LABORATOIRE DE MECANIQUE, MATERIAUX ET STRUCTURES
LABORATORY OF MECHANICS, MATERIALS AND STRUCTURES

ON VIBRATION CONTROL OF OFFSHORE PLATFORM

Thesis submitted and defended in partial fulfillment of the requirements for the award of degree of Doctor of Philosophy (Ph.D.) in Physics.

Speciality : **Mechanics, Materials and Structures**

By

NGOUNOU Armel Martial

*Registration number : **10W0606***

Master of Science in Physics

Option : **Fundamental Mechanics and Complex Systems**

Under the supervision of

NANA NBENDJO Blaise Roméo

Professor

University of Yaoundé I

© *Year 2023*

UNIVERSITÉ DE YAOUNDÉ I
THE UNIVERSITY OF YAOUNDE I

FACULTÉ DES SCIENCES
FACULTY OF SCIENCE

DÉPARTEMENT DE PHYSIQUE
DEPARTMENT OF PHYSICS

ATTESTATION DE CORRECTION DE LA THÈSE DE DOCTORAT/Ph.D

Nous, Professeur **TCHAWOUA** Clément et Professeur **WOAFO Paul**, respectivement Examinateur et Président du jury de la Thèse de Doctorat/Ph.D de Monsieur NGOUNOU Armel Martial, Matricule **10W0606**, préparée sous la direction du Professeur NANA NBENDJO Blaise Roméo, intitulée : « **On vibration control of offshore platform**», soutenue le Mercredi, 22 Février 2022, en vue de l'obtention du grade de Docteur/Ph.D en Physique, Spécialité Mécanique, Matériaux et Structures, Option **Mécanique Fondamentale et Systèmes Complexes**, attestons que toutes les corrections demandées par le jury de soutenance ont été effectuées.

En foi de quoi, la présente attestation lui est délivrée pour servir et valoir ce que de droit.

Fait à Yaoundé le ....0.9. MARS 2023.............

Examinateur

Pr. **TCHAWOUA** Clément

Le Chef de Département de Physique

Pr. NDJAKA Jean-Marie Bienvenu

Le Président du jury

Pr. WOAFO Paul

DEPARTMENT OF PHYSICS

On vibration control of offshore platform

Thesis

Submitted and defended for the award of

Doctorat/ PhD in Physics

Specialty: Mechanics, materials and structure

Option: Fundamental mechanics and complex systems

By

NGOUNOU Armel Martial

Registration Number: 10W0606

MASTER DEGREE in Physics

supervised by

NANA NBENDJO Blaise Roméo

Professor

e-mail address: martialngounou@yahoo.fr

Year 2023

Contents

List of Figures

List of Tables

Dedications

I dedicate this work:

To **Almighty God** who by his powerful hand, his love, graciously gave me the health, the strength, the intelligence necessary to carry out this work. All glory to him

To my mother **KWADO Emilienne**, for his love, advices and encouragements. May you find in this work the achievement of some of your dreams and a real reason of satisfaction;

To my brothers and sisters: **Mr. Happi Leopold**, **Mme. NGUEYEP Mireille**, **Mrs. PAKEDJOU Cendrine**, **Mr. NJANJOUO Boris Hermann**, **Mrs. KEMBOU Sephora**

Acknowledgements

This thesis is the fruit of severals supports of special persons, and I will take this occasion to give them this few words. I would like to address my very king gratitude:

- To Professor **NANA NBENDJO Blaise Roméo**, who cordially admitted me in his research group, defined the topic of this thesis. For his insightful guidance, constant encouragement, the supervision of this work and his dedicated attention to me. I will never forget his entire disponibility and implication for this work. I have learnt to pursue perfection from his serious attitude towards everything. Without his patient instruction, this thesis would not have been completed.

- To Professor **WOAFO Paul**, Head of LaMSEBP for his theoretical and practical teachings that he gave us through seminars so that we can innovate in new technologies.

- To **Prof. Dr.-Ing Uwe Dorka**, of University of Kassel, in Germany for his collaboration, constructive discussions and helpful suggestions during my stay in Germany.

- To Professor **NDJAKA Jean-Marie Bienvenu**, the Head of Department of Physics, for the teachings, advices and encouragements that He gave to me during the academic cycle of Master.

- I wish to express my acknowledgements to all the members of the public defence jury,
  - Prof. **WOAFO Paul**
  - Prof. **NANA NBENDJO Blaise Roméo**
  - Prof. **TCHAWOUA Clément**
  - Prof. **FEWO Serge Ibraïd**
  - Prof. **LOUODOP FOTSO Patrick Hervé**
  - Prof. **ENYEGUE A NYAM Françoise**

- To Professor **KOFANE Timoléon Crépin** for the wide advices during courses in nonlinear physics and in the research have been very beneficial for me in my work.

- To Professor **TCHAWOUA Clément** for his courses in vibration and elasticity and the large number of advices during the Master's courses.

- To All the teaching staff and personnel of the Department of Physics, Faculty of Science, University of Yaoundé I, for their teachings and help since my Master degree in this institution.

- To **Steel and composite structures team of University of Kassel, Germany**, For the opportunity that they give me to follow part of this research study in their laboratory through Humboldt Fellowship.

- To **Dr. MBA Cloriant**, for his support, guidance, availability, exchanges and advice. The one who devoted a lot of his time to me, in order to clarify the gray areas that I encountered in this work.

- To my elders in the lab, **Dr. NANHA Armand**, **Dr. NDEMANOU Peggy**, **Dr. METSEBO Jules**, **Dr. ANAGUE Merveil**, **Dr. SONFACK Hervé**, **Dr. FANKEM Éliane**, **Dr. PIEDJOU Alex**, for your fruitful exchanges during my stay; One more time thank you .

- To my pairs and labmates **YOUTHA Octave**, **DJUITCHOU Thomas**, **YANKAM Gaëlle**, **FEULEFACK Ashley**, **MOKOLA Dalahaï**, **ESSAMBA MAH Ursule**, **YOUMBI Dorota**, **MBOYO Réné**, **NGATCHA Nelly**, **POUOKAM Paola** and all the others, thank for your trust.

- To my elder brother **NGUEYEP Yannick**, for all his advice, encouragement and financial support throughout this work.

- To my brother and friend **KAMGA FOUALENG Arnauld Samuel**, for his multifaceted support.

- To **Maman PANTA Madeleine**, **Uncle DIEUPPA Roger**, **Mr. YOMBOU Duclair**, **Mr. HAPPI Adrien**, for their support.

- To my friends **TSEYEP Rodrigue, SIME Litvine Vanessa, NANA Gaëlle**, NGANKAM Gautier for the presence and encouragements that helped me to accomplish easily this work To all my parents, uncles, aunts, brothers, sisters, nephews,

nieces, friends those whose names have not been mentioned here, those reading this work for their active support.

Please, receive all of you moreover, my gratefulness for this achievement, your achievement for you guide me unconditionally with love and I will respond also with unconditional and pure love.

List of abbreviations

A-B-M: Adams-Bashforth-Moulton

BOP: Blow Out Preventer

DDEs: Delay Differential equation(s)

DOF: Degree Of Freedom

DPS:Dynamic Position Keeping Systems

FDEs: Fractional Differential Equation(s)

FEED: Front-End Engineering Design

FPS: Floating Production Systems

FPSO: Floating Production, Storage and Offloading

FPU: Floating Production Unit

FSO: Floating Storage and Ofloading

GBS: Gravity-Based Structures

HB: Harmonic Balance

ODE(s): Ordinary Differential Equation(s)

PDE(s): Partial Differential Equation(s)

RK4: Fourth-Order Runge-Kutta

TLCD: Tuned Liquid Column Damper

TLP: Tension Leg Platforms

Abstract

This Thesis describes the vibratory, including dynamics analysis and vibration control of an offshore platform. After the description of the different types of offshore platforms, particular attention is paid to tension leg platforms subjected to sea wave excitations. Firstly, one establishes the analytical framework consisting of mathematical modeling of tension leg platform taking into account the tendons and the delay. We analyse the stability and determine the physical characteristics of tendon system that allow the system to be always stable. Secondly, new nonlinear viscoelastic model describing the surge movement of tension leg platform is presented. To make the model more meaninful and practical, fractional derivative damping within the meaning of Caputo is taking into account in the modeling of the system. Finally, a tuned liquid column damper (TLCD) is used to modify the dynamic response of the structural system. By means of the appropriate mathematical concepts (modal approximation, harmonic balance method, D-subdivision method, Melnikov method, multi-scales method, average method) and numerical simulation (Fourth-order Runge-Kutta method for ordinary differential equations, Fourth-order-Runge-Kutta method for delay differential equations, numerical method for fractional differential equations, bisection method), the dynamic behavior of the structure under wave excitation is studied. It is well known that due to the presence of time delay the stability and vibration amplitude of the structure are affected. We show that this effect could be compensated by making a good choice of tendons parameters when designing offshore platforms. We demonstrate that the installation of control device (tuned liquid column damper) at the top of tension leg platform can effectively contribute to reduce the vibrations. Also, a proper selection of the material used to build the tendons can contribute to reduce the amplitude of vibrations and to suppress chaos in the tension leg platform system.

Keywords: Offshore platform, Tension leg platform, Wave, Cantilever beam, Rayleigh beam theory, Amplitude of vibration, Delay effect, Tuned liquid column damper, Fractional order derivative.

Résumé

Cette thèse décrit l'analyse dynamique et le contrôle des vibrations d'une plateforme offshore. Après la description des différents types de plateformes offshore, une attention particulière est portée aux plateformes à jambes de tension soumises aux excitations des vagues de mer. Premièrement, on établit le cadre analytique consistant en une modélisation mathématique de la plateforme à jambe de tension prenant en compte les cables et le retard. Nous analysons la stabilité et déterminons les caractéristiques physiques du système des cables qui permettent au système structurel d'être toujours stable. Deuxièmement, un nouveau modèle viscoélastique non linéaire décrivant le mouvement de surtension de la plateforme à jambe de tension est présenté. Pour rendre le modèle plus significatif et pratique, l'amortissement à dérivé fractionnaire au sens de Caputo est pris en compte dans la modélisation du système. Enfin, un amortisseur de colonne de liquide accordé (TLCD) est utilisé pour modifier la réponse dynamique du système structurel. Par le biais des méthodes mathématiques appropriées (approximation modale, méthode de la balance des harmoniques, méthode de D-subdivision, méthode de l'échelle à temps multiple, méthode de Melnikov, méthode de la moyenne) et méthodes de simulation numérique (la méthode de Runge-Kutta d'ordre quatre pour les équations aux dérivées ordinaires, la méthode de Runge-Kutta d'ordre quatre pour les équations aux dérivées ordinaires avec retard, méthode numérique pour les différentielles fractionnaire. Il est bien connu qu'en raison de la présence du retard dans un système, la stabilité et l'amplitude de vibration du système sont affectées. Nous montrons que cet effet pourrait être compensé en faisant un bon choix des paramètres des câbles lors de la conception des plates-formes offshore. Nous démontrons que l'installation d'un dispositif de contrôle (amortisseur de colonne de liquide réglé) au sommet de la plate-forme à jambe de tension peut contribuer à réduire efficacement les vibrations. Par ailleurs, nous montrons qu'un choix approprié du matériau utilisé pour la construction des plateformes à jambe de tension peut contribuer à réduire l' amplitude de vibrations et à supprimer des comportements non désirés (tels que le chaos) dans la superstructure.

Mots-clés: Plate-forme offshore, Plate-forme à jambe de tension, Vague, Poutre cantilever, Théorie de poutre de Rayleigh, Amplitude de vibration, Effet du retard, Amortisseur à colonne de liquide réglé, Dérivée fractionnaire.

General introduction

Since the dawn of modern civilization, man has been in an ever-increasing need of more and cheaper energy. Resources on land are heading towards extinction due to their rapid depletion. In recent decades, the vast ocean bed has been the target of exploration. It is in this context, the offshore structures in particular offshore platforms may be regarded as the greatest extention of engineering expertise in recent years. Offshore platforms are extensively used to explore, drill, produce, storage and transport ocean oil and/or gas resources in different depths. The earliest offshore structure for oil drilling was built about 1887 off the cost of southern California near Santa Barbara [1]. There are several types of offshore platforms, such as self-elevating platforms, gravity platforms, steel jacket platforms, tension-leg platforms (TLPs), articulated leg platforms, guyed tower platforms, spar platforms, floating production systems, and very large floating structures. These platforms can be divided into fixed-bottom platforms and buoyant platforms, which have their own particular purposes and different configurations. . Specifically, offshore platforms which are located in a very tough ocean environment over a long period of time, are inevitably affected by environmental loading, such as waves, winds, ice, currents, flow, and earthquakes [2–9]. This environmental loading may lead to failure of deck facilities, fatigue failure of platforms, inefficiency of operation, and even discomfort of crews. In order to ensure reliability and safety of offshore platforms, it is of great significance to explore a proper way of suppressing vibration of offshore platforms. To meet an increasing demand for marine sources of energy and minerals, in the past several decades, a lot of research effort has been made on offshore platforms. The related investigations are mainly focused on structure design and monitoring, damage detection, fatigue analysis and reliability assessment, mathematical modeling, dynamic analysis and vibrations control of these structures . Note that reduction of vibration amplitude of an offshore platform by 15 percent can extend service life over two times and can result in decreasing expenditure on maintenance and inspection of structures [10, 11].

Notice that a direct and simple way to mitigate vibration of offshore platforms is to increase the stiffness of the platforms. As a result, natural frequencies can be shifted away from resonating frequencies [12]. However, such schemes generally require extra construction material, which unavoidably leads to increase the costs. Thus, an alternative way is to choose a proper structural control method to reduce structural vibration to an acceptable level [13, 14]. In the past several decades, structural control schemes, such as passive control schemes [15], semi-active control schemes [16], and active control schemes [17], were widely utilized to reduce vibrations of offshore platforms. The tendon systems can also be used, they are constituted by viscoelastic materials.

Therefore, the long memory effects of these viscoelastic materials can be modelled by means of fractional derivatives. We demonstrate that this viscoelastic physical property of the tendons can be beneficial for the platform offshore safety.

Predicting the dynamic behavior of an offshore platform under the action of irregular and regular waves is a well-known challenging subject in structural dynamics and it is considered in this thesis. In particular, the dynamics of tension leg platforms under the action of irregular and regular waves analyzed by using the vibrational and chaotic approaches. More precisely, the aim of the research presented in this thesis is to:

- Model mathematically this structural systems under irregular and regular sea wave excitation.

- Compensate the time-delay effect on the stability and the amplitude of vibration of the TLP.

- Use mathematical and numerical tools to access the behaviour of the structural system and analyse the influence of the control device.

- Explore the effects of main parameters, namely : number of tendons, the order of the fractional viscoelastic material that constitutes the tendon and the tendon viscosity coefficient on the amplitude of TLP and the on the threshold condition for the appearance of chaos and the basins of attraction.

Following this introduction, the dissertation is organized as follows

Chapter one is devoted to the state of the art, on the types of platform offshore as well as the different types of environmental loads on offshore structures, the dynamics of elastic beam and rigid beam are also presented. Afterwards, generalities on the vibration control of mechanical structures are given.

Chapter two consists of the presentation of some analytical and numerical technics used to analysis and solve the problematic of the thesis.

Chapter three is devoted to the presentation and discussion of the results of mathematical analysis and numerical simulations. We end with a general conclusion where we summarize the main results obtained, and perspectives related to our future investigations are suggested.

Litterature review

1.1   Introduction

Offshore platforms vibrations due to thier hostile environment are a source of nuisance that affects the longevity and the comfort of their users. Vibration control are therefore widely used to subdue vibrations in order to lengthen the service life of equipments and structures, also to provide a more comfortable and safe condition for human beings. Due to their structural easiness, offshore platform are particularly vulnerable to damages and sometimes collapse when subjected to sea wave and other external excitation such as earthquakes, wind, ice and tsunamis. In recent years, tendon systems and tuned liquid column damper have become increasingly design and vibration control technique to protect offshore platforms from severe loads. Despite the decades of previous studies, design and vibration control of offshore platforms remains an important problem. The chapter is organized as follows: Section 1.2 presents the types of platform , while Section 1.3 is devoted to the different types of environmental loads on offshore structures. Section 1.4 presents general mathematical formalism of offshore platform (in particular a tension leg platform). Section 1.5 will give an overview on vibration control techniques especially tendon systems and tuned liquid column damper. Section 1.6 deals with the presentation of the problems to be solved in the thesis. Finally in Section 1.7, a brief conclusion will mark the end of this chapter.

1.2   Types of offshore platform

Offshore platforms fall under three major categories : fixed platforms, compliant platforms and floating platforms. They are further classified as follows:

1.2.1   Fixed platforms

1.2.1.1 Jacket platform

A typical jacket platform (Bullwinkle platform) is shown in Fig. 1.1 [1]. A typical jacket platform consists of process, wellhead, riser, flare support, and living quarters. The advantages of offshore jacket platforms are: (i) support large deck loads; (ii) possibility of being constructed in sections and transported; (iii) suitable for large field and long-term production (supports a large number of wells); (iv) piles used for foundation result in good stability; and (v) not influenced by seafloor scour. Few disadvantages are as follows : (i) cost increases exponentially with increase in water

depth; (ii) high initial and maintenance costs; (iii) not reusable (iv) steel structural members are subjected to corrosion, causing material degradation in due course of service life,(v) installation process is time consuming and expensive.

Figure 1.1: Jacket platform

1.2.1.2 Gravity platform

In addition to steel jackets, concrete was also prominently used to build some offshore structures. These structures are called gravity platforms or gravity-based structures (GBS). A gravity platform relies on the weight of the structure to resist the encountered loads instead of piling [18–20]. In regions where driving piles become difficult, structural forms are designed to lie on its own weight to resist the environmental loads [21]. Gravity platforms are the large bottom mounted reinforced concrete structures that are capable of supporting large topside loads during tow-out, which minimizes the hook-up work during installation [22]. Additional large storage spaces for hydrocarbons add up to their advantage. Their salient advantages include: (i) constructed on-shore and transported; (ii) towed to the site of installation; (iii) quick installation by flooding; (iv) no special foundation is required; and (v) use of traditional methods and labor for installation. These platforms are also known to be responsible for seabed scouring due to large foundations, causing severe environmental impact [23, 24]. Gravity platforms had serious limitations namely : (i) not suitable for sites of poor soil conditions, as this would lead to significant settlement of foundation ; (ii) long construction period which there by delays the early start of production ; and (iii) natural frequencies falling within the range of significant power of the input wave spectrum [25]. Advantages of gravity platforms over jacket platforms are namely: (i) Greater

safety for people on board and topside; (ii) Towing to site with deck is possible, which minimizes installation time and cost; (iii) Low maintenance cost because concrete submerged in water will have less problems than that of steel structure; (iv) Adjustable crude oil capacity; (v) Capability to support large deck areas; (vi) Risers are protected as they are placed inside the central shaft; and (vii) Possible access to sea floor from the cell compartment in the foundation, resulting in healthy monitoring. Fig. 1.2 [1] shows the Hibernia gravity base structure. The platform is a steel gravity base structure with a weight of 112,000 ton, height of 241 m, and has steel skirts for penetration into the seabed.
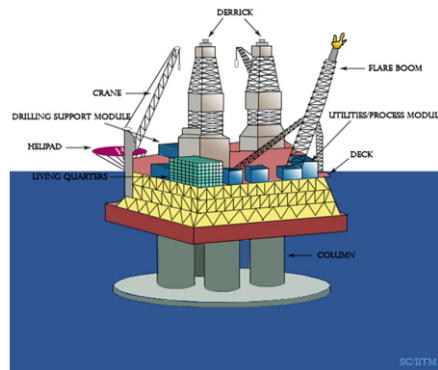
Figure 1.2: Gravity platform

1.2.1.3 Jack-up rigs

Jack-up (rigs) platforms are temporary structures, meant for exploratory drilling. They are similar to barges with movable legs. They are mobile as their hulls have the requisite floating characteristics to enable towing from site to site. When the legs are projecting upwards, the rig can be easily towed from one location to another location. Jacking system provides an effective method to quickly lower or raise the hull. The legs are lattice, truss-type, and transparent to wave loads. When the jack-up is being towed to the site for exploratory drilling, the legs will be projecting upwards from the deck. On installation, the legs will be pushed inside the sea bed while the deck is lifted up. Hence called "Jack-up rig". After installation, one-third height of the leg should be left above the hull for maintaining the stability of the platform. The failure in the platform occurs during sailing when the legs are completely above the hull due to overturning moment caused by the wind load and by spud can pull off. The latter may cause serious damage to the drill pipes and risers but the system will remain floating. The spud can foundation is not an ideal hinged

joint. It offers partial fixity to the structure so that the structure may also fail under bending. The jack-up rigs are capable of working under harsh environments of wave heights up to 24 m and wind speed exceeding 100 knots. Advantages of the platform include (i) high mobility; (ii) low cost and efficient; (iii) easy fabrication and repair; (iv) easy decommissioning; and (v) simple construction. These platforms also have some serious limitations such as (i) suitable only for shallow depth; (ii) subjected to sea bed scouring which leads to differential settlement; (iii) not suitable for rocky stratum. The name jack-up is assigned as the legs will be pulled up while they are transported from one site to another. On reaching the installation site, legs will be driven into the seabed for a better stability. Jack-up rigs have significant mobility but the geometric configuration is comparable to that of a fixed-base structure. Fig. 1.3 [1] shows a schematic view of a typical jack-up rig.
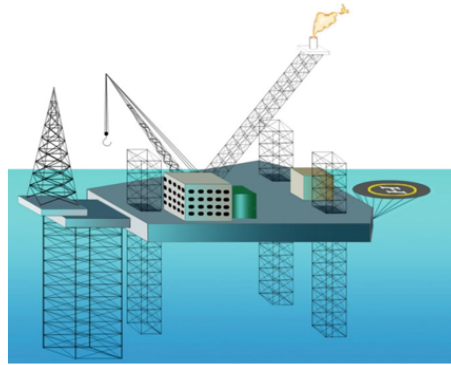
Figure 1.3: Jack-up rig platform

1.2.2 Compliant platform

To overcome the above negative factors, one should design a structural form, which should attract fewer forces and remain flexible to withstand the cyclic forces. The structural action and the form are corrected based on the "mistakes" learnt from the fixed type platforms. This is a special kind of reverse engineering, which makes offshore platforms unique. This leads to continuous improvement from one platform to the other. Hence, FEED is on a constant update as new structural forms are being tried for oil and gas exploration in deep and ultra-deep waters [26,27]. Fixed type offshore structures became increasingly expensive and difficult to install in greater water depths. Hence, modified design concept evolved for structures in water depths beyond 500m. A compliant offshore tower is similar to that of a traditional platform, which extends from

surface to the sea bottom and transparent to waves. A compliant tower is designed to flex with the forces of waves, wind, and current. Classification under compliant structure includes those structures that extend to the ocean bottom and are anchored directly to the seafloor by piles and/or guidelines [28]. Guyed towers, articulated tower, and tension leg platform fall under this category.

1.2.2.1 Guyed tower

Guyed tower is a slender structure made up of truss members that rest on the ocean floor and is held in place by a symmetric array of catenary guy lines. The foun-dation of the tower is supported with the help of spud can arrangement, which is similar to the inverted cone placed under suction. The structural action of the guyed tower makes its innovation more interesting, which is one of the successful improvements in the structural form in the offshore structural design. The upper part of the guy wire is a lead cable, which acts as a stiff spring in moderate seas. The lower portion is a heavy chain, which is attached with clump weights called touch-down point. This feature has allowed the tower to be designed with a constant square cross section along its length, reducing the structural steel weight as compared with that of a conventional platform [29]. The advantages of guyed towers are (i) low cost (lower than steel jacket) ; (ii) good stability as guy lines and clump weights improve restoring force ; and (iii) possible reuse. The disadvantages are as follows : (i) high maintenance costs ; (ii) applicable to small fields only ; (iii) exponential increase in cost with increase in water depth; and (iv) difficult mooring. These factors intuited further innovation in the platform geometry, which resulted in articulated towers [30]. Fig. 1.4 [1] shows the schematic view of the Lena tower (Guyed tower)
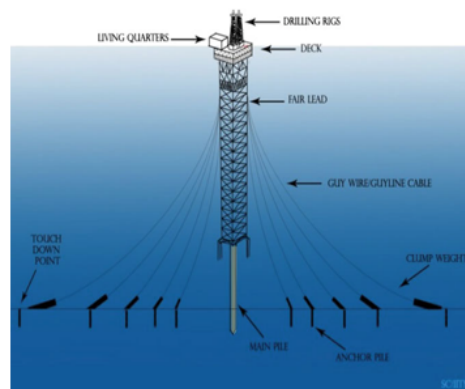
Figure 1.4: Guyed tower

1.2.2.2 Articulated tower

One of the earliest compliant structures that started in relatively shallow waters and slowly moved into deep water is the articulated tower. An articulated tower is an upright tower that is hinged at its base with a universal joint, which enables free rotation about the base. When there was a need to improve the structural form from fixed to compliant, researchers thought of both modes of compliancy namely : (i) rotational and (ii) translational. Enabling large translational motion could make the platform free from position-restrained, and hence rotational compliancy was attempted. In such geometric forms, it is important to note that the design introduces a single-point failure deliberately, which is the universal joint. The tower is ballasted near the universal joint and has a large buoyancy tank at the free surface to provide large restoring force (moment). This is achieved by the dynamic change in water plane area or variable submergence of the member. In addition, the compliancy of the articulated tower avoids the concentration of high overturning moments and the resulting stress. The advantages of articulated towers are as follows : (i) low cost; (ii) large restoring moments due to high center of buoyancy; and (iii) protection of risers by tower. There are few disadvantages : (i) suitable only for shallow water as the tower shows greater oscillations for increased water depth ; (ii) cannot operate in bad weather; (iii) limited to small fields; and (iv) fatigue of universal joint leads to a single-point failure [31–33]. Fig. 1.5 [1] shows a typical articulated tower, supporting the storage activities of a vessel.
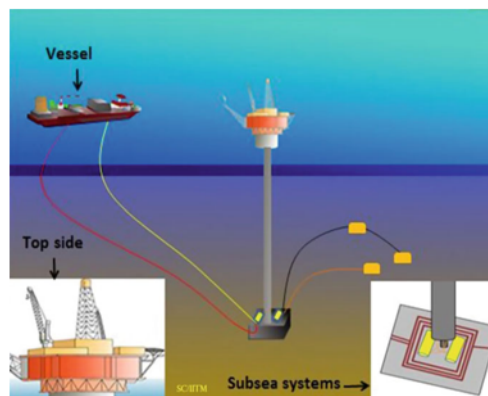
Figure 1.5: Articulated tower

1.2.2.3 Tension leg platform

A tension leg platform (TLP) is a vertically moored compliant platform [34]. Fig. 1.6 [1] shows a typical TLP, highlighting its various components. Taut mooring lines vertically moor the floating platform, with its excess buoyancy ; they are called tendons or tethers. The structure is vertically restrained, while it is compliant in the horizontal direction permitting surge, sway, and yaw motions. The structural action resulted in low vertical force in rough seas, which is the key design factor [35–37]. Columns and pontoons in TLP are constructed with tubular members due to which the buoyancy force exceeds the weight of the platform. The excess buoyancy created is balanced by the pretension in the taut moorings. Substantial pretension is required to prevent the tendons from falling slack even in the deepest trough, which is achieved by increasing the free-floating draft [37, 38]. As the requirement of pretension is too high, pretension cannot be imposed in tethers by any mechanical means. During commissioning, void chambers (columns and pontoon members) are filled with ballast water to increase the weight; this slackens the tendons. After tendons are securely fastened to the foundation in the seabed, de-ballasting is carried out to impose necessary pretension in the tendons. Advantages of TLPS are as follows: (i) mobile and reusable; (ii) stable as the platform has minimal vertical motion; (iii) low increase in cost with increase in water depth; (iv) deepwater capability; and (v) low maintenance cost. Few disadvantages are namely: (i) high initial cost; (ii) high subsea cost; (iii) fatigue of tension legs; (iv) difficult maintenance of subsea systems; and (v) little or no storage.
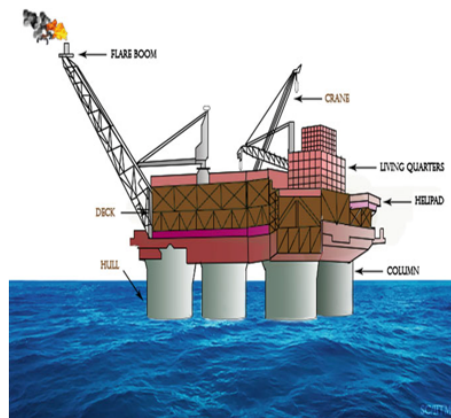
Figure 1.6: Tension leg platform

1.2.3 Floating platforms

Semisubmersibles, FPSO systems, FPUs, FSO systems, and spar platforms are grouped under this category.

1.2.3.1 Semisubmersible

Semisubmersible marine structures are well known in the oil and gas industries and belong to the category of neutrally buoyant structure. These structures are typically moveable only by towing. These semisubmersibles have a relatively low transit draft, with a large water plane area, which allows them to be floated to a stationing location. On location, it is ballasted, usually by seawater, to assume a relatively deep draft or semi-submerged condition, with a smaller water plane area, for operation. Semisubmersible platforms have the principal characteristic of remaining in a substantially stable position and have minimal motions in all the degrees of freedom due to environmental forces such as the wind, waves, and currents. The main parts of the semisubmersibles are the pontoons, columns, deck, and the mooring lines. When submerged for stationing and operations, the columns connecting the pontoons to the upper deck present a lower water plane area, thereby attracting less wave loads and thus reducing the motions. Generally, dynamic position keeping systems (DPS) are deployed to hold the semisubmersibles in position while production and drilling [39]. Fig. 1.7 [1] shows a typical semisubmersible. The advantages of semisubmersibles are as follows: (i) mobility with high transit speed ; (ii) stable as they show minimal response to wave action; and (iii) large deck area. The disadvantages are (i) high initial and operating costs; (ii) limited deck load (low reserve buoyancy); (iii) structural fatigue; (iv) expensive to move large distances.

1.2.3.2 Floating production unit (FPU), floating storage and offsloading (FSO), floating production, storage, and offsloading (FPSO)

FPSO is an acronym for Floating Production, Storage and Offloading systems. Offloading of the crude oil is usually to a shuttle tanker. Typically converted or newly built tankers are custom-made for production and storage of hydrocarbons. These stored hydrocarbons are subsequently transported by other vessels to terminals or deepwater ports. The design variants of FPSO are FPS and FSO. FPS is an acronym for Floating Production Systems devoid of storage facility. Now, it is a universal term to refer to all production facilities that float rather than structurally
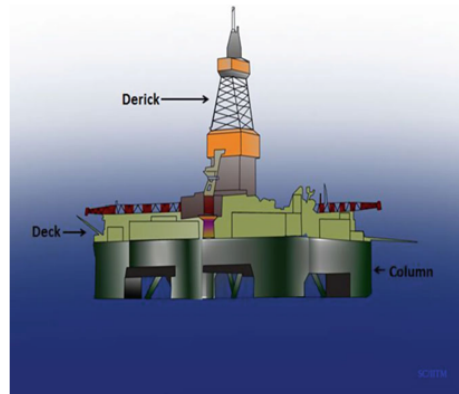
Figure 1.7: Semisubmersible platform

supported by the seafloor, and typical examples include TLPs, spars, semisubmersibles, ship-shape vessels, etc. FSO is an acronym for Floating, Storage, and Offloading system. Like the FPSO, these are typically converted or newly built tankers, and they different from the FPSO by not incorporating the processing equipment for production; the liquids are stored for shipment to another location for processing. An FPSO relies on subsea technology for the production of hydrocarbons and typically involves pipeline export of produced gas with shuttle tanker (offloading) transport of produced liquids [40]. Salient advantages of the FPSOs are asfollows: (i) low cost; (ii) mobile and reusable; (iii) reduced lead time; (iv) quick disconnecting capability, which can be useful in iceberg-prone areas; (v) little infrastructure required; and (vi) turret mooring system enables FPS (converted ship type) to head into the wind/waves reducing their effect. The disadvantages are (i) limited to small fields; (ii) low deck load capacity; (iii) damage to risers due to motion; (iv) poor stability in rough sea.
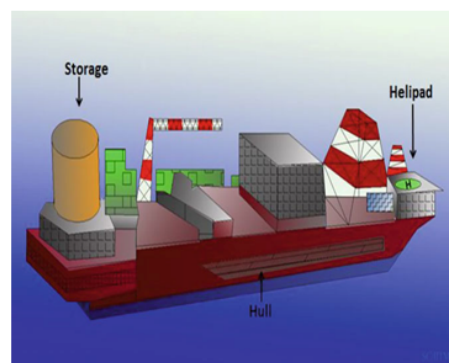
Figure 1.8: Floating production unit (FPU), floating storage and offsloading (FSO), floating production storage and offsloading (FPSO)

1.2.3.3 Spar platform

Spar platform belongs to the category of neutrally buoyant structures and consists of a deep draft floating caisson. This caisson is a hollow cylindrical structure similar to a very large buoy. Its four major components are hull, moorings, topsides, and risers. The spar relies on a traditional mooring system, i.e., anchor-spread mooring or catenaries mooring system, to maintain its position. The spar design is now being used for drilling, production, or both. The distinguishing feature of a spar is its deep draft hull, which produces very favorable motion characteristics. The hull is constructed by using normal marine and shipyard fabrication methods, and the number of wells, surface wellhead spacing, and facilities weight dictate the size of the center well and the diameter of the hull. Fig. 1.9 [1] shows a typical spar platform. In the classic or full cylinder hull forms, the whole structure is divided into upper, middle and lower sections. The upper section is compartmentalized around a flooded center well housing different type of risers namely production riser, drilling riser, and export/import riser. This upper section provides buoyancy for the spar. The middle section is also flooded but can be configured for oil storage. The bottom section, called keel, is also compartmentalized to provide buoyancy during transport and to contain any field-installed, fixed ballast. The mooring lines are a combination of spiral strand wire and chain. Advantages of spar platforms are as follows: (i) low heave and pitch motion compared to other platforms; (ii) use of dry trees (i.e., on surface); (iii) ease of fabrication; (iv) unconditional stability as its center of gravity is always lower than the center of buoyancy. Disadvantages include the following: (i) installation is difficult as the hull and the topsides can only be combined offshore after the spar hull is upended; (ii) have little storage capacity which brings along the necessity of a pipeline or an additional FSO; and (iii) have no drilling facilities.
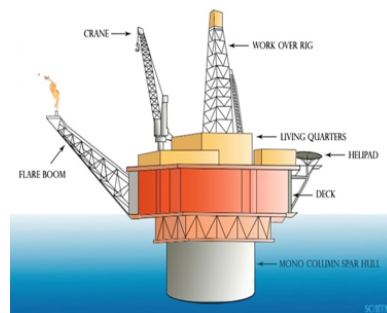
Figure 1.9: Spar platform

Fixed structures are economically feasible only up to water depths. In the range 1, 000 to 1,600 ft. Fixed platforms are indeed the most popular and prolific structures for water depths of 400 to 500 ft. However, they become impractical for deep water because they must be built stronger and more bulky than the equivalent compliant structures. In recent years, the need to explore for oil in deeper water has made compliant structures more popular. Compliant towers are believed to be economically feasible in water depths exceeding 2, 000 ft. Here, we will consider compliant structures. In particular, we are interested in tension leg platforms (TLP) in this thesis.

1.3   Environmental forces

This section deals with different types of environmental loads on offshore structures. It also includes code information regarding the loads. Step-by-step method for load estimate on a cylindrical member and an example structure is detailed. The procedure for estimating wave loads is illustrated through examples. Loads for which an offshore structure must be designed can be classified into the following categories:

- Permanent loads or dead loads

- Operating loads or live loads

- Other environmental loads including earthquake loads

- Construction and installation loads

- Accidental loads

While the design of buildings onshore is influenced mainly by the permanent and operating loads, the design of offshore structures is dominated by environmental loads, especially waves loads, and the loads arising in the various stages of construction and installation. These include

▷ Wave Forces (regular and irregular)

▷ Wind Forces

▷ Current Forces

▷ Earthquake Loads

▷Ice and Snow Loads

1.3.1   Morison's equation

J.R. Morison [41] presented a theory for determination of forces on a vertical cylinder in the presence of regular and irregular sea waves. The theory evaluates the inertia and drag forces

without modifying the wave characteristics. This Theory makes us of linear or Airy's theory for determination of velocity and accelaration of the water particles at the axis of the cylinder. According to Morison's formulation [41], the wave force at any elevation z at the time t is given by Eq.(1.1)

$$f_M\left(z,t\right) = \rho_w c_M \frac{\pi}{4} D^2 \dot{u}_x\left(t\right) - \rho_w\left(c_M - 1\right)\frac{\pi}{4}D^2 \dot{v}\left(t\right) + \rho_w c_D \frac{D}{2}\left(u_x\left(t\right) - v\left(t\right)\right)\left|u_x\left(t\right) - v\left(t\right)\right|,$$

$$(1.1)$$

where, ρ_w is a water density, D is a diameter of the cylinder, v and $\dot{v}$ are the velocity and acceleration of the structure, u_x and $\dot{u}_x$ are the horizontal velocity and accelaration of water particle, c_M is the inertia coefficient, c_D is the drag coefficient and $||$ is the absolute value.

1.3.2 Regular sea wave excitation

In the wave theory, the wave is assumed to be sinusoidal with constant wave amplitude, wavelength, and wave period. Thus, the regular propagation wave in defined as,

$$\eta\left(x,t\right) = \eta_a \sin\left(kx - \omega t\right),$$

$$(1.2)$$

where η is the time-and position-dependent wave elevation. The linear wave theory, usually called the Airy theory, can be used to represent the wave kinematics. The seawater is assumed to be incompressible and inviscid. The fluid motion is irrotational. Then, a velocity potential exists and satisfies the Laplace equations. By applying the kinematic boundary conditions and the dynamic free-surface conditions, the velocity potential, and the wave kinematics can be found [42]. Based on the Airy theory [42], the horizontal water particle kinematics are described by Eq.(1.3) and Eq.(1.4).

$$u\left(x,z,t\right) = \omega \eta_a \frac{\cosh k\left(z+h\right)}{\sinh kh} \cos\left(kx - \omega t\right)$$

$$(1.3)$$

$$\dot{u}\left(x,z,t\right) = \omega^2 \eta_a \frac{\cosh k\left(z+h\right)}{\sinh kh} \sin\left(kx - \omega t\right),$$

$$(1.4)$$

where u and $\dot{u}$ are the water particle velocity and acceleration in the x-direction (wave propagation direction), respectively, ω is the wave frequency, η_a is the regular wave amplitude, k is the wave number, the z axis is upward, and h is the mean water depth.

1.3.3 Irregular sea wave excitation

The natural seaway on the oceans is irregular. It is also referred to as random sea. The sea shows rarely a unidirectional, regular sinusoidal wave pattern, but we observe a mixture of wave of different length and direction. The nature seaway can be decomposes to a sum of partial sinusoidal waves, each having a relatively small steepness, even for a severe sea. Therefore, the spectral approch with a sum of partial waves constitutes a valid representation for a random sea. Form careful observation, certain typical or characteristic parameters can be estimated, such as a significant wave height, period and direction of progress. S. Denis and Pierson [45] introduced a mathematical description of natural seaways. Their work was a milestone to allow a calculation of random seas and linear ship motion. The Unidirectional, irregular wave ζ in seen as the sum of regular partial waves, as showns in Figure 1.10 ($x = 0$). From a record of the irregular sea, the wave velocities are determined using random wave theory, and characterized by the Pierson-Moskowitz power spectrum, and converted to the time domain using Borgman's method [43, 44]. Based on Airy wave theory, irregular wave shape is determined by Eq.(1.5)
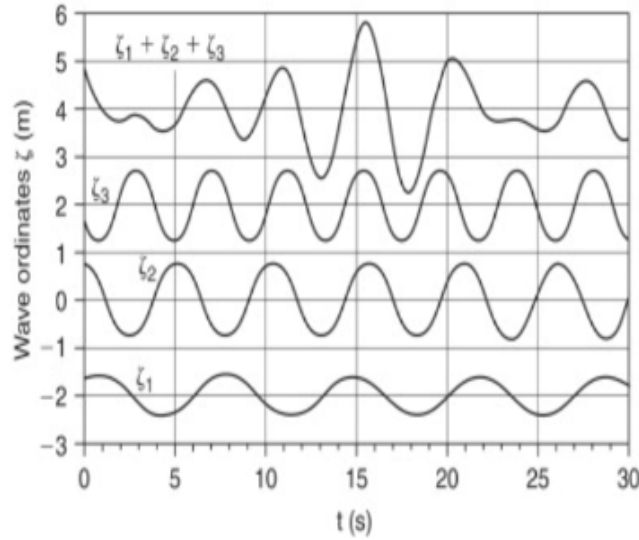
Figure 1.10: Irregular wave from sum of regular wave

$$\zeta(x, t) = \sum_{i=1}^{n} a_i \cos(k_i x - \omega_i t + \varepsilon_i). \tag{1.5}$$

Velocity and acceleration of water particles are given by Eqs.(1.6) and (1.7)

$$u(x, z, t) = \sum_{i=1}^{n} a_i \omega_i \frac{\cosh k(z + h)}{\sinh kh} \cos(k_i x - \omega_i t + \varepsilon_i) \tag{1.6}$$

$$\dot{u}(x,z,t) = \sum_{i=1}^{n} a_i \omega_i^2 \frac{\cosh k(z+h)}{\sinh kh} \sin(k_i x - \omega_i t + \varepsilon_i), \qquad (1.7)$$

where ζ is the wave cordinate, expressing surface elevation, i is the number of wave component (partial wave), a_i is the amplitude of the ith partial wave, ω_i is the frequency of partial wave, n is the total number of partial wave, k_i is the wave number, x and t are the way of progress and time, ε_i is a phase angle of partial wave (the phase is randomly distribution).

1.4 General mathematical formalism of TLP

According to the modelling of compliant offshore structure, in particular a Tension Leg Platform, in litterature, there are two majors ways to model: as Cantilever elastic beams or rigid body beams. This part of work is devoted to the generalities on dynamics of beams

1.4.1 Rigid model

It should be noted that the system responds as a soft spring system. This can be shown by looking at the rigid model. The equation of motion for this system is given by

$$m\ddot{x}(t) + c\dot{x}(t) + (T_0 + \Delta T(x(t)))\sin\theta = f(t), \qquad (1.8)$$

where m is the mass of the structure, T_0 is the initial pre-tension in the tendon, x is the displacement in the surge direction, θ is the angle between the initial and the displaced position of the tether, c is the structural damping coefficient, $\Delta T(x)$ increase in the initial pre-tension due to the arbitrary displacement, $f(t)$ is the external force

1.4.2 Elastic model

An exact formulation of the beam problem was first investigated in terms of general elasticity equations by Love [46]. They derived the equations that describe a vibrating solid cylinder. However, it is not practical to solve the full problem because it yields more information than usually needed in applications. Therefore, approximate solutions for transverse displacement are sufficient. The beam theories under consideration all yield the transverse displacement as a solution.

Euler-Bernoulli beam model

Detailed derivations for the Euler-Bernoulli model can be found in text books by Benaroya [47]. Here, the equation of motion is obtained using Hamilton's variational principle. The potential energy of a uniform beam due to bending is given by

$$PE = \frac{1}{2}\int_0^L EI\left(\frac{\partial^2 w\left(x,t\right)}{\partial x^2}\right)^2 dx. \tag{1.9}$$

The kinetic energy is given by

$$KE = \frac{1}{2}\int_0^L \rho A\left(\frac{\partial^2 w\left(x,t\right)}{\partial t^2}\right)^2 dx. \tag{1.10}$$

The Lagrangian, defined by KE - PE, is given by

$$L = \frac{1}{2}\int_0^L \rho A\left(\frac{\partial^2 w\left(x,t\right)}{\partial t^2}\right)^2 dx - \frac{1}{2}\int_0^L EI\left(\frac{\partial^2 w\left(x,t\right)}{\partial x^2}\right)^2 dx \tag{1.11}$$

Using the extended Hamilton's principle, by including the non conservative forcing, the governing differential equation of motion is given by

$$\rho A\frac{\partial^2 w\left(x,t\right)}{\partial t^2} + EI\frac{\partial^4 w\left(x,t\right)}{\partial x^4} = f\left(x,t\right), \tag{1.12}$$

where E is the modulus of elasticity, I is the area moment of inertia of the cross-section about the neutral axis, $w\left(x,t\right)$ is the transverse deflection at the axial location x and time t, L is the length of the beam, ρ is the density of the beam, A is the cross-sectional area of the beam and $f\left(x,t\right)$ is the external force. The boundary conditions to be satisfied

$\frac{\partial^2 w}{\partial x^2} = 0, \quad w = 0$ for hinged end

$\frac{\partial w}{\partial x} = 0, \quad w = 0$ for clamped end

$\frac{\partial^2 w}{\partial x^2} = 0, \quad \frac{\partial^3 w}{\partial x^3} = 0$ for free end

$\frac{\partial w}{\partial x} = 0, \quad \frac{\partial^3 w}{\partial x^3} = 0$ for sliding end

we proceed with the Rayleigh beam model

Rayleigh beam model

The Rayleigh beam adds the rotary inertia effects to the Euler-Bernoulli beam. The kinetic energy due to the rotation of the cross-section is given by

$$KE_{rot} = \frac{1}{2}\int_0^L \rho I\left(\frac{\partial^2 w\left(x,t\right)}{\partial x\partial t}\right)^2 dx. \tag{1.13}$$

Combining Equation 1.6 with Equations 1.2 and 1.3 to form the Lagrangian and using Hamilton's principle, we obtain the equation of motion given by

$$\rho A \frac{\partial^2 w(x,t)}{\partial t^2} + EI \frac{\partial^4 w(x,t)}{\partial x^4} - \rho I \frac{\partial^4 w(x,t)}{\partial x^2 \partial t^2} = f(x,t),$$ (1.14)

with the boundary conditions given by

$\frac{\partial^2 w}{\partial x^2} = 0, \quad w = 0$ for hinged end

$\frac{\partial w}{\partial x} = 0, \quad w = 0$ for clamped end

$\frac{\partial^2 w}{\partial x^2} = 0, \quad \frac{\partial^3 w}{\partial x^3} - \rho I \frac{\partial^3 w}{\partial x \partial t^2} = 0$ for free end

$\frac{\partial w}{\partial x} = 0, \quad \frac{\partial^3 w}{\partial x^3} - \rho I \frac{\partial^3 w}{\partial x \partial t^2} = 0$ for sliding end

Shear beam model

This model consider the effect of shear distortion. We introduce new variables α, the angle of rotation of the cross-section due to the bending moment, and β, the angle of distortion due to shear. The total angle of rotation is the sum of α and β and is approximately the first derivative of the deflection,

$$\alpha(x,t) + \beta(x,t) = \frac{\partial w(x,t)}{\partial x}$$ (1.15)

The equations of motion, using Hamilton's principle, are given by:

$$\begin{aligned} \rho A \frac{\partial^2 w(x,t)}{\partial t^2} - k_s GA \left(\frac{\partial^2 w(x,t)}{\partial x^2} - \frac{\partial \alpha(x,t)}{\partial x} \right) = 0 \\ EI \frac{\partial^2 \alpha(x,t)}{\partial x^2} + k_s GA \left(\frac{\partial w(x,t)}{\partial x} - \alpha(x,t) \right) = 0 \end{aligned}$$ (1.16)

with the boundary conditions given by

$w(x,t$ is the dimensionless displacement, $\alpha(x,t$ is the angle of rotation due to the bending moment, G is the shear modulus of elasticity and k_s is the shape factor.

$\frac{\partial \alpha}{\partial x} = 0, \quad w = 0$ for hinged end

$\alpha = 0, \quad w = 0$ for clamped end

$\frac{\partial \alpha}{\partial x} = 0, \quad \left(\frac{\partial w}{\partial x} - \alpha \right) = 0$ for free end

$\alpha = 0, \quad \left(\frac{\partial w}{\partial x} - \alpha \right) = 0$ for sliding end

Timoshenko beam model

Timoshenko [48,49] proposed a beam theory which consider the effects of shear distortion and rotary inertia, the Lagrangian includes the effects of bending moment, lateral displacement, rotary

inertia, and shear distortion. We assume that there is no rotational kinetic energy associated with shear distortion, but only with the rotation due to bending. Takinhg into account the previous comment, the equations of motion, using Hamilton's principle, are given by:

$$
\rho A \frac{\partial^2 w(x,t)}{\partial t^2} - k_s G A \left(\frac{\partial^2 w(x,t)}{\partial x^2} - \frac{\partial \alpha(x,t)}{\partial x} \right) = f(x,t)
$$
$$
\rho I \frac{\partial^2 \alpha(x,t)}{\partial t^2} - E I \frac{\partial^2 \alpha(x,t)}{\partial x^2} - k_s G A \left(\frac{\partial w(x,t)}{\partial x} - \alpha(x,t) \right) = 0
$$

$$(1.17)$$

with the boundary conditions given by $\frac{\partial \alpha}{\partial x} = 0$, $w = 0$ for hinged end

$\alpha = 0$, $w = 0$ for clamped end

$\frac{\partial \alpha}{\partial x} = 0$, $\left(\frac{\partial w}{\partial x} - \alpha \right) = 0$ for free end

$\alpha = 0$, $\left(\frac{\partial w}{\partial x} - \alpha \right) = 0$ for sliding end

1.5 An overview on structural control system and vibration control techniques

For several years, always with the aim of improving the performance of controllers and having stronger structures, new structural control system and vibrations control techniques have emerged and is now more and more widespread in the word. It can be passive, active, semi-active or hybrid.

1.5.1 Tendon systems

The tendon system consists of the tendons, and ancillary components needed for operation, including load measurement systems and inspection or monitoring apparatus (Figure 1.11). The tendon system restrains motion of the platform in response to wind, waves, current, and tide within specified limits [50, 51]. The tendons connect points on the platform to corresponding points on a seafloor foundation. By restraining, the platform at a draft deeper than that required displacing its weight; the tendons are ideally under a continuous tensile load that provides a horizontal restoring force when the platform is displaced laterally from its still water position. Generally very stiff in the axial direction, the tendon system limits heave, pitch, and roll response of the platform to small amplitudes while its softer transverse compliance restrains surge, sway, and yaw response to within operationally acceptable 1limits [50, 52].
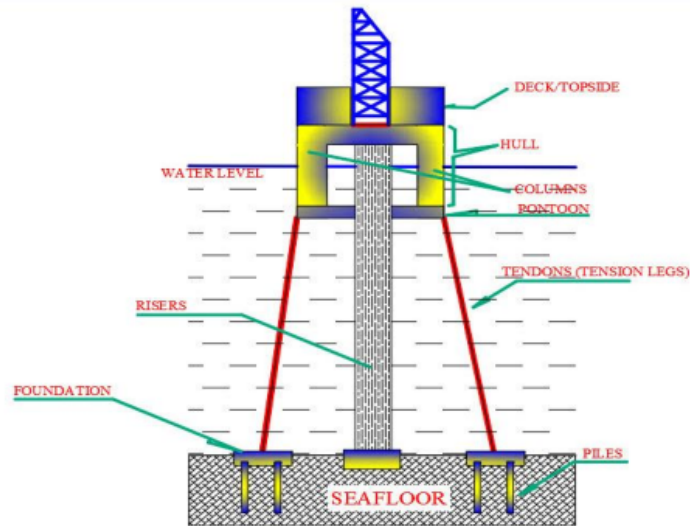
Figure 1.11: Principle of Tendon System on the TLP [50]

1.5.2 Tuned liquid column damper(TLCD)

The idea of utilising liquid in a U-tube to create damping effect for reducing structural vibration by merely allowing it to pass through a small orifice opening in the U-tube was first introduced by Sakai F. in the year of 1989. This device is termed as Tuned Liquid Column Damper as shown in Figure 1.12 [53]
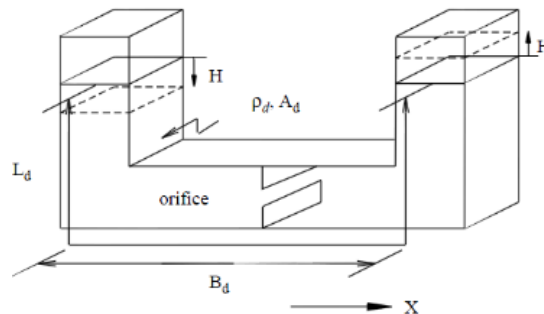
Figure 1.12: Illustration of TLCD [54]

This idea has then be used, further developed extensively and even several modification has been made to the original TLCD. The classification of TLCD available is shown at Figure 1.13

The term LCVA stands for liquid column vibration absorber. The difference between LCVA and TLCD is that a LVCA has a different cross-section in the horizontal and vertical column while TLCD has a same cross-section in the horizontal and vertical column. Double tuned liquid column damper, DTLCD, hybrid tuned liquid column damper, as well as pressurized tuned liquid
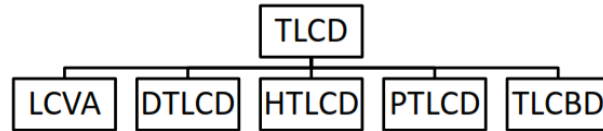
Figure 1.13: Family of TLCD [55]

column damper, PTLCD is not popular due to the complexity in building it and predicting their damping behaviour [56]. On the other hand, tuned liquid column ball damper, TLCBD is the use of a rolling ball instead of an orifice to induce a head loss in the fluid flow of the TLCD [57].

1.6 Problem of the thesis

Various works of art and mechanical constructions emerge daily across the word. We are thus talking about bridges, roads, buildings, boats, offshore platforms that are customizable and varied. All these constructions are essential to the socio-economic development of a region or even a country. In the sense that they allow and participate in the mobility of people (tourists and travellers), the explore, drill, produce, storage, and transport ocean oil and/or gas resources. Hence the need to continually ensure that they are in good working order in order to avoid disasters that will cost the lives of people and their property. The study of the dynamics and the control of the vibrations of offshore platforms (in particular tension leg platfrom) under the action of irregular and regular waves are investigated in this scientific work. Therefore, we propose three techniques to reduce the vibrations of a TLP. First, the rigidity and the damping coefficient of the tendon are increased this by taking into account the time-delay. Second, the fractional nonlinear viscoelastic behavior of the material that constitutes the tendons is taken into account. Finally the tuned liquid column damper will be used as the integral part of the structural system to attenuate the vibration induced by the irregular sea wave excitation.

1.7 Conclusion

This chapter has provided an overview of the dynamics and generalities, on the types of offshore platform, the beam models (elastic, rigid and boundary conditions) and structural vibration control system. To analyse and to solve the problems of the thesis, one needs the use of some analytical and numerical methods. The chapter 2 will be devoted to these methods.

MATHEMATICAL FORMALISMS AND NUMERICAL METHODS

2.1 Introduction

The present chapter is devoted to the presentation of the principles of each method used along the thesis. Theoretical methods concerning both analytical and numerical methods are presented: Galerkin method for modal approximation of partial differential equations, Harmonic Balance (HB) method and method of multiple scales for analytical resolution of ordinary differential equations (ODEs),Average method, Linear stability of delay differential equations,Routh-Hurwitz stability criterion, Melnikov's method,Fourth-order-Runge-Kutta method for delay differential equations,fourth-order Runge- Kutta (RK4) method for numerical resolution, numerical method for fractional differential equation and Bisection method for complex polynomial equations.

2.2 Mathematical formalism

In this subsection, different theories and mathematical methods used to propose solutions to the systems of differential equations of this thesis are stated.

2.2.1 Galerkin approximation for partial differential equations

Vibrations of continuous systems (strings, rods, beams, plates and shells) are governed by PDEs. Galerkin decomposition method is used to simplify the problems of vibrating structures through the reduction of the PDEs into ODEs [58, 59].

Lets $w(x, t)$ describes the displacement of a structure at the time t and spatial location x. Any sufficiently smooth deflection field $w(x, t)$ satisfying any fixed boundary conditions can then be represented as a weighted sum of mode shapes:

$$w(x, t) = \sum_{n=1}^{N} q_n(t) \phi_n(x) \tag{2.1}$$

,

where N represents the number of modes used in the approximation, $q_n(t)$ represents the amplitude of vibrations of the structure associated with the nth mode and $\phi_n(x)$ represents the modal function solution of the nth mode of the beam linear natural equation. These mode shape functions depend on the boundary conditions and are eigenfunctions of the governing equations, of uniform Rayleigh beam in absence of external excitation, obtained from the dimensionles Eq.(1.14) as follows

$$\frac{\partial^2 w(x,\tau)}{\partial \tau^2} + \frac{\partial^4 w(x,\tau)}{\partial x^4} - \mu \frac{\partial^4 w(x,\tau)}{\partial x^2 \partial \tau^2} = 0 \tag{2.2}$$

First, assume that $w(x,\tau)$ is separable so that one can write $w(x,\tau) = \phi(x) q(\tau)$. Then, the equation of motion becomes

$$\phi(x) \ddot{q}(\tau) + \phi''''(x) q(\tau) - \mu \phi''(x) \ddot{q}(\tau) = 0 \tag{2.3}$$

Assuming that $q(\tau)$ is harmonic with frequency ω such that $\ddot{q}(\tau) = -\omega^2 q(\tau)$ with solution $q(\tau) = a \cos \omega \tau + b \sin \omega \tau$, we can write Eq.(2.3) as

$$\phi''''(x) + \left(\mu \omega^2\right) \phi''(x) - \omega^2 \phi(x) = 0 \tag{2.4}$$

The mode function for transverse vibration of the beam is expressed as

$$\phi(x) = d_1 \sin(\alpha x) + d_2 \cos(\alpha x) + d_3 \sinh(\beta x) + d_4 \cosh(\beta x) \tag{2.5}$$

where α, β are given as follows

$$\alpha = \sqrt{\frac{(\mu \omega^2) + \sqrt{(\mu \omega^2)^2 + 4\omega^2}}{2}}, \quad \beta = \sqrt{\frac{-(\mu \omega^2) + \sqrt{(\mu \omega^2)^2 + 4\omega^2}}{2}}. \tag{2.6}$$

After using the following dimensionless boundary conditions

$$w(0,\tau) = 0$$

$$w''(0,\tau) - \frac{kL}{EI} w'(0,\tau) = 0$$

$$\tag{2.7}$$

$$w'''(1,\tau) - \frac{\rho I \omega_0^2 L^2}{EI} (\ddot{w}(1,\tau))' - \frac{M_p \omega_0^2 L^3}{EI} \ddot{w}(1,\tau) = 0$$

$$w''(1,\tau) = 0,$$

one obtain four simultaneous equations which can be written in the matrix form as

$$\begin{vmatrix} 0 & 1 & 0 & 1 \\ -\frac{KL}{EI}\alpha & -\alpha^2 & -\frac{KL}{EI}\beta & \beta^2 \\ -\alpha^2 \sin\alpha & -\alpha^2 \cos\alpha & \beta^2 \sinh\beta & \beta^2 \cosh\beta \\ A_1 & A_2 & A_3 & A_4 \end{vmatrix} \begin{bmatrix} d_1 \\ d_2 \\ d_3 \\ d_4 \end{bmatrix} = \begin{bmatrix} 0 \\ 0 \\ 0 \\ 0 \end{bmatrix} \tag{2.8}$$

where

$$A_1 = -\alpha^3 \cos\alpha + \left(\left(\tfrac{r}{L}\right)^2 \alpha^2\beta^2 + \tfrac{M_p}{\rho AL}\omega^2\alpha^2 \sin\alpha A_2 = \alpha^3 \sin\alpha - \left(\left(\tfrac{r}{L}\right)^2 \alpha^2\beta^2 + \tfrac{M_p}{\rho AL}\omega^2\alpha^2 \cos\alpha A_3 = \beta^3 \cosh\beta\right.$$

In order to have a non-trivial solution, the determinant of the matrix in Eq.(2.8) has to be zero. The first transversability equation is given by

$$A_1 \left(\tfrac{KL}{EI}\beta^3 \sinh\beta + \beta^4 \sinh\beta + \alpha^2\beta^2 \cosh\beta - \tfrac{KL}{EI}\alpha^2\beta \cos\alpha\right) - A_2 \left(\tfrac{KL}{EI}\alpha\beta^2 \sinh\beta + \tfrac{KL}{EI}\alpha^2\beta \sin\alpha\right)$$
$$+ A_3 \left(-\tfrac{KL}{EI}\alpha\beta^2 \cosh\beta + \alpha^2\beta^2 \sin\alpha - \tfrac{KL}{EI}\alpha^3 \sin\alpha + \alpha^4 \sin\alpha\right) + A_4 \left(\tfrac{KL}{EI}\alpha\beta^2 \sinh\beta + \tfrac{KL}{EI}\alpha^2\beta \sin\alpha\right) = 0$$

$$(2.9)$$

The second transversability equation is given by

$$\beta = \sqrt{\tfrac{\alpha^2}{1+\mu\alpha^2}} \tag{2.10}$$

Finally the constants d_1, d_2, d_3 , d_4 can be expressed in the terms of d_1, and they are given by the following relations

$$d_2 = \left(\frac{-\left(\alpha^2 \sin\alpha + \alpha\beta \sinh\beta\right)}{\alpha^2 \cos\alpha + \beta^2 \cosh\beta + \tfrac{EI}{KL}\beta(\alpha^2+\beta^2)\sinh\beta}\right) d_1$$

$$d_3 = \left(-\tfrac{\alpha}{\beta} + \tfrac{EI}{KL}\left(\tfrac{\alpha^2+\beta^2}{\beta}\right) \frac{\left(\alpha^2 \sin\alpha + \alpha\beta \sinh\beta\right)}{\alpha^2 \cos\alpha + \beta^2 \cosh\beta + \tfrac{EI}{KL}\beta(\alpha^2+\beta^2)\sinh\beta}\right) d_1$$

$$d_4 = \left(\frac{\left(\alpha^2 \sin\alpha + \alpha\beta \sinh\beta\right)}{\alpha^2 \cos\alpha + \beta^2 \cosh\beta + \tfrac{EI}{KL}\beta(\alpha^2+\beta^2)\sinh\beta}\right) d_1$$

The value of d_1 is obtained such that the eigenfunctions $\phi(x)$ are normalized $\int_0^1 \phi_n^2(x)dx = 1$

.

2.2.2 Method of multiple scales for ordinary differential equations

Let's Consider a nonlinear oscillator described by the equation of motion

$$\ddot{y} + \Omega_0^2 y = \varepsilon f(t, y, \dot{y}), \tag{2.11}$$

where ε is a dimensionless parameter, assumed to be small. The dot over y denotes differentiation with respect to time t and $f(t, y, \dot{y})$ is a nonlinear function which can depends explicitly on time.

With the method of multiple scales, it is assumed that the solution of Eq. (2.11) depends on multiple independent variables (two in its simplest form). Accordingly, this solution is expressed in terms of different time scales as

$$y(t) = \sum_{m=0}^{\infty} \varepsilon^m y_m(t_0, t_1, ...) = y_0(t_0, t_1, ...) + \varepsilon y_1(t_0, t_1, ...) + ..., \qquad (2.12)$$

where t_m represents different independent time scales given by

$$t_m = \varepsilon^m t, m = 0, 1, ... \qquad (2.13)$$

There is a normal time scale $t_0 = t$, slow time scale $t_1 = \varepsilon t$, a super slow time scale $t_2 = \varepsilon^2 t$, etc. Thus,

$$\frac{d}{dt} = D_0 + \varepsilon D_1 + \dots, \qquad (2.14a)$$

$$\frac{d^2}{dt^2} = D_0^2 + 2\varepsilon D_0 D_1 + \dots, \qquad (2.14b)$$

where

$$D_m = \frac{\partial}{\partial t_m}, \text{ i.e. } D_0 = \frac{\partial}{\partial t_0} \text{ and } D_1 = \frac{\partial}{\partial t_1} \qquad (2.15)$$

Substituting Eq. (2.12) into Eq. (2.11) and taking into account Eqs. (2.14) and (2.15), the following set of linear ordinary differential equations result

$$\varepsilon^0 : D_0^2 y_0 + \Omega_0^2 y_0 = 0, \qquad (2.16a)$$

$$\varepsilon^1 : D_0^2 y_1 + \Omega_0^2 y_1 = -2D_0 D_1 y_0 + f(y_0, D_0 y_0, t_0), \qquad (2.16b)$$

The expansion gets more and more tedious with increasing order in ε. Let's carry this procedure out to first order in ε. At order ε^0,

$$y_0 = A\cos(\Omega_0 t_0 + \varphi), \qquad (2.17)$$

where A and φ are arbitrary (at this point) functions of $\{t_1, t_2, ...\}$. Now we solve the next equation in the hierarchy, for y_1.

Let $\theta = \Omega_0 t_0 + \varphi$. Then $D_0 = \frac{\partial}{\partial t_0} = \Omega_0 \frac{\partial}{\partial \theta}$ and we have

$$D_0^2 y_1 + \Omega_0^2 y_1 = 2\Omega_0 \sin\theta D_1 A + 2A\Omega_0 \cos\theta D_1 \varphi + f(A\cos\theta, -A\sin\theta, t_0). \qquad (2.18)$$

Since the arguments of f are periodic under $\theta \rightarrow \theta + 2\pi$, we may expand f in a Fourier series as

$$f(\theta) = f(A\cos\theta, -A\sin\theta, t_0) = \sum_{k=1}^{\infty} \alpha_k(A)\sin(k\theta) + \sum_{k=1}^{\infty} \beta_k(A)\cos(k\theta). \qquad (2.19)$$

The inverse of this relation is

$$\alpha_k(A) = \frac{1}{\pi} \int_0^{2\pi} f(\theta) \sin(k\theta) \, d\theta \qquad (k > 0), \tag{2.20a}$$

$$\beta_0(A) = \frac{1}{2\pi} \int_0^{2\pi} f(\theta) \, d\theta, \tag{2.20b}$$

$$\beta_k(A) = \frac{1}{\pi} \int_0^{2\pi} f(\theta) \cos(k\theta) \, d\theta \qquad (k > 0). \tag{2.20c}$$

We now demand that the secular terms on the right-hand side (Eq. (2.18)) – those terms proportional to $\cos\theta$ and $\sin\theta$ – must vanish. This means

$$2\Omega_0 D_1 A + \alpha_1(A) = 0, \tag{2.21a}$$

$$2A\Omega_0 D_1 \varphi + \beta_1(A) = 0. \tag{2.21b}$$

These two first order equations require two initial conditions, which is sensible since our initial equation $\ddot{y} + \Omega_0^2 y = \varepsilon f(y, \dot{y}, t)$ is second order in time. With the secular terms eliminated, we may obtain y_1 as follows

$$y_1 = \sum_{k \neq 1}^{\infty} \left\{ \frac{\alpha_k(A)}{1 - k^2} \sin(k\theta) + \frac{\beta_k(A)}{1 - k^2} \cos(k\theta) \right\} + B_0 \cos\theta + C_0 \sin\theta, \tag{2.22}$$

the constants B_0 and C_0 are arbitrary functions of t_1, t_2, etc..

The equations for A and φ (Eqs. (2.21)) are both first-order in t_1. They will therefore involve two constants of integration – call them A_0 and φ_0. At second order, these constants are taken as dependent upon the super slow time scale t_2. The method itself may break down at this order.

2.2.3 Average method

In the quest for approximate solution techniques for vibration problems, the method of averaging has proved to be a powerful analytic tool. This method was originally introduced by Bogoliubov and Mitropolsky [60]. In this thesis, we have used the averaging technique which is now illustrated with the following single-degree-of-freedom system of linear stiffness:

$$\ddot{X} + \omega_0^2 X = \varepsilon f\left(X, \dot{X}\right) + \varepsilon h\left(X, \dot{X}\right) D^\alpha [X(t)] \tag{2.23}$$

where ε is a small parameter, indicating that the damping term is of order ε.

$f\left(X, \dot{X}\right)$ and $h\left(X, \dot{X}\right)$ are linear or nonlinear functions with respect to X, $\dot{X}$,

$D^{\alpha}\left[X\left(t\right)\right]$ Caputo-type fractional derivative and defined by

$$D^{\alpha}\left[X\left(t\right)\right] = \frac{1}{\Gamma\left(n-1\right)} \int_{0}^{t} \frac{X^{(n)}\left(t-\tau\right)}{\tau^{\alpha}} d\tau \qquad (2.24)$$

where $n-1 < \alpha \leq n$ and $\Gamma\left(z\right)$ is Gamma function that satisfies $\Gamma\left(z+1\right) = z\,\Gamma\left(z\right)$. At first, the original system (2.23) is transformed into a diffusion differential equation by using the following generalized Van der Pol transformation:

$$X = A\left(t\right)\cos\theta, \;\; \dot{X} = -A\left(t\right)\sin\theta, \;\; \theta = \omega_0 t + \phi\left(t\right) \qquad (2.25)$$

Therefore, the joint response process $(\mathrm{X}, \dot{X})$ is needed to be transformed to a pair of slowly varying processes (A, ϕ). After some elementary calculations, Eq. (2.23) may be replaced by the following two first-order equations:

$$\dot{A} = -\frac{\sin\theta}{\omega_0}\left[\varepsilon f\left(A\cos\theta, \; -A\omega_0\sin\theta\right) + \varepsilon h\left(A\cos\theta, \; -A\omega_0\sin\theta\right) D^{\alpha}\left[A\cos\theta\right]\right] \qquad (2.26)$$

$$\dot{\phi} = -\frac{\cos\theta}{A\omega_0}\left[\varepsilon f\left(A\cos\theta, \; -A\omega_0\sin\theta\right) + \varepsilon h\left(A\cos\theta, \; -A\omega_0\sin\theta\right) D^{\alpha}\left[A\cos\theta\right] \qquad (2.27)$$

To apply the averaging method, we average at the period T of which one could select as $T = 2\pi/\omega_0$ in the case of periodic function or $T = \infty$ in the case of aperiodic $\left(D_{\tau}^{\alpha}\left(A\cos\left(\omega_0\tau + \varphi\right)\right)\right)$ [61–64]. We obtain the following pair of first order differential equations for the amplitude $A\left(\tau\right)$ and the phase $\varphi\left(\tau\right)$.

$$<\dot{A}>=<-\frac{\sin\theta}{\omega_0}\left[\varepsilon f\left(A\cos\theta, \; -A\omega_0\sin\theta\right) + \varepsilon h\left(A\cos\theta, \; -A\omega_0\sin\theta\right) D^{\alpha}\left[A\cos\theta\right]\right]> \quad (2.28)$$

$$<\dot{\phi}>=<-\frac{\sin\theta}{\omega_0}\left[\varepsilon f\left(A\cos\theta, \; -A\omega_0\sin\theta\right) + \varepsilon h\left(A\cos\theta, \; -A\omega_0\sin\theta\right) D^{\alpha}\left[A\cos\theta\right]\right]> \quad (2.29)$$

where

$$<\left[.\right]>_t = \frac{1}{T}\int_{t_0}^{t_0+T}\left[.\right]dt \qquad (2.30)$$

It is seen that the fractional derivative with Caputo definition is essentially a generalized integral with derivative of time-delay in it, usually, it is very difficult to deal with a higher fractional

order in mathematics. Here in only the case $0 < \alpha \leq 1$ in this thesis is considered, other values will be discussed further in our future work. So, according to formula (2.25) and Eq. (2.26), the Caputo-type fractional derivative can be rewritten as

$$\frac{1}{\Gamma(1-\alpha)} \int_0^t \frac{\dot{X}^{(n)}(t-\tau)}{\tau^\alpha} d\tau = \frac{A\omega_0}{\Gamma(1-\alpha)} \left[\cos\theta \int_0^t \frac{\sin\omega_0\tau}{\tau^\alpha} d\tau - \sin\theta \int_0^t \frac{\cos\omega_0\tau}{\tau^\alpha} d\tau \right] \quad (2.31)$$

It turns out that how to calculate or approximate the integrals appeared in (2.31) is an important task to replace the complicated Caputo-type fractional derivative in terms of envelope and frequency. Fortunately, the following two generalized integrals can play a role to solve this problem, they are respectively

$$\int_0^t \frac{\sin\omega_0\tau}{\tau^\alpha} d\tau = \omega_0^{\alpha-1} \left[\Gamma(1-\alpha)\cos\frac{\pi\alpha}{2} - \frac{\cos\omega_0 t}{(\omega_0 t)^\alpha} + o(\omega_0 t)^{-\alpha} \right] \quad (2.32)$$

$$\int_0^t \frac{\cos\omega_0\tau}{\tau^\alpha} d\tau = \omega_0^{\alpha-1} \left[\Gamma(1-\alpha)\sin\frac{\pi\alpha}{2} - \frac{\sin\omega_0 t}{(\omega_0 t)^\alpha} + o(\omega_0 t)^{-\alpha} \right] \quad (2.33)$$

2.2.4 Stability of the non-trivial steady states solutions of the nonlinear system response

It is well known that the steady states solutions of any nonlinear system only exist if they are stable. Hence the interest to perform a stability analysis of these solution. To do so, we shall define first what we mean by a steady state solution and how can appreciate their stability. So, formally, we can say that

Definition [65]

The constant vector $Y_0 \in C^n$ is a steady state solution of differential equations

$$\frac{dy(t)}{dt} = F(y(t)) \quad (2.34)$$

if it satisfies the equation $F(y(t)) = 0$, where 0 is the null vector and $F(y(t))$ is a differentiable vector function. when $Y_0 \neq 0$, the steady state solution is non-trivial.

As we have seen, if such a system is required to satisfy the initial condition given by $Y(0) = Y_0$, then its solution will be $Y(t) = Y_0$ for all times t. (So, Y_0 will be a constant solution of the system). What about the stability of this solution? We can get some information about the stability of the solution of the nonlinear systems models by using Taylor's Theorem to "relate" it to a linear system. In fact, the version of Taylor's Theorem which we shall use is the following

Theorem[Taylor's Theorem] [65]

If $F : C^n \to C^n$ is a continuously differentiable function and Y_0 is some constant vector in C^n, then for a vector $\delta y(t) \in C^n$,

$$F(Y_0 + \delta y(t)) = F(Y_0) + DF(Y_0) + R(\delta y(t)) \tag{2.35}$$

Note that if the function $F(Y) = (f_1(Y), f_2(Y), f_3(Y), ..., f_n(Y))$, then DF is the Jacobian

$$DF = \begin{pmatrix} \frac{\partial f_1}{\partial Y_1} & \cdots & \frac{\partial f_1}{\partial Y_n} \\ \vdots & \ddots & \vdots \\ \frac{\partial f_n}{\partial Y_1} & \cdots & \frac{\partial f_n}{\partial Y_n} \end{pmatrix} \tag{2.36}$$

and the matrix $DF(Y_0)$ is the Jacobian evaluated at Y_O. Further, $R(\delta y(t))$ has the property that: $\frac{R(\delta y)}{\|\delta y\|} \to 0$, as $\delta y \to 0$. Loosely speaking, this means that if each entry of δY is small, then

$$F(Y_0 + h) \simeq F(Y_0) + DF(Y_0) \tag{2.37}$$

Where $\simeq$ can be interpreted as "is approximately".

Now, suppose that Y_0 is a state solution of the previous system (37), i.e. $F(Y_0) = 0$, and take $Y(t)$ to be a solution of the system such that $Y(0) - Y_0$ is small. If we now take $Y(t) = Y_0 + \delta Y(t)$, system (34) becomes

$$\frac{d}{dt}\{Y_0 + \delta Y(t)\} = F(Y_0 + \delta Y) \tag{2.38}$$

Consequently, using Taylor's theorem, we have

$$F(Y_0 + h) \simeq F(Y_0) + DF(Y_0) \tag{2.39}$$

$$\frac{d\delta Y(t)}{dt} = \frac{d}{dt}\{Y_0 + \delta Y(t)\} = DF(Y_0)\delta Y(t) + R(Y(t)) \tag{2.40}$$

and if $\delta Y(t)$ is small, we can ignore the term $R(\delta Y(t))$. This means that if the quantity $\delta Y(0) = Y(0) - Y_0 = $ is small, then the behaviour of the vector $\delta Y(t) = Y(t) - Y_0$ is qualitatively the same as the solution to linear system

$$\frac{d\delta Y(t)}{dt} = DF(Y_0)\delta Y(t) \tag{2.41}$$

This analysis result in the following theorem:

Theorem [65]

Let the constant vector Y_0 be a steady state solution of the system (2.34) and let the matrix $DF(Y_0)$ denote the Jacobian evaluated at Y_0

-If the n eigenvalues of the Jacobian matrix $DF(Y_0)$ have real parts less than zero, then the steady state solution Y_0 is stable.

-If at least one of the n eigenvalues of Jacobian matrix $DF(Y_0)$ has real part greater than zero, them the steady state solution Y_0 is unstable

Generally, the determination of the sign of the real parts of the eigenvalues is carried out by using the Routh-Hurwitz criterion [66]

This mathematical formalism will be used in the following chapter to analyze the stability of the steady state solution of the beam responses.

2.2.5 Linear stability of delay differential equations

The question of stability for delayed nonlinear equations near their steady-state solutions or fixed points is particularly important when the dynamical states of any system are investigated, as it is the case in this thesis. Indeed, the study of the stability makes possible to realize what happens if a system is disturbed slightly near an equilibrium condition.

• Linearization near an equilibruium solution

Let consider a set of autonomous DDEs of first order defined as [66]

$$\frac{d\mathbf{X}(t)}{dt} = \mathbf{H}\left[\mathbf{X}(t), \mathbf{X}(t-\tau), \alpha\right] \tag{2.42}$$

where $\mathbf{X}(t) = (x_1(t), x_2(t), \ldots, x_n(t))$ is the vector of n-dynamical variables of the system, $\mathbf{X}(t-\tau) = (x_1(t-\tau), x_2(t-\tau), \ldots, x_n(t-\tau))$ is the delayed vector of n-dynamical variables, $\mathbf{H} = (h_1(t), h_2(t), \ldots, h_n(t))$ is a n-dimensional vectorial function and $\alpha = (\alpha_1, \alpha_2, \ldots, \alpha_p)$ is a set of control parameters of the system.

Let us denote an equilibrium point $\mathbf{X}_0$ and consider small variations $\delta\mathbf{X}$ of the system around this equilibrium point, defined by

$$\mathbf{X}(t) = \mathbf{X}_0 + \delta\mathbf{X}(t) \tag{2.43}$$

Substituting Eq. (2.43) into Eq.(2.42) and expanding this equation in a Taylor series about $\mathbf{X}_0$, and discarding terms of order higher than the first in the $\delta\mathbf{X}$'s leads to the variational

equation

$$\frac{d\delta \mathbf{X}(t)}{dt} = \mathbf{J}_0(\alpha)\,\delta \mathbf{X}(t) + \mathbf{J}_1(\alpha)\,\delta \mathbf{X}(t-\tau) \tag{2.44}$$

where $\mathbf{J}_0$ and $\mathbf{J}_1$ are matrix $(n \times n)$ of partial derivatives at the equilibrium point $\mathbf{X}_0$ and are called Jacobian matrix.

• Linearization near an equilibruium solution

The eigenvalues of the linear set of the Eq. (2.44) can be found from the characteristic equation of the system. In that case, the characteristic equation becomes

$$G(s;\alpha) = \det\left(s\mathbf{I} - \mathbf{J}_0(\alpha) - \mathbf{J}_1(\alpha)\,e^{-s\tau}\right) \tag{2.45}$$

where $\mathbf{I}$ is the unit matrix and s are the eigenvalues of the system (2.45) and roots of the characteristic equation.

The algorithm of the D-subdivision method can be summarized as follows [67]:

1. First, solve the equation

$$G(j\omega;\alpha) = 0 \tag{2.46}$$

for s as a function of $j\omega$ (including the origin of the complex plane) in order to find (stability crossing) surfaces in the parameter space $\mathbb{R}^{n_p}$ such that for each s on such a surface, there exists at least one characteristic root on the imaginary axis.

2. Second, these surfaces divide the parameter space into several regions and sometimes it is possible to conclude, by using appropriate additional arguments, for which region the stability is guaranteed. As additional arguments, we can find, for example, a particular point (on some of the axis of the parameter space) for which the stability analysis becomes easier to perform (finite-dimensional systems, eventually). Each region derived in this way is characterized by the same number of strictly unstable characteristic roots for all the points of the corresponding domain.

2.2.6 Melnikov's method to predict Smale horseshoe chaos

Melnikov's method [68] is one of relatively few analalytical method used to predict the onset of chaotic notion in dynamical systems with deterministic or random perturbation. It gives a

bound on the parameters of a system such that chaos is predicted not to occur. It is applicable to conservative one DOF systems which include a separatrix loop, and which are perturbed by small forcing and damping.

The idea is to show by perturbation expansions that there exists an intersection of the stable and unstable manifolds of an equilibrium point in two-dimensional pointcare map M. this implies that there is a horseshoe in the map M, which in turn implies that there exist periodic motions of all periods, as well as motions which are not periodic. The horseshoe mapalso exhibits sensitive dependence on initial conditions. The method was first applied by Holmes [69] to study a periodically forced Duffing oscillator with negative linear stiffness.

To perform the general Melnikov technique for horseshoe chaos analysis, let's consider a single-degree-of-freedom Hamiltonian system subject to light damping and external or parametric excitation. This system has the following form:

$$
\begin{cases}
\dot{x} = \frac{\partial H}{\partial y} \\
\dot{y} = -\frac{\partial H}{\partial x} - \varepsilon \lambda (x, y) \frac{\partial H}{\partial y} + \varepsilon f (x, y) \eta(t),
\end{cases}
\tag{2.47}
$$

where x and y are generalized displacement and velocity respectively; $H = H(x, y)$ is Hamiltonain with can be purely periodic excitation or random noise excitation. $\lambda (x, y)$ represents the coefficient of danping; (x, y) represents the amplitude of excitation.

We assume that $(x_0(t), y_0(t))$ is a solution on separatrix loop in the $\varepsilon = 0$ system will generally be "broken" when the pertubation is appleid. The question of whether or not chaos can occur in a particular system depends upon what happens to broken pieces of the separatrix loop (the stable and unstable manifolds of the saddle), that is , whether they intersect or not. In the case of Eq. (2.48) and based on a formula given by Wiggins [70, 71] , Melnikov's method involves the following integral:

$$
M(t_0) = \int\limits_{-\infty}^{+\infty} \frac{\partial H}{\partial y} \left[-\varepsilon \lambda (x, y) \frac{\partial H}{\partial y} + \varepsilon f (x, y) \eta(t + t_0) \right] dt,
\tag{2.48}
$$

where before integrate the provious Eq. (2.39), the couple (x, y) is substituded by the orbit $(x_0(t), y_0(t))$.

2.3 Numerical method

It is well known that the validation of results obtained through analytical inves- tigation is guaranteed by the perfect match with the results obtained through direct numerical simulation of the mathematical model. In this thesis, three numerical methods including , a classical RK4 to integrate the ODEs, Newton-Leipnik and A-B-M predictor-corrector schemes to integrate the FDEs and the bisection method to solve a complex or non-trivial polynomial equations are presented.

2.3.1 Fourth-order Runge-Kutta method for ordinary differential equations

An ODE is solved analytically considering some assumption to obtain approximate solutions. In contrast, a numerical method proposes solutions which are closed with the experiment. In this thesis, RK4 is used for numerical resolution of ODEs. Fortran 90, with Matlab software language are also used as programming languages. RK4 method has been elaborated for the first time in 1894 by Carle Runge and has been improved by Martin W. Kutta in 1901. This method is widely used because of its stability. It combines trapezium numerical integration and Simpson methods. Let us consider the first-order ODE as

$$\frac{dy}{dt} = f(t, y), \tag{2.49}$$

with the initial condition $y(t_0) = y_0$.

The aim of the RK4 method is to find solutions after each time step h i.e. to determine the point $(t + h; y(t + h))$ knowing the point $(t; y(t))$. This method establishes the following relations [72, 73]:

$$y(t + h) = y(t) + \frac{1}{6}(L_1 + 2L_2 + 2L_3 + L_4), \tag{2.50}$$

where

$L_1 = hf(t, y(t))$,

$L_2 = hf\left(t + \frac{h}{2}, y(t) + \frac{L_1}{2}\right)$,

$L_3 = hf\left(t + \frac{h}{2}, y(t) + \frac{L_2}{2}\right)$ and

$L_4 = hf(t + h, y(t) + L_3)$.

This procedure needs in its iteration only the initial value y_0, to calculate all the other values taken by the function y at other times separated by the time step h.

In the case of second-order differential equation

$$\begin{cases} \frac{d^2y}{dt^2} = f\left(t, y, \frac{dy}{dt}\right) \\ y\left(t_0\right) = y_0, \quad \left.\frac{dy}{dt}\right|_{t=t_0} = y_0^{(1)} \end{cases}, \tag{2.51}$$

it can be divided in order to obtain two first order equations. With variables change, let's consider Eq. (2.51) under the following form

$$\begin{cases} \frac{dy}{dt} = z \\ \frac{dz}{dt} = f\left(t, y, z\right) \\ y\left(t_0\right) = y_0, \quad z\left(t_0\right) = z_0 \end{cases}, \tag{2.52}$$

The RK4 iterations are given by the following equation

$$\begin{cases} y\left(t+h\right) = y\left(t\right) + \frac{1}{6}\left(L_1 + 2L_2 + 2L_3 + L_4\right) \\ z\left(t+h\right) = z\left(t\right) + \frac{1}{6}\left(K_1 + 2K_2 + 2K_3 + K_4\right) \end{cases}, \tag{2.53}$$

where $L_1 = hz\left(t\right),$

$K_1 = hf\left(t, y, z\right),$

$L_2 = h\left(z\left(t\right) + \frac{K_1}{2}\right),$

$K_2 = hf\left(t + \frac{h}{2}, y\left(t\right) + \frac{L_1}{2}, z\left(t\right) + \frac{K_1}{2}\right),$

$L_3 = h\left(z\left(t\right) + \frac{K_2}{2}\right),$

$K_3 = hf\left(t + \frac{h}{2}, y\left(t\right) + \frac{L_2}{2}, z\left(t\right) + \frac{K_2}{2}\right),$

$L_4 = h\left(z\left(t\right) + K_3\right)$ and

$K_4 = hf\left(t + \frac{h}{2}, y\left(t\right) + L_3, z\left(t\right) + K_3\right).$

This generalized form can also serve to solve numerically second-order coupled ODEs.

2.3.2 Fourth-order-Runge-Kutta method for delay differential equations

In the case of delay differential equations (DDEs), the dynamical state of a system at each time t depends both on the value of the vector of n-dynamical variables $\mathbf{X}$ at time t, and also on the value of $\mathbf{X}$ at a prior time $t - \tau$, with $\tau > 0$ [74, 75]. Taking into account the delayed variable $\mathbf{X}(t - \tau) = (x_1(t - \tau), x_2(t - \tau), ..., x_n(t - \tau))$ with $n-$dimensional vectorial flow $\mathbf{G} = (G_1, G_2, ..., G_n)$, a DDE can be written as

$$\frac{d\mathbf{X}(t)}{dt} = \mathbf{G}(t, \mathbf{X}(t), \mathbf{X}(t - \tau))$$

$$\text{with} \quad \mathbf{X}(t) = \mathbf{g}(t) \quad \text{for} \quad t \in [-\tau, 0]\,, \tag{2.54}$$

where $\mathbf{g}$ is a $n-$dimensional vector which depends of the time t, $\mathbf{X}(t) = [x_1(t), x_2(t), ..., x_n(t)]$ and $\mathbf{X}(t - \tau) = (x_1(t - \tau), x_2(t - \tau), ..., x_n(t - \tau))$ are unknown vectorial variables. At the difference of ODEs where the initial conditions were given by a discrete and finite set of value, initial conditions in DDEs should be indicated (through the use of a function) for all the values contained into the continuous interval $[-\tau, 0]$, so an infinity of values should be known to characterize the system. The RK4 iterative scheme for the case DDEs defined by Eq. (2.54) can be given by

$$
\begin{aligned}
x_{i+1,j} &= x_{i,j} + h \left(L_{1,j} + 2L_{2,j} + 2L_{3,j} + L_{4,j} \right)/6 \\
t &= t + h\,,
\end{aligned}
\tag{2.55}
$$

where

$$
\begin{aligned}
L_{1,j} &= \mathbf{G}(t_i, x_{\tau,i,j}, x_{i,j}) \\
L_{2,j} &= \mathbf{G}(t_i + h/2, x_{\tau,i,j}, x_{i,j} + hL_{1,j}/2) \\
L_{3,j} &= \mathbf{G}(t_i + h/2, x_{\tau,i,j}, x_{i,j} + hL_{2,j}/2) \\
L_{4,j} &= \mathbf{G}(t_i + h, x_{\tau,i,j}, x_{i,j} + hL_{3,j})\,,
\end{aligned}
\tag{2.56}
$$

where i represents the time incrementation and j labels the variables related to x_j. $L_{1,j}$, $L_{2,j}$, $L_{3,j}$, $L_{4,j}$ are intermediate variables and h represents the time step.

2.3.3 Numerical method for fractional differential equations

To solve a fractional differential equation, one has to approximate the corresponding derivative operator, which means including information about previous states of the system (the so-called memory effect). For numerical solutions of the FDEs, the Newton-Leipnik and A-B-M predictor-corrector schemes [76–79] are the most used. Accordingly, particular attention will be put on these two numerical methods in this section.

Firstly, a method on the basis of the A-B-M type predictor-corrector schemes is suitable for Caputo's fractional order derivative becaause it just requires the initial conditions and for

unknown function it has clear physical meaning. The method is based on the fact that fractional differential equation

$$\begin{cases} D_t^q Y(t) = \frac{d^q Y(t)}{dt^q} = F(t, Y(t)) \\ Y^{(k)}(0) = Y_0^{(k)}, \quad k = 0, 1, 2, \dots\dots, m-1 \end{cases} \tag{2.57}$$

is equivalent to the Volterra integral equation

$$Y(t) = \sum_{k=0}^{[q]-1} Y_0^{(k)} \frac{t^k}{k!} + \frac{1}{\Gamma(q)} \int_0^t (t-\tau)^{q-1} F(\tau, Y(\tau)) d\tau \tag{2.58}$$

Discretizing the Voterra equation Eq. (2.58) for uniform grid $t_n = nh$ $(n = 0, 1, 2, \dots, N)$, $h = T_{sim}/N$ and using the short memory principle (fixed or logarithmic) [76,80], we obtain a close numerical approximation of the true solution $Y(t_n)$ of fractional differential equation while preserving the order of accuracy. Assume that we have calculated approximations $Y_h(t_j)$, $j = 1, 2, \dots, n$ and we want to obtain $Y_h(t_{n+1})$ by means of the equation

$$Y_h(t_{n+1}) = \sum_{k=0}^{m-1} Y_0^{(k)} \frac{t_{n+1}^k}{k!} + \frac{h^q}{\Gamma(q+2)} F\left[t_{n+1}, Y_h^p(t_{n+1})\right] +$$
$$\frac{h^q}{\Gamma(q+2)} \sum_{j=0}^{n} a_{j,n+1} F\left[t_j, Y_n(t_j)\right] \tag{2.59}$$

where

$$a_{j,n+1} = \begin{cases} n^{q+1} - (n-q)(n+1)^q, & , \ if \ j = 0 \\ (n-j+2)^{q+1} + (n-j)^{q+1} + 2(n-j+1)^{q+1}, & if \ 1 \le j \le n \\ 1, & if \ j = n+1 \end{cases} \tag{2.60}$$

The preliminary approximation $Y_h^p(t_{n+1})$ is called predictor and it is given by

$$Y_h^p(t_{n+1}) = \sum_{k=0}^{m-1} Y_O^{(k)} \frac{t_{n+1}^k}{k!} + \frac{1}{\Gamma(q)} \sum_{j=0}^{n} b_{j,n+1} F\left[t_j, Y_n(t_j)\right] \tag{2.61}$$

where

$$b_{j,n+1} = \frac{h^p}{q} \left[(n+1-j)^q - (n-j)^q\right] \tag{2.62}$$

Secondly, a method on the Newton-Leipnik algorithm is suitable for Grunwald-Letnkov fractional order derivative. This approach is based on the fac that for a wide class of functions, three definitions Grunwald-Letnikov, Riemman-Liouville and Caputo's are equivament. In this case ,

the relation to explicit numerical approximation of qth derivative at the points $kh, (k = 1, 2, ...)$ has the following form [80]:

$$_{K-}L_{m/h}D_{tk}^{q}f(t) \approx h^{-q}\sum_{j=0}^{k}(-1)^{j}\begin{pmatrix} q \\ j \end{pmatrix}f(t_{k-j}) \tag{2.63}$$

where L_m is the "memory length", $t_h = kh$, h is the time step of calculation and $(-1)^{j}\begin{pmatrix} q \\ j \end{pmatrix}$ are binomial coefficients $C_j^{(q)}$ $(j = 0, 1, ...)$. For their calculation we can use the following expression

$$C_{0}^{(q)} = 1, \quad C_{j}^{(q)} = \left(1 - \frac{1+q}{j}\right)C_{j-1}^{(q)} \tag{2.64}$$

According to the short memory principle [76, 80], the length of system memory can be substantially reduced in numerical algorithm to get reliable results. Therefore, general numerical solution of the following fractional differential equation

$$_{a}D_{t}^{q}Y(t) = F(t, X(t)) \tag{2.65}$$

can be expressed as

$$Y(t) = F(t_{k}, Y(t_{k}))h^{q} - \sum_{j=1}^{k}C_{j}^{(q)}Y(t_{k-j}) \tag{2.66}$$

In Eq. (2.55), the memory term is expressed by the sum. As shown in paper [81], both mentioned time-domain numerical methods (Newton-Lepnik and A-B-M) have approximately the same order of accuracy and good match of numerical solutions. Since that the last one method is easy to code, we will used it in the following chapter to approximate the numerical solutions of the FDEs describing our reduced systems models.

2.2.2.4 Bisection method for complex polynomial equations

Bisection method is the simplest among all the numerical schemes to solve the complex polynomial equations. The method is also called the interval having method, the binary search method, or the dichotomy method. The bisection method is based on the following result from calculus:

The Intermediate Value Theorem:

Assume $f : R \to R$ is a continuous function and there are two real numbers a and b such that $f(a)f(b) < 0$. them $f(x)$ has at least one zero between a and b

In other words, if a continuous function has different signs at two points, it has to go through zero somewhere in between!

The bisection method of finding two such numbers a and b, then halving the interval $[a, b]$ and keeping the half on which $f(x)$ changes sign and repeating the procedure until this interval shrinks to give the required accuracy for the root. An algorithm of this method could be defined as follows. Suppose we need a root for $f(x) = 0$ and we have an error tolerance of ε (the absolute error in calculating the root must be less that ε).

Bisection Algorithm :

Step 1: Find two numbers a and b at which f has different signs.

Step 2: Define $c = \frac{a+b}{2}$.

Step 3: If $b - a \leq \varepsilon$ them accept c as the root and stop.

Step 4: If $f(a)f(b) \leq 0$ then set c as the new b. Otherwise set c as the new a. Return to **Step 1**

Let α be the value of the root, $a \leq \alpha \leq b$. Let a_n, b_n and c_n be the values of a,b and c on the nth iteration of the algorithm. Then the error bound for c_n is given by

$$|\alpha - c_n| \leq \frac{1}{2^n}(b - a) \tag{2.67}$$

This inequality can give us the number of iterations needed for a required accuracy ε

$$n \geq \frac{\log\left(\frac{b-a}{\varepsilon}\right)}{\log(2)} \tag{2.68}$$

Advantages and disadvantages of the bisection method

- The method is guaranteed to converge

- The error bound decreases by half with each iteration

- The bisection method converges very slowly

- The bisection method cannot detect multiple roots

This method will be used in the next chapter in order to ge the non-trivial steady states solutions of some nonlinear Amplitude-Frequency equations governing one of our systems models response.

2.3.4 Hardware and software

Throughout this thesis, we used a Laptop having Window 10 as operating system. For mathematical expansions and numerical simulations, the following software were used: Matlab, Fortran and Maple. These software are enormously used in scientific research and engineering.

2.3.5 Conclusion

The present chapter has been devoted to the presentation of mathematical and numerical methods used to solve the differential equations describing the reduced mathematical models of our excited tension leg platform systems as well as the hardware and software used. These methods will be used in the next chapter to obtain the different results that give us informations about the different states of the studied systems.

RESULTS AND DISCUSSION

3.1 Introduction

This chapter is devoted to the results and discussions on the work carried out in this thesis. Section 3.2 analyse the effect of the delay between the detection of vibration and the action of tendons on the dynamics response of tension leg platform (TLP) under sea waves excitation. Section 3.3 presents the new nonlinear viscoelastic model describing the surge movement of tension leg platform. Section 3.4 analyses the influence of tuned liquid column device to the amplitude reduction of an offshore platform under irregular sea wave excitation. The last section concludes the chapter.

3.2 Effect of the delay between the detection of vibration and the action of tendons on the dynamics response of tension leg platform (TLP) under sea waves excitation.

3.2.1 Physical model

A TLP structure which includes, deck, hull, pontoon, risers, tendons and foundation template is shown schematically in Fig. 3.1 and equivalent model, consisting of a vertical beam and two tendons which are coupled through the platform is shown in Fig. 3.2
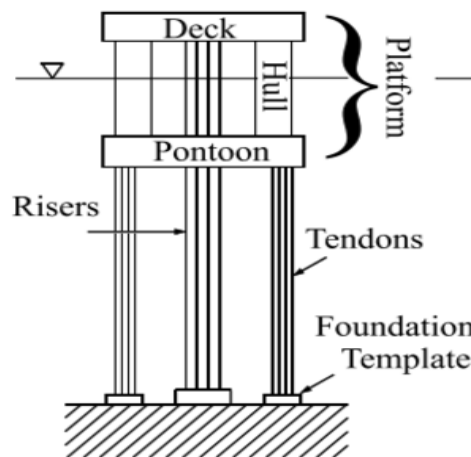
Figure 3.1: Schematics of offshore structures [82]
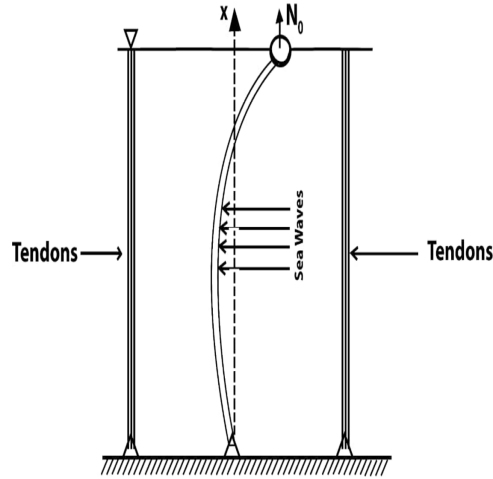
Figure 3.2: A simplified model of a TLP

3.2.2 Mathematical modeling

Consider a pinned free beam of length l, with density ρ, Young's module E, cross sectional area A and moment of inertia I, after using the physical and mathematical concept, the governing equation for TLP (Beam) model system under waves excitation given by equation [83–85].

$$\begin{cases} \rho A \frac{\partial^2 u(x,t)}{\partial t^2} + c_1 \frac{\partial u(x,t)}{\partial t} = EA \frac{\partial^2 u(x,t)}{\partial x^2} + \frac{EA}{2} \frac{\partial}{\partial x} \left(\left(\frac{\partial w(x,t)}{\partial x} \right)^2 \right) \\[3mm] \rho A \frac{\partial^2 w(x,t)}{\partial t^2} + EI \frac{\partial^4 w(x,t)}{\partial x^4} + c_2 \frac{\partial w(x,t)}{\partial t} - \rho I \frac{\partial^4 w(x,t)}{\partial t^2 \partial x^2} - EA \frac{\partial}{\partial x} \left(e \frac{\partial w(x,t)}{\partial x} \right) + z_c(t) = f(x,t) \end{cases}$$
$$(3.1)$$

where

$$e = \frac{\partial u(x,t)}{\partial x} + \frac{1}{2} \left(\frac{\partial w(x,t)}{\partial x} \right)^2$$

with the boundary and initial conditions

$$w(0,t) = \frac{\partial^2 w}{\partial x^2}(0,t) = \frac{\partial^2 w}{\partial x^2}(l,t) = \frac{\partial^3 w}{\partial x^3}(l,t) = 0 \tag{3.2}$$

$$u(0,t) = 0, \ u(l,t) = \frac{lN_0}{EA} \tag{3.3}$$

Assuming that the radius of gyration r is small enough, the longitudinal inertia force and

dissipative force are neglected. Using the boundaries conditions (3.3) and after some simplification its comes out the following equation

$$e = \frac{N_0}{EA} + \frac{1}{2l}\int_0^l \left(\frac{\partial w}{\partial x}\right)^2 dx \tag{3.4}$$

Thus the general equation governing the behaviour of the system is given by

$$
\begin{aligned}
\rho A\frac{\partial^2 w(x,t)}{\partial t^2} + EI\frac{\partial^4 w(x,t)}{\partial x^4} + c_2\frac{\partial w(x,t)}{\partial t} - \rho I\frac{\partial^4 w(x,t)}{\partial t^2 \partial x^2} - N_0\frac{\partial^2 w(x,t)}{\partial x^2} \\
- \frac{EA}{2l}\left(\int_0^l \left(\frac{\partial w(x,t)}{\partial x}\right)^2 dx\right)\frac{\partial^2 w(x,t)}{\partial x^2} + z_c(t) = f(x,t),
\end{aligned}
\tag{3.5}
$$

where $w = w(x,t)$ is the lateral deflexion, EI denotes the flexural rigidity of the beam, c_2 is the damping coefficient, ρI is the transverse Rayleigh beam coeffcient, and N_0 is axial load.

The sea waves excitation is formulated using Morisons equation [41] and airy theory [84] is given by

$$
\begin{aligned}
f(x,t) = \frac{1}{2}C_d\rho_w(2r_{out})\frac{\pi^2 H}{T^2}\frac{\cosh^2 k(x+d_1)}{\sinh^2 kd_1}\cos(\omega t)|\cos(\omega t)| \\
- C_M\rho_w A\frac{2\pi^2 H}{T^2}\frac{\cosh k(x+d_1)}{\sinh kd_1}\sin(\omega t) - C_m\rho A\frac{\partial^2 w(x,t)}{\partial t^2}
\end{aligned}
\tag{3.6}
$$

, where C_D, C_M and C_m are the coefficient of the drag, and inertia forces of the beam and the added mass respectively. ρ_w is density of sea water, r_{out} is the outher radius of beam.

$z_c(t)$ represent the tendons force which is produced by the deplacement of tendon. In fact, tendons are viscoelastic structures which mean they exhibit both elastic and viscous behaviors. Zhang and al [86], proposed a mathematical model given by

$$z_c(t) = 4k_c\cos\alpha_c\left[s_1 w(t - t_x) + s_2\dot{w}(t - t_{\dot{x}})\right] \tag{3.7}$$

where k_c is tendon stiffness, α_c is tendon inclination, s_1 and s_2 are control parameters, t_x and $t_{\dot{x}}$ time delays for displacement and velocity feedback force in the system, respectively. We notice that w and $\dot{w}$ are written as functions of $t - t_x$ and $t - t_{\dot{x}}$, respectively. This lag between the structure response and the corrective action may be attributed to the time required to sense and to gather the information and the computation time for determining the proper action.

Taking into account the following dimensionless variable

$$
\begin{aligned}
q &= \frac{w}{r}, \quad y = \frac{x}{l_0}, \quad \tau = \frac{r}{l_0^2}\sqrt{\frac{E}{\rho}}t, \quad l^* = \frac{l}{l_0}, \quad k_3 = C_m\frac{\rho_w}{\rho} \\
\lambda &= \frac{c_2 l_0^2}{Ar\sqrt{\rho E}}, \quad N_0' = \frac{N_0 l_0}{EI}, \quad \beta = \frac{I}{Al_0^2} \\
\alpha &= \frac{l_0^4}{EIr}, \quad d^* = \frac{d_1}{l_0}, \quad \Gamma_1 = 4k_c s_1\frac{l_0^4}{EI}\cos\alpha_c \\
\Gamma_2 &= 4k_c s_2\frac{l_0^2 r}{EI}\sqrt{\frac{E}{\rho}}\cos\alpha_c, \quad r = \left(\frac{I}{A}\right)^{\frac{1}{2}}
\end{aligned}
\tag{3.8}
$$

Eqs.(3.5) - (3.6) are reduced to a non-dimensional equation

$$\frac{\partial^4 q(y,\tau)}{\partial y^4} - \beta \frac{\partial^4 q(y,\tau)}{\partial \tau^2 \partial y^2} + (1 + k_3) \frac{\partial^2 q(y,\tau)}{\partial \tau^2} + \lambda \frac{\partial q(y,\tau)}{\partial \tau} - N_0' \frac{\partial^2 q(y,\tau)}{\partial y^2}$$
$$- \frac{l_0}{2l} \left(\int_0^{l^*} \left(\frac{\partial q(y,\tau)}{\partial y} \right)^2 dy \right) \frac{\partial^2 q(y,\tau)}{\partial y^2} + \Gamma_1 q\left(y, \tau - \tau_y\right) + \Gamma_2 \frac{\partial q\left(y, \tau - \tau_y\right)}{\partial \tau} = \alpha f_1\left(y, \tau\right) \tag{3.9}$$

$$f_1\left(y, \tau\right) = \tfrac{1}{2} C_d \rho_w \left(2r_{out}\right) \frac{\pi^2 H^2}{T^2} \frac{\cosh^2 k l_0(y+d^*)}{\sinh^2 k l_0 d^*} \cos\left(\omega\tau\right) \left|\cos\left(\omega\tau\right)\right| - C_M \rho_w A \frac{2\pi^2 H}{T^2} \frac{\cosh k l_0(y+d^*)}{\sinh k l_0 d^*} \sin\left(\omega\tau\right) \tag{3.10}$$

with the boundary conditions

$$q\left(0, \tau\right) = \frac{\partial^2 q}{\partial y^2}\left(0, \tau\right) = \frac{\partial^2 q}{\partial y^2}\left(l^*, \tau\right) = \frac{\partial^3 q}{\partial y^3}\left(l^*, \tau\right) = 0 \tag{3.11}$$

Here l_0 is a reference lenght of the beam.

3.2.3 Modal equation

To deal with the analytical analysis, we resort to an assumed mode expansion. Specifically, it is assumed that q can be written as the finite sum

$$q\left(y, \tau\right) = \sum_{n=1}^{N} v_n\left(\tau\right) \phi_n\left(y\right) \tag{3.12}$$

where $v_n(\tau)$ is the amplitude of the nth mode, and $\phi_n(y)$ is the solution of the eigenvalue problem obtained by solving Eq.(3.9) and without damping, non linearity, excitation and tendon effect, and $\phi_n(y)$ is given by

$$\phi_1\left(y\right) = Ky \quad if \ n = 1 \tag{3.13}$$

or

$$\phi_n\left(y\right) = \frac{\cos(k_n)}{\cosh(k_n)} \sinh\left(k_n y\right) + \sin\left(k_n y\right) \quad if \ n \geq 2 \tag{3.14}$$

where

$$k_n = \left(n - \tfrac{3}{4}\right) \pi \tag{3.15}$$

It should be noted that the first natural frequency occurs at 0. This mode corresponds to the rigid body motion which has a mode shape given as ϕ_1, which is not considered in our problem,

since this mode has no relation with the elastic deflection of the beam [87]. In the rest of this part, we limit ourselves to elastic mode, in particular in first elastic mode.

After substituting Eq.(3.12) into Eq.(3.9), multiplying both sides of the resultant equation by the shape function then integrating with respect to the beam axis y over the length l^*, and taking into account the orthogonality condition, the modal equation is given by

$$\ddot{v}_2\left(\tau\right) + 2\eta\dot{v}_2\left(\tau\right) + \omega_2^2 v_2\left(\tau\right) + \gamma v_2^3\left(\tau\right) + pv_2\left(\tau - \tau_x\right)$$
$$+d\dot{v}_2\left(\tau - \tau_{\dot{x}}\right) = p_0\cos\left(\omega\tau\right)\left|\cos\left(\omega\tau\right)\right| + p_1\sin\left(\omega\tau\right) \tag{3.16}$$

with

$$I_0 = \frac{\int_0^{l^*}\phi_n^2(y)dy}{\int_0^{l^*}(1+k_3)\phi_n^2(y)dy - \beta\int_0^{l^*}\phi''_n(y)\phi_n(y)dy}, \quad \eta = \frac{\lambda}{2}I_0,$$
$$\omega_1^2 = \frac{\int_0^{l^*}\phi''''_n(y)\phi_n(y)dy}{\int_0^{l^*}(1+k_3)\phi_n^2(y)dy - \beta\int_0^{l^*}\phi''_n(y)\phi_n(y)dy}, \quad \omega_2^2 = \omega_1^2 - N$$

$$N = N_0'\frac{\int_0^{l^*}\phi''_n(y)\phi_n(y)dy}{\int_0^{l^*}(1+k_3)\phi_n^2(y)dy - \beta\int_0^{l^*}\phi''_n(y)\phi_n(y)dy}, \quad p_0 = \frac{1}{2}C_d\rho_w\left(2r_{out}\right)\frac{\pi^2 H}{T^2}I_2 \tag{3.17}$$

$$I_2 = \frac{\int_0^{l^*}\frac{\cosh^2 kl_0(y+d^*)}{\sinh^2 kl_0 d^*}\phi_n(y)dy}{\int_0^{l^*}(1+k_3)\phi_n^2(y)dy - \beta\int_0^{l^*}\phi''_n(y)\phi_n(y)dy}, \quad p_1 = -C_M\rho_w A\frac{2\pi^2 H}{T^2}I_3,$$
$$I_3 = \frac{\int_0^{l^*}\frac{\cosh kl_0(y+d^*)}{\sinh kl_0 d^*}\phi_n(y)dy}{\int_0^{l^*}(1+k_3)\phi_n^2(y)dy - \beta\int_0^{l^*}\phi''_n(y)\phi_n(y)dy}, \quad p = \Gamma_1 I_0, \quad d = \Gamma_2 I_0$$

Eq.(3.16) represents the modal equation of the TLP under sea waves excitation, with its different parameters defined by (3.17)

3.2.4 Effect of tendon on the stability of the structure

The aims of this section is to show how the tendon can affect parameter on the stability of the structure taking into account the time-delay. This is done using the D-subdivision method [86].

Thus, Eq.(3.16) can be rewritten as follows

$$\dot{v}_2 = g$$
$$\dot{g} = -2\eta g - \omega_0^2 v_2 - \gamma v_2^3 - pv_2\left(\tau - \tau_x\right) - dy\left(\tau - \tau_x\right) \tag{3.18}$$
$$+p_0\cos\left(\omega\tau\right)\left|\cos\left(\omega\tau\right)\right| + p_1\sin\left(\omega\tau\right)$$

point $v_{20}(0,0)$ is an equilibruim point of Eq.(3.18). The characteristic equation of the linearized version of Eq.(3.18) related to this equilibrium point is

$$s^2 + \left(2\eta + d\exp\left(-s\tau_{\dot{x}}\right)\right)s + \left(\omega_2^2 + p\exp\left(-s\tau_x\right)\right) = 0 \tag{3.19}$$

To obtain the stability boundary in the plane of the tendon parameter (d, p), we use the D-subdivision method. According to that method, the stability boundary in the plane are determined by the points that yield either to a root $s = 0$ or a pair of pure imaginary roots of Eq.(3.19).

Substituting $s = 0$ into Eq.(3.19), one finds

$$p = -\omega_2^2 \tag{3.20}$$

Setting $s = ib$ (where b is a real constant) into the characteristic Eq.(3.19), and after some algebraic manipulation we obtained

$$
\begin{aligned}
(\cos b\tau_x)\, p + (b \sin b\tau_{\dot{x}})\, d &= b^2 - \omega_2^2 \\
(b \cos b\tau_{\dot{x}})\, d - (\sin b\tau_x)\, p &= -2\eta b
\end{aligned}
\tag{3.21}
$$

which leads to

$$
\begin{aligned}
p &= \left(b^2 - \omega_2^2\right) \cos b\tau_0 + 2\eta b \sin b\tau_0 \\
d &= \frac{\left(b^2 - \omega_2^2\right)}{b} \sin b\tau_0 - 2\eta \cos b\tau_0 \qquad \tau_x = \tau_{\dot{x}} = \tau_0
\end{aligned}
\tag{3.22}
$$

Properties of the beam and characteristics of the sea waves which are used for numerical purpose are given in Tables 3.1 and 3.2 [82, 84]

Table 3.1: Properties of the beam.

Parameter name	Symbol	Value
beam length (m)	l	415
inertial coefficient of beam	C_M	1.7
drag coefficient of beam	C_d	0.8
Inertial coefficient of added mass	C_m	1
Density of beam $(kg.m^{-3})$	ρ	7800
Young's module of beam(Gpa)	E	204
Outer raduis of beam (m)	r_{out}	0.4
Axial force (N)	N_0	3.462e7

Table 3.2: properties of sea.

Parameter name	Symbol	Value
Sea depth	d	415 m
Wave height	H	2 m
Wave period	T	25 s
water density	ρ_w	kg/m^3

In this part, the simulation solutions are obtainted using the fourth-order runge kutta method, and the matlab software is used for plotting the curves. The Hopf bifurcation boundary in the $(p,\,d)$ space delimiting the stability boundary can be found from the bifurcation curve defined by Eq.(3.22) and bifurcation line defined by Eq.(3.20). In Fig. 3.3, the stable area consists of the region of the plane limited by the straight line given by Eq.(3.20) and the curve associated with each value of time delay given by Eq.(3.22).
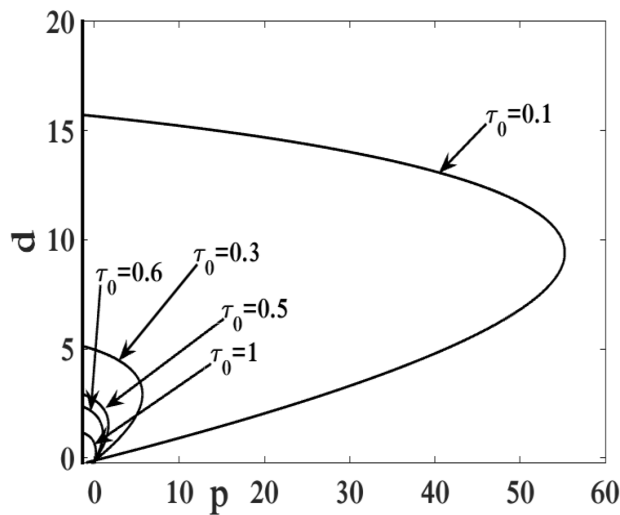
Figure 3.3: Stability boundary in the space $(p,\,d)$ and various values of time delay, with $\eta = 0.06$, $\omega_2 = 1.36$
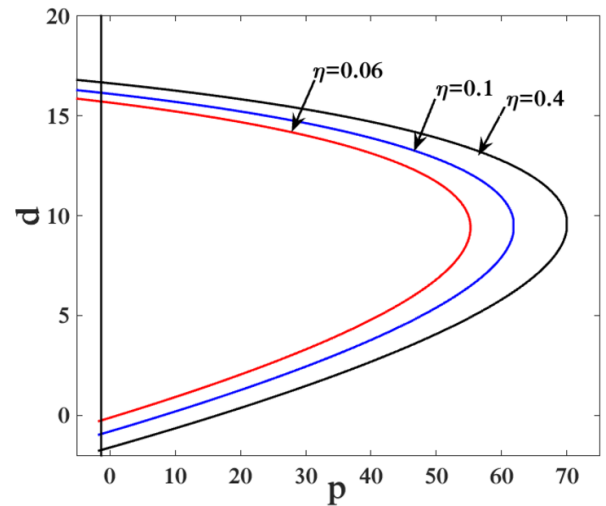
Figure 3.4: Stability boundary in the space $(p,\,d)$ and various values of damping, with $\tau_0 = 0.1$, $\omega_2 = 1.36$

Fig. 3.3 shows that the increase of the value of time-delay contributes to reduce the stability area. In Fig. 3.4 the stability boundary in the space $(p,\,d)$ and various values of damping is

plotted. The interest here is the effect of delay on the stability. One can observe that when the damping coefficient increase, the stability area increase. This means that by increasing the damping coefficient, the area will be increased; so one could choose the parameters of the tendon, so that the structure remains stable.

In Fig. 3.5 the evolution of the amplitude of vibration as a function of time is plotted. It is viewed in Fig. 3.5(a) that the amplitude decreases as function of time leading to stability, while in Fig. 3.5(b) the amplitude increases with time leading to instability of the system.
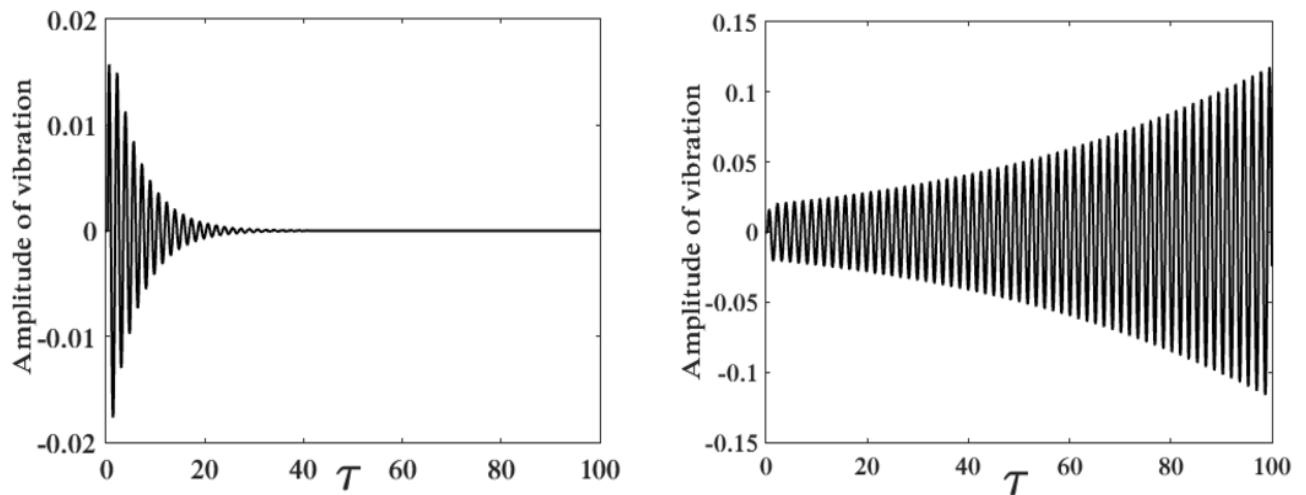
Figure 3.5: Effect of tendons parameter on the stability of the TLP, (a)the tendons parameter taken in the stable region $\tau_0 = 0.3$, $p = 4$, $d = 3$; (b)the tendons parameter taken in the unstable region $\tau_0 = 0.3$, $p = 6.5$, $d = 3$, with $\eta = 0.06$, $\gamma = -4.388$, $\omega_2 = 1.36$

.

3.2.5 Compensation of the time-delay effect for amplitude reduction

In this section, a particular attention is focused on the analytical and numerical analysis in order to determine a parameter of the system that will compensate the time-delay effect leading to amplitude reduction.

For that purpose the multiple time scale method [88–90], which provides an analytical approximate solution and thus permits to detect the effects of the time-delay on the system response is used.

We suppose that $|\cos(\omega\tau)| = \xi\cos(\omega\tau)$, where $\xi = \pm 1$ Eq.(3.16) can be written as

$$\ddot{v}_2(\tau) + 2\eta\dot{v}_2(\tau) + \omega_2^2 v_2(\tau) + \gamma v_2^3(\tau - \tau_x) + p v_2(\tau)$$
$$+ d\dot{v}_2(\tau - \tau_{\dot{x}}) = \xi p_0(\cos(\omega\tau))^2 + p_1\sin(\omega\tau) \qquad \xi = \pm 1 \tag{3.23}$$

Taking into account the following relation: $(\cos(\omega\tau))^2 = \frac{1+\cos(2\omega\tau)}{2}$ and by substituting it in the Eq.(3.23), one obtain

$$\ddot{v}_2(\tau) + 2\eta\dot{v}_2(\tau) + \omega_2^2 v_2(\tau) + \gamma v_2^3(\tau) + p v_2(\tau - \tau_x)$$
$$+ d\dot{v}_2(\tau - \tau_{\dot{x}}) = \xi\frac{p_0}{2} + \xi\frac{p_0}{2}\cos(2\omega\tau) + p_1\sin(\omega\tau) \tag{3.24}$$

One focus our attention on applying the multiple scales method to find the uniform analytical approximations solution at resonance. One would like to obtain a first-order approximate solution so that we define two-time scales as a fast-time, slow-time, so that the derivative with respect to time expanded as

$$\frac{d}{d\tau} = \frac{dT_0}{d\tau}\frac{\partial}{\partial T_0} + \varepsilon\frac{\partial}{\partial T_1} = D_0 + \varepsilon D_1 + ...$$

$$\tag{3.25}$$

$$\frac{d^2}{d\tau^2} = D_0^2 + 2\varepsilon D_0 D_1 + ...$$

where ϵ refers to a very small perturbation parameter. The expansions of the solution $v_2(\tau, \varepsilon)$ and $v_2(\tau - \tau_x, \varepsilon)$ have the form

$$v_2(\tau) = v_{20}(T_0, T_1) + \varepsilon v_{21}(T_0, T_1) + ... \tag{3.26}$$

$$v_2(\tau - \tau_x, \varepsilon) = v_{20}(T_0 - T_x, T_1 - \varepsilon T_x) + \varepsilon v_{21}(T_0 - T_x, T_1 - \varepsilon T_x) + ... \tag{3.27}$$

where $T_n = \varepsilon^n\tau$

Assuming that T_x is small enough, after using Taylor expansion on Eq.(3.27) one gets

$$
\begin{aligned}
v_2 \left(\tau - \tau_x, \varepsilon \right) \ &= v_{20} \left(T_0 - T_x, T_1 \right) - \varepsilon D_1 T_x v_{20} \left(T_0 - T_x, T_1 \right) \\
&+ \varepsilon v_{21} \left(T_0 - T_x, T_1 \right) - \varepsilon^2 T_x D_1 v_{21} \left(T_0 - T_x, T_1 \right)
\end{aligned}
\tag{3.28}
$$

After this expansion, we focus on the different type of resonance that one can have when the structure is subjected to the sea waves excitation.

Harmonic resonance

Substituting Eqs.(3.26) and (3.28) into the Eq.(3.24) and equating the same power of the coefficients, we obtain

$$
D_0^2 v_{20} + \omega_2^2 v_{20} = 0
\tag{3.29}
$$

$$
\begin{aligned}
D_0^2 v_{21} + \omega_2^2 v_{21} = &-2D_0 \left(D_1 v_{20} + \eta v_{20} \right) - \gamma v_{20}^3 - p v_{20} \left(T_0 - T_x, T_0 \right) \\
&- d D_0 v_{20} \left(T_0 - T_x, T_0 \right) + \xi \tfrac{p_0}{2} + \xi \tfrac{p_0}{2} \cos 2\omega T_0 + p_1 \sin \omega T_0
\end{aligned}
\tag{3.30}
$$

The solution of Eq.(3.29) can be written as

$$
v_{20} \left(T_0, T_1 \right) = A \left(T_1 \right) \exp \left(i\omega_2 T_0 \right) + cc
\tag{3.31}
$$

Substituting the above equations into Eq.(3.30) we obtain

$$
\begin{aligned}
D_0^2 v_{21} + \omega_2^2 v_{21} = &\left[-2i\omega_2 \left(A' + \eta A \right) - 3\gamma \bar{A} A^2 - p A \exp \left(-i\omega_2 T_x \right) \right. \\
&- i\omega_2 d A \exp \left(-i\omega_2 T_x \right) \times \exp \left(i\omega_2 T_0 \right) - \gamma A^3 \exp \left(3i\omega_2 T_0 \right) + \xi \tfrac{p_0}{2} + \xi \tfrac{p_0}{4} \exp \left(2\omega T_0 \right) + \tfrac{p_1}{2i} \exp \left(\omega T_0 \right) + cc
\end{aligned}
\tag{3.32}
$$

Two types of resonance could occur from the above equation during the vibration of the system

-First case: $\omega_2 \simeq \omega$

The deviations of ω from ω_2 are shown as the following definition

$\omega = \omega_2 + \varepsilon \sigma$

where σ is the detuning parameter. After considering the above definition and by eliminating the secular terms from Eq.(3.32), one will arrive at

$$
-2i\omega_2 \left(A' + \mu A \right) - 3\gamma \bar{A} A^2 - p A \exp \left(-i\omega_2 T_x \right) - i\omega_2 d A \exp \left(-i\omega_2 T_x \right) + \tfrac{p_1}{2i} \exp \left(i\sigma_1 T_1 \right) \ = 0
\tag{3.33}
$$

Using the polar notation $A\left(T_1\right) = \frac{a(T_1)}{2}\exp\left(i\theta_1\right)$ of the above equation and by separating the real and the imaginary parts, we obtain

$$
\begin{aligned}
&\omega_2 a' + \eta\omega_2 a - \frac{p}{2}a\sin\left(\omega_2 T_x\right) + \frac{d}{2}\omega_2 a\cos\left(\omega_2 T_x\right) + \frac{p_1}{2}\cos\phi_1 = 0 \\
&\omega_2\sigma a - \omega_2 a\phi' - \frac{p}{2}a\cos\left(\omega_2 T_x\right) - \frac{d}{2}\omega_2 a\sin\left(\omega_2 T_x\right) - \frac{3}{8}\gamma a^3 - \frac{p_1}{2}\sin\phi_1 = 0
\end{aligned}
\tag{3.34}
$$

In which $\phi_1 = \sigma T_1 - \theta_1$. For the sake of the steady state response, the parameters ϕ'_1, θ'_1 and a' must be set to zero and, after some mathematical simplification of Eq.(3.34), the following equation is obtained

$$
\left(\eta\omega_2 a - \frac{p}{2}a\sin\omega_2 T_x + \frac{d}{2}\omega_2 a\cos\omega_2 T_x - \frac{d}{2}\omega_2 a\sin\omega_2 T_x\right)^2 = \frac{p_1^2}{4}
$$

(3.35)

-Second case: $\omega_2 \simeq 2\omega$ and $\omega = \frac{\omega_2}{2} + \varepsilon\sigma_2$

Therefore, the secular terms would be

$$
\begin{aligned}
&-2i\omega_2\left(A' + \mu A\right) - 3\gamma\bar{A}A^2 - pA\exp\left(-i\omega_2 T_x\right) - i\omega_2 dA\exp\left(-i\omega_2 T_x\right) \\
&\quad + \xi\frac{p_0}{2}\exp\left(2i\sigma_1 T_1\right) = 0
\end{aligned}
$$

(3.36)

Similarly, by applying the polar forms and separating the imaginary and the real parts, and after some mathematical simplification, the steady-state response will be obtained

$$
\begin{aligned}
&\left(\eta\omega_2 a - \frac{p}{2}a\sin\omega_2 T_x + \frac{d}{2}\omega_2 a\cos\omega_2 T_x\right)^2 + \Big(2\sigma\omega_2 a \\
&\quad -\frac{3}{8}\gamma a^3 - \frac{p}{2}a\cos\omega_2 T_x - \frac{d}{2}\omega_2 a\sin\omega_2 T_x\Big)^2 = \frac{p_0^2}{16}
\end{aligned}
\tag{3.37}
$$

After making these different calculations, the simulation solutions are obtinted using the bisection method, and the matlab software is used for plotting the curves. Fig. 3.6 shows a comparative analysis of the amplitude response as function of the detuning parameter from the results of analytical derivations and numerical simulation. The result obtained shows a qualitative agreement between the numerical and analytical analysis.

The effects of time-delay on the amplitude response of the TLP under sea wave excitation for the first and second resonance state are shown in Fig. 3.7 and Fig. 3.8. As depicted
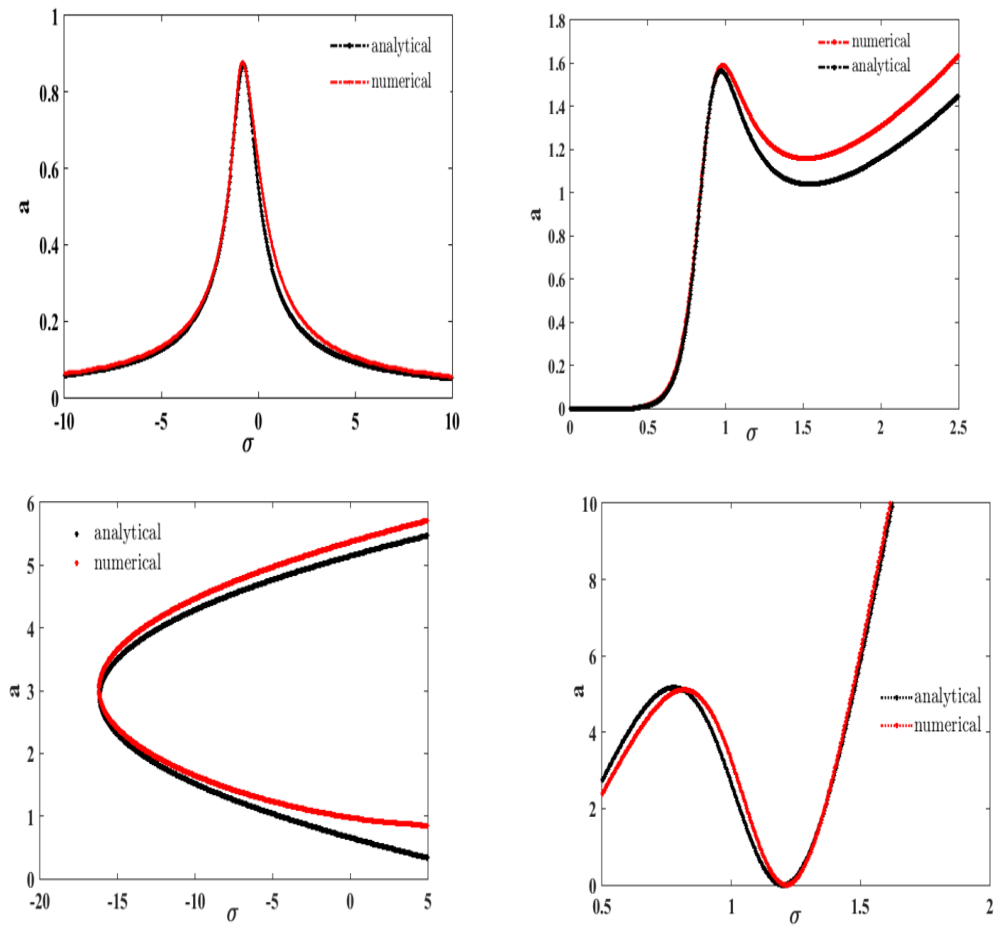
Figure 3.6: Frequency response curves, (a)Primary resonance, (b)Superharmonic resonance, (b)Subharmonic resonance, (d)Combination resonance, with $\tau_0 = 0.0$, $p = 4$, $d = 3$, $\eta = 0.06$, $\gamma = -4.388$, $\omega_2 = 1.36$.

in Fig. 3.7 and Fig. 3.8, increasing the time-delay parameter results in an increase of the amplitude response of the TLP. Fig. 3.9 and figure 3.10 shown the amplitude response curves for different values of naturels frequency. For the primary and secondary resonance state, the natural frequency have the same effects, increasing the natural frequency results in decreasing the amplitude response of TLP. For example, it has been shown that, taking the two values of the following natural frequencies, $\omega_2 = 1.36$ (ie 0.453 rad/s) and $\omega_2 = 1.6$ (ie 0.987 rad/s) , one notes that the effect of the delay on the amplitude is attenuated for the value of the frequency $\omega_2 = 1.6$ (ie 0.987 rad/s). One conclude that, by making a good choice of the natural frequency of the structure one can compensate the time-delay effect on the amplitude. The effects of the damping coefficient on the frequency response for the first and second resonance state are shown in Fig. 3.11 and Fig. 3.12. From both figures, it can be observed that increasing the damping coefficient will reduce the amplitudes of vibration, the effect of time-delay of the amplitudes of vibration meaning that is reduced. It has been found that, for a delay value equal to 0.1 (ie 0.22 second), taking a value of the damping coefficient of $\eta = 0.1$ (ie $c_2 = 66.67Ns/m$) instead of $\eta = 0.06$ (ie $c_2 = 40Ns/m$), one could compensate for the effect of the delay on the stability of the structure.
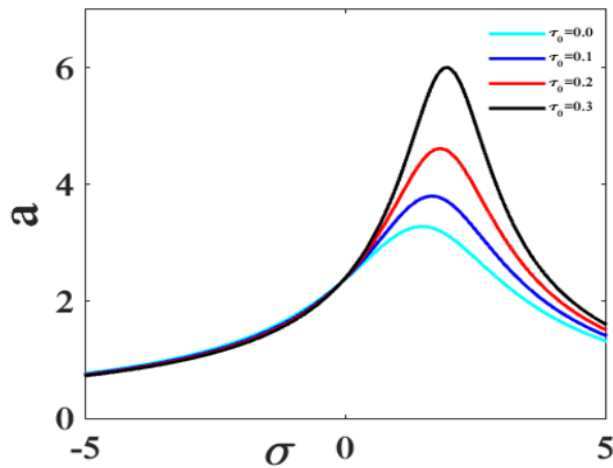
Figure 3.7: Effect of time-delay on the TLP amplitude, $\omega = \omega_2 + \varepsilon\sigma$, with $\eta = 0.06, \gamma = -4.388, \omega_2 = 1.36, p = 4, d = 3$
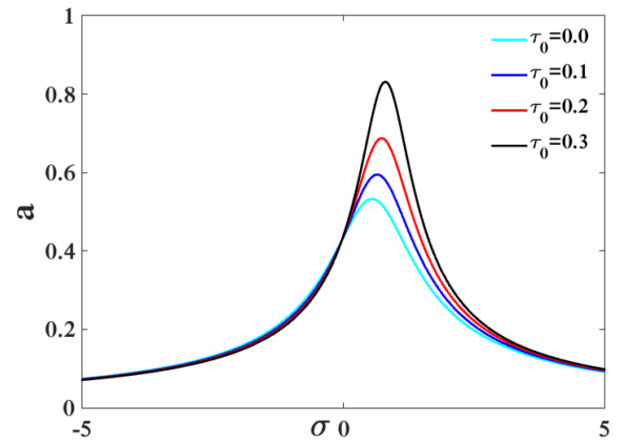
Figure 3.8: Effect of time-delay on the TLP amplitude, $\omega = \frac{1}{2}\omega_2 + \varepsilon\sigma$, with $\eta = 0.06, \gamma = -4.388, \omega_2 = 1.36, p = 4, d = 3$
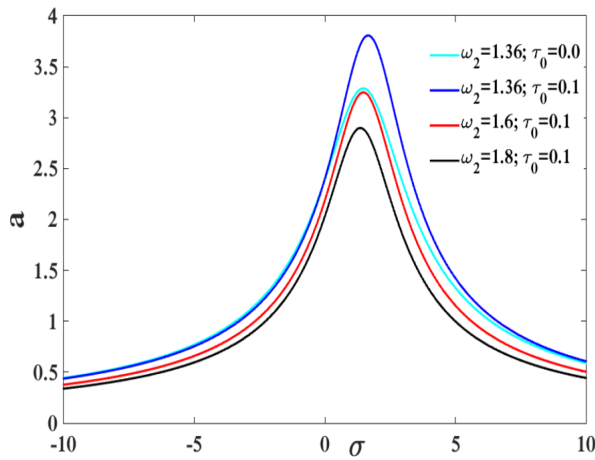
Figure 3.9: Primary resonance curve, effect of natural frequency ω_2, with $\eta = 0.06$, $\gamma = -4.388$, $p = 4, d = 3$
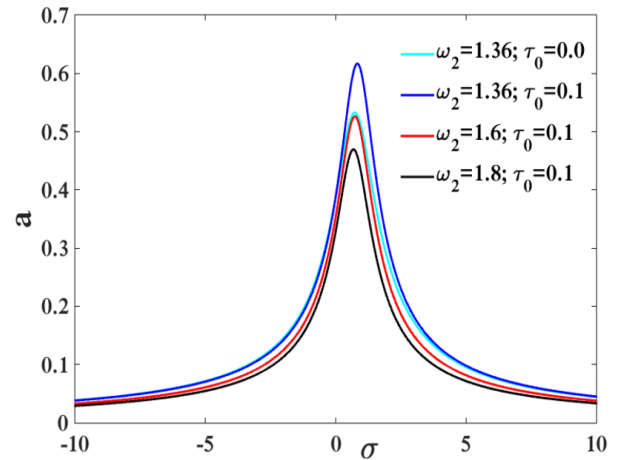
Figure 3.10: Secondary resonance curve, effect of natural frequency ω_2, with $\eta = 0.06$, $\gamma = -4.388$, $p = 4, d = 3$
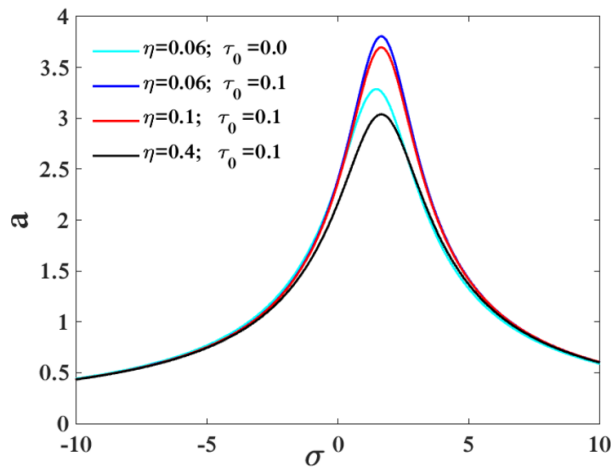
Figure 3.11: Primary resonance curve, effect of damping η , with $\omega_2 = 1.36$, $\gamma = -4.388$, $p = 4, d = 3$
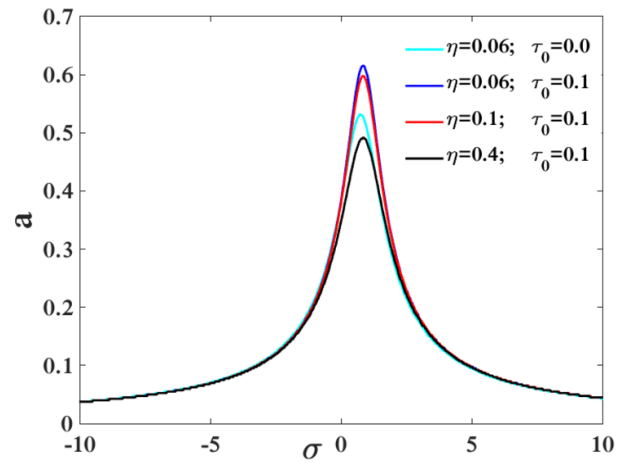
Figure 3.12: Secondary resonance curve, effect of damping η, with $\omega_2 = 1.36$, $\gamma = -4.388$, $p = 4, d = 3$

Superharmonic, subharmonic and combination resonances

In the following section we shall investigate the superharmonic resonance, subharmonic resonance and combination resonance. When the amplitude of the sinusoidal external force is large, other type of oscillations can be displayed by the model, namely the superharmonic, the subharmonic and combination resonance states. Using the multiple timescale method, we obtain

$$D_0^2 v_{20} + \omega_2^2 v_{20} = \xi \frac{p_0}{2} + \xi \frac{p_0}{2} \cos 2\omega T_0 + p_1 \sin \omega T_0 \tag{3.38}$$

$$D_0^2 v_{21} + \omega_2^2 v_{21} = -2D_0 \left(D_1 v_{20} + \eta v_{20} \right) - \gamma v_{20}^3 - p v_{20} \left(T_0 - T_x, T_0 \right) - d D_0 v_{20} \left(T_0 - T_x, T_0 \right) \tag{3.39}$$

The solution of Eq.(3.38) can be written as

$$v_{20} \left(T_0, T_1 \right) = A \left(T_1 \right) \exp \left(i\omega_2 T_0 \right) + \beta_0 + \beta_1 \exp \left(2i\omega T_0 \right) + \beta_2 \exp \left(i\omega T_0 \right) + cc \tag{3.40}$$

$$\beta_0 = \frac{\xi p_0}{\omega_2^2}, \ \beta_1 = \frac{\xi p_0}{4 \left(\omega_2^2 - 4\omega^2 \right)}, \ \beta_2 = \frac{p_1}{2 \left(\omega_2^2 - \omega^2 \right)}, \ i^2 = -1$$

Substituting Eq.(3.40) into Eq.(3.39) we gets

$$D_0^2 v_{21} + \omega_2^2 v_{21} = \left(-2i\omega_2\left(A' + \eta A\right) - 3\gamma\bar{A}A^2 - pA\exp\left(-i\omega_2 T_x\right) - i\omega_2 dA\exp\left(-i\omega_2 T_x\right)\right.$$

$$-3\gamma\beta_0^2 A - 6\gamma\beta_1^2 A + 6\gamma\beta_2^2 A\big) \times \exp\left(i\omega_2 T_0\right)$$

$$-\gamma\left(A^3\exp\left(3i\omega_2 T_0\right) + \beta_1^3\exp\left(6i\omega T_0\right) + \beta_2^3\exp\left(3i\omega T_0\right)\right)$$

$$-\left(2i\eta\omega\beta_2 + p\beta_2\exp\left(-i\omega T_x\right) + id\omega\beta_2\exp\left(-i\omega T_x\right)\right.$$

$$\left.+6\gamma\beta_2 A\bar{A} + 3\gamma\beta_0^2\beta_2 + 6\gamma\beta_1^2\beta_2 - 6\gamma\beta_0\beta_1\beta_2 - 3\gamma\beta_2^3\right) \times \exp\left(i\omega T_0\right)$$

$$-\left(4i\eta\omega\beta_1 + p\beta_1\exp\left(-2i\omega T_x\right) + 2id\omega\beta_1\exp\left(-2i\omega T_x\right)\right.$$

$$\left.+6\gamma\beta_1 A\bar{A} + 3\gamma\beta_0^2\beta_1 - 6\gamma\beta_2^2\beta_1 + 3\gamma\beta_2^2\beta_0 + 3\gamma\beta_1^3\right) \times \exp\left(2i\omega T_0\right)$$

$$-\gamma\left(3\ \beta_0 A^2\exp\left(2i\omega_2 T_0\right) + 3\beta_1 A^2\exp\left(2i\left(\omega_2 - \omega\right)T_0\right)\right.$$

$$+3\beta_1 A^2\exp\left(2i\left(\omega_2 + \omega\right)T_0\right) + 3\beta_2 A^2\exp\left(i\left(2\omega_2 + \omega\right)T_0\right)$$

$$-3\beta_2 A^2\exp\left(i\left(2\omega_2 - \omega\right)T_0\right) + 2\beta_0\beta_1 A\exp\left(i\left(\omega_2 - 2\omega\right)T_0\right)$$

$$+2\beta_0\beta_1 A\exp\left(i\left(\omega_2 + 2\omega\right)T_0\right)\ + 2\beta_0\beta_2 A\exp\left(i\left(\omega_2 + \omega\right)T_0\right)$$

$$+\beta_1^2 A\exp\left(i\left(\omega_2 + 4\omega\right)T_0\right) + \beta_2^2 A\exp\left(i\left(\omega_2 + 2\omega\right)T_0\right)$$

$$+\beta_1^2 A\exp\left(i\left(\omega_2 - 4\omega\right)T_0\right) - 2\beta_0\beta_2 A\exp\left(i\left(\omega_2 - \omega\right)T_0\right)$$

$$+2\beta_1\beta_2 A\exp\left(i\left(\omega_2 + 3\omega\right)T_0\right) - 2\beta_1\beta_2 A\exp\left(i\left(\omega_2 + \omega\right)T_0\right)$$

$$+\beta_2^2 A\exp\left(i\left(\omega_2 - 2\omega\right)T_0\right)\ - 2\beta_1\beta_2 A\exp\left(i\left(\omega_2 - 3\omega\right)T_0\right)$$

$$+2\beta_1\beta_2 A\exp\left(i\left(\omega_2 - \omega\right)T_0\right) + 6\beta_0\beta_1\beta_2\exp\left(3i\omega T_0\right)$$

$$-3\beta_2\beta_1^2\exp\left(3i\omega T_0\right) + 3\beta_1\beta_2^2\exp\left(4i\omega T_0\right) + 3\beta_2\beta_1^2\exp\left(5i\omega T_0\right)$$

$$\left.+\beta_0^3 + 3\beta_0\beta_2^2 - 6\beta_0\beta_2^2 - 6\beta_1\beta_2^2 + 6\beta_0 A\bar{A}\right) + cc$$

$$(3.41)$$

cc is the complex conjugate of the previous terms. One noticed that the system can presented two superharmonic, two subharmonic and two combinations resonant states, when the following conditions are satisfied:

-Superharmonic resonance

$6\omega = \omega_2 + \varepsilon\sigma; \quad 3\omega = \omega_2 + \varepsilon\sigma$

-Subharmonic resonance

$\omega = 3\omega_2 + \varepsilon\sigma; \quad \omega = \frac{3}{2}\omega_2 + \varepsilon\sigma$

-Combination resonance

$4\omega = \omega_2 + \varepsilon\sigma; \quad 5\omega = \omega_2 + \varepsilon\sigma$

a) Superharmonic resonance

Considering $3\omega = \omega_2 + \varepsilon\sigma$, and injecting this condition into Eq. (3.41) and setting secular terms to 0, we obtained

$$-2i\omega_2\left(A' + \mu A\right) - 3\gamma\bar{A}A^2 - pA\exp\left(-i\omega_2 T_x\right) - i\omega_2 dA\exp\left(-i\omega_2 T_x\right) - 3\gamma\left(\beta_0^2 + 2\beta_1^2 + 2\beta_3^2\right)$$
$$-i\gamma\left(\beta_3^3 - 6\beta_0\beta_1\beta_3 + 3\beta_3\beta_1^2\right)\exp\left(i\sigma T_1\right) = 0$$

$$(3.42)$$

where $\beta_3 = \frac{p_1}{2\left(\omega_2^2 - \omega^2\right)}$

Using the polar notation $A\left(T_1\right) = \frac{a(T_1)}{2}\exp\left(i\theta_1\right)$ of in Eq.(3.41) and by separating the real and the imaginary parts, we obtain

$$\begin{cases} \omega_2 a' + \eta\omega_2 a - \frac{p}{2}a\sin\left(\omega_2 T_x\right) + \frac{d}{2}\omega_2 a\cos\left(\omega_2 T_x\right) + \gamma\left(\beta_3^3 - 6\beta_0\beta_1\beta_3 + 3\beta_3\beta_1^2\right)\cos\phi_1 = 0 \\ \\ \omega_2\sigma a - \omega_2 a\phi_1' - \frac{p}{2}a\cos\left(\omega_2 T_x\right) - \frac{d}{2}\omega_2 a\sin\left(\omega_2 T_x\right) - \frac{3}{8}\gamma a^3 - 3\gamma\left(\beta_0^2 + 2\beta_1^2 + 2\beta_3^2\right)\frac{a}{2} \\ \qquad -\gamma\left(\beta_3^3 - 6\beta_0\beta_1\beta_3 + 3\beta_3\beta_1^2\right)\sin\phi_1 = 0 \end{cases}$$

$$(3.43)$$

.

For the sake of the steady state response, the parameters θ_1', a' ϕ_1' must be set to zero and, after some mathematical simplification of Eq.(3.43), the following equation is obtained

$$\left(\mu a\right)^2 + \left(\sigma\omega_2 a - \frac{3}{8}\gamma a^3 - \frac{p}{2}a\cos\left(\omega_2 T_x\right)\right.$$
$$\left. - \frac{d}{2}\omega_2 a\sin\left(\omega_2 T_x\right) - \frac{3}{2}\gamma\left(\beta_0^2 + 2\beta_1^2 + 2\beta_3^2\right)a\right)^2 = f_0^2$$

$$(3.44)$$

,

where $f_0 = \gamma\left(\beta_3^3 - 6\beta_0\beta_1\beta_3 + 3\beta_3\beta_1^2\right)$, $\quad \mu = \eta\omega_2 - \frac{p}{2}\sin\left(\omega_2 T_x\right) + \frac{d}{2}\omega_2\cos\left(\omega_2 T_x\right)$.

Let us consider now $6\omega = \omega_2 + \varepsilon\sigma$, and injecting this condition into Eq. (3.41) and setting secular terms to 0, one gets

$$-2i\omega_2 \left(A' + \mu A\right) - 3\gamma \bar{A}A^2 - pA \exp\left(-i\omega_2 T_x\right) - i\omega_2 dA \exp\left(-i\omega_2 T_x\right)$$
$$-3\gamma \left(\beta_0^2 + 2\beta_1^2 + 2\beta_3^2\right) - \gamma\beta_1^3 \exp\left(i\sigma T_1\right) = 0 \tag{3.45}$$

.

Similarly, by applying the polar forms and separating the imaginary and the real parts, and after some mathematical simplification, the steady-state response we gets

$$\left(\mu a\right)^2 + \left(\sigma\omega_2 a - \tfrac{3}{8}\gamma a^3 - \tfrac{p}{2}a \cos\left(\omega_2 T_x\right) - \tfrac{d}{2}\omega_2 a \sin\left(\omega_2 T_x\right) - \tfrac{3}{2}\gamma\left(\beta_0^2 + 2\beta_1^2 + 2\beta_3^2\right) a\right)^2 = f_0^2 \tag{3.46}$$

,

where $f_0 = \gamma\beta_1^3$

b) Subharmonic resonance

In this part, we treat two cases: $\omega = 3\omega_2 + \varepsilon\sigma$ and $\omega = \tfrac{3}{2}\omega_2 + \varepsilon\sigma$. In the first case($\omega = 3\omega_2 + \varepsilon\sigma$) ,the secular terms are eliminated when

$$-2i\omega_2 \left(A' + \mu A\right) - 3\gamma \bar{A}A^2 - pA \exp\left(-i\omega_2 T_x\right) - i\omega_2 dA \exp\left(-i\omega_2 T_x\right)$$
$$-3\gamma \left(\beta_0^2 + 2\beta_1^2 + 2\beta_3^2\right) - 3i\gamma\beta_3 \bar{A}^2 \exp\left(i\sigma T_1\right) = 0 \tag{3.47}$$

.

Inserting the polar form of A, putting $\phi_1 = \sigma T_1 - 3\theta_1$, and proceeding in the same way as in the case of superharmonic, we obtain the following equation

$$\left(\mu\right)^2 + \left(\tfrac{\sigma}{3}\omega_2 - \tfrac{3}{8}\gamma a^2 - \tfrac{p}{2}\cos\left(\omega_2 T_x\right) - \tfrac{d}{2}\omega_2 \sin\left(\omega_2 T_x\right) - \tfrac{3}{2}\gamma\left(\beta_0^2 + 2\beta_1^2 + 2\beta_3^2\right)\right)^2 = \left(f_0 a\right)^2 \tag{3.48}$$

,

where $f_0 = 3\gamma\beta_3$.

The second case let us consider $\omega = \frac{3}{2}\omega_2 + \varepsilon\sigma$ proceeding in the same way as in the case, one obtain the following equation

$$(\mu)^2 + \left(\frac{\sigma}{3}\omega_2 - \frac{3}{8}\gamma a^2 - \frac{p}{2}\cos\left(\omega_2 T_x\right) - \frac{d}{2}\omega_2 \sin\left(\omega_2 T_x\right) - \frac{3}{2}\gamma\left(\beta_0^2 + 2\beta_1^2 + 2\beta_3^2\right)\right)^2 = \left(f_0 a\right)^2$$
(3.49)

Where $f_0 = 3\gamma\beta_1$

c) combination resonance

In this part, the following situation is considered: $4\omega = \omega_2 + \varepsilon\sigma$; $5\omega = \omega_2 + \varepsilon\sigma$

frist case $4\omega = \omega_2 + \varepsilon\sigma$; The corresponding solvability condition is

$$-2i\omega_2\left(A' + \mu A\right) - 3\gamma\bar{A}A^2 - pA\exp\left(-i\omega_2 T_x\right) - i\omega_2 dA\exp\left(-i\omega_2 T_x\right) - 3\gamma\left(\beta_0^2 + 2\beta_1^2 + 2\beta_3^2\right)$$
$$+3\gamma\beta_3^2\beta_1\exp\left(i\sigma T_1\right) = 0$$
(3.50)

.

Subtutiting the polar form of A, putting $\phi_1 = \sigma T_1 - 3\theta_1$ in the above equation, and proceeding in the same way as in the case of superharmonic, the resonance equation is given by

$$(\mu a)^2 + \left(\sigma\omega_2 a - \frac{3}{8}\gamma a^3 - \frac{p}{2}a\cos\left(\omega_2 T_x\right) - \frac{d}{2}\omega_2 a\sin\left(\omega_2 T_x\right) - \frac{3}{2}\gamma\left(\beta_0^2 + 2\beta_1^2 + 2\beta_3^2\right)a\right)^2 = f_0^2$$
(3.51)

where $f_0 = 3\gamma\beta_3^2\beta_1$

second case $5\omega = \omega_2 + \varepsilon\sigma$. In this case, the resonance equation is given by

$$(\mu a)^2 + \left(\sigma\omega_2 a - \frac{3}{8}\gamma a^3 - \frac{p}{2}a\cos\left(\omega_2 T_x\right) - \frac{d}{2}\omega_2 a\sin\left(\omega_2 T_x\right) - \frac{3}{2}\gamma\left(\beta_0^2 + 2\beta_1^2 + 2\beta_3^2\right)\right)^2 = f_0^2$$
(3.52)

where $f_0 = 3\gamma\beta_1^2\beta_3$

Figs. 3.13, 3.14, 3.15, 3.16, 3.17, 3.18 represent the influence of the natural frequency on the amplitude response for the superhamonic, subharmnic and combination resonance state . As can be seen from these figures, increasing the natural frequency results in decreasing the oscillation amplitude, this allows us to say that increasing the natural frequency of the structure could increase the life of the structure because the vibrations of the structure are reduced. Each black curves of these figures are obtained for different values of time-delay. This allow us to say that time-delay has no effect on the superhamonic, subharmonic and combination resonant states.
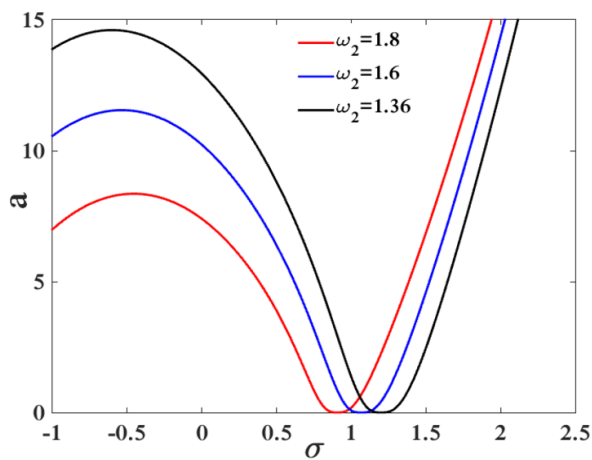
Figure 3.13: Superharmonic resonance curve: $3\omega = \omega_2 + \varepsilon\sigma$, effect of natural frequency ω_2, $\eta = 0.06$, $\gamma = -4.388$, $p = 4, d = 3$
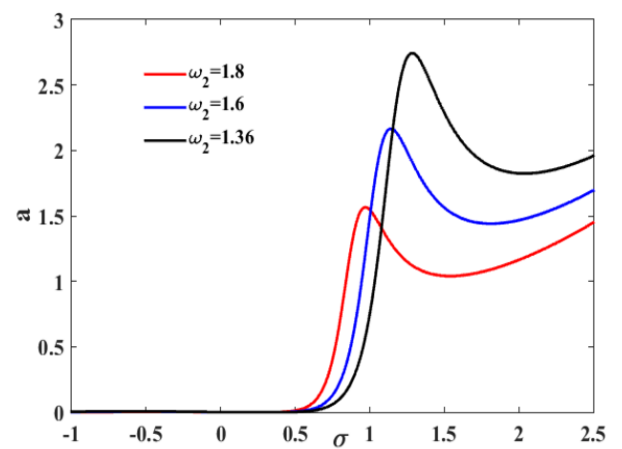
Figure 3.14: Superharmonic resonance curve: $6\omega = \omega_2 + \varepsilon\sigma$, effect of natural frequency ω_2, $\eta = 0.06$, $\gamma = -4.388$, $p = 4, d = 3$
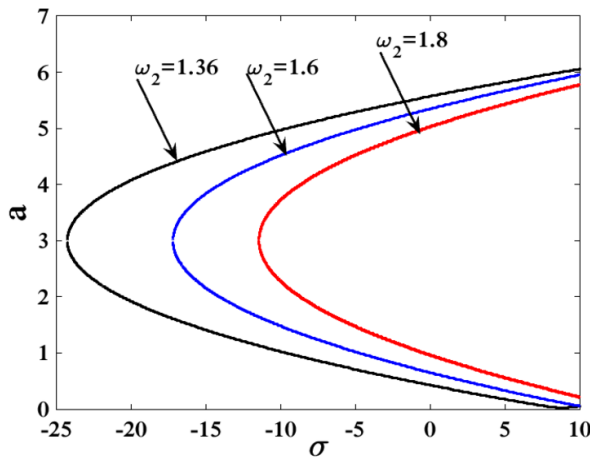
Figure 3.15: Subharmonic resonance curve: $\omega = 3\omega_2 + \varepsilon\sigma$, effect of natural frequency ω_2, $\eta = 0.06$, $\gamma = -4.388$, $p = 4, d = 9$
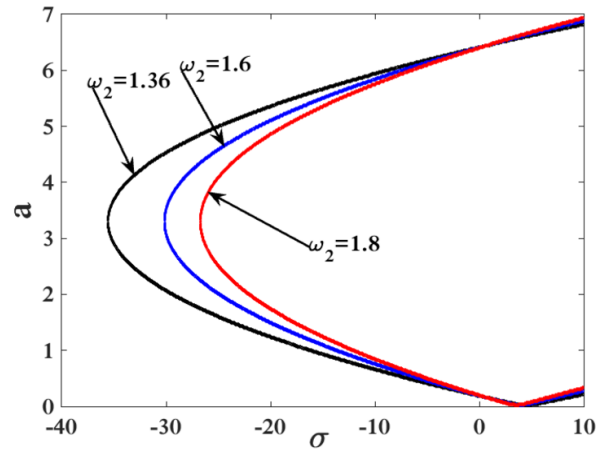
Figure 3.16: Subharmonic resonance curve: $\omega = \frac{1}{2}\omega_2 + \varepsilon\sigma$, effect of natural frequency ω_2, $\eta = 0.06$, $\gamma = -4.388$, $p = 4, d = 3$
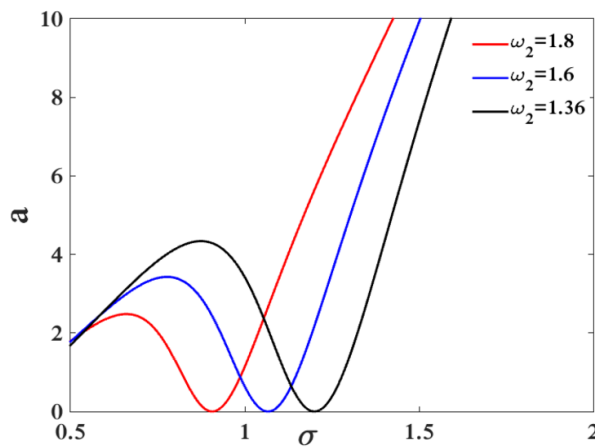
Figure 3.17: Combination resonance curve: $4\omega = \omega_2 + \varepsilon\sigma$, effect of natural frequency ω_2, $\eta = 0.06$, $\gamma = -4.388$, $p = 4, d = 3$
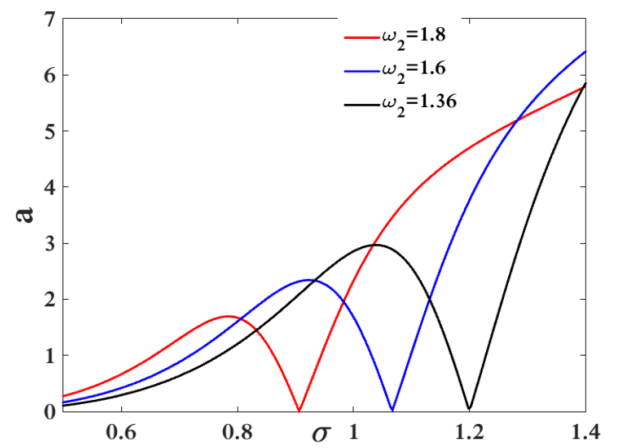
Figure 3.18: Combination resonance curve: $5\omega = \omega_2 + \varepsilon\sigma$, effect of natural frequency ω_2, $\eta = 0.06$, $\gamma = -4.388$, $p = 4, d = 3$

3.3 Design, analysis and horseshoes chaos control on Tension Leg Platform system with fractional non-linear viscoelastic tendon force under regular sea wave excitation.

3.3.1 Model description, mathematical modeling and wave force

3.3.1.1 Model description

The supporting structure of TLP consists of a hull, tethers, and templates. The hull is a buoyant structure with a deck at its top. The pontoons and columns provide sufficient buoyancy to maintain the deck above the sea waves during all sea states. The hull is anchored to the sea bed through tethers and fixed in place with templates as presented in Fig. 3.19 and equivalent model is shown in Fig. 3.20. Where F_B is a total buoyancy force, W is a total weight of the platform in the air, T_0 is the initial pre-tension in the tether, D_c is the diameter of TLP columns, D_p is the diameter of pontoon, D_r is the draft .
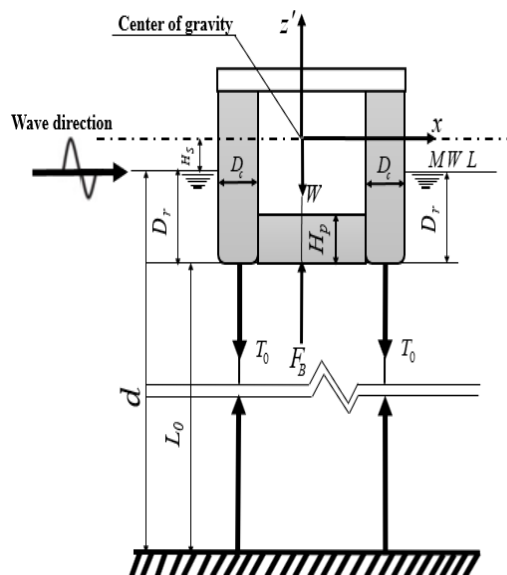
Figure 3.19: Schematic tension leg platform
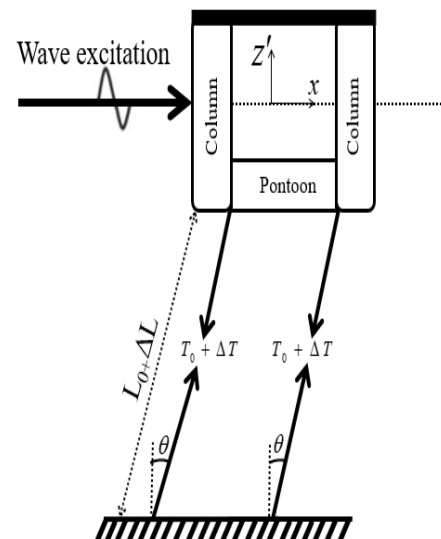
Figure 3.20: Surge displacement of TLP : simplified model

D_r is calculated from the following relation [91]

$$D_r = \frac{4}{D_c^2}\left(\frac{F_B - n\rho g L_p H_p W_p}{n\rho\pi g}\right) \tag{3.53}$$

where n is the number of tendon and ρ is the water density

3.3.1.2 Mathematical model of the vibration of tension leg platform

In this section, we have limited the analysis to the single DoF in order to give a first rough estimate of the sea wave and the fractional viscoelastic tendon force effects. Therefore, the equation of motion in horizontal direction of the whole system Fig. 3.20 is given as follows:

$$m\ddot{x} + c\dot{x} + F(x) = F_w \tag{3.54}$$

$$F(x) = (nT_0 + n\Delta T(x))\sin\theta + n\mu D_t^\alpha x \tag{3.55}$$

$$\Delta T(x) = AE\left(\frac{\sqrt{L_0^2 + x^2} - L_0}{L_0}\right) \tag{3.56}$$

The model used in this section is based on the model proposed by [92]. In order to get closer in a more practical and meaningful case, we propose in this section a model which taking into account that the structure can have a catastrophic behavior.

Assuming that the displacement x is small enough and taking into account the previous comment, one obtains

$$\Delta T(x) = \frac{AE}{2L_0^2}x^2 - \frac{AE}{8L_0^4}x^4 \tag{3.57}$$

$$\sin\theta = \frac{x}{\sqrt{L_0^2 + x^2}} \simeq \frac{x}{L_0}\left(1 - \frac{x^2}{2L_0^2} + \frac{3x^4}{8L_0^4}\right) \simeq \frac{x}{L_0} - \frac{x^3}{2L_0^3} + \frac{3x^5}{8L_0^5} \tag{3.58}$$

$$(nT_0 + n\Delta T(x))\sin\theta \simeq \frac{nT_0}{L_0}x + n\left(\frac{AE - T_0}{2L_0^3}\right)x^3 - 3n\left(\frac{AE - T_0}{8L_0^5}\right)x^5 \tag{3.59}$$

Taking into account Eq.(3.59), Eq.(3.54) becomes

$$m\ddot{x} + \frac{nT_0}{L_0}x + c\dot{x} + n\left(\frac{AE - T_0}{2L_0^3}\right)x^3 - 3n\left(\frac{AE - T_0}{8L_0^5}\right)x^5 + n\mu D_t^\alpha x = F_w \qquad (3.60)$$

where, x is the displacement in the surge direction, θ is the angle between the initial and the displaced position of the tether, c is the structural damping coefficient, L_0 is the initial length of each tether, E is the Young's modulus of the tether, $\Delta T(x)$ increases in the initial pre-tension due to the arbitrary displacement, $F(x)$ is the nonlinear viscoelastic force of tendon, F_w is the wave force, A is the cross-sectional area of tether, μ is the tendon viscosity coefficient and D_t^α is the fractional derivative with order $\alpha \in (0, 1)$.

3.3.1.3 Wave force

According to Morison [41], the generalized wave force due to sea wave on the members of TLP is calculated by the Morison equation on TLP columns as below:

$$F_{morison} = \sum (F_{inertia} + F_{drag})_{column} \qquad (3.61)$$

Assuming that the force coefficients C_m and C_d are constants and integrating over the still-water-depth on column yields [93].

$$F_{morison} = \sum_{column} \int_V c_m \rho \dot{u} dV - \int_V c_a \rho \ddot{x} dV + \int_{z_1}^{z_2} 0.5 c_d \rho \left| u - \dot{x} \right| (u - \dot{x}) dz \qquad (3.62)$$

Taking into account the wave theory, the horizontal water particle velocity and acceleration at the vertical centreline of a circular cylinder at $x = 0$ are given [94]

$$u(x, t) = \frac{\pi H}{T} \frac{\cosh kz}{\sinh kd} \cos(kx - \Omega t) \qquad (3.63)$$

$$\dot{u}(x, t) = \frac{2\pi^2 H}{T^2} \frac{\cosh kz}{\sinh kd} \sin(kx - \Omega t) \qquad (3.64)$$

The relation between Ω and k is given by [93].

$$\Omega^2 = gk \tanh kd \qquad (3.65)$$

In the deep water $\frac{d}{L} > 0.5$, the following equation used to replace Eq.(3.65) becomes

$$L = \frac{0.5gT^2}{\pi} \tag{3.66}$$

where, H is the wave height, L is the wave length, Ω is the wave frequency k is the wave number, C_a, C_m are inertia and added mass coefficient respectively, z_1 and z_2 are the bottom level and the still water level, T is the wave period. Also, m_{add} is the added mass on TLP columns, V is the volume of column.

Ignoring the drag force [93] and substituting Eq.(3.63) and Eq.(3.64) into Eq.(3.62) one obtains:

$$F_{morison} = \sum_{column} \int_V c_a \rho \ddot{x} dV + \sum_{column} c_m \rho \frac{2\pi^2 H}{T^2} \frac{\pi D_c^2}{4 \sinh kd} \left(\frac{\sinh kz_2 - \sinh kz_1}{k} \right) \sin \Omega t \tag{3.67}$$

Substituting Eq.(3.67)into Eq.(3.60) one could obtain

$$
\begin{aligned}
(m + m_{add}) \ddot{x}(t) + c\dot{x}(t) + \frac{nT_0}{L_0}x + n\left(\frac{AE-T_0}{2L_0^3}\right)x^3(t) - 3n\left(\frac{AE-T_0}{8L_0^5}\right)x^5(t) \\
+ n\mu D_t^\alpha x(t) = \sum_{column} c_m \rho \frac{2\pi^2 H}{T^2} \frac{\pi D_c^2}{4 \sinh kd} \left(\frac{\sinh kz_2 - \sinh kz_1}{k} \right) \sin \Omega t
\end{aligned}
\tag{3.68}
$$

where $m_{add} = \sum_{column} \int_V c_a \rho dV$

Taking into account the following dimensionless variables and parameters and after some manipulations, the dimensionless nonlinear equations of the system can be obtained as follows

$$y = \frac{x}{L_0}, \quad \Omega_0 = \sqrt{\frac{nT_0}{(m+m_{add})L_0}}, \quad \gamma_1 = \frac{AE-T_0}{2T_0}, \quad \omega = \frac{\Omega}{\Omega_0}, \quad \lambda = c\sqrt{\frac{L_0}{n(m+m_{add})T_0}}$$

$$\eta = \frac{n\mu\Omega_0^{\alpha-2}}{(m+m_{add})}, \quad F_0 = \varepsilon \sum_{column} c_m \rho \frac{2\pi^2 H}{T^2} \frac{\pi D_c^2}{4 \sinh kd} \left(\frac{\sinh kz_2 - \sinh kz_1}{k} \right), \quad \varepsilon = \frac{1}{nT_0}, \quad \tau = \Omega_0 t$$

$$\ddot{y}(\tau) + \lambda\dot{y}(\tau) + \omega_0^2 y(\tau) + \gamma_1 y^3(\tau) - \frac{3}{4}\gamma_1 y^5(\tau) + \eta D_\tau^\alpha y(\tau) = F_0 \sin \omega\tau \tag{3.69}$$

The previous equation represents the dimensionless equation of the system.

3.3.2 Approximate solution of the TLP response subjected to the wave excitations and stability analysis

3.3.2.1 Analytical investigation

In this section, we are interested on the effect of the order of derivative α, the tendon viscosity coefficient η and the number of tendon n on the dynamic response of the platform.

Averaging method is applied here. First of all, we assume that γ_1, γ_2, η and F_0 are small perturbations, and considered $\omega^2 = \omega_0^2 + \xi\sigma$, $\omega_0^2 = 1$

For that consideration, let us assume that the solution of Eq.(3.69) can be written as

$$y(\tau) = A(\tau)\cos(\omega\tau + \varphi(\tau)) \tag{3.70}$$

$$\dot{y}(\tau) = -\omega A(\tau)\sin(\omega\tau + \varphi(\tau)) \tag{3.71}$$

where the amplitude $A(\tau)$ and the phase $\varphi(\tau)$ are slow-varying functions of time τ. Substituting Eq.(3.70) and Eq.(3.71) into Eq.(3.69) after some mathematical manipulations, one obtains

$$\begin{cases} \dot{A} = -\frac{1}{\omega}[P_1(A,\varphi) + P_2(A,\varphi)]\sin(\omega\tau + \varphi) \\ A\dot{\varphi} = -\frac{1}{\omega}[P_1(A,\varphi) + P_2(A,\varphi)]\cos(\omega\tau + \varphi) \end{cases} \tag{3.72}$$

$$P_1(A,\varphi) = \tilde{F}_0\sin(\omega\tau) + \sigma A\cos(\omega\tau + \varphi) + \tilde{\lambda}\omega A\sin(\omega\tau + \varphi)$$
$$-\tilde{\gamma}_1 A^3\cos^3(\omega\tau + \varphi) + \frac{3}{4}\tilde{\gamma}_1 A^5\cos^5(\omega\tau + \varphi) \tag{3.73}$$
$$P_2(A,\varphi) = -\tilde{\eta}D_\tau^\alpha(A\cos(\omega\tau + \varphi))$$

To apply the averaging method, we average at the period T_1 of which one could select as $T_1 = 2\pi/\omega$ in the case of periodic function or $T_1 = \infty$ in the case of aperiodic $D_\tau^\alpha(A\cos(\omega\tau + \varphi))$ [95–98]. We obtain the following pair of first order differential equations for the amplitude $A(\tau)$ and the phase $\varphi(\tau)$.

$$\dot{A} = -\frac{F_0}{2\omega}\cos\varphi + \frac{\lambda}{2}A + \eta A\omega^{\alpha-1}\sin\left(\frac{\alpha\pi}{2}\right) \tag{3.74}$$

$$A\dot{\varphi} = \frac{F_0}{2\omega}\sin\varphi - \frac{\xi\sigma A}{2\omega} + \frac{3\gamma_1 A^3}{8\omega} - \frac{15\gamma_1 A^5}{64\omega} + \eta A\omega^{\alpha-1}\cos\left(\frac{\alpha\pi}{2}\right) \tag{3.75}$$

In vibration engineering, the steady-state solution is more important. By eliminating $\sin \varphi$ and $\cos \varphi$

Eq.(3.74) and Eq.(3.75) for the steady-state solution $\left(A = A_0,\ \dot{A} = 0,\ \dot{\varphi} = 0 \right)$, one obtains the following nonlinear algebraic equation

$$c_{10} A_0^{10} + c_8 A_0^8 + c_6 A_0^6 + c_4 A_0^4 + c_2 A_0^2 - F_0^2 = 0 \tag{3.76}$$

with

$$c_2 = \beta_1^2 (\alpha) + \beta_2^2 (\alpha),\ \ c_4 = -\tfrac{3\gamma_1}{2} \beta_1 (\alpha),\ \ c_6 = \tfrac{9\gamma_1^2}{16} + \tfrac{15\gamma_1}{16} \beta_2 (\alpha),\ \ c_8 = -\tfrac{45\gamma_1^2}{64},\ \ c_{10} = \tfrac{225\gamma_1^2}{1024}$$

$$\beta_1 (\alpha) = \lambda \omega + \eta \omega^\alpha \sin \left(\tfrac{\alpha \pi}{2} \right),\ \ \beta_2 (\alpha) = (\omega^2 - \omega_0^2) - \eta \omega^\alpha \cos \left(\tfrac{\alpha \pi}{2} \right) \tag{3.77}$$

This equation has more than one steady-state solution for some parameters. An interesting observation is the dependence of the oscillations amplitude upon the tendons parameters (natural frequency $\omega_0^2 = 1$, nonlinear γ_1 component, the number of tendon n and the dimensionless viscosity coefficient η), the parameters of the wave excitation (wave frequency ω and the dimensionless wave load F_0).

Next, we study the stability of the steady-state solution by using the method of Andronov and Witt [100], $A = A_0 + \Delta A,\ \ \varphi = \varphi_0 + \Delta \varphi$ and substituting them into Eq.(3.74) and Eq.(3.75) one obtains

$$\frac{dA}{d\tau} = -\frac{\beta_1 (\alpha)}{2\omega} \Delta A + \frac{A_0}{2\omega} \left[\beta_2 (\alpha) - \frac{3}{4} \gamma_1 A_0^2 + \frac{15}{32} \gamma_1 A_0^4 \right] \Delta \varphi \tag{3.78}$$

$$\frac{d\varphi}{d\tau} = \frac{1}{2\omega A_0} \left[\frac{9}{4} \gamma_1 A_0^2 - \frac{75}{64} \gamma_1 A_0^4 - \beta_2 (\alpha) \right] \Delta A - \frac{\beta_1 (\alpha)}{2\omega} \Delta \varphi \tag{3.79}$$

where $\beta_1 (\alpha)$ and $\beta_2 (\alpha)$ are given by Eq.(3.77). The stability of the steady-state solution is determined by the eigenvalue of the corresponding Jacobian matrix of Eq.(3.78) and Eq.(3.79) . The corresponding eigenvalues Ψ are the roots of

$$\begin{aligned} \Psi^2 + \tfrac{\beta_1(\alpha)}{2\omega} \Psi + \left(\tfrac{\beta_1(\alpha)}{2\omega} \right)^2 + \tfrac{1}{4\omega^2} \left[\tfrac{3}{4} \gamma_1 A_0^2 - \tfrac{15}{32} \gamma_1 A_0^4 - \beta_2 (\alpha) \right] \\ \times \left[\tfrac{9}{4} \gamma_1 A_0^2 - \tfrac{75}{64} \gamma_1 A_0^4 - \beta_2 (\alpha) \right] = 0 \end{aligned} \tag{3.80}$$

Since $0 < \alpha < 1$, then $\beta_1 (\alpha) > 0$, the determination of signs of the real parts of the roots Ψ may be carried out by making use of the Routh-Hurwitz criterion [101] as

$$\left(\frac{\beta_1\left(\alpha\right)}{2\omega} \right)^2 + \frac{1}{4\omega^2} \left[\frac{3}{4}\gamma_1 A_0^2 - \frac{15}{32}\gamma_1 A_0^4 - \beta_2\left(\alpha\right) \right] \times \left[\frac{9}{4}\gamma_1 A_0^2 - \frac{75}{64}\gamma_1 A_0^4 - \beta_2\left(\alpha\right) \right] < 0 \quad (3.81)$$

The previous inequality represents the instability condition for the steady-state solution.

3.3.2.1 Numerical investigation

It is well known that the validation of results obtained through analytical investigation is guaranteed by the perfect match with the results obtained through direct numerical simulation of the mathematical model. Thus, the numerical scheme used in this paper is based on the Gunwald-Letnikov definition of the fractional order derivative Eq.(3.82) [102, 103]

$$D_\tau^\alpha \left[y\left(\tau_{n_f}\right) \right] \approx h^{-\alpha} \sum_{j=0}^{n_f} C_j^\alpha y\left(\tau_{n_f-j}\right) \quad (3.82)$$

where h is the integration step and the coefficients C_j^α satisfy the following recursive relations :

$$C_0^\alpha = 1, \qquad C_j^\alpha = \left(1 - \frac{1+\alpha}{j} \right) C_{j-1}^\alpha \quad (3.83)$$

Properties of the tendon leg platform and characteristics of the sea waves which are used for numerical and analytical purpose are given in Table 3.3 [104]

Fig. 3.21 shows the effect of the fractional order derivative on the amplitude of vibration of the TLP. It is found that as the order of the fractional derivative increases, the amplitude response of the TLP decreases. The increase of the fractional order derivative also contributes to decrease the unstable range of amplitude. Nevertheless, beyond a certain value of the fractional parameter ($\alpha \in (0.65, 1)$), we rather observe an increase in amplitude. This graph also shows a comparison between the analytical results (curve with dotted lines) and numerical results (curve with a circle line $\alpha = 0.5$). We observe a good agreement between the analytical and numerical results. The same results were obtained by Anague et al [105], who studied the dynamics of a Rayleigh beam resting

Table 3.3: Properties of the tendon leg platform and characteristics of the sea waves.

Parameter name	Symbol	Value
Tendons length (m)	L_0	882.5
Pre-Tension (mt)	T_0	18857
Weight of structure (mt)	W	13154
Young's modulus of a tendon (Pa)	E	2.10^{10}
Tendon stiffness (N/m)	k_0	9.10^6
Tendon Outer Inner Diameter (mm)	D_0, D_i	$813, 781.5$
Pontoon Size (m)	L_p, W_p, H_p	$46, 15, 5$
Columns Size (m)	D_c, H_c	$20, 51$
Number of Tendons Per Tendsion leg	n	$8, 12, 16$
Inertial coefficient of added	C_m	2
Tendon viscosity coefficient (Ns^α/m)	μ	3.10^4
Acceleration of gravity (m/s^2)	g	9.81
Water density (kg/m^3)	ρ	1024
Wave period (s)	T	12
Wave height (m)	H	6

on fractional-order viscoelastic Pasternak foundations subjected to moving loads. But in their case they only observed a decrease in amplitude of vibration of the beam when the fractional parameter increases.

In Fig. 3.22, we have plotted the amplitude response curve of vibration of the TLP A_0 as a function of the wave frequency ω for different values of the dimensionless tendon viscosity coefficient η. It is clearly shown that the system is more stable when the value of the dimensionless tendons viscosity coefficient increases. There is also a fairly significant reduction in the vibration amplitude of the structure with the increase of viscosity coefficient. The multi-value solutions appear for the small value of this coefficient and disappears gradually when this value increase.

Figure 3.21: Steady-state amplitude A_0 of the TLP as function of wave frequency ω for different values of the fractional-order α with $n = 8$.

Fig. 3.23 shows the variation of the amplitude of vibration of the TLP A_0 as function of the tendon viscosity coefficient for different values of wave frequency ω. It is observed from this figure that, for the lowest tendon viscosity coefficient, we only have the multi-value solutions, while for the highest tendon viscosity coefficient the multi-value solutions disappear. This confirms the results obtained and displays in Fig. 3.22. It is also found that for a value frequency $\omega = \omega_0 = 1$, when the tendon viscosity coefficient increases, the amplitude of vibration of TLP continuously decreases Fig. 3.23(a), which is not the case in Fig. 3.23(b), Fig. 3.23(c) and Fig. 3.23(d), where the increase in the tendon viscosity coefficient leads first to increase the amplitude of vibration of the TLP, and then decrease it.

Fig. 3.24 shows the variation of the amplitude of vibration of the TLP as function of the tendon viscous coefficient η for different values of the fractional-order α . From the analysis of this figure, we note that the hysteresis and the amplitude jump phenomena are confirmed and can be controlled by the fractional-order parameter.

Fig. 3.25 shows the behaviour of the amplitude of vibration A_0 in function of excitation
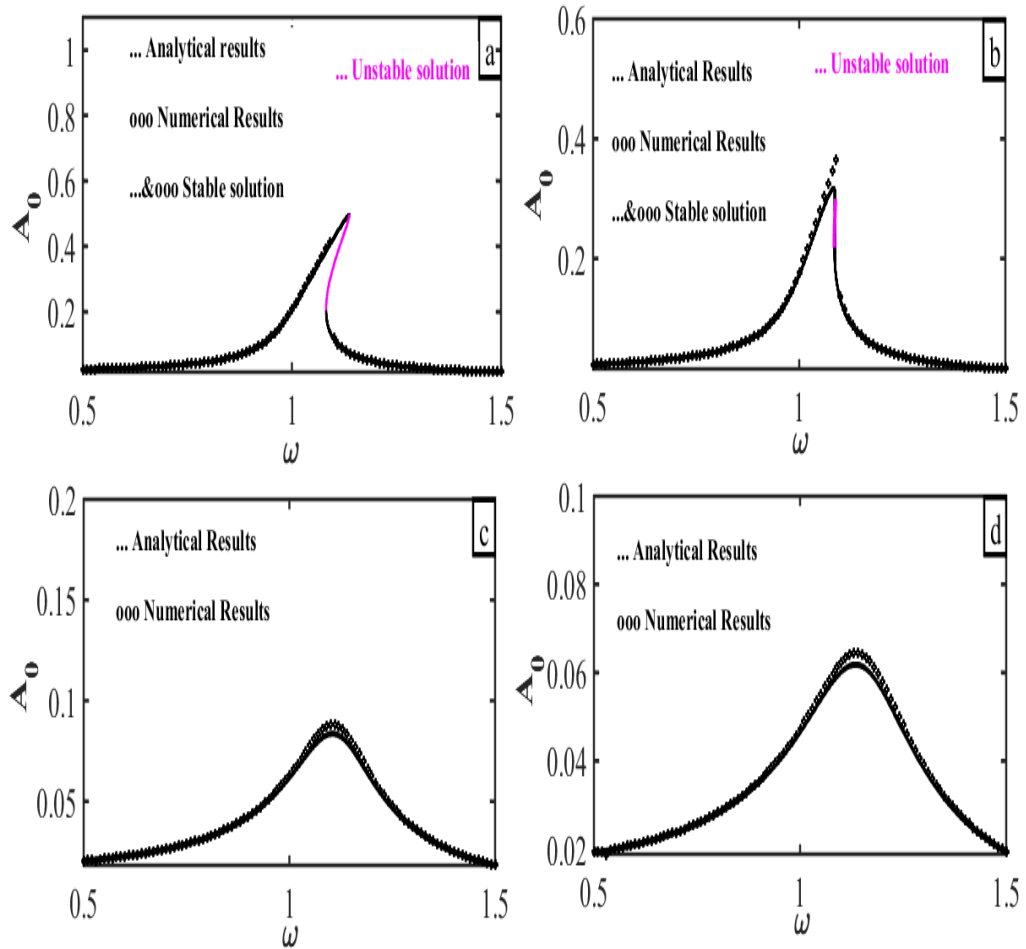
Figure 3.22: Steady-state amplitude A_0 of the TLP as function of wave frequency ω for different values of tendon viscosity coefficient with (a) $\eta = 0.03$, (b) $\eta = 0.08$, (c) $\eta = 0.2$, (d) $\eta = 0.4$ for $n = 8$, $\alpha = 0.5$.
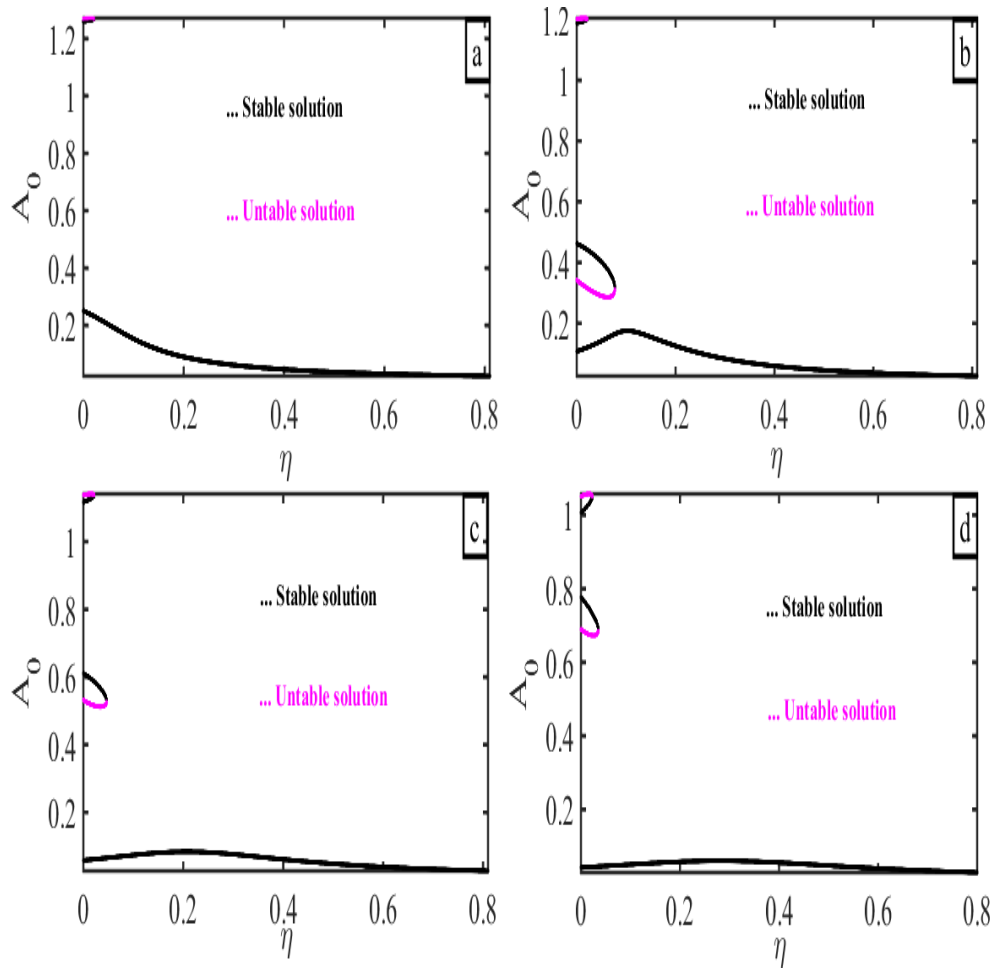
Figure 3.23: Steady-state amplitude A_0 of the TLP as function of tendon viscosity coefficient η for different values of wave frequency with (a) $\omega = 1$, (b) $\omega = 1.09$, (c) $\omega = 1.15$, (d) $\omega = 1.2$ for $n = 8$, $\alpha = 0.5$.
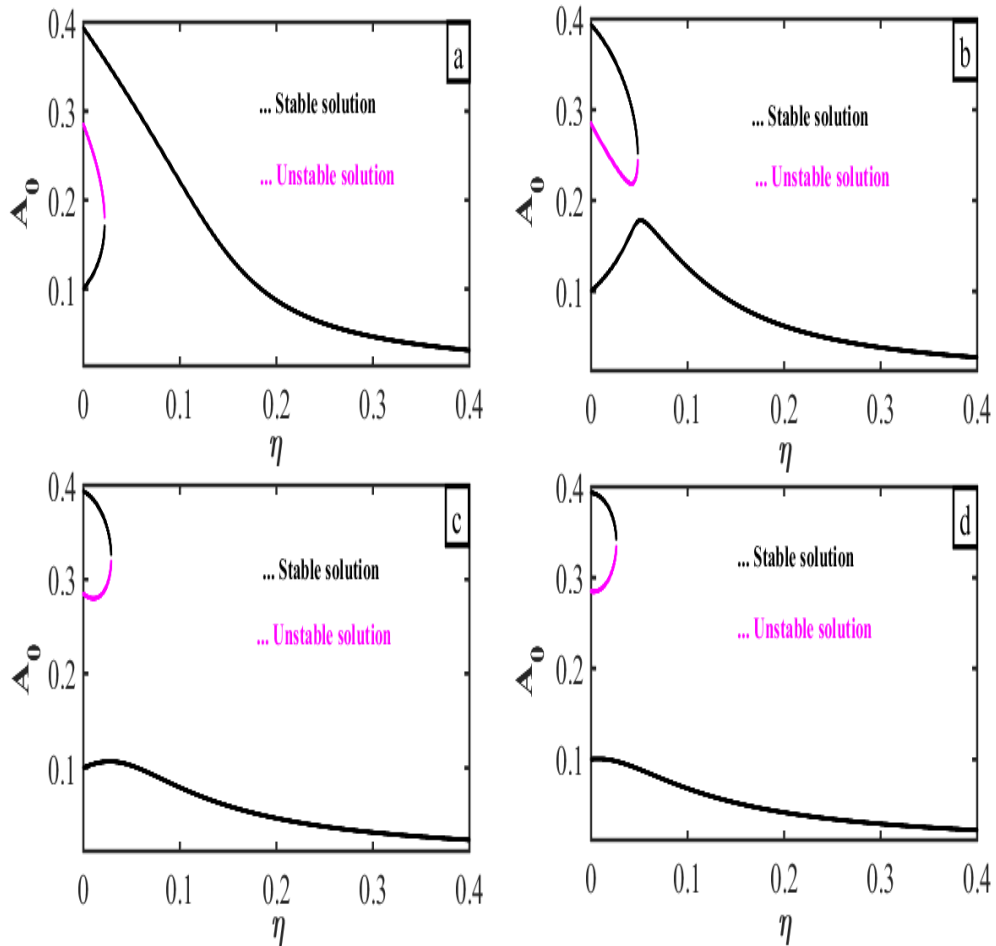
Figure 3.24: Steady-state amplitude A_0 of the TLP as function of tendon viscosity coefficient η for different values of fractional-order with (a) $\alpha = 0.1$, (b) $\alpha = 0.5$, (c) $\alpha = 0.8$, (d) $\alpha = 0.95$ for $n = 8$, $\omega = 1.09$

frequency ω for the different values of number of tendons. One can observe that, when the number of the tendons increases, the vibration amplitude is relevantly reduced and the domain of the unstable solutions also decreases.
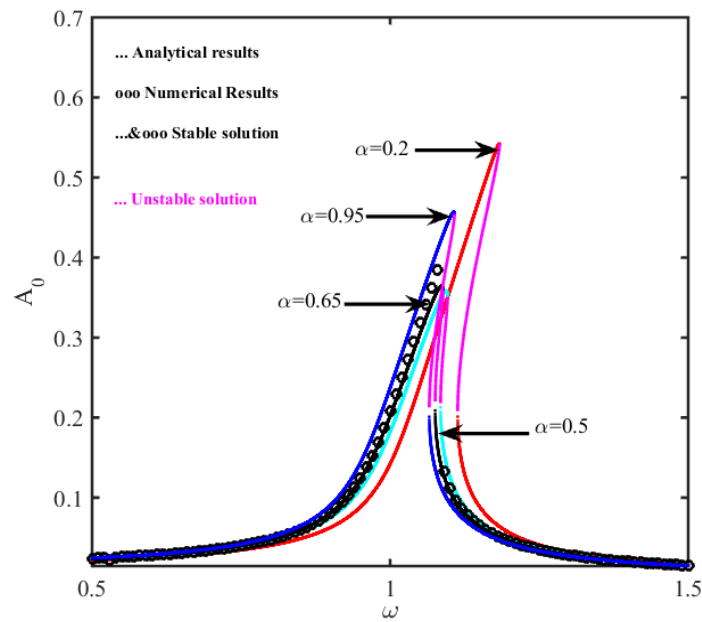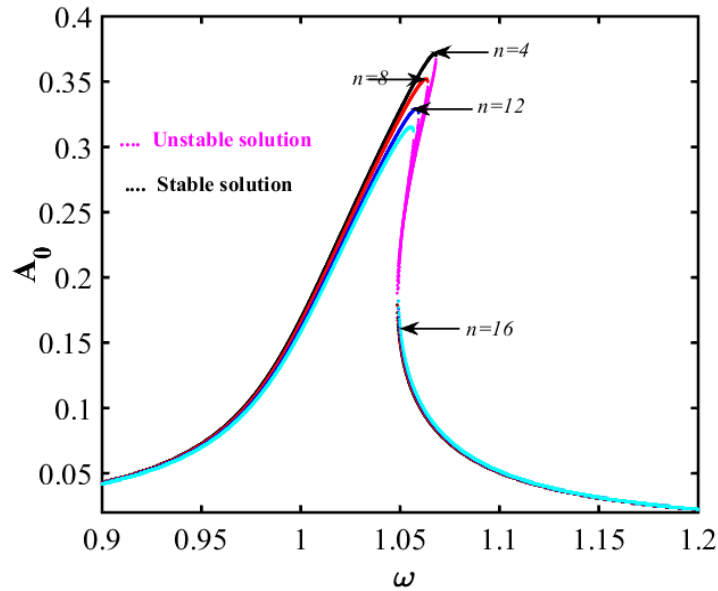

Figure 3.25: Steady-state amplitude A_0 of the TLP as function of wave frequency ω for different values of the number of tendons n, with $\alpha = 0.5$.

3.3.3 Effect of tendon on the appearance of horseshoes chaos on TLP: Melnikov analysis

In this section, it comes to evaluating the Melnikov's function which measures the distance between the border of regular oscillations and that of chaotic movements. Indeed, the aim is to clearly determine the effect of the fractional order parameter, the tendon viscosity coefficient and the number of tendons on the fractality of the basins of attraction and, so to speak, Smale horseshoe chaos through the analysis of the Melnikov's function. The configuration considered here is that of a catastrophic monostable potential.

The mathematical model Eq.(3.69) can be rewritten as a perturbed Hamiltonian system as

$$\frac{d\chi}{d\tau} = F[\chi] + \varepsilon G[\chi, \tau], \tag{3.84}$$

where the vector fields χ, F and G are given by

$$\chi = \begin{bmatrix} y \\ z = \dot{y} \end{bmatrix}, \quad F = \begin{bmatrix} z \\ -y - \gamma_1 y^3 + \frac{3}{4}\gamma_1 y^5 \end{bmatrix}, \quad G = \begin{bmatrix} 0 \\ -\lambda z - \eta D_\tau^\alpha y + F_0 \sin \omega\tau \end{bmatrix}$$
$$\tag{3.85}$$

with ε being a perturbation parameter.

In the unperturbed case ($\varepsilon = 0$), the system of Eq.(3.84) is the Hamiltonian system with Hamiltonian function

$$H(y, z) = \frac{1}{2}z^2 + \frac{1}{4}\gamma_1 y^4 - \frac{3}{24}\gamma_1 y^6 \tag{3.86}$$

and the corresponding potential function is given as

$$U(y) = \frac{1}{4}\gamma_1 y^4 - \frac{3}{24}\gamma_1 y^6 \tag{3.87}$$

The saddle points are connected by heteroclinic orbit that satisfy the following equation:

$$y_{het} = \pm\frac{y_1\sqrt{2}\sinh\left(\frac{\theta}{2}\tau\right)}{[-\beta + \cosh(\theta\tau)]^{\frac{1}{2}}}, \quad z_{het} = \pm\frac{y_1\frac{\sqrt{2}}{2}(1-\beta)\theta\cosh\left(\frac{\theta}{2}\tau\right)}{[-\beta + \cosh(\theta\tau)]^{\frac{3}{2}}} \tag{3.88}$$

where

$$\beta = \frac{5-3G^2}{3G^2-1}, \quad \theta = y_1^2\sqrt{\frac{\gamma_1(1-G^2)}{2}}, \quad G^2 = \frac{y_2^2}{y_1^2}$$

Fig. 3.26(a) shows the potential energy of our system ($\gamma_1 > 0$). The system has three equilibrium points: a center point $y_0 = (0, 0)$ and two saddle points $y_{1,2} = \left(\pm\sqrt{\frac{2(\gamma_1+\sqrt{\gamma_1^2+3\gamma_1})}{3\gamma_1}}, 0\right)$, as shows in Fig. 3.26(b)

Unfortunately, mechanical and civil structures are subject to external stresses. That said, we consider the perturbed case ($\varepsilon \neq 0$). The Melnikov's theorem is used to detect
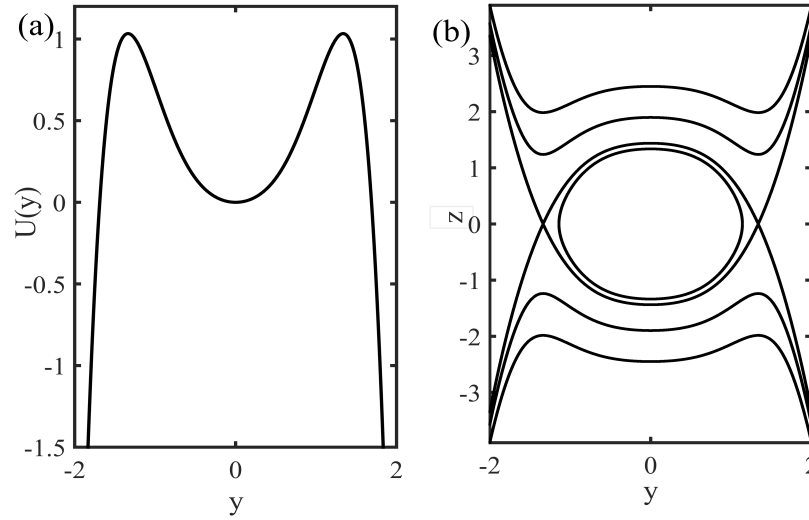
Figure 3.26: Potential (a), separatrix (closed curve) and Phase space trajectories (open line) (b) of the system Eq.(3.69).

transverse intersection points between perturbed and unperturbed orbits or the appearance of the fractality on the basin of attraction, which leads to the occurrence of chaos. Melnikov's theorem which gives the condition of transversality (of the existence of a fractal basin) can be formulated as follows [105–109]. Let the Melnikov function be defined in the case of Eq.(3.84) as

$$
\begin{aligned}
M_D\left(\tau_0\right) &= \int_{-\infty}^{+\infty} F\left[\chi_{het}\left(\tau\right)\right] \wedge G\left[\chi_{het}\left(\tau\right), \tau + \tau_0\right] \\
&= -\lambda \int_{-\infty}^{+\infty} z_{het}^2\left(\tau\right) d\tau - \eta \int_{-\infty}^{+\infty} z_{het}\left(\tau\right) D_\tau^\alpha\left[y_{het}\left(\tau\right)\right] d\tau + F_0 \int_{-\infty}^{+\infty} z_{het}\left(\tau\right) \sin\left(\tau + \tau_0\right) d\tau
\end{aligned}
$$
(3.89)

When the Melnikov function has simple point, the stable manifold and unstable manifold intersect transversally, chaos in the sense of Smale horseshoe transform occurs. So let $M_D\left(\tau_0\right) = 0$, one concludes that horseshoe chaos appears when

$$F_0 \geq F_{0cr} = y_1 \left(\frac{2\eta I_1 + \lambda(1-\beta)\theta I_2}{\sqrt{2} \times I_3} \right) \tag{3.90}$$

where
$$I_1 = \int_{-\infty}^{+\infty} \frac{\cosh\left(\frac{\theta}{2}\tau\right)}{[-\beta+\cosh(\theta\tau)]^{\frac{3}{2}}} D_\tau^\alpha \left[\frac{\sinh\left(\frac{\theta}{2}\tau\right)}{[-\beta+\cosh(\theta\tau)]^{\frac{1}{2}}} \right] d\tau$$

$$I_2 = \frac{(\beta+1)}{2\theta(1-\beta^2)^2} \left[\beta + 2 + \frac{(4\beta+2)(1-\beta^2)}{\sqrt{\beta^2-1}} \ln\left(\frac{-\beta+1+\sqrt{\beta^2-1}}{-\beta+1-\sqrt{\beta^2-1}} \right) \right], \quad I_3 = \frac{2\sqrt{2}\pi\omega}{(1-\beta)\theta^2 \sinh\left(\frac{\pi\omega}{\theta}\right)}$$

Fig. 3.27, Fig. 3.28 and Fig. 3.29 show the threshold conditions as function of wave frequency for different values of the main parameters of the system. Fig. 3.27(a) shows the critical external force for different values of fractional order parameter. One can observe that, when the value of the fractional order parameter increases, the thresholds of the critical values F_{0cr} decrease. Fig. 3.27(a) confirms the fact that as fractional order parameter increases the amplitude of critical force decreases. We can conclude that, by making the good choice of fractional derivative relating to reduce the amplitude of vibration of the system. Fig. 3.28 presents the threshold conditions as a function of wave frequency for different values of tendon viscosity coefficient. For each frequency, it is shown that the limit value predicted by the Melnikov theory is much larger when the tendon viscosity coefficient increases. On the other hand, the effect of the number of the tendons on the threshold amplitude versus the wave frequency is shown in Fig. 3.29. It is clear that the increase of the number of tendons first increases the threshold. One can conclude that the highest value of the number of tendons contributed to increase the degree of stability of the TLP.

To confirm our analytical predictions obtained in Fig. 3.27, Fig. 3.28 and Fig. 3.29, we study the effect tendon viscosity coefficient and fractional order parameters on a basin of attraction of the system. For this purpose, we numerically solve Eq.(3.69) using Newton-Leipnik method [98, 99]. From Fig. 3.30, we notice that, when decreasing the order of derivative, one an erosion of the basin of attraction. This result allows to conclude that, the lowest value of fractional order has a detrimental effect on the stability of the system. Fig. 3.31 presents the effect of the tendon viscosity coefficient on the basin of attraction. It should be noted that, when the tendon viscosity coefficient η greater than 0.27 , the basin
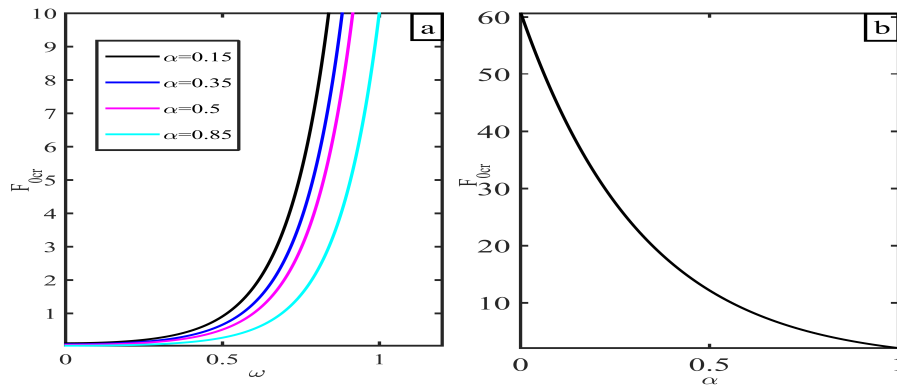
Figure 3.27: Critical external force for the appearance of horsheshoes chaos as function of: (a) wave frequency ω, (b) fractional order parameter α for $n = 8$.
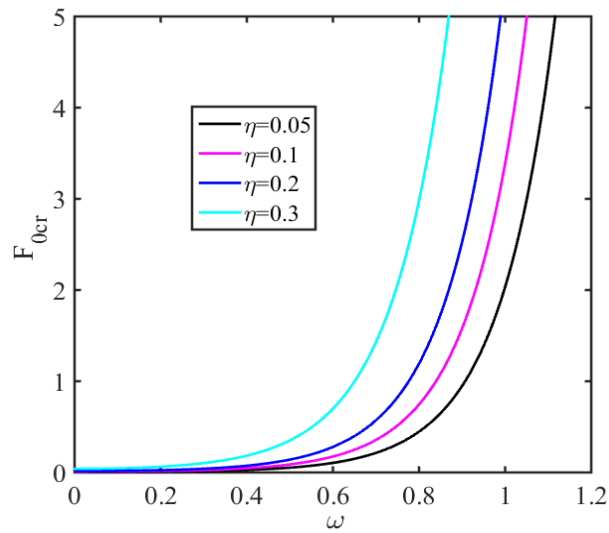
Figure 3.28: Critical external force for the appearance of horsheshoes chaos for different values of tendon viscosity coefficient η for $n = 8$, $\alpha = 0.5$.
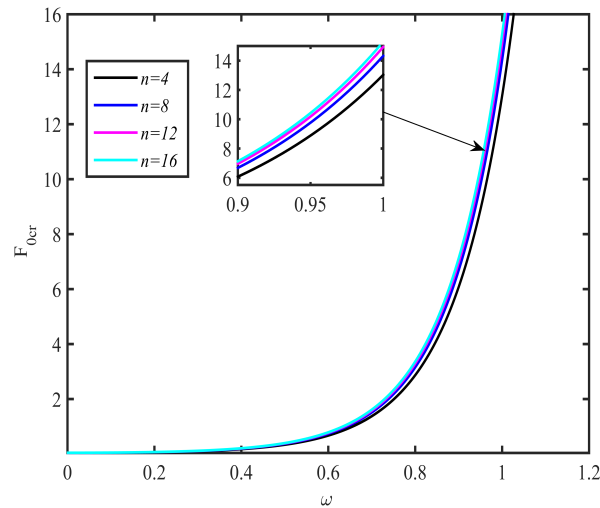
Figure 3.29: Critical external force for the appearance of horsheshoes chaos for different values of the number of tendons n for $\alpha = 0.5$.

of attraction has a regular form Fig. 3.31(d). Those results have already been predicted analytically. We can conclude that, the analytical and numerical predictions are in good agreement.

3.4 Tension leg platform model with tuned liquid column damper under excitation of sea waves

3.4.1 Physical Model, mathematical model of the vibration of tension leg platform with tuned liquid column damper, modal equation and description of the wave excitation

3.4.1.1 Physical model

We focused on compliant platforms, and in particular on tension leg platform. A TLP structure which includes, deck, hull, pontoon, risers, tendons, foundation template and TLCD control device is shown schematically in Fig. 3.32 and equivalent model, consisting of a vertical beam is shown in Fig. 3.33. The TLCD model is given in Fig. 3.34
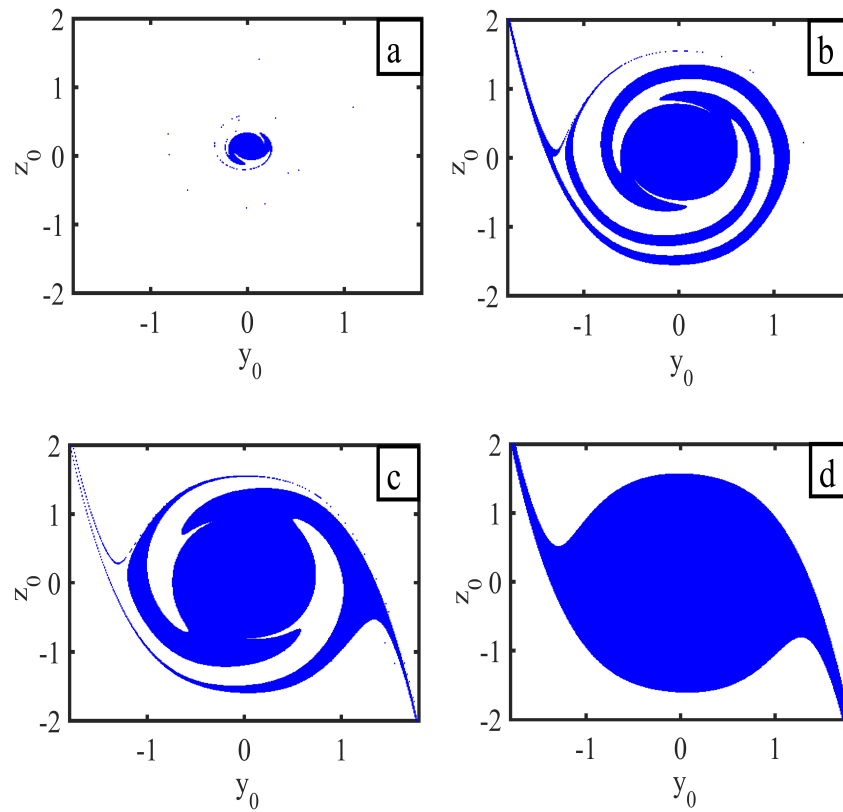
Figure 3.30: Effect of fractional parameter α on basin of attraction with (a) $\alpha = 0.15$, (b) $\alpha = 0.35$, (c) $\alpha = 0.4$, (d) $\alpha = 0.5$ for $n = 8$, $\eta = 0.3$, $\omega = 1$, $F_{0cr} = 0.05$.
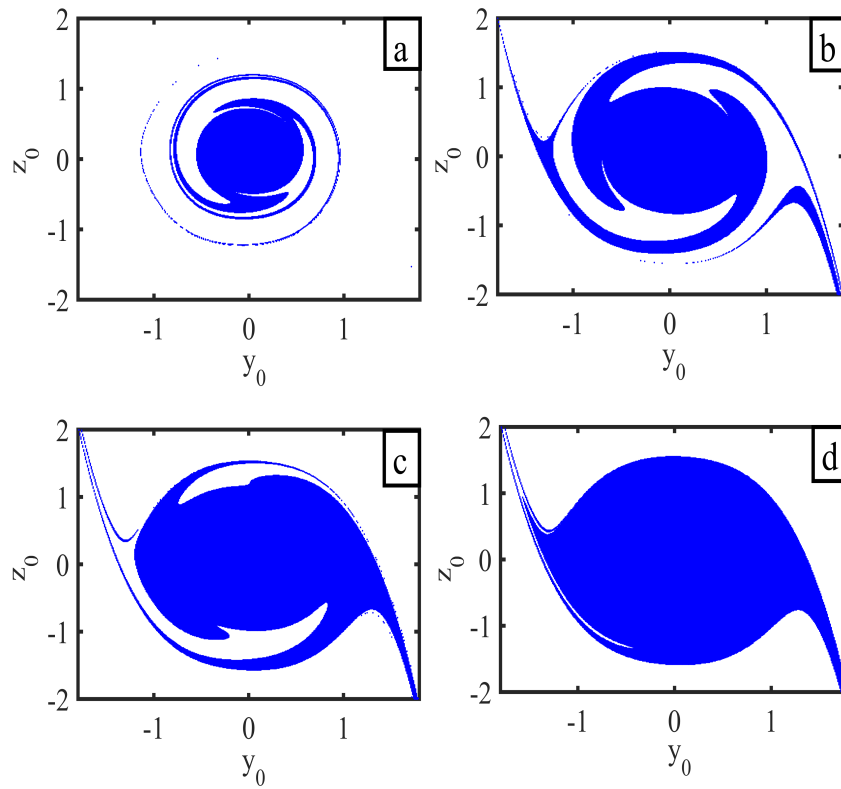
Figure 3.31: Effect of tendon viscosity coefficient η on basin of attraction with (a) $\eta = 0.2$, (b) $\eta = 0.24$, (c) $\eta = 0.26$, (d) $= 0.28$ for $n = 8$, $\alpha = 0.5$,$\omega = 1$, $F_{0cr} = 0.05$.
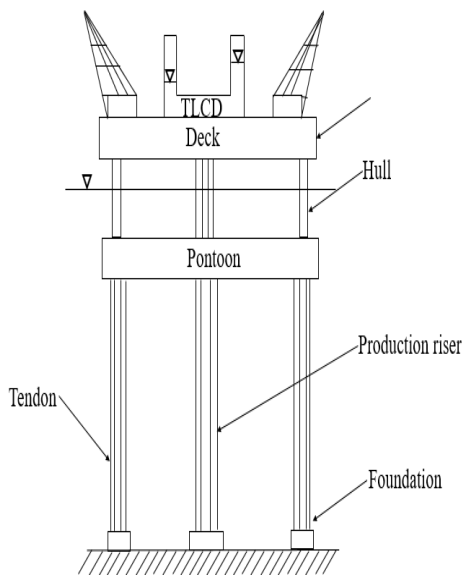
Figure 3.32: Schematics of tension leg platform [110]
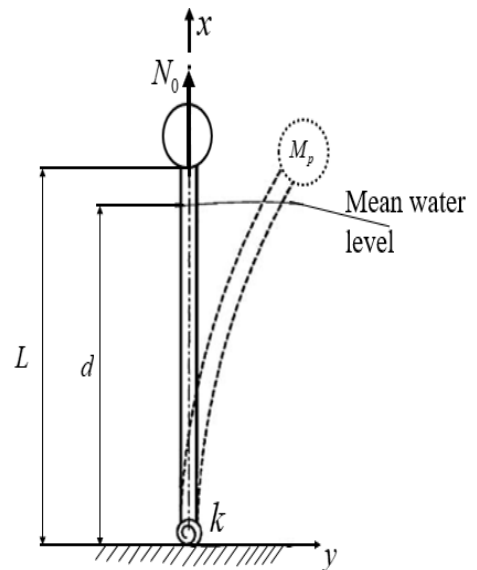
Figure 3.33: A simplified model [110]
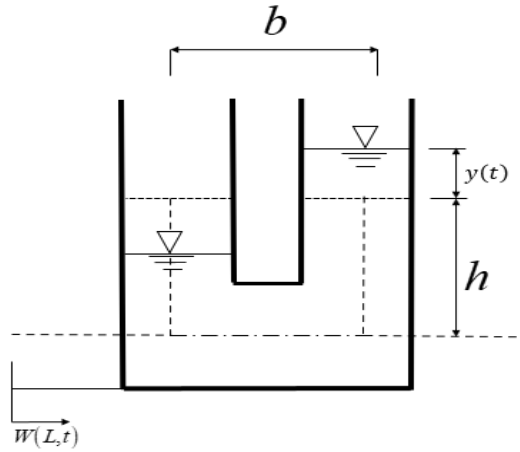
Figure 3.34: Tuned liquid column damper model [111]

3.4.1.2 The mathematical model of the vibration of tension leg platform with tuned liquid column damper

The kinetic energy T of the vibration of tension leg platform with tuned column liquid damper is written [84, 112]:

$$T = T_{TLCD} + T_{structure} \tag{3.91}$$

$$T_{TLCD} = \rho_l A_v \frac{h}{L} \int_0^L \left[\left(\frac{\partial W(L,t)}{\partial t} \right)^2 + \left(\frac{\partial Y(t)}{\partial t} \right)^2 \right] dX + \rho_l A_h \frac{b}{L} \left[\int_0^L \left(\upsilon \frac{\partial Y(t)}{\partial t} + \frac{\partial W(L,t)}{\partial t} \right)^2 dX \right] \tag{3.92}$$

$$T_{structure} = \frac{\rho A}{2} \int_0^L \left[\left(\frac{\partial W(X,t)}{\partial t} \right)^2 + \left(\frac{\partial U(X,t)}{\partial t} \right)^2 \right] dX - \frac{\rho I}{2} \int_0^L \left(\frac{\partial^2 W(X,t)}{\partial X \partial t} \right)^2 dX \tag{3.93}$$

Finally one obtains

$$T = \rho_l A_v \frac{h}{L} \int_0^L \left[\left(\frac{\partial W(L,t)}{\partial t} \right)^2 + \left(\frac{\partial Y(t)}{\partial t} \right)^2 \right] dX + \rho_l A_h \frac{b}{L} \left[\int_0^L \left(\upsilon \frac{\partial Y(t)}{\partial t} + \frac{\partial W(L,t)}{\partial t} \right)^2 dX \right]$$
$$+ \frac{\rho A}{2} \int_0^L \left[\left(\frac{\partial W(X,t)}{\partial t} \right)^2 + \left(\frac{\partial U(X,t)}{\partial t} \right)^2 \right] dX - \frac{\rho I}{2} \int_0^L \left(\frac{\partial^2 W(X,t)}{\partial X \partial t} \right) dX$$

$$(3.94)$$

Simultaneously taking into account geometric nonlinearity, axial force action and potential energy of TLCD. The potential energy given by three paths: bending potential energy V_b, axial potential energy V_n and TLCD potential energy V_{TLCD} [111, 112].

$$V = V_b + V_n + V_{TLCD} \qquad (3.95)$$

$$V = \frac{1}{2} EI \int_0^L \left(\frac{\partial W(X,t)}{\partial X} \right)^2 dX + \frac{1}{2} EA \int_0^L \left(\frac{1}{2} \left(\frac{\partial W(X,t)}{\partial X} \right)^2 + \frac{\partial U(X,t)}{\partial X} \right)^2 dX$$
$$, \qquad + N_0 \frac{\rho A}{2} \int_0^L \left(\frac{\partial^2 W(X,t)}{\partial X^2} \right)^2 dX + \rho_l A_v g \frac{1}{L} \int_0^L \left(h^2 + (Y(t))^2 \right) dX$$

$$(3.96)$$

where ρ and ρ_l are the density of the structure and liquid respectively, A represents the cross-sectional area of the beam, A_v and A_b are the vertical and horizontal column cross-section area of the TLCD respectively, I is the moment of inertia, L is the beam length, h and b are the vertical and horizontal liquid length respectively, g is the gravitational acceleration, υ is the area ratio of the vertical column to the horizontal column of the TLCD , N_0 is the compressive axial force, EI and EA represent the flexural rigidity and axial stiffness, respectively. The non- conservative force Q is composed of three parts: energy consumption of the vibration of TLP, the dissipation force of the liquid and the external force, which can be formulated as

$$Q = - \left[\int_0^L c \frac{\partial W(X,t)}{\partial t} dX + \frac{1}{L} \frac{\rho_l A_h \xi \upsilon^2}{2} \int_0^L \left| \frac{\partial Y(t)}{\partial t} \right| \frac{\partial Y(t)}{\partial t} dX + \int_0^L f(X,Y,t) dX \right] \qquad (3.97)$$

where c is the damping coefficient of the TLP and ξ is the head loss coefficient.

Applying the Rayleigh beam theory and Lagrange's equations, the coupled transverse-longitudinal equations of the TLP and TLCD dynamical equation are given by the following set of equations:

$$\rho A \frac{\partial^2 W(X,t)}{\partial t^2} + \left(\rho_l A_v \frac{h}{L} + \rho_l A_h \frac{b}{L}\right) \frac{\partial^2 W(L,t)}{\partial t^2} + c\frac{\partial W(X,t)}{\partial t} + EI\frac{\partial^4 W(X,t)}{\partial X^4} - \rho I\frac{\partial^4 W(X,t)}{\partial X^2 \partial t^2}$$
$$-EA\frac{\partial}{\partial x}\left[\frac{\partial W(X,t)}{\partial X}\left(\frac{1}{2}\left(\frac{\partial W(X,t)}{\partial X}\right)^2 + \frac{\partial U(X,t)}{\partial X}\right)\right] - N_0\frac{\partial^2 W(X,t)}{\partial X^2} + \rho_l A_h \frac{b}{L}v\frac{\partial^2 Y}{\partial t^2} = f(X,Y,t)$$

(3.98)

$$\left(\rho_l A_v \frac{h}{L} + \rho_l A_h \frac{b}{L}v\right)\frac{\partial^2 y(t)}{\partial t^2} + \frac{2\rho_l A_v g}{L}y(t) + \frac{\rho_l A_h v^2}{2L}\xi\left|\frac{\partial y(t)}{\partial t}\right|\frac{\partial y(t)}{\partial t} = -\rho_l A_h \frac{b}{L}\frac{\partial^2 W(L,t)}{\partial t^2} \qquad (3.99)$$

$$\rho A \frac{\partial^2 U(X,t)}{\partial t^2} - EA\frac{\partial}{\partial x}\left[\left(\frac{1}{2}\left(\frac{\partial W(X,t)}{\partial X}\right)^2 + \frac{\partial U(X,t)}{\partial X}\right)\right] = 0 \qquad (3.100)$$

The boundary conditions are given by [84]

$$U(0,t) = U(L,t) = 0$$

$$W(0,t) = 0$$

$$EIW''(0,t) - kW'(0,t) = 0$$

(3.101)

$$EIW'''(L,t) - \rho I\left(\ddot{W}(L,t)\right)' - N_0 W'(L,t) - M_p\ddot{W}(L,t) = 0$$

Assuming that the radius of gyration r is small enough, the longitudinal inertia force is neglected [112] , Eq. (3.100) can be written as

$$e = \frac{\partial U(X,t)}{\partial X} + \frac{1}{2}\left(\frac{\partial W(X,t)}{\partial X}\right)^2 \qquad (3.102)$$

Using the following boundary conditions $U(0,t) = U(L,t) = 0$ and after some simplification it comes out the following equation

$$e = \frac{1}{2L} \int_0^L \left(\frac{\partial W(X,t)}{\partial X} \right)^2 dX \qquad (3.103)$$

One obtains the general nonlinear equations governing the behavior of the system (TLP+TLCD) is given by

$$\rho A \frac{\partial^2 W(X,t)}{\partial t^2} + \left(\rho_l A_v \frac{h}{L} + \rho_l A_h \frac{b}{L} \right) \frac{\partial^2 W(L,t)}{\partial t^2} + c \frac{\partial W(X,t)}{\partial t} + EI \frac{\partial^4 W(X,t)}{\partial X^4} - \rho I \frac{\partial^4 W(X,t)}{\partial X^2 \partial t^2}$$
$$- EA \left(\frac{1}{2L} \int_0^L \left(\frac{\partial W(X,t)}{\partial X} \right)^2 dX \right) \frac{\partial^2 W(X,t)}{\partial X^2} - N_0 \frac{\partial^2 W(X,t)}{\partial X^2} + \rho_l A_h \frac{b}{L} \upsilon \frac{\partial^2 Y(t)}{\partial t^2} = f(X,Y,t)$$
$$(3.104)$$

$$\left(\rho_l A_v \frac{h}{L} + \rho_l A_h \frac{b}{L} \upsilon \right) \frac{\partial^2 Y(t)}{\partial t^2} + 2 \frac{\rho_l A_v g}{L} Y(t) + \frac{\rho_l A_h \upsilon^2}{2L} \xi \left| \frac{\partial Y(t)}{\partial t} \right| \frac{\partial Y(t)}{\partial t} = -\rho_l A_h \frac{b}{L} \frac{\partial^2 W(L,t)}{\partial t^2}$$
$$(3.105)$$

Taking into account the following dimensionless variables and parameters and after some manipulations, the dimensionless nonlinear equations of the controlled system can be obtained as follows

$$w(x,\tau) = \frac{W(X,t)}{r}, \ x = \frac{X}{L}, \ \tau = \omega_0 t, \ \omega_0 = \frac{1}{L^2}\sqrt{\frac{EI}{\rho A}}, \ y(\tau) = \frac{Y(t)}{h}, \ \lambda = \frac{cL^2}{\sqrt{\rho AEI}},$$
$$P_0 = \frac{N_0 L^2}{EI}, \ \eta = \frac{\rho_l}{\rho AL}(A_v h + A_h b), \ c_p = \frac{\rho_l A_h bh\upsilon}{\rho ALr}, \ \lambda_2 = \frac{A_h h\upsilon^2 \xi}{2(A_v h + A_h b\upsilon)}$$
$$\omega_2^2 = \frac{2\rho A_v AgL^4}{EI(A_v h + A_h b\upsilon)}, \ c_q = \frac{A_h br}{(A_v h^2 + A_h bh\upsilon)}, \ \mu = \left(\frac{r}{L}\right)^2$$

$$\frac{\partial^2 w(x,\tau)}{\partial \tau^2} + \eta \frac{\partial^2 w(1,\tau)}{\partial \tau^2} + \lambda \frac{\partial w(x,\tau)}{\partial \tau} + \frac{\partial^4 w(x,\tau)}{\partial x^4} - \mu \frac{\partial^4 w(x,\tau)}{\partial x^2 \partial \tau^2}$$
$$- \frac{1}{2} \left(\int_0^1 \left(\frac{\partial w(x,\tau)}{\partial x} \right)^2 dx \right) \frac{\partial^2 w(x,\tau)}{\partial x^2} - P_0 \frac{\partial^2 w(x,\tau)}{\partial x^2} + c_p \frac{\partial^2 y(\tau)}{\partial \tau^2} = \frac{L^3}{EI} f(x,y,\tau) \qquad (3.106)$$

$$\frac{\partial^2 y(\tau)}{\partial \tau^2} + \omega_2^2 y(\tau) + \lambda_2 \left| \frac{\partial y(\tau)}{\partial \tau} \right| \frac{\partial y(\tau)}{\partial \tau} = -c_q \frac{\partial^2 w(1,\tau)}{\partial \tau^2} \qquad (3.107)$$

The dimensionless boundary condition given by

$$w\left(0, \tau\right) = 0$$

$$w''\left(0, \tau\right) - \frac{kL}{EI} w'\left(0, \tau\right) = 0$$

$$(3.108)$$

$$w'''\left(1, \tau\right) - \frac{\rho I \omega_0^2 L^2}{EI}\left(\ddot{w}\left(1, \tau\right)\right)' - \frac{N_0 L^2}{EI} w'\left(1, \tau\right) - \frac{M_p \omega_0^2 L^3}{EI} \ddot{w}\left(1, \tau\right) = 0$$

$$w''\left(1, \tau\right) = 0$$

3.4.1.3 Irregular sea waves excitation

According to Morison, the generalized transverse force on an oscillating cylindrical beam element in sea waves can be modelled as [41]:

$$f\left(X, Y, t\right) = C_d \rho_w r_o \left(V_Y\left(X, Y, t\right) - \dot{W}\left(X, t\right)\right) \left|V_Y\left(X, Y, t\right) - \dot{W}\left(X, t\right)\right|$$
$$+ C_M \pi r_0^2 \rho_w \dot{V}_Y\left(X, Y, t\right) - C_A \pi r_0^2 \rho_w \ddot{W}\left(X, t\right)$$

$$(3.109)$$

According to dimensionless parameters one obtains

$$f\left(x, y, \tau\right) = C_d \rho_w r_o \left(v_y\left(x, y, \tau\right) - \dot{w}\left(x, \tau\right)\right) \left|v_y\left(x, y, \tau\right) - \dot{w}\left(x, \tau\right)\right|$$
$$+ C_M \pi r_0^2 \rho_w \dot{v}_y\left(x, y, \tau\right) - C_A \pi r_0^2 \rho_w \ddot{w}\left(x, \tau\right)$$

$$(3.110)$$

where v_y and $\dot{v}_y$ are the dimensionless transverse velocity and acceleration of the water particles in the sea, respectively; x and y are the dimensionless position in the longitudinal and transverse direction of beam, respectively; C_d, C_M, and C_A are the coefficients of the drag, inertia forces of the beam and the added mass, respectively; ρ_w is the material density of the water; r_0 is the outer radius of the TLP. By assuming that longitudinal velocity of water particles are much bigger than longitudinal velocity of beam $V_y >> \dot{W}\left(X, t\right)$ at $Y = 0$, Eq.(3.110) can be simplified as [112]:

$$f\left(x, y, \tau\right) = C_d \rho_w r_o \left(v_y\left(x, y, \tau\right)\right) \left|v_y\left(x, y, \tau\right)\right| + C_M \pi r_0^2 \rho_w \dot{v}_y\left(x, y, \tau\right) - C_A \pi r_0^2 \rho_w \ddot{w}\left(x, \tau\right)$$

$$(3.111)$$

Taking into account the third term of Eq. (3.111) , Eq. (3.106) becomes

$$
\begin{aligned}
(1 + k_3) \frac{\partial^2 w(x,\tau)}{\partial \tau^2} + \eta \frac{\partial^2 w(1,\tau)}{\partial \tau^2} + \lambda \frac{\partial w(x,\tau)}{\partial \tau} + \frac{\partial^4 w(x,\tau)}{\partial x^4} - \mu \frac{\partial^4 w(x,\tau)}{\partial x^2 \partial \tau^2} \\
- \frac{1}{2} \left(\int_0^1 \left(\frac{\partial w(x,\tau)}{\partial x} \right)^2 dx \right) \frac{\partial^2 w(x,\tau)}{\partial x^2} - P_0 \frac{\partial^2 w(x,\tau)}{\partial x^2} + c_p \frac{\partial^2 y(\tau)}{\partial \tau^2} = \frac{L^3}{EI} f_1 (x, y, \tau)
\end{aligned}
\tag{3.112}
$$

with

$$
f_1 (x, y, \tau) = C_d \rho_w r_o (v_y (x, y, \tau)) |v_y (x, y, \tau)| + C_M \pi r_0^2 \rho_w \dot{v}_y (x, y, \tau)
\tag{3.113}
$$

$$
k_3 = \frac{C_A \pi r_0^2 \rho_w}{\rho A}
$$

The wave velocities are determined using random wave theory, and characterized by the Pierson-Moskowitz power spectrum, and converted to the time domain using Borgman's method [41, 43]: Based on Airy wave theory, irregular wave shape is determined by wave profile η defined in Eq. (3.114) as

$$
\eta (y, \tau) = \frac{H_s}{4} \sqrt{\frac{2}{N}} \sum_{n=1}^{N} \cos \left(\bar{k}_n y - \frac{\bar{\omega}_n}{\omega_0} \tau + \varphi_n \right)
\tag{3.114}
$$

Therefore, velocity and acceleration of water particles are computed by Eqs. (3.115) and (3.116) :

$$
V_y (x, y, \tau) = \frac{H_s}{4} \sqrt{\frac{2}{N}} \sum_{n=1}^{N} \bar{\omega}_n \frac{\cosh \bar{k}_n x}{\sinh \bar{k}_n d} \cos \left(\bar{k}_n y - \frac{\bar{\omega}_n}{\omega_0} \tau + \varphi_n \right)
\tag{3.115}
$$

$$
\dot{V}_y (x, y, \tau) = \frac{H_s}{4} \sqrt{\frac{2}{N}} \sum_{n=1}^{N} \bar{\omega}_n^2 \frac{\cosh \bar{k}_n x}{\sinh \bar{k}_n d} \sin \left(\bar{k}_n y - \frac{\bar{\omega}_n}{\omega_0} \tau + \varphi_n \right)
\tag{3.116}
$$

in which H_s ,N, $\bar{k}_n$ and $\bar{\omega}_n$ are significant wave height, number of frequency sample, *nth* wave number and *nth* angular frequency of the ocean wave motion, respectively; φ_n is a uniform random number between 0 and 2π ; d is the ocean depth.

$$
\bar{\omega}_n = \frac{\omega_n + \omega_{n-1}}{2}, \bar{k}_n = k (\bar{\omega}_n) , n = 1, \cdots , N
\tag{3.117}
$$

The frequency ω_0 is zero, ω_N and is chosen so that most of the area is contained between ω_0 and ω_N. The frequencies ω_0 to ω_N are chosen so that the area under the spectrum curve for each interval is equal [114]

3.4.1.4 Modal equation

In oder to reduce the partial differential equations to a set of ordinary differential equations, this to assess the dynamic behaviour response of the structural system, the general solution of the Eq. (3.106) and Eq. (3.107) can be written as separation variables of $q(\tau)$, which is the time dependent function and the shape function $\phi(x)$. The spatial function is obtained from Equation Eq. (3.106) without the term of nonlinearity, the wave excitation and the coupling term. Then, Eq. (3.106) is reduced to

$$\frac{\partial^2 w(x,\tau)}{\partial \tau^2} + \frac{\partial^4 w(x,\tau)}{\partial x^4} - \mu \frac{\partial^4 w(x,\tau)}{\partial x^2 \partial \tau^2} - P_0 \frac{\partial^2 w(x,\tau)}{\partial x^2} = 0 \qquad (3.118)$$

First, assume that $w(x,\tau)$ is separable so that one can write $w(x,\tau) = \phi(x) q(\tau)$. Then, the equation of motion becomes

$$\phi(x)\ddot{q}(\tau) + \phi''''(x) q(\tau) - \mu\phi''(x)\ddot{q}(\tau) - P_0\phi''(x) q(\tau) = 0 \qquad (3.119)$$

Assuming that $q(\tau)$ is harmonic with frequency ω such that $\ddot{q}(\tau) = -\omega^2 q(\tau)$ with solution $q(\tau) = a\cos\omega\tau + b\sin\omega\tau$, we can write Eq. (3.119) as

$$\phi''''(x) + (\mu\omega^2 - P_0)\phi''(x) - \omega^2\phi(x) = 0 \qquad (3.120)$$

The mode function for transverse vibration of the beam is expressed as

$$\phi(x) = d_1 \sin(\alpha x) + d_2 \cos(\alpha x) + d_3 \sinh(\beta x) + d_4 \cosh(\beta x) \qquad (3.121)$$

where α, β are given as follow

$$\alpha = \sqrt{\frac{(\mu\omega^2 - P_0) + \sqrt{(\mu\omega^2 - P_0)^2 + 4\omega^2}}{2}}, \quad \beta = \sqrt{\frac{-(\mu\omega^2 - P_0) + \sqrt{(\mu\omega^2 - P_0)^2 + 4\omega^2}}{2}} \qquad (3.122)$$

After using the boundary conditions in Eq.(3.108), we obtain four simultaneous equations which can be written in the matrix form as

$$\begin{vmatrix} 0 & 1 & 0 & 1 \\ -\frac{KL}{EI}\alpha & -\alpha^2 & -\frac{KL}{EI}\beta & \beta^2 \\ -\alpha^2\sin\alpha & -\alpha^2\cos\alpha & \beta^2\sinh\beta & \beta^2\cosh\beta \\ A_1 & A_2 & A_3 & A_4 \end{vmatrix} \begin{bmatrix} d_1 \\ d_2 \\ d_3 \\ d_4 \end{bmatrix} = \begin{bmatrix} 0 \\ 0 \\ 0 \\ 0 \end{bmatrix} \qquad (3.123)$$

where

$$A_1 = -\alpha^3 \cos\alpha + \left(\left(\tfrac{r}{L}\right)^2 \alpha^2 \beta^2 - \tfrac{N_0 L^2}{EI}\right) \alpha \cos\alpha + \tfrac{M_p}{\rho AL} \omega^2 \alpha^2 \sin\alpha$$
$$A_2 = \alpha^3 \sin\alpha - \left(\left(\tfrac{r}{L}\right)^2 \alpha^2 \beta^2 - \tfrac{N_0 L^2}{EI}\right) \alpha \sin\alpha + \tfrac{M_p}{\rho AL} \omega^2 \alpha^2 \cos\alpha$$

$$A_3 = \beta^3 \cosh\beta + \left(\left(\tfrac{r}{L}\right)^2 \alpha^2 \beta^2 - \tfrac{N_0 L^2}{EI}\right) \beta \cosh\beta + \tfrac{M_p}{\rho AL} \omega^2 \beta^2 \sinh\beta$$

$$A_4 = \beta^3 \sinh\beta + \left(\left(\tfrac{r}{L}\right)^2 \alpha^2 \beta^2 - \tfrac{N_0 L^2}{EI}\right) \beta \sinh\beta + \tfrac{M_p}{\rho AL} \omega^2 \beta^2 \cosh\beta$$

In order to have a non-trivial solution, the determinant of the matrix in Eq. (3.123) has to be zero. The first transversability equation is given by

$$A_1 \left(\tfrac{KL}{EI}\beta^3 \sinh\beta + \beta^4 \sinh\beta + \alpha^2\beta^2 \cosh\beta - \tfrac{KL}{EI}\alpha^2\beta \cos\alpha\right) - A_2 \left(\tfrac{KL}{EI}\alpha\beta^2 \sinh\beta + \tfrac{KL}{EI}\alpha^2\beta \sin\alpha\right)$$
$$+ A_3 \left(-\tfrac{KL}{EI}\alpha\beta^2 \cosh\beta + \alpha^2\beta^2 \sin\alpha - \tfrac{KL}{EI}\alpha^3 \sin\alpha + \alpha^4 \sin\alpha\right) + A_4 \left(\tfrac{KL}{EI}\alpha\beta^2 \sinh\beta + \tfrac{KL}{EI}\alpha^2\beta \sin\alpha\right) = 0$$

$$(3.124)$$

The second transversability equation is given by

$$\beta = \sqrt{\tfrac{\alpha^2 + P_0}{1 + \mu\alpha^2}} \qquad (3.125)$$

Finally the constants d_1, d_2, d_3, d_4 can be expressed in the terms of d_1, and they are given by the following relations

$$d_2 = \left(\frac{-\left(\alpha^2 \sin\alpha + \alpha\beta \sinh\beta\right)}{\alpha^2 \cos\alpha + \beta^2 \cosh\beta + \frac{EI}{KL}\beta(\alpha^2+\beta^2)\sinh\beta}\right) d_1$$

$$d_3 = \left(-\frac{\alpha}{\beta} + \frac{EI}{KL}\left(\frac{\alpha^2+\beta^2}{\beta}\right) \frac{\left(\alpha^2 \sin\alpha + \alpha\beta \sinh\beta\right)}{\alpha^2 \cos\alpha + \beta^2 \cosh\beta + \frac{EI}{KL}\beta(\alpha^2+\beta^2)\sinh\beta}\right) d_1$$

$$d_4 = \left(\frac{\left(\alpha^2 \sin\alpha + \alpha\beta \sinh\beta\right)}{\alpha^2 \cos\alpha + \beta^2 \cosh\beta + \frac{EI}{KL}\beta(\alpha^2+\beta^2)\sinh\beta}\right) d_1$$

The value of d_1 is obtained such that the eigenfunctions $\phi(x)$ are normalized $\int_0^1 \phi_n^2(x)dx = 1$. To reduce the partial differential equations to a set of ordinary differential equations,

the general solution of $w\left(x,\tau\right)$ can be written as separation variables of $q\left(\tau\right)$ which is the time dependent functions by the shape functions $\phi\left(x\right)$.

$$w\left(x,\tau\right) = \sum_{n=1}^{\infty} \phi_n\left(x\right) q_n\left(\tau\right) \tag{3.126}$$

Substituting the mode decomposition of Eq. (3.126) into Eqs. (3.106) and (3.107), multiplying by the spatial expression, integrating from 0 to 1 and considering the first vibration mode, one obtains the modal forms of above equations, that are defined as follow

$$\begin{cases} \ddot{q}\left(\tau\right) + \lambda_1 \dot{q}\left(\tau\right) + \left(\omega_1^2 - p_0\right) q\left(\tau\right) + \gamma q^3\left(\tau\right) + c_{p_1} \ddot{y}\left(\tau\right) = f\left(\tau\right) \\ \\ \ddot{y}\left(\tau\right) + \lambda_2 \left|\dot{y}\left(\tau\right)\right| \dot{y}\left(\tau\right) + \omega_2^2 y\left(\tau\right) = -c_{q_1} \ddot{q}\left(\tau\right) \end{cases} \tag{3.127}$$

with

$$\lambda_1 = \frac{\lambda \int_0^1 \phi^2(x)dx}{(1+k_3)\int_0^1 \phi^2(x)dx - \mu \int_0^1 \phi''(x)\phi(x)dx + \eta\phi(1)\int_0^1 \phi(x)dx}$$

$$\omega_1^2 = \frac{\int_0^1 \phi''''(x)\phi(x)dx}{(1+k_3)\int_0^1 \phi^2(x)dx - \mu \int_0^1 \phi''(x)\phi(x)dx + \eta\phi(1)\int_0^1 \phi(x)dx}$$

$$p_0 = \frac{P_0 \int_0^1 \phi''(x)\phi(x)dx}{(1+k_3)\int_0^1 \phi^2(x)dx - \mu \int_0^1 \phi''(x)\phi(x)dx + \eta\phi(1)\int_0^1 \phi(x)dx}$$

$$c_{p_1} = \frac{c_p \int_0^1 \phi(x)dx}{(1+k_3)\int_0^1 \phi^2(x)dx - \mu \int_0^1 \phi''(x)\phi(x)dx + \eta\phi(1)\int_0^1 \phi(x)dx}$$

$$c_{q_1} = \frac{c_q \phi(1) \int_0^1 \phi(x)dx}{\int_0^1 \phi(x)dx} \quad , \quad \gamma = \frac{-\frac{1}{2}\int_0^1 \left(\int_0^1 \phi'^2(x)dx\right)\phi''(x)\phi(x)dx}{(1+k_3)\int_0^1 \phi^2(x)dx - \mu \int_0^1 \phi''(x)\phi(x)dx + \eta\phi(1)\int_0^1 \phi(x)dx}$$

$$f\left(\tau\right) = \frac{\frac{L^4}{EIr} f_1(x,y,\tau)}{(1+k_3)\int_0^1 \phi^2(x)dx - \mu \int_0^1 \phi''(x)\phi(x)dx + \eta\phi(1)\int_0^1 \phi(x)dx}$$

c_{p_1} and c_{q_1} represent the control gain parameters.

3.4.2   Linear stability analysis

Following the classical local stability analysis of Lyapunov, the fixed points of the system are first examined. Consider the system of Eq. (3.127), the fixed points are $(0, 0, 0, 0)$, $\left(\pm\sqrt{-\frac{\omega_1^2 - p_0}{\gamma}}, 0, 0, 0\right)$. The characteristic equation is given as follows

$$s^4 + a_0 s^3 + a_1 s^2 + a_2 s + a_3 = 0 \tag{3.128}$$

with

$$a_0 = \frac{\lambda_1 + 2\varepsilon\lambda_2 v_0}{1 - c_{p_1} c_{q_1}}, \; a_1 = \frac{2\varepsilon\lambda_1\lambda_2 v_0 + \omega_1^2 + 3\gamma q_0^2 - p_0 + \omega_2^2}{1 - c_{p_1} c_{q_1}}, \; a_2 = \frac{2\varepsilon\lambda_1\lambda_2 v_0\left(\omega_1^2 + 3\gamma q_0^2 - p_0 + \omega_2^2\right) + \lambda_1\omega_2^2}{1 - c_{p_1} c_{q_1}}, \; a_3 = \frac{\left(\omega_1^2 + 3\gamma q_0^2 - p_0\right)\omega_2^2}{1 - c_{p_1} c_{q_1}}$$

From the classical local stability analysis of Lyapunov, it is known that the fixed points are stable if the real parts of the roots of the characteristics equation are all negative. Otherwise (if at least one root has a positive real part), the fixed points are unstable. Using Routh-Hurwitz criterion, for the sign of the real part of roots, we obtain that the real parts of the roots are negative provided that all the coefficients a_0, a_1, a_2 and a_3 are positive and that all the determinants $\Delta_1 = a_0 a_1 - a_2$ and $\Delta_2 = a_0\left(a_1 a_2 - a_0 a_3\right) - a_2^2$ are also positive. Knowing that all these coefficients are positive and considering the case where the parameters c_{p_1} and c_{q_1} are also positive, the above analysis leads to the following condition for the control for the stability of the fixed points for the system under TLCD controller

$$0 < c_{p_1} c_{q_1} < 1 \tag{3.129}$$

This condition allows us to obtain the following stability diagram shown in Fig. 3.35 where the white region represent the stable region and the blue one the unstable.
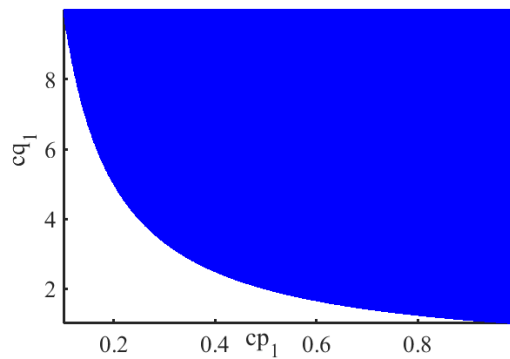
Figure 3.35: Stability boundary in the control parameter space $c_{p_1} - c_{q_1}$.

3.4.3 Numerical analysis of the modal equation

In this section, the dynamical states of the TLP are explored, and by varying the parameters of the TLCD the effect of the control system on general behavior of the TLP is also investigated. The numerical simulations are carried out through the fourth-order Runge Kutta scheme. Properties of the beam and characteristics of the sea waves which are used for numerical purpose are given in Tables 3.4, 3.5 and 3.6 [115, 116].

Table 3.4: Physical properties of the TLP.

Parameter name	Symbol	Value
tendons length (m)	l	200
tendon outer raduis (m)	r_0	0.3048
tendon inner raduis (m)	r_i	0.1112
tendon density (kg/m^3)	ρ	7800
young's modulus of a tendon (Gpa)	E	204
inertial coefficient of beam	C_M	1.7
drag coefficient of beam	C_d	0.8
inertial coefficient of added mass	C_m	1
hull mass, (kg)	M_p	210^7
water density (kg/m^3)	ρ_w	1025

Fig. 3.36 shows the irregular wave excitation versus dimensionless time respectively. One observe that, increase of the number of frequency sample N generates several harmonics on the wave excitation.

Fig. 3.37 shows the response of the TLP without TLCD controller in time domain under different values of number of frequency sample N. It is found that the increase of the number of frequency sample increases both the response amplitude of the TLP and the range of frequencies.
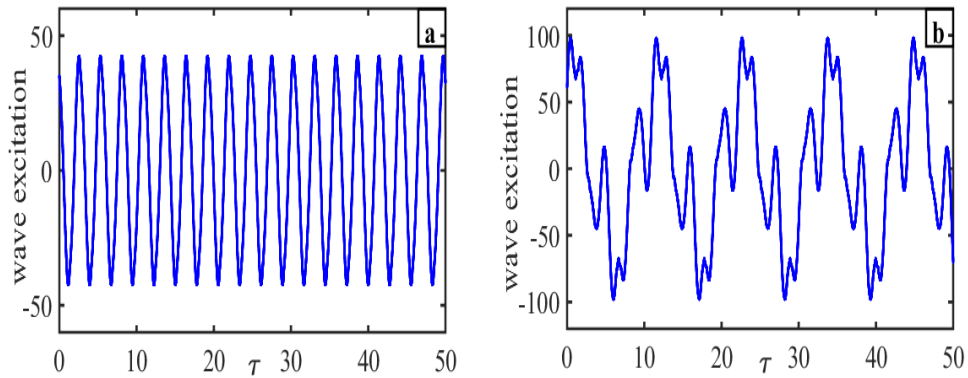
Figure 3.36: Sea wave acting on the TLP with parameters defined in Tables 3.4, 3.5 for $H_s = 3.5m$. a) $N = 5$, b) $N = 15$
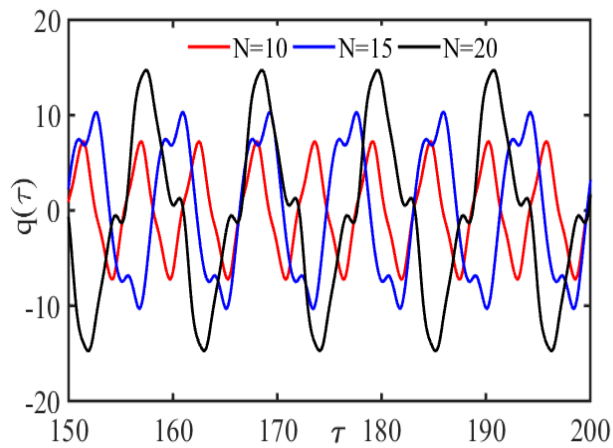
Figure 3.37: Vibration response of the TLP without TLCD controller in time domain under different values of number of frequency sample N with parameters defined in Tables 3.4, 3.5 for $H_s = 3.5m$.

Table 3.5: Physical properties of the simplified model.

Parameter name	Symbol	Value
mass per unit length of the beam	ρA (kg/m)	334.9
transverse Rayleigh beam coefficient	ρI $(kg.m)$	151.3
axial stiffness of the beam	EA (kg/ms^2)	$9.52.10^9$
flexural rigidity of the beam	EI (Nm^2)	$4.18.10^9$
compressive axial force	N_0 (N)	$1.8.10^5$
damping coefficient of the beam	c (Ns/m)	360

Fig. 3.38 and Fig. 3.39 illustrate the effect of the controller on the displacement and velocity of the TLP with different values of the number of frequency sample N. Fig. 3.38 shows that the vibrations caused by the sea wave excitation are reduced when the structure is controlled by a TLCD device. Fig. 3.39 shows that the velocity of the TLP decreases, when the structure is subjected to the action of the control device. As depicted in those figures, the action of the TLCD controller also contributes to the suppression of the complex motions observed as the number of frequency sample N increases. This shows that the TLCD device acts efficiently on the dynamics response of the structure.
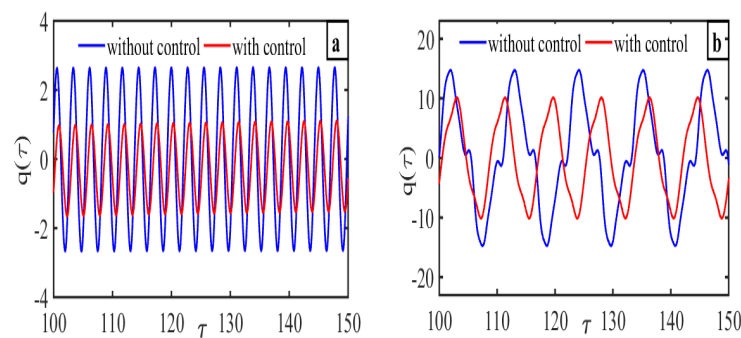
Figure 3.38: Vibration responses of the beam in time domain with parameters defined in Tables 3.4, 3.5 and 3.6 for $H_s = 3.5m$. a) $N = 5$, b) $N = 15$
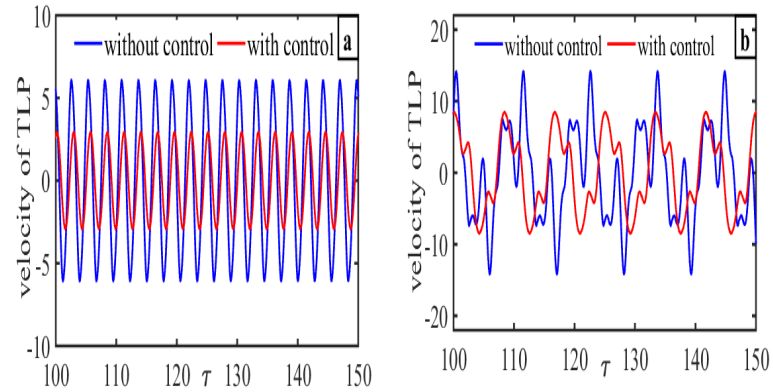
Figure 3.39: The curves of velocities of TLP versus the time with parameters defined in Tables 3.4, 3.5 and 3.6 for $H_s = 3.5m$. a) $N = 5$, b) $N = 15$
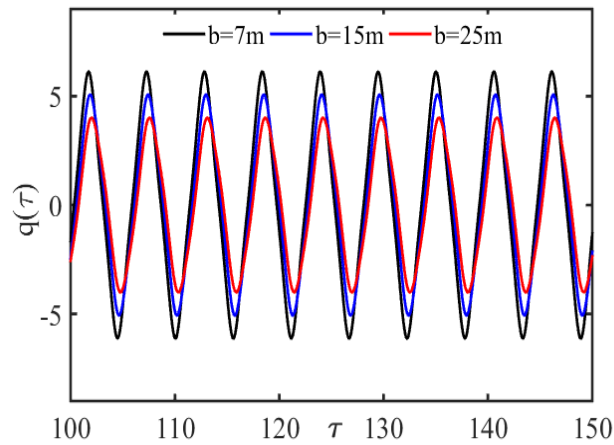
Figure 3.40: Vibration response of the TLP with TLCD controller in time domain for different horizontal liquid length of the TLCD with parameters defined in Tables 3.4, 3.5 and 3.6 for $N{=}10$ $H_s = 3.5m$.

Table 3.6: Physical properties of the TLCD.

Parameter name	Symbol	Value
vertical column cross-section (m^2)	A_v	10
horizontal column cross-section, (m^2)	A_v	10
vertical liquid length m	h	4
horizontal liquid length (m)	b	15
density of the liquid kg/m^3	ρ_l	1000
area ratio of the vertical column to the horizontal column	υ	1
Head loss coefficient	ξ	500
Acceleration of gravity (m/s^2)	g	9.81

Fig. 3.40 represents the influence of the horizontal liquid length of the TLCD on the response of TLP. This figure allows to observe that the increase of the horizontal liquid length of the TLCD results to decrease the response of the system. Fig. 3.41 displays the peak RMS versus the horizontal liquid column of TLCD. It is observed from this figure that the increase of this horizontal liquid column length affects the performance of tuned liquid column damper in reducing the amplitude response of the structure. This result confirms the observation made in the Fig. 3.40. It is important to note that the choice of the parameters of the TLCD is done such as the control device cannot increase the mechanical energy in the structural system. In order words the control device should reinforce the stability of the structure in order to avoid its premature destruction. Fig. 3.42 illustrated the peak RMS versus the head loss coefficient of TLCD. It is found that for $0 < \xi < 850$ the amplitude of TLP decreases and for $850 < \xi < 4000$, it increases. It appears that is exists and optimal value of the head loss coefficient ($\xi = 850$). It is also noticed that, for the value of ξ greater than 2700, the control is no longer efficient. One concludes that, by making a good choice of the head loss coefficient results to reduce the vibration response of the structure.
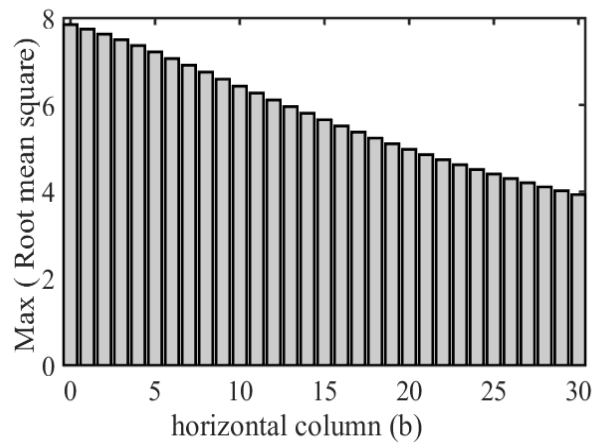
Figure 3.41: Root square response versus horizontal liquid column of TLCD length of the TLCD with parameters defined in Tables 3.4, 3.5 and 3.6 for N=10, $H_s = 3.5m$.
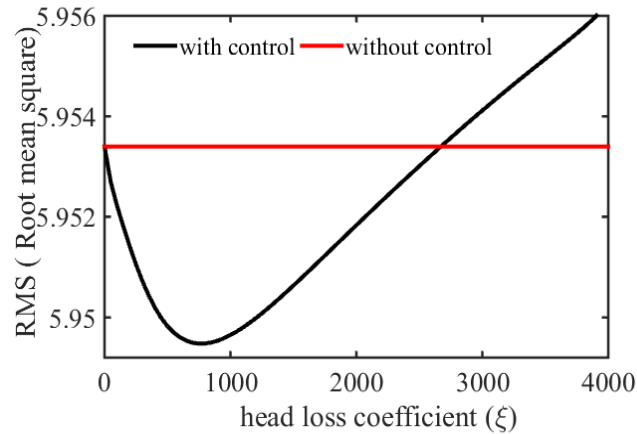
Figure 3.42: Root square response versus head loss coefficient with parameters defined in Tables 3.4, 3.5 and 3.6 for N=10, $H_s = 3.5m$.

3.4.4   Conclusion

The present chapter has presented the results obtained in this thesis work. We firstly modelled the TLP by the full partial differential equation that we have thereafter reduced to the nonlinear ordinary differential equation. the effect of the time-delay on the stability of the structure have been analyzed. Results of the analysis shown, that increase of the value of time-delay contributes to reduce the stability area. Secondly a new nonlinear viscoelastic model describing the surge movement of tension leg platform is presented. The effect of main parameters, namely: number of tendons, the order of the fractional viscoelastic material that constitutes the tendon and the tendon viscosity coefficient on the amplitude as well as the appearance of horseshoe chaos of TLP have been analyzed.The result shown that, the amplitude of TLP is affected by the number of tendons, the fractional order derivative and the tendon viscosity coefficient and the horseshoes chaos decreases and disappears as these parameters increase. Thirdly the Rayleigh beam approach is used to develop mathematical formulation for dynamic analysis of the compliant offshore structure taking into account the TLCD controller. The influence of the TLCD on the dynamic responses of TLP is analyzed. The results obtained shown that, a passive structural control device, i.e. tuned liquid column damper is a good candidate to cancel the vibration on the TLP structure subjected under irregular sea wave excitation.

General Conclusion

This dissertation has dealt with an analysis of the dynamic behavior and vibration control of an offsohre platform excited by the regular and irregular wave. Specific analytical and numerical analysis methods have been formulated to evaluate the response of the structure. The main results obtained in this work are summarized as follows :

In the first chapter the review of the literature on the types of offshore platforms as well as their importance in the exploration, drilling, production, storage and transportion of the ocean oil and/or gas resources in different depths is done. Then we introduced the various types of solicitation to which platforms are submitted. Finally, the derivation of the equations of motion of beam models and the vibratory control of the mechanical are presented. These beam models and precisely the Rayleigh beam model as well as the rigid model are used to model the tendons of a TLP.

In the second chapter, methods and techniques used to solve the problematic of the thesis have been described. Firstly the analytical methods has been presented, such as the Galerkin method used to transform a problem of the PDEs into a set of ODEs, the multiple scales method to solve the nonlinear ODEs with the time delay, the classical averaging technique and harmonic balance method to approach the nonlinear ODEs, Melnikov's method to predict Smale horseshoe type chaos, Routh-Hurwitz criterion to give the decision on the stability of the non-trivial steady-states solutions of the nonlinear ODEs and the D-subdivision method to investigate through linear stability of delay differential equations. Finally, numerical methods have been presented, such as the RK4 for the ODEs, the RK4 for the DDEs, the Newton-Leipnik and the A-B-M predictor-corrector schemes to integrate the nonlinear FDEs, the bisection method to solve complex or non-trivial polynomial equations.

The third chapter was devoted to the presentation and discussion of the results obtained in the thesis.

- Firstly, the effect of the delay between the detection of vibration and the action of tendons on the dynamics response of tension leg platform (TLP) under sea waves excitation was analyse. An analytical and numerical solution for the dynamic response of a TLP under sea wave excitation are presented. The TLP is modeled by the full partial differential equation that we have thereafter reduced to the nonlinear

ordinary differential equation. The effect of tendon on the stability of the structure have been analyzed. Results of the analysis shown that increase of the value of time-delay contributes to reduce the stability area. Then the effect of time-delay on the primary, secondary, superharmonic, subharmoncic and combination resonance state has been illustred. The analysis leads us to the conclusion that increasing the time-delay will increase the amplitude response in the case of the primary and secondary resonaces, but is without effects on the superharmonic, subharmonic and combination resonants states. One also analysed the effect of the natural frequency on the amplitude response. It has been found that the amplitude of oscillation decreases by increasing the natural frequency, this for all types of resonant states, which allows to cancel the time-delay effect in the case of primary and secondary resonances.

- In the second set of result, we have analysed the surge movement of tension leg platform under regular sea wave excitation. We have supposed that, the tendons exhibit a nonlinear viscoelastic behavior and fractional properties. The TLP is modeled by the nonlinear ordinary differential equation. Then the averaging method has been used to evaluate the effect of different parameters, namely : fractional order, tendon viscosity coefficient, number of tendons on the vibration amplitude of the tendon leg platform and on its stability. It was observed that as the order of the fractional derivative increases the amplitude response of the TLP decreases. The increase of the fractional order derivative also contributes to decrease the unstable range of amplitude. Nevertheless, beyond a certain value of the fractional parameter ($\alpha \in (0.65, 1)$), we have rather observed an increase in amplitude. It was also observed that, the amplitude response of tension leg platform is relevantly reduced and the domain of the unstable solutions also decreases when the number of tendons increases. On the basis of the Melnikov method, we have demonstrated that increase the number of tendons, the tendon viscosity coeffcient and fractional derivative can be contributed to enlarge de regular domain.

- Finally, we have used TLCD as control device to reduce vibration on a compliant offshore under irregular sea wave excitation. The effect of TLCD device on the

stability of the structure has been analyzed, along with the dynamic responses of the structure. The influence of different parameters on the dynamics response of the system on the control strategy has been presented. The results of the analysis show that increase the number of frequency sample generates several harmonics on the dynamic response of the structure. When the horizontal liquid length of the TLCD becomes large, the controller becomes more efficient. The optimum head loss coefficient is obtained to minimize the vibration response of the structure.

In this thesis, some of the results have opened interesting perspectives for future investigations. In this sense, it would be interesting for us to study the dynamics of TLPs taking into account the 3-DOF or 6-DOF. It will also be interesting to carry out an experimental study in order to validate the theoretical results obtained.

Bibliography

Bibliography

[1] Voditel SS (1985) Dynamic analysis of offshore structures *Department of Earthquake Engineering University of Roorkee* (India).

[2] Adrezin R, Bar-Avi P, BenaroyaH (1996) Dynamic response of compliant offshore structures: review. *J. of Aerospace Eng.* 9(4):114-31.

[3] Adrezin R, Benaroya H (1999) Non-linear stochastic dynamics of tension leg platforms. *J. of Sound and Vib.* 220:27-65.

[4] Adrezin R, Benaroya H. (1999) Response of a tension leg platform to stochastic wave forces. *Prob. Eng. and Mech.* 14:3-17.

[5] Taflanidis AA, Vetter C, Loukogeorgaki E (2013) Impact of modeling and excitation uncertainties on operational and structural reliability of tension leg platforms. *Appl. Ocean Res.* 43:131-147.

[6] Yigit AS, Christoforou AP (1996) Coupled axial and transverse vibrations of oilwell drillstrings. *J. of sound and Vib.* 195:6172721.

[7] Patel MH, Park HI (1991) Dynamics of tension leg platform tethers at low tension. Part I-Mathieu stability at large parameters. *Marine struct.* 4:257-273.

[8] Mohammad RT, Ali A (2021) Sensitivity analysis of methods in determination of offshore jacket structures levels sitiffness. *J. Mar. sci. Technol.*

[9] Mohammad RT, Rahim S (2018) Pertubation nonlinear response of tension leg platform under regular wave excitation. *J. Ma.r sci. Technol.* 23:132-140.

[10] Ou J, Long X, Li QS, Xiao YQ (2007) Vibration control of steel jacket offshore platform structures with damping isolation systems. *Eng. Struct.* 29(7):1525-1538.

[11] Shenoi J, Xiong A (2016) A review of vibration control methods for marine offshore structures. *Ocean Eng.* 127:279-297.

[12] Soong TT, Dargush GF (1997) Passive Energy Dissipation Systems in Structural Engineering. *Wiley, Buffalo.*

[13] Yao JT (1972) Concept of structural control.*J. Struct. Div.* 98(7):1567-1574.

[14] Korkmaz S (2011) A review of active structural control: challenges for engineering informatics. *Comput. Struct.* 89:23-24.

[15] Lee H.H (1997) Stochastic analysis for offshore structures with added mechanical dampers. *Ocean Eng.* 24(5):817-834.

[16] Li H, Wang S, Ji C (2002) Semi-active control of waveinduced vibration for offshore platforms by use of MR damper. *China Ocean Eng.* 16(1):33-40.

[17] Abdel-Rohman M (1996) Structural control of a steel jacket platform. *Struct. Eng. Mech.* 4(2): 125-138.

[18] API-RP 2A-WSD (2000) Recommended practice for planning, designing and constructing fixed offshore platforms. *American Petroleum Institute* Washington, D.C.

[19] Tromans P, Swan C, Masterton S (2006) Nonlinear potential flow forcing: the ringing of concrete gravity based structures.*Research Report No. 468, Ocean Wave Engineering Ltd, Health Safety Executive Publication* Norwich, UK.

[20] Hoeg K (1976) Foundation engineering for fixed offshore structures. *In: Proceedings first international conference behaviour of offshore structures* 1:39-69.

[21] Hove K, Foss I (1974) Quality assurance for offshore concrete gravity structures. *In: In: Proceedings of offshore technology conference* Paper No. 2113.

[22] Young AG, Kraft LM, Focht JA (1975) Geotechnical considerations in foundation design of offshore gravity structures. *In: Proceedings of offshore technology conference* Paper No. 2371.

[23] Chandrasekaran S, Madhavi N (2015a) Estimation of force reduction on ocean structures with perforated members. *In: Proceedings of 34th international conference on ocean, offshore and arctic engineering* (OMAE2015), St. John's, NL, Canada, 31 May 5 June 2015, OMAE2015-41153.

[24] Chandrasekaran S, Madhavi N (2015b) Flow field around a outer perforated circular cylinder under regular waves: numerical study. *Int J Marine Syst Ocean Technol.* doi:10.1007/s40868-015-0008-1.

[25] Boaghe OM, Billings SA, Stansby PK (1998) Spectral analysis for non-linear wave forces. *J. Appl. Ocean Res.* 20:199-212.

[26] Chandrasekaran S, Madhavi N, Natarajan C (2014) Variations of hydrodynamic characteristics with the perforated cylinder. *In: Proceedings of 33rd international conference on ocean, offshore and arctic engineering* OMAE 8-13 2014 June , San Francisco, USA.

[27] Stansberg CT, Ormberg H, Oritsland O (2002) Challenges in deep water experiments: hybrid approach. *J. Offshore Mech. Arctic Eng.* 124:90-96.

[28] Mather A (2000) Offshore engineering: an introduction, 2nd edn. *Witherby Co Ltd.* London.

[29] Moe G, Verley RLP (1980) Hydrodynamic damping of offshore structures in wave and currents. *In: Offshore technology conference, 12th annual OTC, Houston, Texas* pp.37-44.

[30] Choi HS, Lou Jack YK (1991) Nonlinear behavior of an articulated offshore loading platform. *Appl. Ocean Res.* 13(2):63-74.

[31] Chandrasekaran S, Pannerselvam R (2009) Offshore structures: materials, analysis, design and construction. *In: Proceedings of short course on offshore structures and materials* IITM, Chennai, 14-18 Dec, pp.156.

[32] Chandrasekaran S, Bhaskar K, Hashim M (2010a) Experimental study on dynamic response behavior of multi-legged articulated tower. *In: Proceedings of 29th international conference on ocean, offshore and arctic engineering* OMAE 6-11 June 2010 Shanghai, China.

[33] Chandrasekaran S, Bhaskar K, Harilal Lino Brijit R (2010b) Dynamic response behavior of multi-legged articulated tower with and without TMD. *In: Proceedings of international conference of marine technology MARTEC-2010, 11-12 Dec, Dhaka, Bangladesh* pp.131-136.

[34] Zeng X et al (2007) Parametric studies of tension leg platform with large amplitude motions. *In: Proceedings of 17th international offshore and polar engineering conference, Lisbon, Portugal* pp.202-209.

[35] Chandrasekaran S, Jain AK (2002a) Dynamic behavior of square and triangular offshore tension leg platforms under regular wave loads. *Ocean Eng.* 29(3):279-313.

[36] Chandrasekaran S, Jain AK (2002b) Triangular con?guration tension leg platform behavior under random sea wave loads. Ocean Eng 29(15):1895-1928.

[37] Basim MB, Johnson C, Philip J, Roesset M (1996) Implication of tendon modeling on nonlinear response of TLP. *J. Struct. Eng.* 122(2):142-149.

[38] Kawanishi T, Ohashi S, Takamura H, Koboyashi H (1993) Earthquake response of tension leg platform under unbalanced initial tension. *Proc ISOPE* Singapore:319-325.

[39] Witz JA, Patel MH, Harrison JH (1986) On the hydrodynamics of semisubmersibles with articulated members. *Proc. Roy. Soc. London Ser. A Math. Phys. Sci.* 403:81-109.

[40] Leffler WL, Pattarozzi R, Sterling G (2011) Deep-water petroleum: exploration and production. *Pennwell Corp.* Oklahoma, pp 350.

[41] Morison JR, O'Brien MP, Johnson JW, Schaaf SA (1950) The force exerted by surface waves on piles, *Pet. Trans. AIME* 189:149-57.

[42] Ivan Young R (2017) Rgular, irregular waves and the wave spectrum. *wiley*

[43] Gadagi MM, Benaroya H (2006) Dynamic response of an axially loaded tendon of a tension leg platform. *J. Sound. Vib.* 29:38-58.

[44] S. Chakrabarti (1987) Hydrodynamics of offshore structures. *Comput. Mech. Pub.*

[45] Dennis M, Pierson WJ (1953) On the motions of ships in confused seas. *Transactions, society of Naval Architects and Marine Eng.* 61:280-357.

[46] Love A (1927) A Treatise on the mathematical theory of elasticity. Dover publications, Inc.

[47] Benaroya H (1998) Mechanical Vibration. Prentice Hall, Inc.

[48] Timoshenko S (1921) On the correction for shear of the differential equation for transverse vibrations of bars of uniform cross-section. *Philosophical Magazine* 41:744.

[49] Timoshenko S (1922) On the transverse vibration of bars of uniform cross-section. *Philosophical Magazine* 43:125.

[50] Kabir S, Hüdaverdi T (2018) Tension leg platforms : an overview of planning, design, construction and installation. *Academic Research Int.* Vol. 9(2)

[51] Sadeghi K (2007) An overview of design, analysis, construction and installation of offshore petroleum platforms suitable for Cyprus oil/gas fields. *GAU Journal of Soc. Applied Sciences.* 2(4):1-16.

[52] Sadegh, K (2008). Significant guidance for design and construction of marine and offshore structure. *GAU Journal of Soc. Applied Sciences.* 4(7):67-92.

[53] Sakai F, Takeda S and Tamaki T (1989). Tuned liquid column damper-New type device for suppression of building vibrations. *In: Proceedings of the International Conference on Highrise Buildings.* Nanjing, China, 25-27th March 1989

[54] Lee HH, Wong SH and Lee RS (2005) Response mitigation on the offshore floating platform system with tuned liquid column damper. *Ocean Eng.* 33(8-9):1118-1142.

[55] Venkateswara RK (2013) Experimental and numerical studies on tuned liquid damper. *Master, National Institute of Technology Rourkela.*

[56] Tanmoy C, Subrata C (2014) Vibration mitigation of structures subjected torandom wave forces by liquid column dampers. *Ocean Eng.* 87:151-161.

[57] Wu JC, Shih MH and Lin YY (2005) Design guidelines for tuned liquid column damper for structures responding to Wind. *Eng. Struct.* 27(13):1893-1905.

[58] Thomsen JJ (2013) Vibrations and stability: advanced theory, analysis, and tools. Springer Science Business Media, 99.

[59] Timoshenko SP, Young DH, Weaver W (1967) Vibrations in engineering. *Mashinostroenie* Moscow.

[60] Bogoliubov NN, Mitropolsky YA (1961) Asymptotic Methods in the Theory of Nonlinear Oscillations. *Gordon and Breach* New York.

[61] Kargarnovin MH, Younesian D (2004) Dynamics of timoshenko beams on pasternak foundation under moving load. *Mech. Res. Commun.* 31:713-23.

[62] Fryba L (1999) Vibration of solids and structures under moving loads. London: Thomas Telford.

[63] Wang YH, Tham LG, Cheung YK (2005) Beams and plates on elastic foundations: a review. *Progr. Struct. Eng. Mater* 7(4):174-82.

[64] Beskou ND, Theodorakopoulos DD (2011) Dynamic effects of moving loads on road pavements: a review. *Soil Dyn. Earthq. Eng.* 31:547-67.

[65] Simon CP, Blume L (1994) Mathematics for economists. W.W. Norton and company New York.

[66] Hayashi C (1964) Nonlinear oscillations in physical systems. *McGraw-Hill* New York.

[67] Michiels W, Niculescu SL (2007) Stability and stabilization of time-delay systems : an eigenvalue-based approach. *SIAM.*

[68] Melnikov VK (1963) On the stability of the center for time periodic perturbations. *Trans. Moscow Math.* 12:1-57.

[69] Holmes P (1979) A nonlinear oscillator with a strange attractor. *Philos. Trans. R. Soc.* A292:419-418.

[70] Wiggins S (1990) Introduction to Applied Nonlinear Dynamical Systems and Chaos. *Springer Verlag New York.*

[71] Guckenheimer J, Holmes P (1983) Nonlinear Oscillations, Dynamical Systems, and Bifurcations of Vector Fields. *Springer-Verlag New York.*

[72] William HP, Teukolsky SA, William TV, Brian PF (1992) Numerical recipes in c++. *The art of scientific comput.* 2:1002.

[73] Steven HS (2018) Nonlinear dynamics and chaos: with applications to physics, biology, chemistry, and engineering. *CRC Press.*

[74] Thomas E (2009) Applied delay differential equations. *volume 3. Springer Science Business Media.*

[75] Alfredo B, Marino Z (2013) Numerical methods for delay differential equations. *Higher Education Press Beijing Oxford university press.*

[76] Petras I (2011) Fractional-order Nonlinear Systems: Modeling, Analysis and Simulation. *Higher Education Press Beijing.*

[77] Deng W (2007) Short memory principle and a predictor-corrector approach for fractional differential equations. *J. Comput. Appl. Math.* 206:174-188.

[78] Diethelm K, Ford NJ, Freed D (2002) A predictor-corrector approach for the numerical solution of fractional differential equations. *Nonlinear Dyn.* 29:3-22.

[79] Ngueteu Mbouna GS, Woafo P (2012) Dynamics and synchronization analysis of coupled fractional-order nonlinear electromechanical systems. *Mech. Res. Commun.* 46:20-25.

[80] Podlubny I (1999) Fractional Differential Equations. *Academic Press San Diego.*

[81] Petras I (2009) Chaos in the fractional-order Volta's system : modeling and simulation. *Nonlinear Dyn.* 57:157-170.

[82] Han SM, Benaroya H (2002) Comparison of linear and nonlinear responses of a compliant tower to random wave forces, *Chaos Solitons and Fract.* 14:269-291.

[83] Nayfeh AH, Mook DH (1995) Nonlinear Oscillations, *Wiley Classics Library, New York.*

[84] Jahangiri V, Mirab H, Fathi R, Ettefaghand MM (2016) TLP Structural Health Monitoring Based on Vibration Signal of Energy Harvesting System, *Latin American J. of Solids Struct.* 13:897-915.

[85] Anii KA, Kosaka SH, Yamanaka H (1994) Stability of active-trndon structural control with time delay, *J. Eng. Mech.* 120:2240-2243.

[86] Zhang L, Yang CY, Chajes MJ, Cheng AHD (1993) Stability of active-tendon structural control with time delay, *J. Eng. Mech.* 119:1017-1024.

[87] Korak S, Ranjan G (2013) Rotating beams and non-rotating beams with shared eigenpair for pinned-free boundary condition, *Meccanica* 48:1661-1676.

[88] Bernstein A, Rand R (2016) Delay-Coupled Mathieu Equations in Synchrotron Dynamics, *J. of Appl. Nonlinear Dyn.* 5(3):337-348.

[89] Bernstein A, Rand R (2018) Delay-Coupled Mathieu Equations in Synchrotron Dynamics Revisited: Delay Terms in the Slow Flow, *J. of Appl. Nonlinear Dyn.* 7(4):349-360.

[90] Yang T, Fang B, Chen Y, Zhen Y (2009) Approximate solutions of axially moving viscoelastic beams subject to multi-frequency excitations. *International J. and Non-Linear Mech.* 44:230-238.

[91] Abou-Rayan AM, Ayman AS, El-gamal AR (2012) Response of square tension leg platforms to hydrodynamic forces. *Ocean Sys. Eng.* 2:000-000.

[92] Mohammad RT, Rahim S (2014) Nonlinear dynamic analysis of TLP surge motion using homotopy perturbation method. *Ships Off. Struct.* 9(6):569-577.

[93] Mohammad RT, Rahim S (2018) Perturbation nonlinear response of tension leg platform Under regular wave excitation. *J. Mar. Sci. Tech.* 23:132-140.

[94] Journée JMJ, Massie WW (2001) Offshore Hydromechanics. *Delft University of Technology.*

[95] Hayashi C (1964) Nonlinear oscillations inphysicals Systems. *New York* Mc-Graw-Hill.

[96] Sanders JA, Verhulst F ,Murdock J (2007) Averaging method sin nonlinear dynamical systems. *New York* Springer Science Business Media.

[97] Shen Y, Yang Xing H, Ma H (2012) Primary resonance of duffing oscillator with two kinds of fractional-order derivatives. *Int. J. Non-linear Mech.* 47:975-83.

[98] Deng J, Xie W-C, Pandey MD (2014) Stochasticstability of a fractional viscoelastic column under bounded noise excitation. *J. Sound Vib.* 333:1629-43.

[99] Debnath L (2003) Recent applications of fractional calculus to science and engineering. *Int. J. Math. Math. Sci.* 54:3413-3442.

[100] Anadronov AA, Witt A (1930) Towards mathematical theory of capture. *Archiv fur Electrotechnik* 24:99-110.

[101] Wiggins S (1990) Introduction to applied Nonlinear dynamical systems and chaos. NewYork :Springer.

[102] Ortigueira MD (2011) Fractional Calculus for Scientists and Engineers, Lecture Notes in Electrical Engineering (Springer, Berlin, Heidelberg).

[103] Samko S, Kilbas A, Marichev O (1993) Fractional Integrals and Derivatives : Theory and Applications Gordon and Breach Science Publishers, Amsterdam.

[104] Xu N, Zhang J (2010) Pitch/Roll static stability of tension leg platforms. *International Conference on Ocean, Offshore and Arctic Engi.* Shanghai, China.

[105] Anague Tabejieu LM, Nana Nbendjo BR, Woafo P (2016) On the dyanamics of Rayleigh beams resting on fractional-order viscoelastic pasternak foundations subjected to moving loads. *Chaos Solitons and Fract.* 93:39-47.

[106] Awrejcewicz J, Yuriy P (2006) Chaos prediction in the Duffing type system with friction using Melnikov's functions. *Nonlinear Analysis: Real World and Applications* 7(1):12-24.

[107] Awrejcewicz J, Holicke M (2007) Analytical prediction of chaos in rotated Froude pendulum. *Nonlinear Dyn.* 47:3-24.

[108] Youtha Ngouoko ON, Nana Nbendjo BR, Dorka U (2021) On the appearance of horseshoes chaos in a nonlinear hysteretic system with negative stiffness. *Archiv Appl Mech.*

[109] Awrejcewicz J, Krysko VA (2006) Introduction to asymptotic methods. *New York: Chapmanand Hall, CRC Press, Boca Raton.*

[110] Han SM, Benaroya H (2002) Comparison of linear and nonlinear responses of a compliant tower to random wave forces. *Chaos Solitons and Fract.* 14:269-291.

[111] Dimateo AM, Iacono FL, Navarra G, Pirrotta A (2014) Innovative Modeling of Tuned Liquid Column Damper Motion. *Communications in Nonlinear Science and Numerical Simulation.* 5704(14):00525-5.

[112] Shihua Z, Qi L, Dong D, Tianzhuang Y, Yongchao Z (2020) Dynamic characteristic analysis of harmonically excited cracked vibration platform with intermediate nonlinear support. *Chaos Solitons and Fract.* 140:1100228.

[113] S.M. Han, H. Benaroya (2002) Nonlinear and Stochastic Dynamics of Compliant Offshore Structure. Kluwer Academic Publishers, Dordrecht, The Netherlands.

[114] Lee HH, Wong SH, Lee RS (2006) Response mitigation on the offshore floating platform system with tuned liquid column damper. *Ocean Eng.* 33(8-9):1118-1142.

[115] Chatjigeorgiou IK (2019) Nonlinear dynamics of statically displaced tendons with non-conventional end conditions. *Appl. Math. Model.* 81:211-231.

[116] You LX (1991) Vibration control of wind-excited tall/slender structures. *Dip.Mech.Eng, M. Eng. sc.* A thesis presented for the degree of Doctor of Philosophy.

List of publications

1-**A.M. Ngounou**, B.R. Nana Nbendjo, U. Dorka, (2021), Effect of the delay between the detection of vibration and the action of tendons on the dynamics response of tension leg platform (TLP) under sea waves excitation. *Journal of Applied Nonlinear Dynamics 10(4) 663-659.*

2-**A.M. Ngounou**, S.C. Mba Feulefack, L.M. Anague Tabejieu, B.R. Nana Nbendjo, (2022), Design, analysis and horseshoes chaos control on Tension Leg Platform system with fractional nonlinear viscoelastic tendon force under regular sea wave excitation. *Chaos Solitons and Fractals 157(2022)111952.*

Other publications

1-M.S. Kana Nguemo, **A.M. Ngounou**, S.C. Mba Feulefack, A.A. Nanha Djanan, B.R. Nana Nbendjo, Alessandro N. Vargas, (2022), Tuned liquid column for dampering rotational motion of a nonlinear horizontal deck. *Journal of Vibration Engineering Technologies.*

Collection of the published papers

Effect of the Delay Between the Detection of Vibration and the Action of Tendons on the Dynamics Response of Tension Leg Platform (TLP) Under Sea Waves Excitation

A.M. Ngounou[1], B.R. Nana Nbendjo[1,2†], U. Dorka[2]

[1] Laboratory of Modelling and Simulation in Engineering, Biomimetics and Prototypes, Faculty of Science, University of Yaounde I, P.O. Box 812, Yaounde, Cameroon

[2] Steel and Composite Structures, University of Kassel,Kurt-Wolters-Strasse 3, Kassel 34125, Germany

Abstract

In this study, the dynamic response of the tension leg platform (TLP) under sea waves excitation is investigated. One establishes the analytical framework consisting of mathematical modeling of TLP taking into account the tendons and the delay. We analyse the stability and determine the physical characteristics of tendon system that allow the system to be always stable. Conditions on the space parameters of the system for which harmonic, subharmonic, superharmonic, combination resonants states are obtained using the multiple time scales method. The results show that the stability area of the system decreases when the delay increases and increases when the damping coefficient increases. Furthermore, increasing the time- delay only increases the value of the maximum amplitude response of the system. However, reasonable selection of the system parameters can effectively reduce the level of vibration of the system.

1 Introduction

Offshore structures are used in the oil industry as exploratory, producction, oil storage, and oil landing facilities. In general, there are two types of stationary offshore structures: fixed and compliant. In recent years, the need to explore for oil in deeper water has made compliant structures more popular. Compliant towers are believed to be economically feasible in water depths exceeding 2000 ft. In particular,we are interested in tension leg platforms (TLP). Those structures being constructed in harsh environment are affected by wave and wind forces which can also affect their reliability. Moreover, stability of TLP structures is highly dependent on tendons.

Many studies are done about modeling and dynamic response of TLP structures under sea wave excitation. A review on the dynamic response of compliant platforms was made by Adrezin and al [1]. Adrezin and Benaroya [2,3] they examined the nonlinear transverse behavior of a tension leg platform

---

†Corresponding author.

Email address: nananbendjo@yahoo.com

with being a time dependent tension due to gravity and buoyancy. It appeared that the inclusion of hydrodynamic forces on tendons will result in greater surge amplitude and offset position. Han and Benaroya [4] modeled a vertical member of compliant offshore structure as a beam which is under going bending and extension. The beam is contituted with a mass point and is subjected to its free end with an axial load. They also compared linear and non-linear responses. They showed that the transverse response of the linear model is as good as the nonlinear coupled models. However, they also found that the nonlinear coupled method is more suitable for the axial vibration response. Yigit and Chrostoforou [5] studied the coupled vibration of the oil well drill strings in compression and also they solved the equations of motion by using the assumed model method. They arrive to the conclusion that the coupled model at a lower load yields an unstable behavior in comparison of the uncoupled model. Patel and Park [6] investigated on the dynamics of tension leg platform tethers at low tension. Besides, they analyzed the effect of tension on the dynamic behavior of the structure and it was observed that the increase in the axial force frequency has no effect on the transverse response, only the axial response is influenced. Gadagi and Benaroya [7] studied the dynamic response of an axially loaded tendon of a tension leg platform and they derived a set of non-linear equations of motion for a coupled axial and transverse vibration of a tether subjected to end tension. Kim and Yang [8] developed a numerical study of the transient effect of tendon disconnection on global performance of an extended tension leg platform during harsh environmental conditions of Gulf of Mexico and found that tendon breakage affects natural periods of heave and pitch. Taflanidis and al [9] determined a dynamic response of the platform, by considering the uncertainties related to the excitation characteristics such as significant wave height or uncertainties related to the TLP model properties such as, Young module of tendons and they concluded that uncertainties related to excitation characteristics are the dominant risk factors. Clearly and al [10] studied the effect of wave impact angle on the platform motion and also they determined how pre-tension modifies motion of the platform and behavior of mooring lines. Additionally, they concluded that the wave angle has a little impact on the broad nature of the platform dynamics and the maximum tension in mooring cables highly depend on the impact angle. An investigation by Srinivasan and al [11] was to analyse non-linear phenomena such as ringing and springing responses [12,13] that have been observed in TLPs under impact and non-impact wave conditions. These phenomena can pose a threat to platform stability and can result to an eventual fatigue failure of the tendons [11,14].

In this paper, we analyze the time-delay effect on the stability and the amplitude of vibration of the TLP. This consists to determine the physical parameters of the structure leading to reduce the effect of this delay on the stability and amplitude of vibration of the structure.

The paper is organized as follows. After Introduction, the physical model of the system which taking into account tendon and the equivalent modal equation is illustrated in Section 2. In Section 3, the effect of the tendon on the stability of the structure taking into account the time-delay are presented. In Section 3, analytical and numerical methods are used to analyse the effects of the main parameters of the system on the amplitude response. Section 5 is devoted to the conclusion.

2 Modelling of the dynamics of TLP taking into account the tendons

A TLP structure which includes, deck, hull, pontoon, risers, tendons and foundation template is shown schematically in figure 1 and equivalent model, consisting of a vertical beam and two tendons and which are coupled through the platform is shown in figure 2.
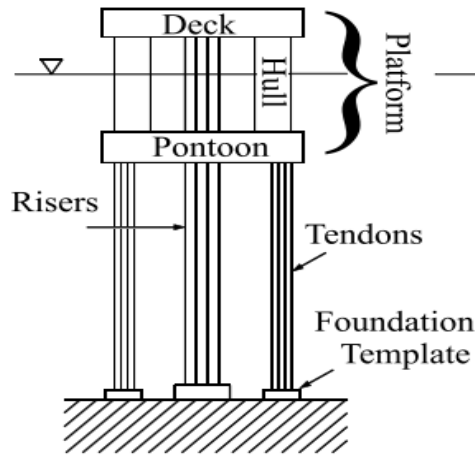
Fig. 1 Schematics of offshore structures [4].
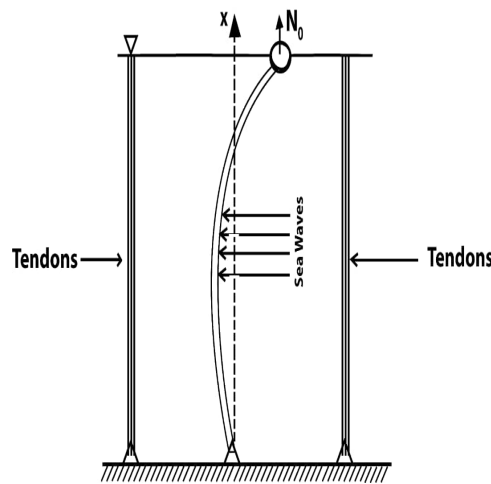
Fig. 2 A simplified model of a TLP.

2.1 Mathematical modeling

Consider a pinned free beam of length l, with density ρ, Young's module E, cross sectional area A and moment of inertia I, after using the physical and mathematical concept,the governing equation for TLP (Beam) model system under waves excitation given by equation [15–17].

$$\begin{cases} \rho A \dfrac{\partial^2 u(x,t)}{\partial t^2} + c_1 \dfrac{\partial u(x,t)}{\partial t} = EA \dfrac{\partial^2 u(x,t)}{\partial x^2} + \dfrac{EA}{2} \dfrac{\partial}{\partial x}\left(\left(\dfrac{\partial w(x,t)}{\partial x}\right)^2\right) \\ \rho A \dfrac{\partial^2 w(x,t)}{\partial t^2} + EI \dfrac{\partial^4 w(x,t)}{\partial x^4} + c_2 \dfrac{\partial w(x,t)}{\partial t} - \rho I \dfrac{\partial^4 w(x,t)}{\partial t^2 \partial x^2} - EA \dfrac{\partial}{\partial x}\left(e \dfrac{\partial w(x,t)}{\partial x}\right) + z_c(t) = f(x,t) \end{cases} \tag{1}$$

with the boundary and initial conditions

$$w(0,t) = \frac{\partial^2 w}{\partial x^2}(0,t) = \frac{\partial^2 w}{\partial x^2}(l,t) = \frac{\partial^3 w}{\partial x^3}(l,t) = 0, \tag{2}$$

$$u(0,t) = 0,\, u(l,t) = \frac{lN_0}{EA}. \tag{3}$$

Assuming that the radius of gyration r is small enough, the longitudinal inertia force and dissipative force are neglected. Using the boundaries conditions (3) and after some simplification its comes out the following equation

$$e = \frac{N_0}{EA} + \frac{1}{2l} \int_0^l (\frac{\partial w}{\partial x})^2 dx. \tag{4}$$

Thus the general equation governing the behaviour of the system is given by

$$\rho A \frac{\partial^2 w(x,t)}{\partial t^2} + EI \frac{\partial^4 w(x,t)}{\partial x^4} + c_2 \frac{\partial w(x,t)}{\partial t} - \rho I \frac{\partial^4 w(x,t)}{\partial t^2 \partial x^2} - N_0 \frac{\partial^2 w(x,t)}{\partial x^2}$$
$$- \frac{EA}{2l} (\int_0^l (\frac{\partial w(x,t)}{\partial x})^2 dx) \frac{\partial^2 w(x,t)}{\partial x^2} + z_c(t) = f(x,t) \tag{5}$$

where $w = w(x,t)$ is the lateral deflexion EI denotes the flexural rigidity of the beam, c_2 is the damping coefficient, ρI is the transverse Rayleigh beam coeffcient, and N_0 is axial load.

The sea waves excitation is formulated using Morisons equation [18] and airy theory [16] is given by

$$f(x,t) = \frac{1}{2} C_d \rho_w (2r_{out}) \frac{\pi^2 H}{T^2} \frac{\cosh^2 k(x+d_1)}{\sinh^2 kd_1} \cos(\omega t) |\cos(\omega t)|$$
$$- C_M \rho_w A \frac{2\pi^2 H}{T^2} \frac{\cosh k(x+d_1)}{\sinh kd_1} \sin(\omega t) - C_m \rho A \frac{\partial^2 w(x,t)}{\partial t^2} \tag{6}$$

where C_D, C_M and C_m are the coefficient of the drag, and inertia forces of the beam and the added mass respectively. ρ_w is density of sea water, r_{out} is the outher radius of beam.

$z_c(t)$ represent the tendons force which is produced by the displacement of tendon. In fact, tendons are viscoelastic structures which mean they exhibit both elastic and viscous behaviors. Zhang and al [19], proposed a mathematical model given by

$$z_c(t) = 4k_c \cos \alpha_c [s_1 w(t - t_x) + s_2 \dot{w}(t - t_{\dot{x}})] \tag{7}$$

where k_c is tendon stiffness, α_c is tendon inclination, s_1 and s_2 are control parameters, t_x and $t_{\dot{x}}$ time delays for displacement and velocity feedback force in the system, respectively. We notice that w and $\dot{w}$ are written as functions of $t - t_x$ and $t - t_{\dot{x}}$, respectively. This lag between the structure response and the corrective action may be attributed to the time required to sense and to gather the information and the computation time for determining the proper action.

Taking into account the following dimensionless variable

$$q = \frac{w}{r}, \ y = \frac{x}{l_0}, \ \tau = \frac{r}{l_0^2} \sqrt{\frac{E}{\rho}} t, \ l^* = \frac{l}{l_0}, \ k_3 = C_m \frac{\rho_w}{\rho}$$
$$\lambda = \frac{c_2 l_0^2}{Ar\sqrt{\rho E}}, \ N_0' = \frac{N_0 l_0}{EI}, \ \beta = \frac{I}{Al_0^2}$$
$$\alpha = \frac{l_0^4}{EIr}, \ d^* = \frac{d_1}{l_0}, \ \Gamma_1 = 4k_c s_1 \frac{l_0^4}{EI} \cos \alpha_c$$
$$\Gamma_2 = 4k_c s_2 \frac{l_0^2 r}{EI} \sqrt{\frac{E}{\rho}} \cos \alpha_c, \ r = (\frac{I}{A})^{\frac{1}{2}}. \tag{8}$$

Eqs.(5) - (6) are reduced to a non-dimensional equation

$$\frac{\partial^4 q(y,\tau)}{\partial y^4} - \beta \frac{\partial^4 q(y,\tau)}{\partial \tau^2 \partial y^2} + (1+k_3) \frac{\partial^2 q(y,\tau)}{\partial \tau^2} + \lambda \frac{\partial q(y,\tau)}{\partial \tau} - N_0' \frac{\partial^2 q(y,\tau)}{\partial y^2}$$
$$- \frac{l_0}{2l} (\int_0^{l^*} (\frac{\partial q(y,\tau)}{\partial y})^2 dy) \frac{\partial^2 q(y,\tau)}{\partial y^2} + \Gamma_1 q(y,\tau-\tau_y) + \Gamma_2 \frac{\partial q(y,\tau-\tau_{\dot{y}})}{\partial \tau} = \alpha f_1(y,\tau) \tag{9}$$

$$f_1(y,\tau) = \frac{1}{2}C_d\rho_w(2r_{out})\frac{\pi^2 H^2}{T^2}\frac{\cosh^2 kl_0(y+d^*)}{\sinh^2 kl_0 d^*}\cos(\omega\tau)|\cos(\omega\tau)| - C_M\rho_w A\frac{2\pi^2 H}{T^2}\frac{\cosh kl_0(y+d^*)}{\sinh kl_0 d^*}\sin(\omega\tau) \tag{10}$$

with the boundary conditions

$$q(0,\tau) = \frac{\partial^2 q}{\partial y^2}(0,\tau) = \frac{\partial^2 q}{\partial y^2}(l^*,\tau) = \frac{\partial^3 q}{\partial y^3}(l^*,\tau) = 0. \tag{11}$$

Here l_0 is a reference lenght the of beam.

2.2 Modal equation

To deal with the analytical analysis, we resort to an assumed mode expansion. Specifically, it is assumed that q can be written as the finite sums

$$q(y,\tau) = \sum_{n=1}^{N} v_n(\tau)\phi_n(y) \tag{12}$$

where $v_n(\tau)$ is the amplitude of the nth mode, and $\phi_n(y)$ is the solution of the eigenvalue problem obtained by solving Eq.(9) and without damping, non linearity, excitation and tendon effect, and $\phi_n(y)$ is given by

$$\phi_1(y) = Ky, \quad \text{if } n = 1 \tag{13}$$

or

$$\phi_n(y) = \frac{\cos(k_n)}{\cosh(k_n)}\sinh(k_n y) + \sin(k_n y) \quad \text{if } n \geq 2 \tag{14}$$

where

$$k_n = (n - \frac{3}{4})\pi. \tag{15}$$

It should be noted that the first natural frequency occurs at 0. This mode corresponds to the rigid body motion which has a mode shape given as ϕ_1, which is not considered in our problem, since this mode has no relation with the elastic deflection of the beam [20]. In the rest of this paper, we limit ourselves to elastic mode, in particular in first elastic mode.

After substituting Eq.(12) into Eq.(9), multiplying both sides of the resultant equation by the shape function then integrating with respect to the beam axis y over the length l^*, and taking into account the orthogonality condition, the modal equation given by

$$\ddot{v}_2(\tau) + 2\eta\dot{v}_2(\tau) + \omega_2^2 v_2(\tau) + \gamma v_2^3(\tau) + pv_2(\tau - \tau_x) + d\dot{v}_2(\tau - \tau_{\dot{x}})$$
$$= p_0\cos(\omega\tau)|\cos(\omega\tau)| + p_1\sin(\omega\tau) \tag{16}$$

with

$$I_0 = \frac{\int_0^{l^*}\phi_n^2(y)\,dy}{\int_0^{l^*}(1+k_3)\phi_n^2(y)\,dy - \beta\int_0^{l^*}\phi''_n(y)\phi_n(y)\,dy}, \quad \eta = \frac{\lambda}{2}I_0,$$

$$\omega_1^2 = \frac{\int_0^{l^*}\phi''''_n(y)\phi_n(y)\,dy}{\int_0^{l^*}(1+k_3)\phi_n^2(y)\,dy - \beta\int_0^{l^*}\phi''_n(y)\phi_n(y)\,dy}, \quad \omega_2^2 = \omega_1^2 - N$$

$$N = N_0'\frac{\int_0^{l^*}\phi''_n(y)\phi_n(y)\,dy}{\int_0^{l^*}(1+k_3)\phi_n^2(y)\,dy - \beta\int_0^{l^*}\phi''_n(y)\phi_n(y)\,dy}, \quad p_0 = \frac{1}{2}C_d\rho_w(2r_{out})\frac{\pi^2 H}{T^2}I_2 \tag{17}$$

$$I_2 = \frac{\int_0^{l^*}\frac{\cosh^2 kl_0(y+d^*)}{\sinh^2 kl_0 d^*}\phi_n(y)\,dy}{\int_0^{l^*}(1+k_3)\phi_n^2(y)\,dy - \beta\int_0^{l^*}\phi''_n(y)\phi_n(y)\,dy}, \quad p_1 = -C_M\rho_w A\frac{2\pi^2 H}{T^2}I_3,$$

$$I_3 = \frac{\int_0^{l^*} \frac{\cosh k l_0 (y + d^*)}{\sinh k l_0 d^*} \phi_n (y) \, dy}{\int_0^{l^*} (1 + k_3) \phi_n^2 (y) \, dy - \beta \int_0^{l^*} \phi''_n (y) \phi_n (y) \, dy}, \quad p = \Gamma_1 I_0, \quad d = \Gamma_2 I_0.$$

Eq.16 represents the modal equation of the TLP under sea waves excitation, with its different parameters defined by Eq.17.

3 Effect of tendon on the stability of the structure

The aims of this section is to show how the tendon can affect parameter on the stability of the structure taking into account the time-delay. This is done using the D-subdivision method [19].

Thus, Eq.(16) can be rewritten as follows

$$\begin{aligned}
\dot{v}_2 &= g \\
\dot{g} &= -2\eta g - \omega_0^2 v_2 - \gamma v_2^3 - p v_2 (\tau - \tau_x) - d y (\tau - \tau_x) \\
&\quad + p_0 \cos (\omega \tau) |\cos (\omega \tau)| + p_1 \sin (\omega \tau)
\end{aligned} \tag{18}$$

point $v_{20}(0,0)$ is an equilibruim point of Eq.(18). The characteristic equation of the linearized version of Eq.(18) related to this equilibrium point is

$$s^2 + (2\eta + d \exp(-s\tau_{\dot{x}})) s + (\omega_2^2 + p \exp(-s\tau_x)) = 0. \tag{19}$$

To obtain the stability boundary in the plane of the tendon parameter(d, p), we use the D-subdivision method. According to that method, the stability boundary in the plane are determined by the points that yield either to a root $s = 0$ or a pair of pure imaginary roots of Eq.(19).

Substituting $s = 0$ into Eq.(19), one finds

$$p = -\omega_2^2. \tag{20}$$

Setting $s = ib$ (where b is a real constant) into the characteristic equation(19), and after some algebraic manipulation we obtained

$$(\cos b\tau_x) p + (b \sin b\tau_{\dot{x}}) d = b^2 - \omega_2^2 (b \cos b\tau_{\dot{x}}) d - (\sin b\tau_x) p = -2\eta b \tag{21}$$

which leads to

$$\begin{aligned}
p &= (b^2 - \omega_2^2) \cos b\tau_0 + 2\eta b \sin b\tau_0 \\
d &= \frac{(b^2 - \omega_2^2)}{b} \sin b\tau_0 - 2\eta \cos b\tau_0, \quad \tau_x = \tau_{\dot{x}} = \tau_0.
\end{aligned} \tag{22}$$

Properties of the beam and characteristics of the sea waves which are used for numerical purpose are given in Tables 1 and 2 [4, 16].

In this part, the simulation solutions are obtainted using the fourth-order runge kutta method, and the matlab software is used for plotting the curves. The Hopf bifurcation boundary in the (p, d) space delimiting the stability boundary can be found from the bifurcation curve defined by Eq.(22) and bifurcation line defined by Eq.(20). In figure 3, the stable area consists of the region of the plane limited by the straight line given by Eq.(20) and the curve associated with each value of time delay given by Eq.(22). Figure 3 shows that the increase of the value of time-delay contributes to reduce the stability area. In figure 4 the stability boundary in the space (p, d) and various values of damping is plotted. The interest here is the effect of delay on the stability. One can observe that when the damping coefficient increase, the stability area increase. This means that by increasing the damping

Table 1 Properties of the beam.

Parameter name	Symbol	Value
beam length (m)	l	415
inertial coefficient of beam	C_M	1.7
drag coefficient of beam	C_d	0.8
Inertial coefficient of added mass	C_m	1
Density of beam $(kg.m^2)$	ρ	7800
Young's module of beam(Gpa)	E	204
Outer raduis of beam (m)	r_{out}	0.4
Axial force (N)	N_0	$3.462e7$

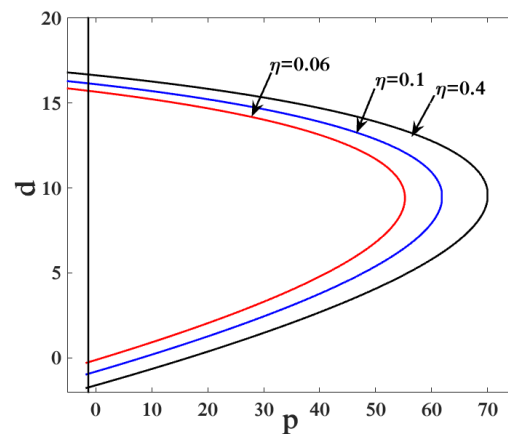**Table 2** Properties of sea.

Parameter name	Symbol	Value
Sea depth	d	415 m
Wave height	H	2 m
Wave period	T	25 s
water density	ρ_w	kg/m^3
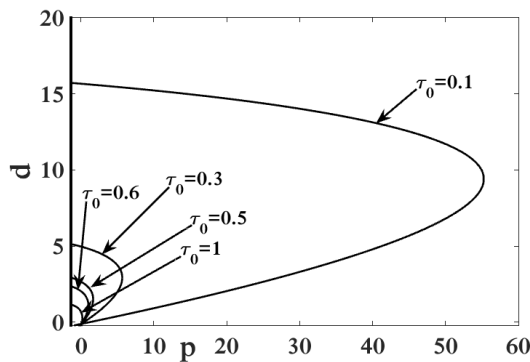
Fig. 3 Stability boundary in the space (p, d) and various values of time delay, with $\eta = 0.06$, $\omega_2 = 1.36$.

Fig. 4 Stability boundary in the space (p, d) and various values of damping, with $\tau_0 = 0.1$, $\omega_2 = 1.36$.

coefficient, the area will be increased; so one could choose the parameters of the tendon, so that the structure remains stable.

In figure 5 the evolution of the amplitude of vibration as a function of time is plotted. It is viewed in figure 5.a that the amplitude decreases as function of time leading to stability, while in figure 5.b the amplitude increases with time leading to instability of the system.

4 Compensation of the time-delay effect for amplitude reduction

In this section, a particular attention is focused on the analytical and numerical analysis in order to determine a parameter of the system that will compensate of time-delay effect leading to amplitude
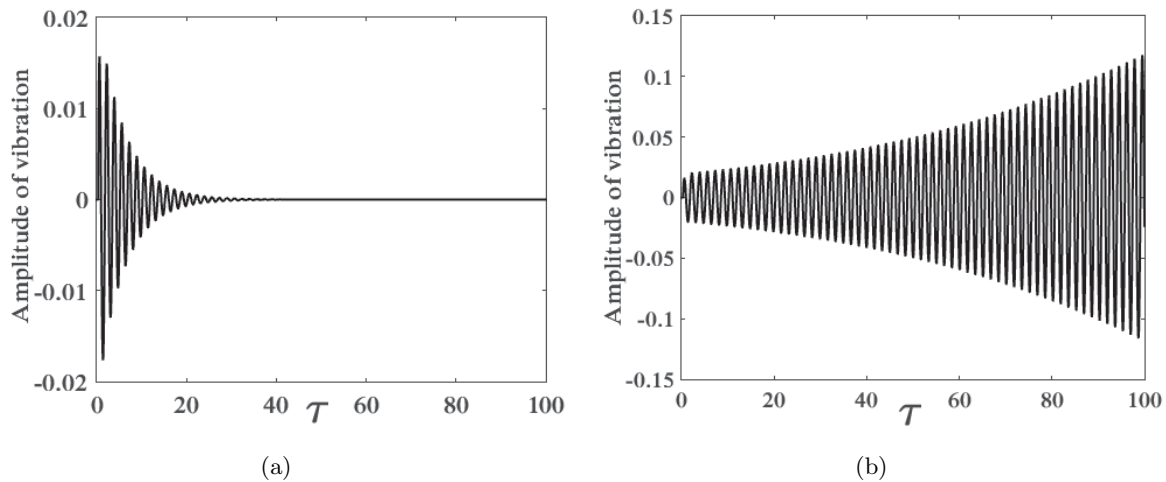
Fig. 5 Effect of tendons parameter on the stability of the TLP, (a) the tendons parameter taken in the stable region $\tau_0 = 0.3$, $p = 4$, $d = 3$; (b) the tendons parameter taken in the unstable region $\tau_0 = 0.3$, $p = 6.5$, $d = 3$, with $\eta = 0.06$, $\gamma = -4.388$, $\omega_2 = 1.36$.

reduction.

For that purpose the multiple time scale method [21–23], which provides an analytical approximate solution and thus permits to detect the effects of the time-delay on the system response is used.

We suppose that $|\cos(\omega\tau)| = \xi\cos(\omega\tau)$, where $\xi = \pm 1$ Eq.(16) can be written as

$$
\begin{aligned}
&\ddot{v}_2(\tau) + 2\eta\dot{v}_2(\tau) + \omega_2^2 v_2(\tau) + \gamma v_2^3(\tau - \tau_x) + p v_2(\tau) \\
&+ d\dot{v}_2(\tau - \tau_{\dot{x}}) = \xi p_0(\cos(\omega\tau))^2 + p_1\sin(\omega\tau), \quad \xi = \pm 1.
\end{aligned}
\tag{23}
$$

Taking into account the following relation: $(\cos(\omega\tau))^2 = \frac{1+\cos(2\omega\tau)}{2}$ and by substituting it in the Eq.(23), one obtain

$$
\begin{aligned}
&\ddot{v}_2(\tau) + 2\eta\dot{v}_2(\tau) + \omega_2^2 v_2(\tau) + \gamma v_2^3(\tau) + p v_2(\tau - \tau_x) + d\dot{v}_2(\tau - \tau_{\dot{x}}) \\
&= \xi\frac{p_0}{2} + \xi\frac{p_0}{2}\cos(2\omega\tau) + p_1\sin(\omega\tau).
\end{aligned}
\tag{24}
$$

One focus our attention on applying the multiple scales method to find the uniform analytical approximations solution at resonance. One would like to obtain a first-order approximate solution so that we define two-time scales as a fast-time, slow-time, so that the derivative with respect to time expanded as

$$
\begin{aligned}
&\frac{d}{d\tau} = \frac{dT_0}{d\tau}\frac{\partial}{\partial T_0} + \varepsilon\frac{\partial}{\partial T_1} = D_0 + \varepsilon D_1 + ... \\
&\frac{d^2}{d\tau^2} = D_0^2 + 2\varepsilon D_0 D_1 + ...
\end{aligned}
\tag{25}
$$

where ε refers to a very small perturbation parameter. The expansions of the solution $v_2(\tau, \varepsilon)$ and $v_2(\tau - \tau_x, \varepsilon)$ have the form

$$
v_2(\tau) = v_{20}(T_0, T_1) + \varepsilon v_{21}(T_0, T_1) + ...
\tag{26}
$$

$$
v_2(\tau - \tau_x, \varepsilon) = v_{20}(T_0 - T_x, T_1 - \varepsilon T_x) + \varepsilon v_{21}(T_0 - T_x, T_1 - \varepsilon T_x) + ...
\tag{27}
$$

Where $T_n = \varepsilon^n \tau$

Assuming that T_x is small enough, after using Taylor expansion on Eq.(27) one gets

$$
\begin{aligned}
v_2 \left(\tau - \tau_x, \varepsilon \right) =& v_{20} \left(T_0 - T_x, T_1 \right) - \varepsilon D_1 T_x v_{20} \left(T_0 - T_x, T_1 \right) \\
&+ \varepsilon v_{21} \left(T_0 - T_x, T_1 \right) - \varepsilon^2 T_x D_1 v_{21} \left(T_0 - T_x, T_1 \right).
\end{aligned}
\tag{28}
$$

After this expansion, we focus on the different type of resonance that one can have when the structure is subjected to the sea waves excitation.

4.1 Harmonic resonance

Substituting Eqs.(26) and (28) into the Eq.(24) and equating the same power of the coefficients, we obtain

$$
D_0^2 v_{20} + \omega_2^2 v_{20} = 0
\tag{29}
$$

$$
\begin{aligned}
D_0^2 v_{21} + \omega_2^2 v_{21} =& - 2D_0 \left(D_1 v_{20} + \eta v_{20} \right) - \gamma v_{20}^3 - p v_{20} \left(T_0 - T_x, T_0 \right) \\
&- d D_0 v_{20} \left(T_0 - T_x, T_0 \right) + \xi \frac{p_0}{2} + \xi \frac{p_0}{2} \cos 2\omega T_0 + p_1 \sin \omega T_0.
\end{aligned}
\tag{30}
$$

The solution of Eq.(29) can be written as

$$
v_{20} \left(T_0, T_1 \right) = A \left(T_1 \right) \exp \left(i \omega_2 T_0 \right) + cc
\tag{31}
$$

Substituting the above equations into Eq.(30) we obtain

$$
\begin{aligned}
D_0^2 v_{21} + \omega_2^2 v_{21} =& \left[-2i\omega_2 \left(A' + \eta A \right) - 3\gamma \bar{A} A^2 - pA \exp \left(-i\omega_2 T_x \right) - i\omega_2 dA \exp \left(-i\omega_2 T_x \right) \right] \\
&\times \exp \left(i\omega_2 T_0 \right) - \gamma A^3 \exp \left(3i\omega_2 T_0 \right) + \xi \frac{p_0}{2} + \xi \frac{p_0}{4} \exp \left(2\omega T_0 \right) + \frac{p_1}{2i} \exp \left(\omega T_0 \right) + cc.
\end{aligned}
\tag{32}
$$

Two types of resonance could occur from the above equation during the vibration of the system

-First case: $\omega_2 \simeq \omega$

The deviations of ω from ω_2 are shown as the following definition

$\omega = \omega_2 + \varepsilon\sigma$

Where σ is the detuning parameter. After considering the above definition and by eliminating the secular terms from Eq.(32), one will arrive at

$$
-2i\omega_2 \left(A' + \mu A \right) - 3\gamma \bar{A} A^2 - pA \exp \left(-i\omega_2 T_x \right) - i\omega_2 dA \exp \left(-i\omega_2 T_x \right) + \frac{p_1}{2i} \exp \left(i\sigma_1 T_1 \right) = 0.
\tag{33}
$$

Using the polar notation $A \left(T_1 \right) = \frac{a(T_1)}{2} \exp \left(i\theta_1 \right)$ of the above equation and by separating the real and the imaginary parts, we obtain

$$
\begin{aligned}
\omega_2 a' + \eta \omega_2 a - \frac{p}{2} a \sin \left(\omega_2 T_x \right) + \frac{d}{2} \omega_2 a \cos \left(\omega_2 T_x \right) + \frac{p_1}{2} \cos \phi_1 = 0, \\
\omega_2 \sigma a - \omega_2 a \phi' - \frac{p}{2} a \cos \left(\omega_2 T_x \right) - \frac{d}{2} \omega_2 a \sin \left(\omega_2 T_x \right) - \frac{3}{8} \gamma a^3 - \frac{p_1}{2} \sin \phi_1 = 0.
\end{aligned}
\tag{34}
$$

In which $\phi_1 = \sigma T_1 - \theta_1$. For the sake of the steady state response, the parameters ϕ_1', θ_1' and a' must be set to zero and, after some mathematical simplification of Eq.(34), the following equation is obtained

$$
\left(\eta \omega_2 a - \frac{p}{2} a \sin \omega_2 T_x + \frac{d}{2} \omega_2 a \cos \omega_2 T_x \right)^2 + \left(\sigma \omega_2 a - \frac{3}{8} \gamma a^3 - \frac{p}{2} a \cos \omega_2 T_x - \frac{d}{2} \omega_2 a \sin \omega_2 T_x \right)^2 = \frac{p_1^2}{4}.
\tag{35}
$$

-Second case: $\omega_2 \simeq 2\omega$ and $\omega = \frac{\omega_2}{2} + \varepsilon\sigma_2$
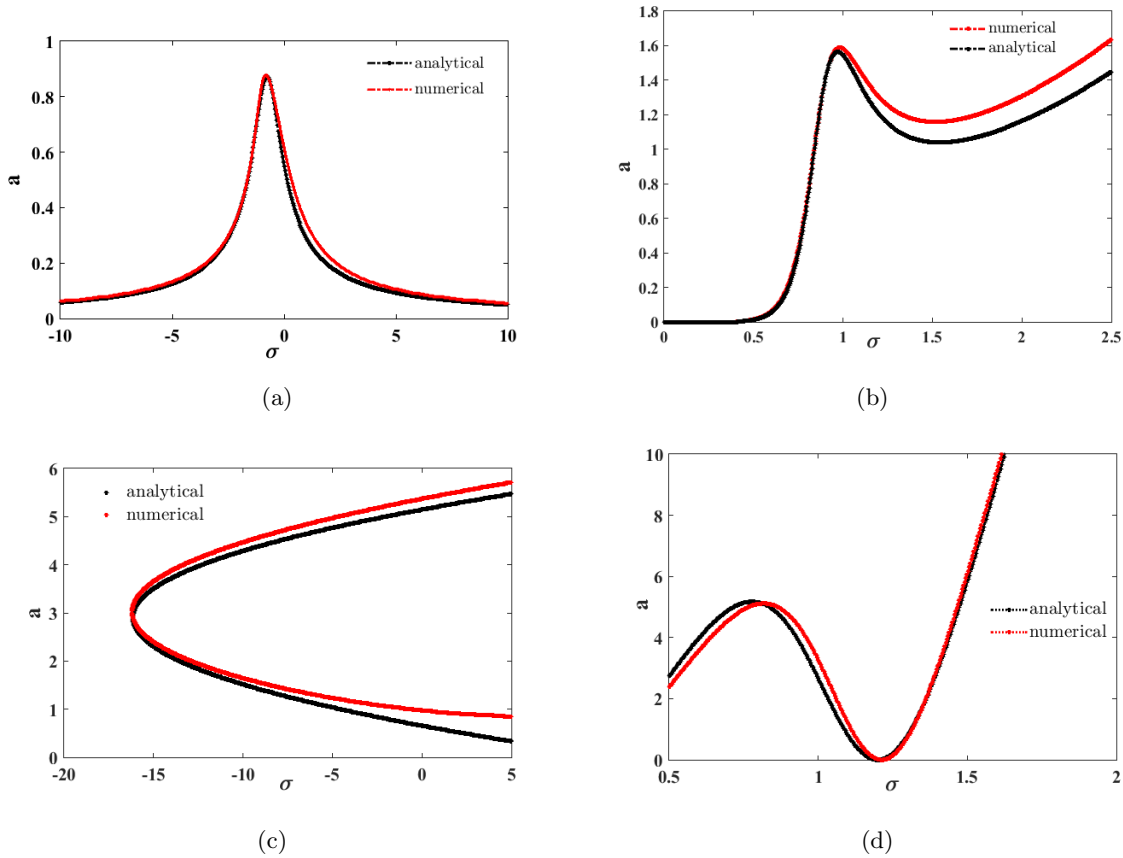
Fig. 6 Frequency response curves, $((a))$ Primary resonance, $((b))$ Superharmonic resonance, $((c))$ Subharmonic resonance, $((d))$ Combination resonance, with $\tau_0 = 0.0$, $p = 4$, $d = 3$, $\eta = 0.06$, $\gamma = -4.388$, $\omega_2 = 1.36$.

Therefore, the secular terms would be

$$-2i\omega_2 \left(A' + \mu A\right) - 3\gamma \bar{A}A^2 - pA\exp\left(-i\omega_2 T_x\right) - i\omega_2 dA\exp\left(-i\omega_2 T_x\right) + \xi\frac{p_0}{2}\exp\left(2i\sigma_1 T_1\right) = 0. \qquad (36)$$

Similarly, by applying the polar forms and separating the imaginary and the real parts, and after some mathematical simplification, the steady-state response will be obtained

$$(\eta\omega_2 a - \frac{p}{2}a\sin\omega_2 T_x + \frac{d}{2}\omega_2 a\cos\omega_2 T_x)^2 + (2\sigma\omega_2 a - \frac{3}{8}\gamma a^3 - \frac{p}{2}a\cos\omega_2 T_x - \frac{d}{2}\omega_2 a\sin\omega_2 T_x)^2 = \frac{p_0^2}{16}. \qquad (37)$$

After making these different calculations, the simulation solutions are obtainted using the bisection method, and the matlab software is used for plotting the curves. Figure 6 shows a comparative analysis of the amplitude response as function of the detuning parameter from the results of analytical derivations and numerical simulation. The result obtained shows a qualitative agreement between the numerical and analytical analysis. The effects of time-delay on the amplitude response of the TLP under sea wave excitation for the first and second resonance state are shown in figure 7 and figure 8. As depicted in figure 7 and figure 8, increasing the time-delay parameter results in an increase of the amplitude respose of the TLP. Figure 9 and figure 10 shown the amplitude response curves for different values of naturels frequency. For the primary and secondary resonance state, the natural frequency have the same effects, increasing the natural frequency results in decreasing the amplitude response of TLP. For example, it has been shown that, taking the two values of the following natural frequencies,
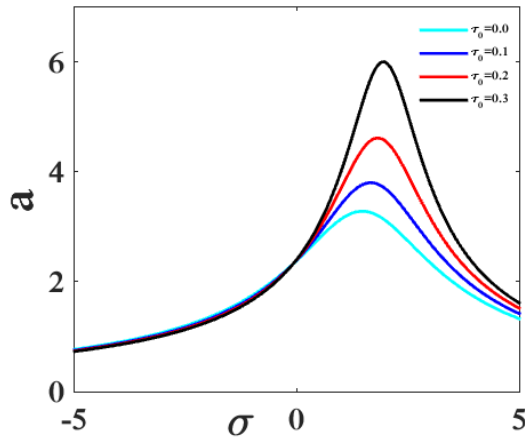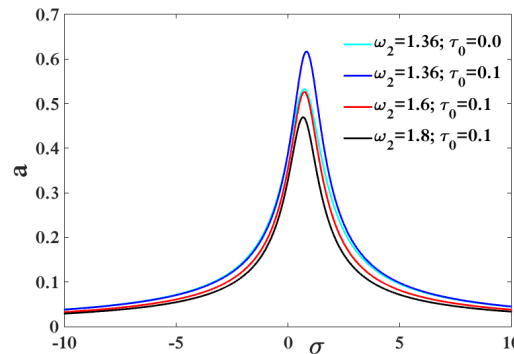
Fig. 7 Effect of time-delay on the TLP amplitude, $\omega = \omega_2 + \varepsilon\sigma$, with $\eta = 0.06$, $\gamma = -4.388$, $\omega_2 = 1.36, p = 4, d = 3$.
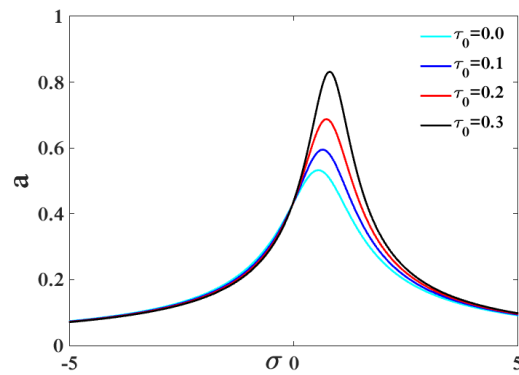
Fig. 8 Effect of time-delay on the TLP amplitude, $\omega = \frac{1}{2}\omega_2 + \varepsilon\sigma$, with $\eta = 0.06$, $\gamma = -4.388$, $\omega_2 = 1.36$, $p = 4$, $d = 3$.
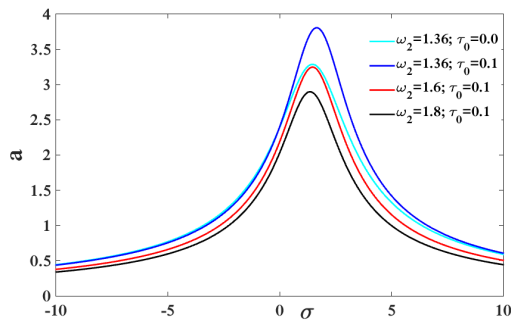
Fig. 9 Primary resonance curve, effect of natural frequency ω_2, with $\eta = 0.06$, $\gamma = -4.388$, $p = 4$, $d = 3$.
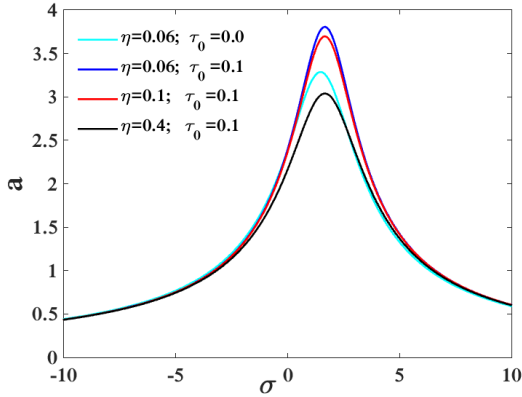

Fig. 10 Secondary resonance curve, effect of natural frequency ω_2, with $\eta = 0.06$, $\gamma = -4.388$, $p = 4$, $d = 3$.

$\omega_2 = 1.36$ (ie 0.453 rad/s) and $\omega_2 = 1.6$ (ie 0.987 rad/s) , one notes that the effect of the delay on the amplitude is attenuated for the value of the frequency $\omega_2 = 1.6$ (ie 0.987 rad/s). One conclude that, by making a good choice of the natural frequency of the structure one can compensate the time-delay effect on the amplitude. The effects of the damping coefficient on the frequency response for the first and second resonance state are shown in figure 11 and figure 12. From both figures, it can be observed that increasing the damping coefficient will reduce the amplitudes of vibration, the effect of time-delay of the amplitudes of vibration meaning that is reduced. It has been found that, for a delay value equal to 0.1(ie 0.22 second), taking a value of the damping coefficient of $\eta = 0.1$ (ie $c_2 = 66.67Ns/m$) instead of $\eta = 0.06$ (ie $c_2 = 40Ns/m$), one could compensate for the effect of the delay on the stability of the structure.

4.2 Superharmonic, subharmonic and combination resonances

In the following section we shall investigate the superharmonic resonance, subharmonic resonance and combination resonance. When the amplitude of the sinusoidal external force is large, other type of oscillations can be displayed by the model, namely the superharmonic, the subharmonic and combination

Fig. 11 Primary resonance curve, effect of damping η, with $\omega_2 = 1.36$, $\gamma = -4.388$, $p = 4$, $d = 3$.
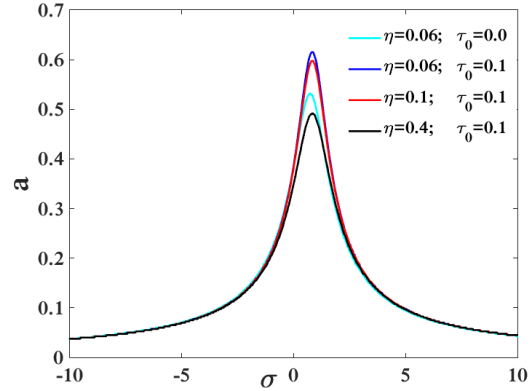
Fig. 12 Secondary resonance curve, effect of damping η, with $\omega_2 = 1.36$, $\gamma = -4.388$, $p = 4$, $d = 3$.

resonance states. Using the multiple timescale method, we obtain

$$D_0^2 v_{20} + \omega_2^2 v_{20} = \xi \frac{p_0}{2} + \xi \frac{p_0}{2} \cos 2\omega T_0 + p_1 \sin \omega T_0, \tag{38}$$

$$D_0^2 v_{21} + \omega_2^2 v_{21} = -2D_0 (D_1 v_{20} + \eta v_{20}) - \gamma v_{20}^3 - p v_{20} (T_0 - T_x, T_0) - dD_0 v_{20} (T_0 - T_x, T_0). \tag{39}$$

The solution of Eq.(38) can be written as

$$v_{20}(T_0, T_1) = A(T_1) \exp(i\omega_2 T_0) + \beta_0 + \beta_1 \exp(2i\omega T_0) + \beta_2 \exp(i\omega T_0) + cc \tag{40}$$

$\beta_0 = \frac{\xi p_0}{\omega_2^2}$, $\beta_1 = \frac{\xi p_0}{4(\omega_2^2 - 4\omega^2)}$, $\beta_2 = \frac{p_1}{2(\omega_2^2 - \omega^2)}$, $i^2 = -1$.

Substituting Eq. (40) into Eq. (39) we gets

$$
\begin{aligned}
D_0^2 v_{21} + \omega_2^2 v_{21} = &\left(-2i\omega_2 (A' + \eta A) - 3\gamma \bar{A} A^2 - pA \exp(-i\omega_2 T_x) - i\omega_2 dA \exp(-i\omega_2 T_x)\right. \\
&\left. -3\gamma \beta_0^2 A - 6\gamma \beta_1^2 A + 6\gamma \beta_2^2 A\right) \times \exp(i\omega_2 T_0) \\
&- \gamma \left(A^3 \exp(3i\omega_2 T_0) + \beta_1^3 \exp(6i\omega T_0) + \beta_2^3 \exp(3i\omega T_0)\right) \\
&- (2i\eta \omega \beta_2 + p\beta_2 \exp(-i\omega T_x) + id\omega \beta_2 \exp(-i\omega T_x) \\
&+ 6\gamma \beta_2 A\bar{A} + 3\gamma \beta_0^2 \beta_2 + 6\gamma \beta_1^2 \beta_2 - 6\gamma \beta_0 \beta_1 \beta_2 - 3\gamma \beta_2^3) \times \exp(i\omega T_0) \\
&- (4i\eta \omega \beta_1 + p\beta_1 \exp(-2i\omega T_x) + 2id\omega \beta_1 \exp(-2i\omega T_x) \\
&+ 6\gamma \beta_1 A\bar{A} + 3\gamma \beta_0^2 \beta_1 - 6\gamma \beta_2^2 \beta_1 + 3\gamma \beta_2^2 \beta_0 + 3\gamma \beta_1^3) \times \exp(2i\omega T_0) \\
&- \gamma (3 \beta_0 A^2 \exp(2i\omega_2 T_0) + 3\beta_1 A^2 \exp(2i(\omega_2 - \omega) T_0) \\
&+ 3\beta_1 A^2 \exp(2i(\omega_2 + \omega) T_0) + 3\beta_2 A^2 \exp(i(2\omega_2 + \omega) T_0) \\
&- 3\beta_2 A^2 \exp(i(2\omega_2 - \omega) T_0) + 2\beta_0 \beta_1 A \exp(i(\omega_2 - 2\omega) T_0) \\
&+ 2\beta_0 \beta_1 A \exp(i(\omega_2 + 2\omega) T_0) + 2\beta_0 \beta_2 A \exp(i(\omega_2 + \omega) T_0) \\
&+ \beta_1^2 A \exp(i(\omega_2 + 4\omega) T_0) + \beta_2^2 A \exp(i(\omega_2 + 2\omega) T_0) \\
&+ \beta_1^2 A \exp(i(\omega_2 - 4\omega) T_0) - 2\beta_0 \beta_2 A \exp(i(\omega_2 - \omega) T_0) \\
&+ 2\beta_1 \beta_2 A \exp(i(\omega_2 + 3\omega) T_0) - 2\beta_1 \beta_2 A \exp(i(\omega_2 + \omega) T_0) \\
&+ \beta_2^2 A \exp(i(\omega_2 - 2\omega) T_0) - 2\beta_1 \beta_2 A \exp(i(\omega_2 - 3\omega) T_0) \\
&+ 2\beta_1 \beta_2 A \exp(i(\omega_2 - \omega) T_0) + 6\beta_0 \beta_1 \beta_2 \exp(3i\omega T_0) \\
&- 3\beta_2 \beta_1^2 \exp(3i\omega T_0) + 3\beta_1 \beta_2^2 \exp(4i\omega T_0) + 3\beta_2 \beta_1^2 \exp(5i\omega T_0) \\
&+ \beta_0^3 + 3\beta_0 \beta_2^2 - 6\beta_0 \beta_2^2 - 6\beta_1 \beta_2^2 + 6\beta_0 A\bar{A}) + cc
\end{aligned}
\tag{41}
$$

cc is the complex conjugate of the previous terms. One noticed that the system can presented two superharmonic, two subharmonic and two combinations resonant states, when the following conditions are satisfied:

-Superharmonic resonance

$6\omega = \omega_2 + \varepsilon\sigma; \ \ 3\omega = \omega_2 + \varepsilon\sigma$

-Subharmonic resonance

$\omega = 3\omega_2 + \varepsilon\sigma; \ \ \omega = \frac{3}{2}\omega_2 + \varepsilon\sigma$

-Combination resonance

$4\omega = \omega_2 + \varepsilon\sigma; \ \ 5\omega = \omega_2 + \varepsilon\sigma$

a) Superharmonic resonance

Considering $3\omega = \omega_2 + \varepsilon\sigma$, and injecting this condition into Eq. (41) and setting secular terms to 0, we obtained

$$
\begin{aligned}
&- 2i\omega_2 \left(A' + \mu A\right) - 3\gamma\bar{A}A^2 - pA\exp\left(-i\omega_2 T_x\right) - i\omega_2 dA\exp\left(-i\omega_2 T_x\right) - 3\gamma\left(\beta_0^2 + 2\beta_1^2 + 2\beta_3^2\right) \\
&- i\gamma\left(\beta_3^3 - 6\beta_0\beta_1\beta_3 + 3\beta_3\beta_1^2\right)\exp\left(i\sigma T_1\right) = 0
\end{aligned}
\tag{42}
$$

where $\beta_3 = \frac{p_1}{2(\omega_2^2 - \omega^2)}$.

Using the polar notation $A\left(T_1\right) = \frac{a(T_1)}{2}\exp\left(i\theta_1\right)$ of in Eq.(41) and by separating the real and the imaginary parts, we obtain

$$
\begin{cases}
\omega_2 a' + \eta\omega_2 a - \dfrac{p}{2}a\sin\left(\omega_2 T_x\right) + \dfrac{d}{2}\omega_2 a\cos\left(\omega_2 T_x\right) + \gamma\left(\beta_3^3 - 6\beta_0\beta_1\beta_3 + 3\beta_3\beta_1^2\right)\cos\phi_1 = 0, \\[2mm]
\omega_2\sigma a - \omega_2 a\phi_1' - \dfrac{p}{2}a\cos\left(\omega_2 T_x\right) - \dfrac{d}{2}\omega_2 a\sin\left(\omega_2 T_x\right) - \dfrac{3}{8}\gamma a^3 - 3\gamma\left(\beta_0^2 + 2\beta_1^2 + 2\beta_3^2\right)\dfrac{a}{2} \\[2mm]
\quad - \gamma\left(\beta_3^3 - 6\beta_0\beta_1\beta_3 + 3\beta_3\beta_1^2\right)\sin\phi_1 = 0.
\end{cases}
\tag{43}
$$

For the sake of the steady state response, the parameters θ_1', a' ϕ_1' must be set to zero and, after some mathematical simplification of Eq.(43), the following equation is obtained

$$
(\mu a)^2 + \left(\sigma\omega_2 a - \frac{3}{8}\gamma a^3 - \frac{p}{2}a\cos\left(\omega_2 T_x\right) - \frac{d}{2}\omega_2 a\sin\left(\omega_2 T_x\right) - \frac{3}{2}\gamma\left(\beta_0^2 + 2\beta_1^2 + 2\beta_3^2\right)a\right)^2 = f_0^2
\tag{44}
$$

Where $f_0 = \gamma\left(\beta_3^3 - 6\beta_0\beta_1\beta_3 + 3\beta_3\beta_1^2\right)$, $\mu = \eta\omega_2 - \frac{p}{2}\sin\left(\omega_2 T_x\right) + \frac{d}{2}\omega_2\cos\left(\omega_2 T_x\right)$.

Let us consider now $6\omega = \omega_2 + \varepsilon\sigma$, and injecting this condition into Eq. (41) and setting secular terms to 0, one gets

$$
\begin{aligned}
&- 2i\omega_2 \left(A' + \mu A\right) - 3\gamma\bar{A}A^2 - pA\exp\left(-i\omega_2 T_x\right) - i\omega_2 dA\exp\left(-i\omega_2 T_x\right) \\
&- 3\gamma\left(\beta_0^2 + 2\beta_1^2 + 2\beta_3^2\right) - \gamma\beta_1^3\exp\left(i\sigma T_1\right) = 0.
\end{aligned}
\tag{45}
$$

Similarly, by applying the polar forms and separating the imaginary and the real parts, and after some mathematical simplification, the steady-state response we gets

$$
(\mu a)^2 + \left(\sigma\omega_2 a - \frac{3}{8}\gamma a^3 - \frac{p}{2}a\cos(\omega_2 T_x) - \frac{d}{2}\omega_2 a\sin(\omega_2 T_x) - \frac{3}{2}\gamma(\beta_0^2 + 2\beta_1^2 + 2\beta_3^2)a\right)^2 = f_0^2
\tag{46}
$$

Where $f_0 = \gamma\beta_1^3$.

b) Subharmonic resonance

In this part, we treat two cases: $\omega = 3\omega_2 + \varepsilon\sigma$ and $\omega = \frac{3}{2}\omega_2 + \varepsilon\sigma$. In the first case($\omega = 3\omega_2 + \varepsilon\sigma$), the secular terms are eliminated when

$$-2i\omega_2\left(A' + \mu A\right) - 3\gamma\bar{A}A^2 - pA\exp\left(-i\omega_2 T_x\right) - i\omega_2 dA\exp\left(-i\omega_2 T_x\right)$$
$$- 3\gamma\left(\beta_0^2 + 2\beta_1^2 + 2\beta_3^2\right) - 3i\gamma\beta_3\bar{A}^2\exp\left(i\sigma T_1\right) = 0. \tag{47}$$

Inserting the polar form of A, putting $\phi_1 = \sigma T_1 - 3\theta_1$, and proceeding in the same way as in the case of superharmonic, we obtain the following equation

$$(\mu)^2 + (\frac{\sigma}{3}\omega_2 - \frac{3}{8}\gamma a^2 - \frac{p}{2}\cos(\omega_2 T_x) - \frac{d}{2}\omega_2\sin(\omega_2 T_x) - \frac{3}{2}\gamma(\beta_0^2 + 2\beta_1^2 + 2\beta_3^2))^2 = (f_0 a)^2 \tag{48}$$

Where $f_0 = 3\gamma\beta_3$.

The second case let us consider $\omega = \frac{3}{2}\omega_2 + \varepsilon\sigma$ proceeding in the same way as in the case, one obtain the following equation

$$(\mu)^2 + (\frac{\sigma}{3}\omega_2 - \frac{3}{8}\gamma a^2 - \frac{p}{2}\cos(\omega_2 T_x) - \frac{d}{2}\omega_2\sin(\omega_2 T_x) - \frac{3}{2}\gamma(\beta_0^2 + 2\beta_1^2 + 2\beta_3^2))^2 = (f_0 a)^2 \tag{49}$$

Where $f_0 = 3\gamma\beta_1$.

c) combination resonance.

In this part, the following situation is consider: $4\omega = \omega_2 + \varepsilon\sigma$; $5\omega = \omega_2 + \varepsilon\sigma$

frist case $4\omega = \omega_2 + \varepsilon\sigma$; The corresponding solvability condition is

$$-2i\omega_2\left(A' + \mu A\right) - 3\gamma\bar{A}A^2 - pA\exp\left(-i\omega_2 T_x\right) - i\omega_2 dA\exp\left(-i\omega_2 T_x\right) - 3\gamma\left(\beta_0^2 + 2\beta_1^2 + 2\beta_3^2\right)$$
$$+ 3\gamma\beta_3^2\beta_1\exp\left(i\sigma T_1\right) = 0. \tag{50}$$

Subtutiting the polar form of A, putting $\phi_1 = \sigma T_1 - 3\theta_1$ in the above equation, and proceeding in the same way as in the case of superharmonic, the resonance equation is given by

$$(\mu a)^2 + \left(\sigma\omega_2 a - \frac{3}{8}\gamma a^3 - \frac{p}{2}a\cos\left(\omega_2 T_x\right) - \frac{d}{2}\omega_2 a\sin\left(\omega_2 T_x\right) - \frac{3}{2}\gamma\left(\beta_0^2 + 2\beta_1^2 + 2\beta_3^2\right)a\right)^2 = f_0^2 \tag{51}$$

Where $f_0 = 3\gamma\beta_3^2\beta_1$.

Second case $5\omega = \omega_2 + \varepsilon\sigma$. In this case, the resonance equation is given by

$$(\mu a)^2 + \left(\sigma\omega_2 a - \frac{3}{8}\gamma a^3 - \frac{p}{2}a\cos\left(\omega_2 T_x\right) - \frac{d}{2}\omega_2 a\sin\left(\omega_2 T_x\right) - \frac{3}{2}\gamma\left(\beta_0^2 + 2\beta_1^2 + 2\beta_3^2\right)\right)^2 = f_0^2. \tag{52}$$

Where $f_0 = 3\gamma\beta_1^2\beta_3$.

Figures 13, 14, 15, 16, 17, 18 represents the influence of the natural frequency on the amplitude response for the superhamonic, subharmnic and combination resonance state . As can be seen from these figures, increasing the natural frequency results in decreasing the oscillation amplitude, this allows us to say that increasing the natural frequency of the structure could increase the life of the structure because the vibrations of the structure are reduced. Each black curves of these figures are obtained for different values of time-delay. This allow us to say that time-delay has no effect on the superhamonic, subharmonic and combination resonant states.

5 Conclusion

An analytical and numerical solution for the dynamic response of a TLP under sea wave excitation are presented. We firstly modelled the TLP by the full partial differential equation that we have thereafter
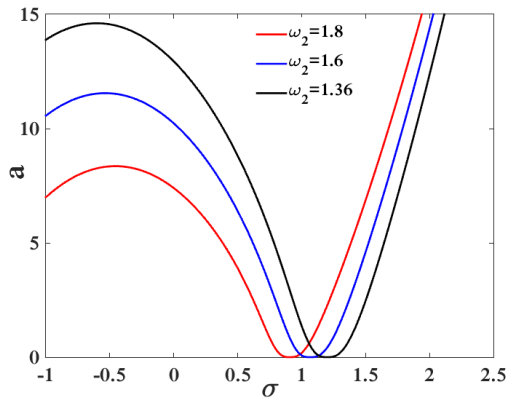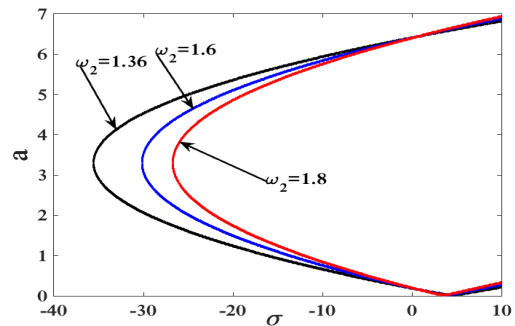
Fig. 13 Superharmonic resonance curve: $3\omega = \omega_2 + \varepsilon\sigma$, effect of natural frequency ω_2, $\eta = 0.06$, $\gamma = -4.388$, $p = 4$, $d = 3$.
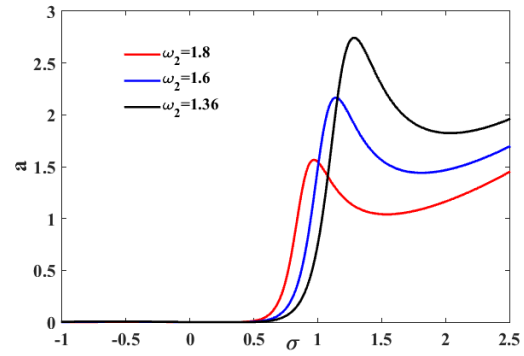
Fig. 14 Superharmonic resonance curve: $6\omega = \omega_2 + \varepsilon\sigma$, effect of natural frequency ω_2, $\eta = 0.06$, $\gamma = -4.388$, $p = 4$, $d = 3$.
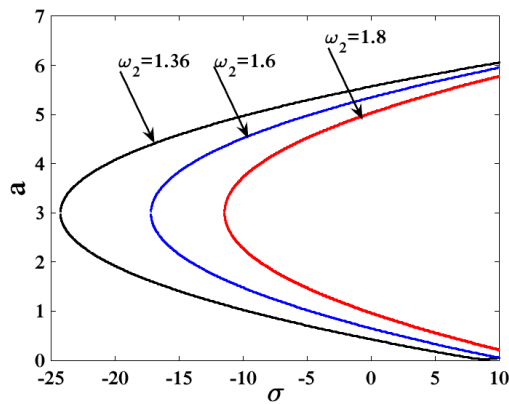
Fig. 15 Subharmonic resonance curve: $\omega = 3\omega_2 + \varepsilon\sigma$, effect of natural frequency ω_2, $\eta = 0.06$, $\gamma = -4.388$, $p = 4$, $d = 9$.

Fig. 16 Subharmonic resonance curve: $\omega = \frac{1}{2}\omega_2 + \varepsilon\sigma$, effect of natural frequency ω_2, $\eta = 0.06$, $\gamma = -4.388$, $p = 4$, $d = 3$.

Fig. 17 Combination resonance curve: $4\omega = \omega_2 + \varepsilon\sigma$, effect of natural frequency ω_2, $\eta = 0.06$, $\gamma = -4.388$, $p = 4$, $d = 3$.

Fig. 18 Combination resonance curve: $5\omega = \omega_2 + \varepsilon\sigma$, effect of natural frequency ω_2, $\eta = 0.06$, $\gamma = -4.388$, $p = 4$, $d = 3$.

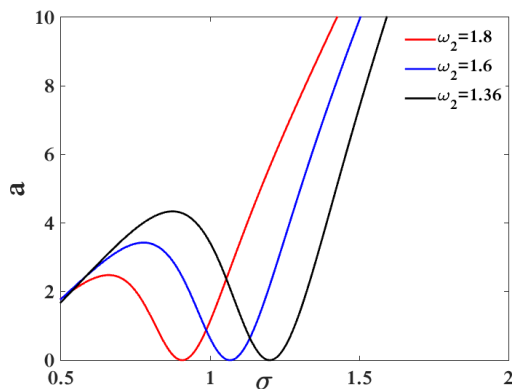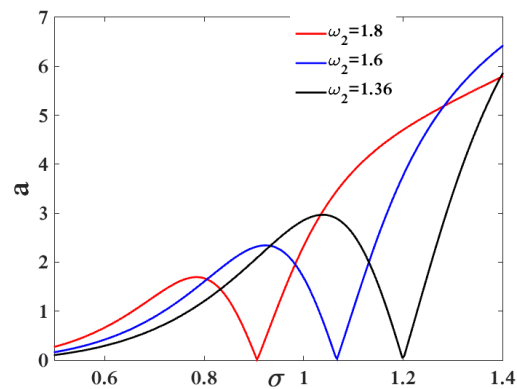reduced to the nonlinear ordinary differential equation. Secondly, the effect of tendon on the stability of the structure have been analyzed. Finally the effects of different parameters, namely, time-delay, natural frequency and damping coefficient, on different types of resonant cases of the system were fully investigated. Results of the analysis show that increase of the value of time-delay contributes to reduce the stability area. Therefore, increasing the value of the damping would increase the stability area. The effects of time-delay on the primary, secondary, superharmonic, subharmoncic and combination resonance state has been illustred. The analysis leads us to the conclusion that increasing of the time-delay would increases the amplitude response in the case of the primary and secondary resonaces, but is without effects on the superharmonic, subharmonic and comobination resonants states. One also analysed the effect of the natural frequency on the amplitude response. It has been found that the amplitude of oscillation decreases by incrising the the natural frequency, this for all types of resonant states, which allows to cancel the time-delay effect in the case of primary and secondary resonances. The same conclusion was drawn by increasing the damping coefficient. Results were also presented taking into account the non-dimensionless parameters. This order to validate the different analyzes that have been made.

Acknowledgements

Nomenclature

l = Beam length
c_M = Inertia coefficient of beam
c_d = Drag coefficient of beam
c_m = Inertia coefficient of added mass
ρ = Density of beam
E = young's module of beam
r_{out}= Outer raduis of beam
N_0 = Axial force
l_0 = Reference length
s_1, s_2 = Control parameters
t_x = Time delay of displacement
$\dot{t}_x$ = Time delay of velocity
k_c = Tendon stiffness
ρ_w = Water density
T= Wave period
d_1 = Sea wave
H = Wave height
I = Moment of Inertia
A = Cross section area
r = Raduis of gyration
c_2 = damping coefficient of beam
k= Wave number
λ = Dimensionless damping cefficient of beam

$N_0' =$ Dimensionless axial force

$\Gamma_1 =$ Dimensionless proportional gain parameter

$\Gamma_1 =$ Dimensionless derivative gain parameter

$\tau =$ Dimensionless time

$\tau_0 =$ Dimensionless time delay

$d^* =$ Dimensionless sea depth

$l^* =$ Dimensionless beam length

References

[1] Adrezin, R., Bar-Avi, P., and Benaroya, H. (1996), Dynamic response of compliant offshore structures: review, *Journal of Aerospace Engineering*, **9**(4), 114-31.

[2] Adrezin, R. and Benaroya, H. (1999), Non-linear stochastic dynamics of tension leg platforms, *Journal of Sound and Vibration*, **220**, 27-65.

[3] Adrezin, R. and Benaroya, H. (1999), Response of a tension leg platform to stochastic wave forces, *Probababilistic Engineering and Mechanics*, **14**, 3-17.

[4] Han, S.M. and Benaroya, H. (2002), Comparison of linear and nonlinear responses of a compliant tower to random wave forces, *Chaos Solitons and Fractals*, **14**, 269-291.

[5] Yigit, A.S. and Christoforou, A.P. (1996), Coupled axial and transverse vibrations of oilwell drillstrings, *Journal of sound and Vibration*, **195**, 617-27.

[6] Patel, M.H. and Park, H.I. (1991), Dynamics of tension leg platform tethers at low tension. Part I-Mathieu stability at large parameters, *Marine structures*, **4**, 257-273.

[7] Gadagi, M.M. and Benaroya, H. (2006), Dynamic response of an axially loaded tendon of a tension leg platform, *Journal of Sound and Vibration*, **293**, 38-58.

[8] Yang, C.K. and Kim, M.H. (2010), Transient effects of tendon disconnection of a TLP by hull-tendon-riser coupled dynamic analysis, *Ocean Engineering*, **37**, 667-677.

[9] Taflanidis, A.A., Vetter, C., and Loukogeorgaki, E. (2013), Impact of modeling and excitation uncertainties on operational and structural reliability of tension leg platforms, *Applied Ocean Research*, **43**, 131-147.

[10] Rudman, M. and Cleary, P.W. (2013), Rogue wave impact on a tension leg platform: the effect of wave incidence angle and mooring line tension, *Ocean Engineering*, **61**, 123-138.

[11] Srinivasan, C., Gaurav, G., Serino, G., and Miranda, S. (2011), Ringing and springing response of triangular TLPs, *International Shipbuild Programm*, **58**, 141-163.

[12] Abdussamie, N., Drobyshevski, Y., Ojeda, R., Thomas, G., and Amin, W. (2017), Experimental investigation of wave-in-deck impact events on a TLP model, *Ocean Engineering*, **142**, 541-562.

[13] Matsui, T., Sakoh, Y., and Nozu, T. (1993), Second-order sum-frequency oscillations of tension-leg platforms: Prediction and measurement, *Applied Ocean Research*, **15**, 107-118.

[14] Feng, W.H., Hua, F.Y., and Yang, L. (2014), Dynamic analysis of a tension leg platform for offshore wind turbines, *Journal of Power Technologie*, **94**, 42-49.

[15] Nayfeh, A.H. and Mook, D.H. (1995), Nonlinear Oscillations, *Wiley Classics Library, New York*.

[16] Jahangiri, V., Mirab, H., Fathi, R., and Ettefaghand, M.M. (2016), TLP Structural Health Monitoring Based on Vibration Signal of Energy Harvesting System, *Latin American Journal of Solids Structures*, **13**, 897-915.

[17] Anii, K.A., Kosaka, S.H., and Yamanaka, H. (1994), Stability of active-trndon structural control with time delay, *Journal of Engineering Mechanics*, **120**, 2240-2243.

[18] Morison, J.R., O'Brien, M.P., Johnson, J.W., and Schaaf, S.A. (1950), The force exerted by surface waves on piles, *Pet Trans, AIME* **189**, 149-57.

[19] Zhang, L., Yang, C.Y., Chajes, M.J., and Cheng, A.H.D. (1993), Stability of active-tendon structural control with time delay, *Jounal of Engineering Mechanics*, **119**, 1017-1024.

[20] Korak, S. and Ranjan, G. (2013), Rotating beams and non-rotating beams with shared eigenpair for pinned-free boundary condition, *Meccanica* , **48**, 1661-1676.

[21] Bernstein, A. and Rand, R. (2016), Delay-Coupled Mathieu Equations in Synchrotron Dynamics, *Journal of Applied Nonlinear Dynamics*, **5**(3), 337-348.

[22] Bernstein, A. and Rand, R., (2018), Delay-Coupled Mathieu Equations in Synchrotron Dynamics Revisited: Delay Terms in the Slow Flow, *Journal of Applied Nonlinear Dynamics*, **7**(4), 349-360.

[23] Yang, T., Fang, B., Chen, Y., and Zhen, Y. (2009), Approximate solutions of axially moving viscoelastic beams subject to multi-frequency excitations, *International Journal and Non-Linear Mechanics*, **44**, 230-238.
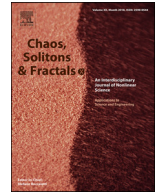
Design, analysis and horseshoes chaos control on tension leg platform system with fractional nonlinear viscoelastic tendon force under regular sea wave excitation

A.M. Ngounou[a], S.C. Mba Feulefack[a],*, L.M. Anague Tabejieu[b], B.R. Nana Nbendjo[a]

[a] *Laboratory of Modelling and Simulation in Engineering, Biomimetics and Prototypes, Faculty of Science, University of Yaounde I, P.O. Box 812, Yaounde, Cameroon*
[b] *Department of Mechanical Engineering National Higher Polytechnic School of Douala, University of Douala P.O. Box 2701, Douala, Cameroon*

A B S T R A C T

In this paper, the dynamic response of a Tension Leg Platform (TLP) system with fractional nonlinear viscoelastic tendon force under regular sea wave is investigated. Analytical and numerical methods are employed to analyse the effect of the fractional viscoelastic parameter, the tendon viscosity coefficient and the number of tendons on the amplitude of the system. It is found that, when the tendon viscosity coefficient and the number of tendons increase, the amplitude of vibration decreases. We also show that, increase of the fractional order derivative also contributes to decrease the unstable range of amplitude. Nevertheless, beyond a certain value of the fractional parameter, we rather observe an increase in amplitude. In other hand, Melnikov technique is used to derive the analytical criterion for the appearance of the heteroclinic chaos in the system. Analytical prediction is tested against numerical simulations based on the basin of attraction. It is found that, the appearance of horseshoes chaos depend of the fractional viscoelastic parameter, the tendon viscosity coefficient and the number of tendons.

1. Introduction

TLP is a floating platform which is moored to the seabed by tendons. This platform consisted of buoyant hull, deck and mooring system. Buoyant hull sustains deck sufficiently above water level and anchored to the seabed by a complex mooring system. The buoyancy of TLP is more than weight. Therefore, it needs stiff and strong pre tensioned tendons to support additional buoyancy. Tendons mostly connect hull to the seabed by suction anchors. Although the tendon mooring system allows lateral wave, wind and current loads move the platform compliantly, it keeps that strongly restricted vertically. Moreover, the stability of TLP structures is highly dependent on tendons. Thus, many researchers have been interested in the modeling and dynamic response of TLP structures under sea wave excitation [1–5].

In the literature many studies have been done with a view to determine the influence of tendon or tether parameters on the dynamic response of tension leg platform under wave excitation. Kurian et al. [6,7] developed a numerical study on the dynamic response of square TLPs subjected to regular and random waves. They also conducted parametric studies with different parameters such as pretension, wave angle, position of center of gravity and water depth. Yang and Kim [8], developed a numerical study of the transient effect of tendon disconnection on the global performance of an extended tension leg platform (ETLP) during harsh environmental conditions of the Gulf of Mexico. Patel and Park [9] investigated on the dynamics of tension leg platform tethers at low tension. Besides, they analyzed the effect of tension on the dynamic behavior of the structure and it was observed that the increase in the axial force frequency has no effect on the transverse response, only the axial response is influenced. Amr R. El-gama et al. [10], analyzed the effect of tethers tension force on the behavior of the triangular tension leg platform. In this study, the analysis was carried out using modified Morison equation in the time domain with water particle kinematics using Airy's linear wave theory to investigate the effect of changing the tether tension force on the stiffness matrix of TLP's, the dynamic behavior of TLP's; and on the fatigue stresses in the cables. The effect was investigated for different parameters of the hydrodynamic forces such as wave periods, and wave heights. And Golafshani et al. [11] presented the analytical response of a continuous model of the tether of TLP, considering the buoyancy and the

---

* Corresponding author.
  E-mail address: steveclorian@yahoo.fr (S.C. Mba Feulefack).

A.M. Ngounou, S.C. Mba Feulefack, L.M. Anague Tabejieu et al.

Chaos, Solitons and Fractals 157 (2022) 111952

Nomenclature

x	horizontal displacement of TLP (m)
$\dot{x}$	velocity of TLP (m/s)
$\ddot{x}$	acceleration of TLP (m/s^2)
m	total mass of the platform (kg)
W	total weight of the platform in the air (N)
F_B	total buoyancy force (N)
x	displacement in the surge direction (m)
θ	angle between the initial and the displaced position of the tendons
L_0	initial length of each tendons (m)
$\Delta T(x)$	increase in the initial pre-tension due to the arbitrary displacement (N)
F_w	wave force (N)
$F(x)$	nonlinear viscoelastic force of tendon (N)
n	number of tendons
A	cross-sectional area of tendons (m^2)
T_0	pre-tension (N)
E	Young's modulus of a tendon (Pa)
k_0	tendon stiffness (N/m)
L_p, W_p, H_p	pontoon size (m)
D_c, H_c	columns size (m)
D_r	draft (m)
C_m	inertial coefficient
C_d	drag coefficient
C_a	added mass coeficient
μ	tendon viscosity coefficient (Ns$^\alpha$/m)
g	acceleration of gravity (m/s^2)
u	water particle velocity (m/s)
$\dot{u}$	water particle acceleration (m/s^2)
ρ	water density (kg/m^3)
d	sea wave (m)
T	wave period (s)
H	wave height (m)
L	wave length (m)
c	damping coefficient of tendons (Ns/m)
k	wave number (m^{-1})
α	fractional-order
V	volume of columns (m^3)
m_{add}	added mass of TLP columns (kg)
Ω	wave frequency (rad/s)
z_1, z_2	bottom level and still water level (m)
σ	tuning parameter (rad/s)
ξ	disturbances parameter

effect of added mass fluctuation under the load simulated as an ocean wave. Recently Ngounou et al. [12] investigated the effect of the delay between the detection of vibration and the action of the tendons on the dynamic response of tension leg platform (TLP) under sea wave excitation. It was shown that, a good choice of the tendons parameters (natural frequency, damping coefficient) makes it possible to compensate the time-delay effect on the amplitude response.

In this paper, a nonlinear viscoelastic model describing the surge movement of tension leg platform is presented. To make the model more meaninful and practical, fractional derivative damping within the meaning of Caputo is taking into account in the modeling of the system. In fact, in the system of viscoelastic materials, the damping term does not only depend on the current state, but also on the previous state. It was shown by Anague et al. [13] that, for material with memory properties, the fractional-order models can better describing the dynamic response of the system. In this work, we firstly propose a nonlinear model of the

tendon leg platform taking into account the fractional viscoelastic behavior. Secondly the effect of main parameters, namely: number of tendons, the order of the fractional viscoelastic material that constitutes the tendon and the tendon viscosity coefficient on the amplitude of TLP have been analyzed. The present study is divided into five sections. After the introduction, the physical model of the system which taking into account tendon and the mathematical model equation is illustrated in Section 2. Section 3 contains the details of analytical and numerical methods (the averaging method [14–17] and Newton–Leipnik method [18,19] respectively) which have been used to analyze the effects of the main parameters of the system on the steady-state amplitude and the stability of the TLP system. In Section 4, the Melnikov theorem is used to detect the effect of the order of the fractional viscoelastic parameter and the tendon viscosity coefficient and the number of tendons on the threshold condition for the appearance of chaos and the basins of attraction are explored to support the obtained results. Our approach follows the earlier methodology introduced and discussed in references [13,20–23]. Section 5 draws some brief conclusions.

2. The tendon leg platform model

The supporting structure of TLP consists of a hull, tethers, and templates. The hull is a buoyant structure with a deck at its top. The pontoons and columns provide sufficient buoyancy to maintain the deck above the sea waves during all sea states. The hull is anchored to the sea bed through tethers and fixed in place with templates as presented in Fig. 1 and equivalent model is shown in Fig. 2. Where F_B is a total buoyancy force, W is a total weight of the platform in the air, T_0 is the initial pre-tension in the tether, D_c is the diameter of TLP columns, D_p is the diameter of pontoon, D_r is the draft.

D_r is calculated from the following relation [24]

$$D_r = \frac{4}{D_c^2}\left(\frac{F_B - n\rho g L_p H_p W_p}{n\rho\pi g}\right) \tag{1}$$

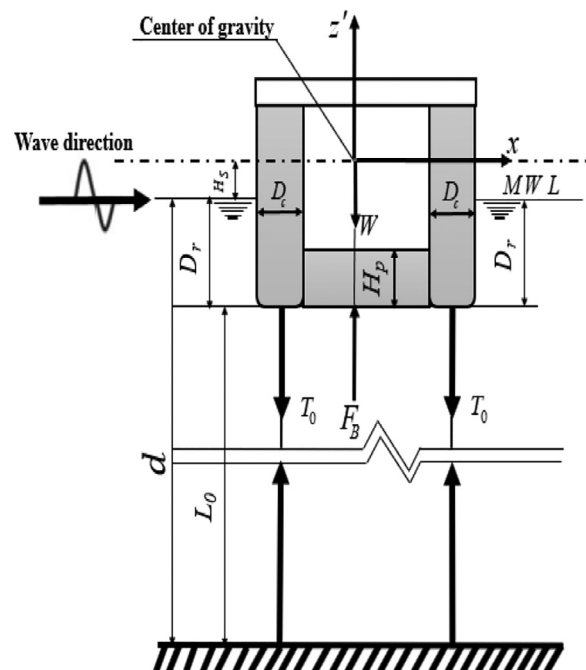where n is the number of tendon and ρ is the water density.

Fig. 1. Schematic tension leg platform.

A.M. Ngounou, S.C. Mba Feulefack, L.M. Anague Tabejieu et al.

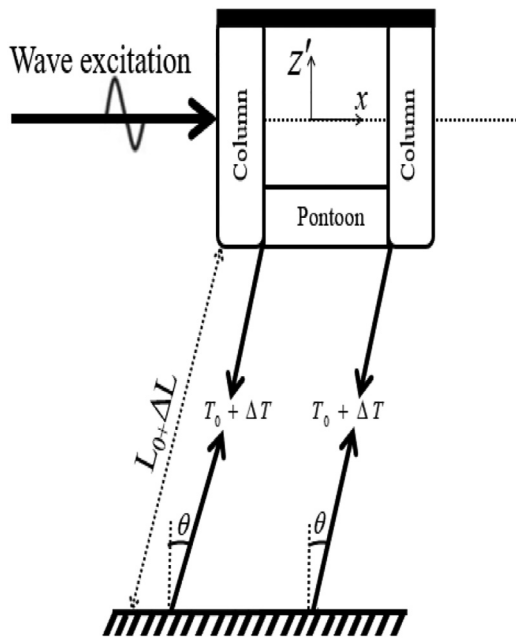*Chaos, Solitons and Fractals 157 (2022) 111952*

Fig. 2. Surge displacement of TLP: simplified model.

2.1. The mathematical model of the vibration of tension leg platform

In this paper, we have limited the analysis to the single DoF in order to give a first rough estimate of the sea wave and the fractional viscoelastic tendon force effects. Therefore, the equation of motion in horizontal direction of the whole system (Fig. 2) is give as follows:

$$m\ddot{x} + c\dot{x} + F(x) = F_w \tag{2}$$

$$F(x) = (nT_0 + n\Delta T(x))\sin\theta + n\mu D_t^\alpha x \tag{3}$$

$$\Delta T(x) = AE\left(\frac{\sqrt{L_0^2 + x^2} - L_0}{L_0}\right) \tag{4}$$

The model used in this paper is based on the model proposed by Mohammad and Rahim [25]. In order to get closer in a more practical and meaningful case, we propose in this paper a model which taking into account that the structure can have a catastrophic behavior.

Assuming that the displacement x is small enough and taking into account the previous comment, one obtains

$$\Delta T(x) = \frac{AE}{2L_0^2}x^2 - \frac{AE}{8L_0^4}x^4 \tag{5}$$

$$\sin\theta = \frac{x}{\sqrt{L_0^2 + x^2}} \simeq \frac{x}{L_0}\left(1 - \frac{x^2}{2L_0^2} + \frac{3x^4}{8L_0^4}\right) \simeq \frac{x}{L_0} - \frac{x^3}{2L_0^3} + \frac{3x^5}{8L_0^5} \tag{6}$$

$$(nT_0 + n\Delta T(x))\sin\theta \simeq \frac{nT_0}{L_0}x + n\left(\frac{AE - T_0}{2L_0^3}\right)x^3 - 3n\left(\frac{AE - T_0}{8L_0^5}\right)x^5 \tag{7}$$

Taking into account Eq. (7), Eq. (2) becomes

$$m\ddot{x} + \frac{nT_0}{L_0}x + c\dot{x} + n\left(\frac{AE - T_0}{2L_0^3}\right)x^3 - 3n\left(\frac{AE - T_0}{8L_0^5}\right)x^5 + n\mu D_t^\alpha x = F_w \tag{8}$$

where, x is the displacement in the surge direction, θ is the angle between the initial and the displaced position of the tether, c is the structural damping coefficient, L_0 is the initial length of each tether, E is the Young's modulus of the tether, $\Delta T(x)$ increases in the initial pre-tension due to the arbitrary displacement, $F(x)$ is the nonlinear viscoelastic force of tendon, F_w is the wave force, A is the cross-sectional area of tether, μ is the tendon viscosity coefficient and D_t^α is the fractional derivative with order $\alpha \in (0, 1)$.

2.2. Wave force

According to Morison [26], the generalized wave force due to sea wave on the members of TLP is calculated by the Morison equation on TLP columns as below:

$$F_{\text{morison}} = \sum \left(F_{\text{inertia}} + F_{\text{drag}}\right)_{\text{column}} \tag{9}$$

Assuming that the force coefficients C_m and C_d are constants and integrating over the still-water-depth on column yields [27].

$$F_{\text{morison}} = \sum_{\text{column}} \int_V c_m\rho\dot{u}dV - \int_V c_a\rho\ddot{x}dV + \int_{z_1}^{z_2} 0.5c_d\rho|u - \dot{x}|(u - \dot{x})dz \tag{10}$$

Taking into account the wave theory, the horizontal water particle velocity and acceleration at the vertical centreline of a circular cylinder at $x = 0$ are given [28]

$$u(x, t) = \frac{\pi H}{T}\frac{\cosh kz}{\sinh kd}\cos(kx - \Omega t) \tag{11}$$

$$\dot{u}(x, t) = \frac{2\pi^2 H}{T^2}\frac{\cosh kz}{\sinh kd}\sin(kx - \Omega t) \tag{12}$$

The relation between Ω and k is given by Mohammad and Rahim [27].

$$\Omega^2 = gk\tanh kd \tag{13}$$

In the deep water $\frac{d}{L} > 0.5$, the following equation used to replace Eq. (13) becomes

$$L = \frac{0.5gT^2}{\pi} \tag{14}$$

where, H is the wave height, L is the wave length, Ω is the wave frequency k is the wave number, C_a, C_m are inertia and added mass coefficient respectively, z_1 and z_2 are the bottom level and the still water level, T is the wave period. Also, m_{add} is the added mass on TLP columns, V is the volume of column.

Ignoring the drag force [27] and substituting Eqs. (11) and (12) into Eq. (10) one obtains:

$$F_{\text{morison}} = \sum_{\text{column}} \int_V c_a\rho\ddot{x}dV + \sum_{\text{column}} c_m\rho\frac{2\pi^2 H}{T^2}$$
$$\frac{\pi D_c^2}{4\sinh kd}\left(\frac{\sinh kz_2 - \sinh kz_1}{k}\right)\sin\Omega t \tag{15}$$

Substituting Eq. (15) into Eq. (8) one could obtain

$$(m + m_{add})\ddot{x}(t) + c\dot{x}(t) + \frac{nT_0}{L_0}x + n\left(\frac{AE - T_0}{2L_0^3}\right)x^3(t)$$
$$- 3n\left(\frac{AE - T_0}{8L_0^5}\right)x^5(t) + n\mu D_t^\alpha x(t)$$
$$= \sum_{\text{column}} c_m\rho\frac{2\pi^2 H}{T^2}\frac{\pi D_c^2}{4\sinh kd}\left(\frac{\sinh kz_2 - \sinh kz_1}{k}\right)\sin\Omega t \tag{16}$$

A.M. Ngounou, S.C. Mba Feulefack, L.M. Anague Tabejieu et al.

Chaos, Solitons and Fractals 157 (2022) 111952

where $m_{add} = \sum\limits_{column} \int\limits_{V} c_a \rho dV$ Taking into account the following dimensionless variables and parameters and after some manipulations, the dimensionless nonlinear equations of the system can be obtained as follows

$$y = \frac{x}{L_0}, \quad \Omega_0 = \sqrt{\frac{nT_0}{(m + m_{add})L_0}}, \quad \gamma_1 = \frac{AE - T_0}{2T_0},$$

$$\omega = \frac{\Omega}{\Omega_0}, \quad \lambda = c\sqrt{\frac{L_0}{n(m + m_{add})T_0}}$$

$$\eta = \frac{n\mu\Omega_0^{\alpha-2}}{(m + m_{add})}, \quad F_0 = \varepsilon \sum\limits_{column} c_m \rho \frac{2\pi^2 H}{T^2} \frac{\pi D_c^2}{4\sinh kd}$$

$$\left(\frac{\sinh kz_2 - \sinh kz_1}{k}\right), \quad \varepsilon = \frac{1}{nT_0}, \quad \tau = \Omega_0 t$$

$$\ddot{y}(\tau) + \lambda\dot{y}(\tau) + \omega_0^2 y(\tau) + \gamma_1 y^3(\tau) - \frac{3}{4}\gamma_1 y^5(\tau) + \eta D_\tau^\alpha y(\tau)$$
$$= F_0 \sin\omega\tau \tag{17}$$

The previous equation represents the dimensionless equation of the system.

3. Approximate solution of the TLP response subjected to the wave excitations and stability analysis

3.1. Analytical investigation

In this section, we are interested in the effect of the order of derivative α, the tendon viscosity coefficient η and the number of tendon n on the dynamic response of the platform.

Averaging method is applied here. First of all, we assume that γ_1, γ_2, η and F_0 are small perturbations, and considered $\omega^2 = \omega_0^2 + \xi\sigma$, $\omega_0^2 = 1$.

For that consideration, let us assume that the solution of Eq. (17) can be written as

$$y(\tau) = A(\tau)\cos(\omega\tau + \varphi(\tau)) \tag{18}$$

$$\dot{y}(\tau) = -\omega A(\tau)\sin(\omega\tau + \varphi(\tau)) \tag{19}$$

where the amplitude $A(\tau)$ and the phase $\varphi(\tau)$ are slow-varying functions of time τ. Substituting Eqs. (18) and (19) into Eq. (17)) after some mathematical manipulations, one obtains

$$\begin{cases} \dot{A} = -\frac{1}{\omega}[P_1(A, \varphi) + P_2(A, \varphi)]\sin(\omega\tau + \varphi) \\ A\dot{\varphi} = -\frac{1}{\omega}[P_1(A, \varphi) + P_2(A, \varphi)]\cos(\omega\tau + \varphi) \end{cases} \tag{20}$$

$$P_1(A, \varphi) = \tilde{F}_0\sin(\omega\tau) + \sigma A\cos(\omega\tau + \varphi) + \tilde{\lambda}\omega A\sin(\omega\tau + \varphi)$$
$$- \tilde{\gamma}_1 A^3\cos^3(\omega\tau + \varphi) + \frac{3}{4}\tilde{\gamma}_1 A^5\cos^5(\omega\tau + \varphi)$$

$$P_2(A, \varphi) = -\tilde{\eta}D_\tau^\alpha(A\cos(\omega\tau + \varphi)) \tag{21}$$

To apply the averaging method, we average at the period T_1 of which one could select as $T_1 = 2\pi/\omega$ in the case of periodic function or $T_1 = \infty$ in the case of aperiodic $D_\tau^\alpha(A\cos(\omega\tau + \varphi))$ [14–17]. We obtain the following pair of first order differential equations for the amplitude $A(\tau)$ and the phase $\varphi(\tau)$.

$$\dot{A} = -\frac{F_0}{2\omega}\cos\varphi + \frac{\lambda}{2}A + \eta A\omega^{\alpha-1}\sin\left(\frac{\alpha\pi}{2}\right) \tag{22}$$

$$A\dot{\varphi} = \frac{F_0}{2\omega}\sin\varphi - \frac{\xi\sigma A}{2\omega} + \frac{3\gamma_1 A^3}{8\omega} - \frac{15\gamma_1 A^5}{64\omega} + \eta A\omega^{\alpha-1}\cos\left(\frac{\alpha\pi}{2}\right) \tag{23}$$

In vibration engineering, the steady-state solution is more important. By eliminating $\sin\varphi$ and $\cos\varphi$.

Eqs. (22) and (23) for the steady-state solution $(A = A_0, \dot{A} = 0, \dot{\varphi} = 0)$, one obtains the following nonlinear algebraic equation

$$c_{10}A_0^{10} + c_8 A_0^8 + c_6 A_0^6 + c_4 A_0^4 + c_2 A_0^2 - F_0^2 = 0 \tag{24}$$

with

$$c_2 = \beta_1^2(\alpha) + \beta_2^2(\alpha), \quad c_4 = -\frac{3\gamma_1}{2}\beta_1(\alpha),$$

$$c_6 = \frac{9\gamma_1^2}{16} + \frac{15\gamma_1}{16}\beta_2(\alpha), \quad c_8 = -\frac{45\gamma_1^2}{64}, \quad c_{10} = \frac{225\gamma_1^2}{1024}$$

$$\beta_1(\alpha) = \lambda\omega + \eta\omega^\alpha\sin\left(\frac{\alpha\pi}{2}\right),$$

$$\beta_2(\alpha) = (\omega^2 - \omega_0^2) - \eta\omega^\alpha\cos\left(\frac{\alpha\pi}{2}\right) \tag{25}$$

This equation has more than one steady-state solution for some parameters. An interesting observation is the dependence of the oscillations amplitude upon the tendons parameters (natural frequency $\omega_0^2 = 1$, nonlinear γ_1 component, the number of tendon n and the dimensionless viscosity coefficient η), the parameters of the wave excitation (wave frequency ω and the dimensionless wave load F_0).

Next, we study the stability of the steady-state solution by using the method of Andronov and Witt [29], $A = A_0 + \Delta A$, $\varphi = \varphi_0 + \Delta\varphi$ and substituting them into Eqs. (22) and (23) one obtains

$$\frac{dA}{d\tau} = -\frac{\beta_1(\alpha)}{2\omega}\Delta A + \frac{A_0}{2\omega}\left[\beta_2(\alpha) - \frac{3}{4}\gamma_1 A_0^2 + \frac{15}{32}\gamma_1 A_0^4\right]\Delta\varphi \tag{26}$$

$$\frac{d\varphi}{d\tau} = \frac{1}{2\omega A_0}\left[\frac{9}{4}\gamma_1 A_0^2 - \frac{75}{64}\gamma_1 A_0^4 - \beta_2(\alpha)\right]\Delta A - \frac{\beta_1(\alpha)}{2\omega}\Delta\varphi \tag{27}$$

where $\beta_1(\alpha)$ and $\beta_2(\alpha)$ are given by Eq. (25). The stability of the steady-state solution is determined by the eigenvalue of the corresponding Jacobian matrix of Eqs. (26) and (27). The corresponding eigenvalues Ψ are the roots of

$$\Psi^2 + \frac{\beta_1(\alpha)}{2\omega}\Psi + \left(\frac{\beta_1(\alpha)}{2\omega}\right)^2 + \frac{1}{4\omega^2}\left[\frac{3}{4}\gamma_1 A_0^2 - \frac{15}{32}\gamma_1 A_0^4 - \beta_2(\alpha)\right]$$
$$\left[\frac{9}{4}\gamma_1 A_0^2 - \frac{75}{64}\gamma_1 A_0^4 - \beta_2(\alpha)\right] = 0 \tag{28}$$

Since $0 < \alpha < 1$, then $\beta_1(\alpha) > 0$, the determination of signs of the real parts of the roots Ψ may be carried out by making use of the Routh–Hurwitz criterion [30] as

$$\left(\frac{\beta_1(\alpha)}{2\omega}\right)^2 + \frac{1}{4\omega^2}\left[\frac{3}{4}\gamma_1 A_0^2 - \frac{15}{32}\gamma_1 A_0^4 - \beta_2(\alpha)\right]$$
$$\times\left[\frac{9}{4}\gamma_1 A_0^2 - \frac{75}{64}\gamma_1 A_0^4 - \beta_2(\alpha)\right] < 0 \tag{29}$$

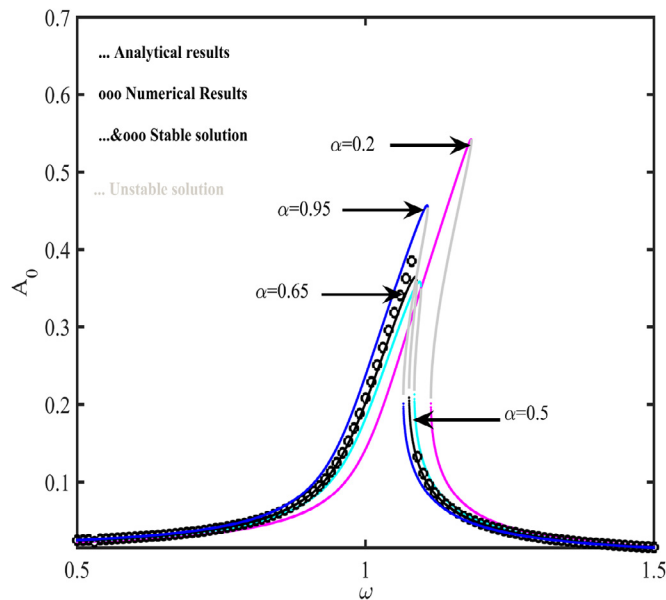The previous inequality represents the instability condition for the steady-state solution.

3.2. Numerical investigation

It is well known that the validation of results obtained through analytical investigation is guaranteed by the perfect match with the results obtained through direct numerical simulation of the mathematical model. Thus, the numerical scheme used in this paper is based on the Grunwald–Letnikov definition of the fractional order derivative Eq. (30) [31,32] and the Newton–Leipnik algorithm [18,19]

$$D_\tau^\alpha[y(\tau_{n_f})] \approx h^{-\alpha}\sum\limits_{j=0}^{n_f} C_j^\alpha y(\tau_{n_f-j}) \tag{30}$$

A.M. Ngounou, S.C. Mba Feulefack, L.M. Anague Tabejieu et al.

Chaos, Solitons and Fractals 157 (2022) 111952

Table 1
Values of the physical parameters of TLP model.

Parameter name	Symbol	Value
Tendons length (m)	L_0	882.5
Pre-Tension (mt)	T_0	18857
Weight of structure (mt)	W	13154
Young's modulus of a tendon (Pa)	E	2.10^{10}
Tendon stiffness (N/m)	k_0	9.10^6
Tendon Outer Inner Diameter (mm)	D_0, D_i	813, 781.5
Pontoon Size (m)	L_p, W_p, H_p	46, 15, 5
Columns Size (m)	D_c, H_c	20, 51
Number of Tendons Per Tendsion leg	n	8, 12, 16
Inertial coefficient of added	C_m	2
Tendon viscosity coefficient (Ns$^\alpha$/m)	μ	3.10^4
Acceleration of gravity (m/s^2)	g	9.81
Water density (kg/m^3)	ρ	1024
Wave period (s)	T	12
Wave height (m)	H	6

Fig. 3. Steady-state amplitude A_0 of the TLP as function of wave frequency ω for different values of the fractional-order α with $n = 8$.

where h is the integration step and the coefficients C_j^α satisfy the following recursive relations:

$$C_0^\alpha = 1, \qquad C_j^\alpha = \left(1 - \frac{1+\alpha}{j}\right)C_{j-1}^\alpha \qquad (31)$$

Properties of the tendon leg platform and characteristics of the sea waves which are used for numerical and analytical purpose are given in Table 1 [33].

Fig. 3 shows the effect of the fractional order derivative on the amplitude of vibration of the TLP. It is found that as the order of the fractional derivative increases, the amplitude response of the TLP decreases. The increase of the fractional order derivative also contributes to decrease the unstable range of amplitude. Nevertheless, beyond a certain value of the fractional parameter ($\alpha \in (0.65, 1)$), we rather observe an increase in amplitude. This graph also shows a comparison between the analytical results (curve with dotted lines) and numerical results (curve with a circle line $\alpha = 0.5$). We observe a good agreement between the analytical and numerical results. The same results were obtained by Anague et al [13]. Who studied the dynamic of a Rayleigh beam resting on fractional-order viscoelastic Pasternak foundations subjected to moving loads. But in their case they only observed a decrease in

amplitude of vibration of the beam when the fractional parameter increases.

In Fig. 4, we have plotted the amplitude response curve of vibration of the TLP A_0 as a function of the wave frequency ω for different values of the dimensionless tendon viscosity coefficient η. It is clearly shown that the system is more stable when the value of the dimensionless tendons viscosity coefficient increases. There is also a fairly significant reduction in the vibration amplitude of the structure with the increase of viscosity coefficient. The multi-value solutions appear for the small value of this coefficient and disappears gradually when this value increase.

Fig. 5 shows the variation of the amplitude of vibration of the TLP A_0 as function of the tendon viscosity coefficient for different values of wave frequency ω. It is observed from this figure that, for the lowest tendon viscosity coefficient, we only have the multi-value solutions, while for the highest tendon viscosity coefficient the multi-value solutions disappear. This confirms the results obtained and displays in Fig. 4. It is also found that for a value frequency $\omega = \omega_0 = 1$, when the tendon viscosity coefficient increases, the amplitude of vibration of TLP continuously decreases Fig. 5a, which is not the case in Fig. 5b–d, where the increase in the tendon viscosity coefficient leads first to increase the amplitude of vibration of the TLP, and then decrease it.

Fig. 6 shows the variation of the amplitude of vibration of the TLP as function of the tendon viscous coefficient η for different values of the fractional-order α. From the analysis of this figure, we note that the hysteresis and the amplitude jump phenomena are confirmed and can be controlled by the fractional-order parameter.

Fig. 7 shows the behavior of the amplitude of vibration A_0 in function of excitation frequency ω for the different values of number of tendons. One can observe that, when the number of the tendons increases, the vibration amplitude is relevantly reduced and the domain of the unstable solutions also decreases.

4. Effect of tendon on the appearance of horseshoes chaos on TLP: Melnikov analysis

In this section, it comes to evaluating the Melnikov's function which measures the distance between the border of regular oscillations and that of chaotic movements. Indeed, the aim is to clearly determine the effect of the fractional order parameter, the tendon viscosity coefficient and the number of tendons on the fractality of the basins of attraction and, so to speak, Smale horseshoe chaos through the analysis of the Melnikov's function. The configuration considers here is that of a catastrophic monostable potential.

The mathematical model Eq. (17) can be rewritten as a perturbed Hamiltonian system as

$$\frac{d\chi}{d\tau} = F[\chi] + \varepsilon G[\chi, \tau] \qquad (32)$$

where the vector fields χ, F and G are given by

$$\chi = \begin{bmatrix} y \\ z = \dot{y} \end{bmatrix}, \qquad F = \begin{bmatrix} z \\ -y - \gamma_1 y^3 + \frac{3}{4}\gamma_1 y^5 \end{bmatrix},$$

$$G = \begin{bmatrix} 0 \\ -\lambda z - \eta D_\tau^\alpha y + F_0 \sin\omega\tau \end{bmatrix} \qquad (33)$$

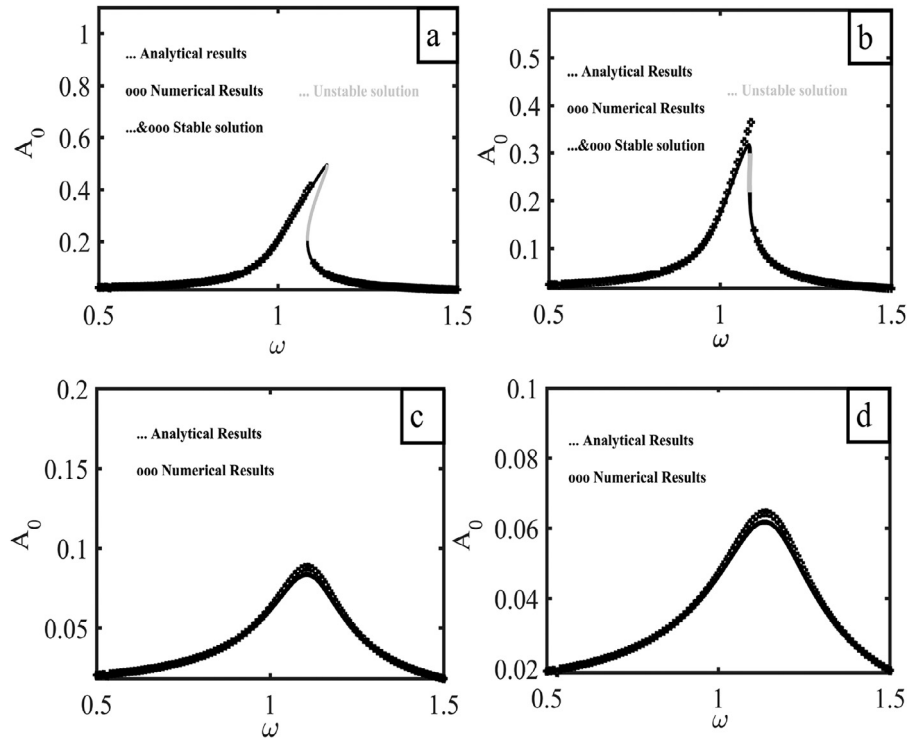with ε being a perturbation parameter.

In the unperturbed case ($\varepsilon = 0$), the system of Eq. (32) is the Hamiltonian system with Hamiltonian function
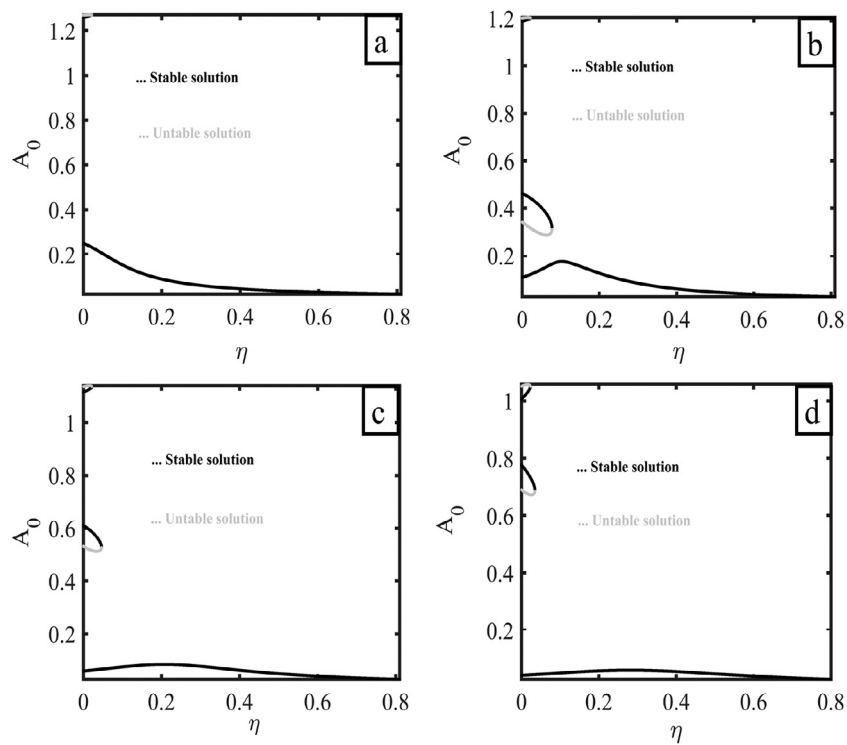
$$H(y, z) = \frac{1}{2}z^2 + \frac{1}{4}\gamma_1 y^4 - \frac{3}{24}\gamma_1 y^6 \qquad (34)$$

and the corresponding potential function is given as

$$U(y) = \frac{1}{4}\gamma_1 y^4 - \frac{3}{24}\gamma_1 y^6 \qquad (35)$$

A.M. Ngounou, S.C. Mba Feulefack, L.M. Anague Tabejieu et al.

Chaos, Solitons and Fractals 157 (2022) 111952

Fig. 4. Steady-state amplitude A_0 of the TLP as function of wave frequency ω for different values of tendon viscosity coefficient with (a) $\eta = 0.03$, (b) $\eta = 0.08$, (c) $\eta = 0.2$, (d) $\eta = 0.4$ for $n = 8$, $\alpha = 0.5$.

Fig. 5. Steady-state amplitude A_0 of the TLP as function of tendon viscosity coefficient η for different values of wave frequency with (a) $\omega = 1$, (b) $\omega = 1.09$, (c) $\omega = 1.15$, (d) $\omega = 1.2$ for $n = 8$, $\alpha = 0.5$.
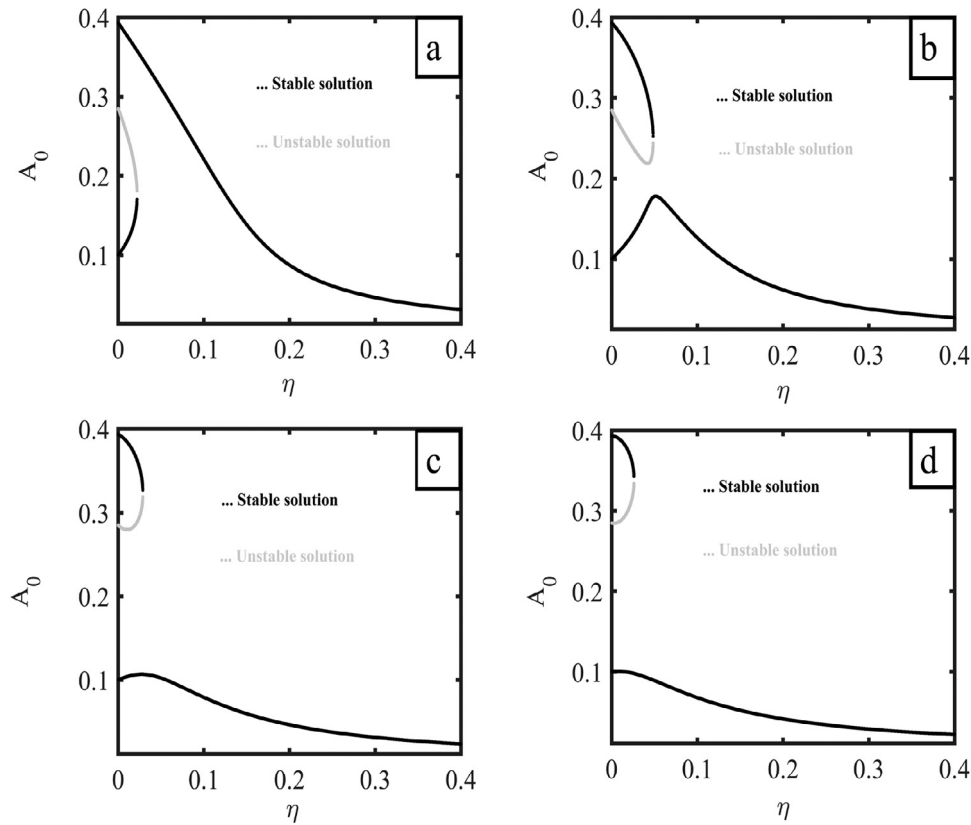
Fig. 6. Steady-state amplitude A_0 of the TLP as function of tendon viscosity coefficient η for different values of fractional-order with (a) $\alpha = 0.1$, (b) $\alpha = 0.5$, (c) $\alpha = 0.8$, (d) $\alpha = 0.95$ for $n = 8$, $\omega = 1.09$.
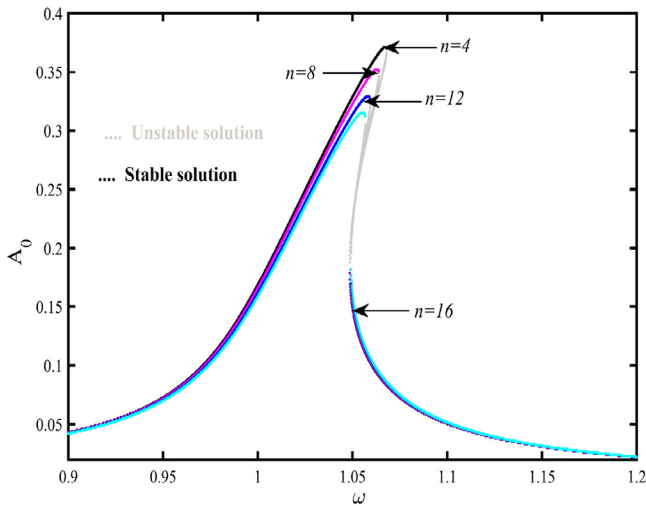
Fig. 7. Steady-state amplitude A_0 of the TLP as function of wave frequency ω for different values of the number of tendons n, with $\alpha = 0.5$.

Fig. 8 a shows the potential energy of our system ($\gamma_1 > 0$). The system has three equilibrium points: a center point $y_0 = (0, 0)$ and two saddle points $y_{1,2} = (\pm\sqrt{\frac{2(\gamma_1 + \sqrt{\gamma_1^2 + 3\gamma_1})}{3\gamma_1}}, \ 0)$, as shows in Fig. 8b.

The saddle points are connected by heteroclinic orbit that satisfy the following equation:

$$y_{het} = \pm\frac{y_1\sqrt{2}\sinh\left(\frac{\theta}{2}\tau\right)}{[-\beta + \cosh(\theta\tau)]^{\frac{1}{2}}}, \quad z_{het} = \pm\frac{y_1\frac{\sqrt{2}}{2}(1-\beta)\theta\cosh\left(\frac{\theta}{2}\tau\right)}{[-\beta + \cosh(\theta\tau)]^{\frac{3}{2}}} \quad (36)$$

where $\beta = \frac{5 - 3G^2}{3G^2 - 1}$, $\theta = y_1^2\sqrt{\frac{\gamma_1(1-G^2)}{2}}$, $G^2 = \frac{y_2^2}{y_1^2}$.

Unfortunately, mechanical and civil structures are subject to external stresses. That said, we consider the perturbed case ($\varepsilon \neq 0$). The Melnikov's theorem is used to detect transverse intersection points between perturbed and unperturbed orbits or the appearance of the fractality on the basin of attraction, which leads to the occurrence of chaos. Melnikov's theorem which gives the condition of transversality (of the existence of a fractal basin) can be formulated as follows [13,20–23]. Let the Melnikov function be defined in the case of Eq. (32) as

$$M_D(\tau_0) = \int_{-\infty}^{+\infty} F[\chi_{het}(\tau)] \wedge G[\chi_{het}(\tau), \tau + \tau_0]$$

$$= -\lambda\int_{-\infty}^{+\infty} z_{het}^2(\tau)\,d\tau - \eta\int_{-\infty}^{+\infty} z_{het}(\tau)\,D_\tau^\alpha[y_{het}(\tau)]d\tau)$$

$$+ F_0\int_{-\infty}^{+\infty} z_{het}(\tau)\sin(\tau + \tau_0)d\tau \quad (37)$$

When the Melnikov function has simple point, the stable manifold and unstable manifold intersect transversally, chaos in the sense of Smale horseshoe transform occurs. So let $M_D(\tau_0) = 0$, one concludes that horseshoe chaos appears when

$$F_0 \geq F_{0cr} = y_1\left(\frac{2\eta I_1 + \lambda(1-\beta)\theta I_2}{\sqrt{2} \times I_3}\right) \quad (38)$$

where

$$I_1 = \int_{-\infty}^{+\infty} \frac{\cosh\left(\frac{\theta}{2}\tau\right)}{[-\beta + \cosh(\theta\tau)]^{\frac{3}{2}}} D_\tau^\alpha\left[\frac{\sinh\left(\frac{\theta}{2}\tau\right)}{[-\beta + \cosh(\theta\tau)]^{\frac{1}{2}}}\right]d\tau$$

$$I_2 = \frac{(\beta+1)}{2\theta(1-\beta^2)^2}\left[\beta + 2 + \frac{(4\beta+2)(1-\beta^2)}{\sqrt{\beta^2 - 1}}\ln\left(\frac{-\beta + 1 + \sqrt{\beta^2 - 1}}{-\beta + 1 - \sqrt{\beta^2 - 1}}\right)\right],$$

$$I_3 = \frac{2\sqrt{2}\pi\omega}{(1-\beta)\theta^2\sinh\left(\frac{\pi\omega}{\theta}\right)}$$

A.M. Ngounou, S.C. Mba Feulefack, L.M. Anague Tabejieu et al.

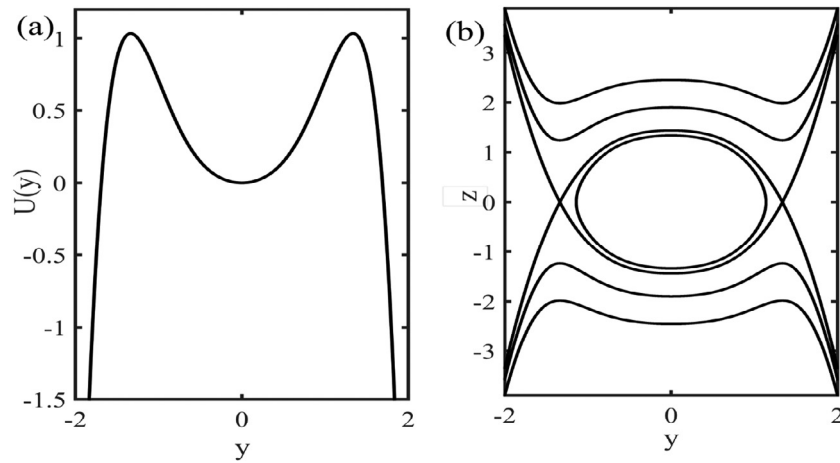*Chaos, Solitons and Fractals 157 (2022) 111952*

Fig. 8. Potential (a), separatrix (closed curve) and Phase space trajectories (open line) (b) of the system Eq. (17).
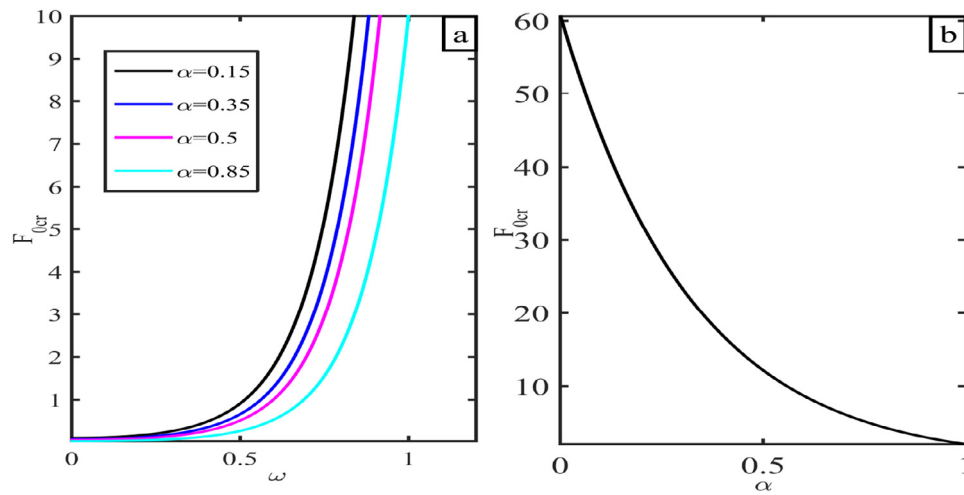

Fig. 9. Critical external force for the appearance of horsheshoes chaos as function of: (a) wave frequency ω, (b) fractional order parameter α for $n = 8$.
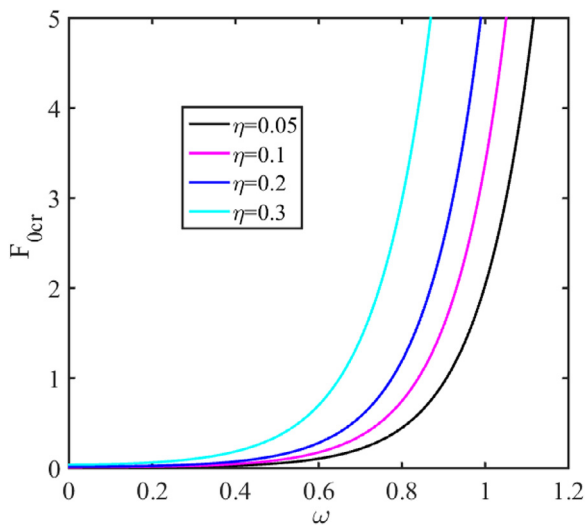

Fig. 10. Critical external force for the appearance of horsheshoes chaos for different values of tendon viscosity coefficient η for $n = 8$, $\alpha = 0.5$.
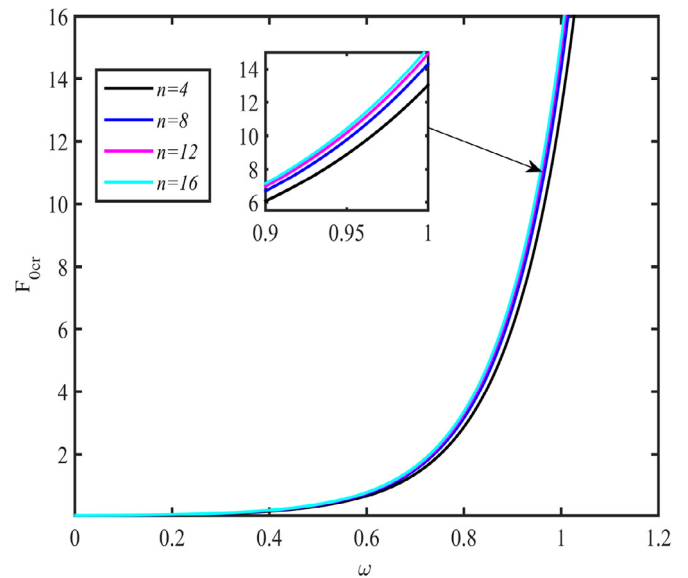

Fig. 11. Critical external force for the appearance of horsheshoes chaos for different values of the number of tendons n for $\alpha = 0.5$.

A.M. Ngounou, S.C. Mba Feulefack, L.M. Anague Tabejieu et al.
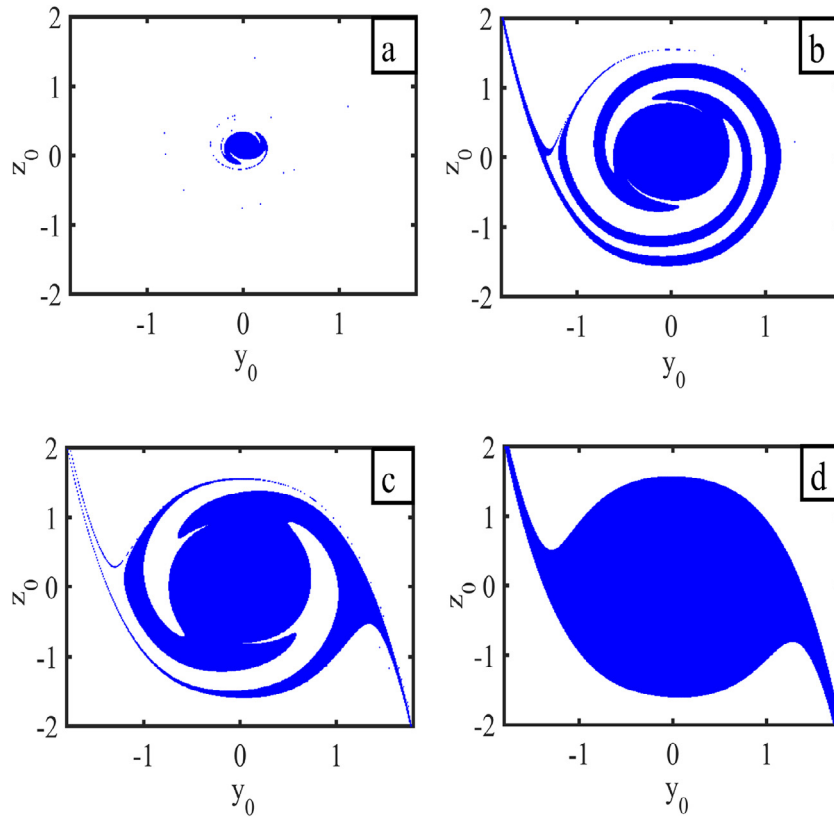
Chaos, Solitons and Fractals 157 (2022) 111952

Fig. 12. Effect of fractional parameter α on basin of attraction with (a) $\alpha = 0.15$, (b) $\alpha = 0.35$, (c) $\alpha = 0.4$, (d) $\alpha = 0.5$ for $n = 8$, $\eta = 0.3$, $\omega = 1$, $F_{0cr} = 0.05$.
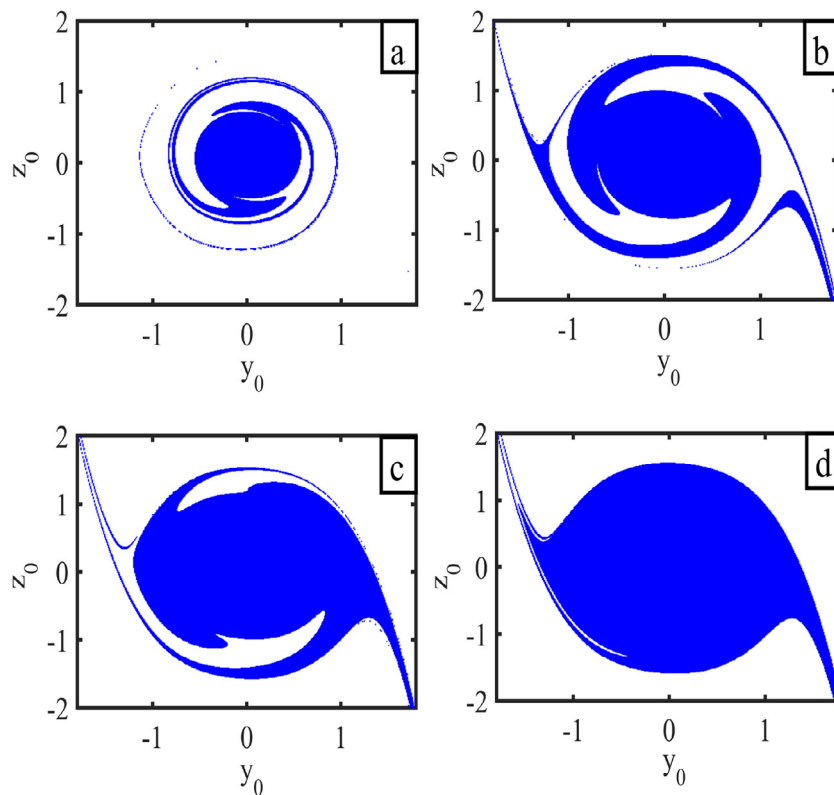

Fig. 13. Effect of tendon viscosity coefficient η on basin of attraction with (a) $\eta = 0.2$, (b) $\eta = 0.24$, (c) $\eta = 0.26$, (d) $= 0.28$ for $n = 8$, $\alpha = 0.5$, $\omega = 1$, $F_{0cr} = 0.05$.

Figs. 9–11 show the threshold conditions as function of wave frequency for different values of the main parameters of the system. Fig. 9a shows the critical external force for different values of fractional order parameter. One can observe that, when the value of the fractional order parameter increases, the thresholds of the critical values F_{0cr} decrease. Fig. 9b confirms the fact that as fractional order parameter increases the amplitude of critical force decreases. We can conclude that, by making the good choice of fractional derivative relating to reduce the amplitude of vibration of the system. Fig. 10 presents the threshold conditions as a function of wave frequency for different values of tendon viscosity coefficient. For each frequency, it is shown that the limit value predicted by the Melnikov theory is much larger when the tendon viscosity coefficient increases. On the other hand, the effect of the number of the tendons on the threshold amplitude versus the wave frequency is shown in Fig. 11. It is clear that the increase of the number of tendons first increases the threshold. One can conclude that the highest value of the number of tendons contributed to increase the degree of stability of the TLP.

To confirm our analytical predictions obtained in Figs. 9–11, we study the effect tendon viscosity coefficient and fractional order parameters on a basin of attraction of the system. For this purpose, we numerically solve Eq. (17) using Newton-Leipnik method [17,18]. From Fig. 12, we notice that, when decreasing the order of derivative, one an erosion of the basin of attraction. This result allows to conclude that, the lowest value of fractional order has a detrimental effect on the stability of the system. Fig. 13 presents the effect of the tendon viscosity coefficient on the basin of attraction. It should be noted that, when the tendon viscosity coefficient η greater than 0.27, the basin of attraction has a regular form Fig. 13b. Those results have already been predicted analytically. We can conclude that, the analytical and numerical predictions are in good agreement.

5. Conclusion

This work has analyzed the surge movement of tension leg platform under regular sea wave excitation. We have supposed that, the tendons exhibit a nonlinear viscoelastic behavior and fractional properties. We firstly modeled the TLP by the nonlinear ordinary differential equation. Secondly, the averaging method has been used to evaluate the effect of different parameters, namely: fractional order, tendon viscosity coefficient, number of tendons on the vibration amplitude of the tendon leg platform and on its stability. It was observed that as the order of the fractional derivative increases the amplitude response of the TLP decreases. The increase of the fractional order derivative also contributes to decrease the unstable range of amplitude. Nevertheless, beyond a certain value of the fractional parameter ($\alpha \in (0.65, 1)$), we have rather observed an increase in amplitude. It was also observed that, the amplitude response of tension leg platform is relevantly reduced and the domain of the unstable solutions also decreases when the number of tendons increases. Thus, it can be concluded that the surge amplitude is affected by the number of tendons, the fractional order derivative and the tendon viscosity coefficient. The Melnikov perturbation method is used to derive the analytical criterion for the appearance of chaos in the system. A convenient demonstration of the use and accuracy of the method is obtained from the basin of attraction. The effect of the number of tendons, the tendon viscosity coefficient and fractional derivative are investigated. It is found that, the horseshoes chaos decreases and disappears as these parameters increase. The basin of attraction is destroyed and the fractal behavior becomes more and more visible as the fractional derivative and the tendon viscosity coefficient decrease.

Declaration of Competing Interest

The authors declare that they have no known competing financial interests or personal relationships that could have appeared to influence the work reported in this paper.

CRediT authorship contribution statement

A.M. Ngounou: Investigation, Software, Writing – original draft. **S.C. Mba Feulefack:** Conceptualization, Investigation, Methodology, Software. **L.M. Anague Tabejieu:** Visualization, Investigation, Validation. **B.R. Nana Nbendjo:** Supervision, Methodology, Writing – review & editing, Validation.

References

[1] Adrezin R, Bar-Avi P, Benaroya H. Dynamic response of compliant offshore structures: review. J Aerosp Eng 1996;9(4):114–31.
[2] Feng WH, Hua FY, Yang L. Dynamic analysis of a tension leg platform for offshore wind turbines. J Power Tech 2014;94:42–9.
[3] Adrezin R, Benaroya H. Response of a tension leg platform to stochastic wave forces. Probab Eng Mech 1999;14:3–17.
[4] Han SM, Benaroya H. Comparison of linear and nonlinear responses of a compliant tower to random wave forces. Chaos, Solitons Fractals 2002;14:269–91.
[5] Taflanidis AA, Vetter C, Loukogeorgaki E. Impact of modeling and excitation uncertainties on operational and structural reliability of tension leg platforms. Appl Ocean Res 2013;43:131–47.
[6] Kurian VJ, Gasin MA, Narayanan SP, Kalaikuman V. Parametric study of TLPs subjected to random waves. ICCBT-C 2008;19:213–22.
[7] Kurian VJ, Gasin MA, Narayanan SP, Kalaikuman V. Response of square and triangular TLPs subjected to random waves. ICCBT-C 2008;12:133–40.
[8] Yang CM, Kim MH. Transient effects of tendon disconnection of TLP by hull-tendon-riser coupled dynamic analysis. Ocean Sys Eng 2010;37(8–9):667–77.
[9] Patel MH, Park HI. Dynamics of tension leg platform tethers at low tension. Part I-Mathieu stability at large parameters. Mar Struct 1991;4:257–73.
[10] El-gamal AR, Ashraf E, Ayman I. Effect of tethers tension force on the behavior of triangular tension leg platform. Am. J Civ Eng Archit 2014;2(3):107–14.
[11] Golafshani AA, Tabeshpour MR, Seif MS. First order perturbation solution for axial vibration of tension leg platforms. Sci Iran 2007;14:414–23.
[12] Ngounou AM, Nana Nbendjo BR, Dorka U. Effect of the delay between the detection of vibration and the action of tendon on the dynamics response of tension leg platform (TLP) under sea waves excitation. J Appl Nonlinear Dyn 2021;10(4):645–61.
[13] Anague Tabejieu LM, Nana Nbendjo BR, Woafo P. On the dyanamics of Rayleigh beams resting on fractional-order viscoelastic Pasternak foundations subjected to moving loads. Chaos, Solitons Fract 2016;93:39–47.
[14] Hayashi C. Nonlinear oscillations inphysicals systems. New York Mc-Graw-Hill; 1964.
[15] Sanders JA, Verhulst F, Murdock J. Averaging method sin nonlinear dynamical systems. New York: Springer Science & Business Media; 2007.
[16] Shen Y, Yang Xing H, Ma H. Primary resonance of duffing oscillator with two kinds of fractional-order derivatives. Int J Nonlinear Mech 2012;47:975–83.
[17] Deng J, Xie W-C, Pandey MD. Stochasticstability of a fractional viscoelastic column under bounded noise excitation. J Sound Vib 2014;333:1629–43.
[18] Debnath L. Recent applications of fractional calculus to science and engineering. Int J Math Math Sci 2003;54:3413–42.
[19] Petráš I. Fractional-order nonlinear systems: modeling, analysis and simulation. Beijing: Higher Education Press; 2011.
[20] Awrejcewicz J, Yuriy P. Chaos prediction in the duffing type system with friction using Melnikov's functions. Nonlinear Anal 2006;7(1):12–24.
[21] Awrejcewicz J, Holicke M. Analytical prediction of chaos in rotated froude pendulum. Nonlinear Dyn 2007;47:3–24.
[22] Youtha Ngouoko ON, Nana Nbendjo BR, Dorka U. On the appearance of horseshoes chaos in a nonlinear hysteretic system with negative stiffness. Archiv Appl Mech 2021;91(12):4621–30.
[23] Awrejcewicz J, Krysko VA. Introduction to asymptotic methods. New York: Chapmanand Hall, CRC Press, Boca Raton; 2006.
[24] Abou-Rayan AM, Ayman AS, El-gamal AR. Response of square tension leg platforms to hydrodynamic forces. Ocean Sys Eng 2012;2(2):115–35.
[25] Mohammad RT, Rahim S. Nonlinear dynamic analysis of TLP surge motion using homotopy perturbation method. Ships Off Struct 2014;9(6):569–77.
[26] Morison JR, O'Brien MP, Johnson JW, Schaaf SA. The force exerted by surface waves on piles. Pet Trans (Am Inst Min Eng) 1950;189:149–54.
[27] Mohammad RT, Rahim S. Perturbation nonlinear response of tension leg platform under regular wave excitation. J Mar Sci Tech 2018;23:132–40.
[28] Journée JMJ, Massie WW. Offshore hydromechanics. Delft University of Technology; 2001.

[29] Anadronov AA, Witt A. Towards mathematical theory of capture. Arch Elec-trotech 1930;24:99–110.

[30] Wiggins S. Introduction to applied nonlinear dynamical systems and chaos. NewYork: Springer; 1990.

[31] Ortigueira MD. Fractional calculus for scientists and engineers. Lecture notes in electrical engineering. Berlin, Heidelberg: Springer; 2011.

[32] Samko S, Kilbas A, Marichev O. Fractional integrals and derivatives: theory and applications. Amsterdam: Gordon and Breach Science Publishers; 1993.

[33] Xu N, Zhang J. Pitch/roll static stability of tension leg platforms. In: Interna-tional conference on ocean, offshore and arctic engineering, Shanghai, China; 2010.